THE GASIFICATION OF VARIOUS COALS IN MOLTEN SALTS

S. J. Yosim and K. M. Barclay

Energy Systems Group
Rockwell International
8900 De Soto Avenue
Canoga Park, California 91304

I. INTRODUCTION

The utilization of the U.S. coal reserves in a manner which does not add to the existing pollution problem is of utmost importance in the interest of conservation of more valuable natural resources in the national economy. Gasification of coal and generation of clean fuel gas offers one of the most promising approaches to the utilization of coal. It has been assigned a high priority in the U.S. Energy Development Program. Several of the coal gasification processes presently under development are now at the initial pilot plant operation stage. One of these processes is the Rockwell International Molten Salt Coal Gasification Process (Rockgas Process).[1,2] In this process, the coal is gasified at a temperature of about 1800°F and at pressures up to 30 atm by reaction with air in a highly turbulent mixture of molten sodium carbonate containing sodium sulfide, ash, and unreacted carbonaceous material. The sulfur and ash of the coal are retained in the melt, a small stream of which is continuously circulated through a process system for regeneration of the sodium carbonate, removal of the ash, and recovery of elemental sulfur.

A molten salt coal gasification process development unit (PDU)[1,2] capable of converting 1 ton of coal per hour into low-Btu fuel gas at pressures up to 20 atm is currently undergoing testing under contract to the Department of Energy. Preliminary to the PDU, a considerable amount of laboratory testing took place. These tests were conducted in a bench-scale, 6-in.-diameter gasifier in which coals of different rank were continuously gasified in the melt. The tests resulted in a better understanding of the gasification process. The purpose of this paper is to describe these laboratory tests and to discuss some of the chemistry taking place in the gasifier. Emphasis is placed on the effect of coal rank on the chemistry.

II. EXPERIMENTAL SECTION

A. COALS GASIFIED

The coals gasified were an anthracite, a medium-volatile bituminous coal, a high-volatile bituminous coal, and lignite. The coals are listed in order of decreasing rank. The first three coals were supplied by the Electric Power Development Corporation of Japan, and the lignite was supplied by Phillips Petroleum Company.

The proximate and ultimate analyses of the coals are listed in Table 1.

B. APPARATUS

A schematic of the bench-scale molten salt gasifier is shown in Figure 1. Approximately 12 lb of molten salt were contained in a 6-in.-ID and 36-in. high alumina tube placed in a Type 321 stainless steel retainer vessel. This stainless steel vessel, in turn, was contained in an 8-in.-ID four-heating-zone furnace. The four heating zones were each 8 in. in height, and the temperature of each zone was controlled by a silicon-controlled rectifier. Furnace and reactor temperatures were recorded by a 12-point Barber-Colman chart recorder.

TABLE 1

COMPOSITION OF COALS (WT %)

	Anthracite	Medium-Volatile Bituminous	High-Volatile Bituminous	Lignite
Proximate Analysis				
Moisture	2.78	2.26	0.85	32.46
Volatile Matter	4.92	30.36	38.71	28.70
Fixed Carbon	87.51	56.53	37.69	25.50
Ash	4.79	10.85	22.75	13.34
Ultimate Analysis				
Moisture	2.78	2.26	0.85	32.46
Carbon	85.27	71.85	62.26	35.34
Hydrogen	3.21	4.60	4.95	2.52
Nitrogen	0.81	0.78	0.82	0.96
Oxygen*	1.97	8.59	5.60	14.85
Sulfur	0.67	1.07	2.77	0.53
Ash	4.79	10.85	22.75	13.34

*By difference

The coal ground in a hand-turned burr mill was metered into the 1/2-in.-ID central tube of the injector by a screw feeder. Rotation of the screw feeder was provided by a 0- to 400-rpm Eberback Corporation Con-Torque stirrer motor. The coal was mixed in the injector with the air being used for gasification, and this coal-air mixture passed downward through the center tube of the injector and emerged into the 1-1/2-in.-ID alumina feed tube. This alumina feed tube was adjusted so that its tip was ~1/2 in. above the bottom of the 6-in.-diameter alumina reactor tube. Thus, the coal-air mixture was forced to pass downward through the feed tube, outward at its bottom end, and then upward through 6 in. of salt in the annulus between the 1-1/2-in. and the 6-in. alumina tubes.

III. RESULTS

A. PRODUCT GAS COMPOSITION FROM GASIFICATION WITH AIR

The test conditions for the gasification tests are listed in Table 2 which gives the melt temperature, the air and coal feed rates, the air/coal ratio, and the percent theoretical air. The last column shows the air feed as a percentage of the amount of air which is required to oxidize the coal completely to CO_2 and H_2O. The air/coal ratios and thus the percent theoretical air were chosen to give a good quality product gas from a heating value point of view. The steady-state composition and the higher heating value (HHV)* of the product gas obtained from the four coals are shown in Table 3. In each case, a good quality (>120 Btu/scf) low-Btu product gas was obtained. The product gas compositions were calculated on the basis of the carbon, hydrogen, and oxygen mass balance and assuming thermodynamic equilibrium for the water-gas shift reaction

$$CO + H_2O \rightleftharpoons CO_2 + H_2 \qquad 1)$$

To perform the mass balance, the coal analytical data shown in Table 1 were expressed in terms of an empirical formula, $C_CH_hO_O$. The results are shown in Table 3. The agreement between the observed and calculated values is, in general, quite good.

*The higher heating values include the heat of condensation of steam to liquid water.

TABLE 2

TEST CONDITIONS FOR GASIFICATION TESTS WITH COALS OF DIFFERENT RANK

Coal	Rank Number*	Melt Temperature (^{o}F)	Air Feed Rate (scfm)	Coal Feed Rate (lb/h)	Air/Coal Ratio (scf/lb)	Percent Theoretical Air
Anthracite	1-2	1791	1.85	1.67	66.7	45.3
Medium-Volatile Bituminous	2-2	1773	1.85	1.97	56.4	44.2
High-Volatile Biruminous	2-5	1740	1.85	2.95	37.7	32.4
Lignite	4-1	1781	1.60	5.06	19.0	32.9

*The rank number shows the ASTM class number followed by the group number. In Class 1, 1-1 is higher than 1-2, etc.

TABLE 3

COMPARISON OF OBSERVED AND CALCULATED PRODUCT GAS COMPOSITION

	Anthracite		Medium-Volatile Bituminous		High-Volatile Bituminous		Lignite	
	Observed	Calculated	Observed	Calculated	Observed	Calculated	Observed	Calculated
CO	29.9	28.9	28.7	26.2	31.4	33.4	24.3	22.2
H_2	9.3	8.0	9.3	11.0	14.7	17.0	15.4	19.4
CH_4	0.3	0.1*	0.0	0.1*	0.3	0.1*	1.7	0.9*
C_2H_6	0.0	0.0*	0.0	0.0*	0.0	0.0*	0.2	0.0*
CO_2	2.9	2.6	4.8	4.1	4.3	0.1	10.9	11.3
N_2	58.6	60.4	57.3	58.6	49.5	49.5	44.6	46.2
Higher Heating Value (Btu/scf)	129.0	120.3	122.7	120.0	151.1	164.2	149.2	143.6

*Arbitrarily assumed values.

As expected, the heating value of the product gas increases as the percent theoretical air decreases. This can be seen in Table 3, where in the case of anthracite and medium volatile bituminous coals, a product gas resulted with an HHV of about 130 Btu/scf at about 45% theoretical air, and the high-volatile bituminous and lignite coals resulted in a product gas with an HHV of about 150 Btu/scf at about 32% theoretical air. However, these are practical lower limits as to the percent theoretical air which should be used. If the percent theoretical air is too low, there will not be sufficient oxygen to gasify all the carbon and the carbon content of the melt will continue to increase. This is most pronounced with high rank coals such as anthracite. In addition, if the percent theoretical air is too low, there will be insufficient heat released to the melt to sustain the operating temperature. This is most pronounced in the low rank coals such as lignite which contain a considerable amount of combined oxygen and moisture. Thus, there is a practical limit to the heating value that can be obtained for the product gas.

B. A MECHANISM OF COAL GASIFICATION

A certain amount of time was required for the heating value of the gas to exceed 100 Btu/scf; this time was different for coals of different rank. A plot of product gas heating value vs cumulative run time is shown for the four coals in Figure 2. It can be seen that the time for the product gas to reach a heating value >100 Btu/scf decreased with decreasing coal rank. In the case of the anthracite and the medium-volatile bituminous coal, the times were about 2 h and 1/2 h, respectively. The product gases from the lignite and the high-volatile bituminous coals both had initial heating values in excess of 100 Btu/scf with the lignite initially producing somewhat richer gas than the high-volatile bituminous coal. During the early stages of an experiment when the product gas heating value was increasing, it was found that the CO_2 concentration was initially very high and continued to decrease while the CO concentration was very low and continued to increase. It was also found that the carbon content of the melt increased with time. This effect is shown for the case of anthracite in Figure 3. This suggests that conversion of carbon to CO_2 is the primary step; reduction of CO_2 to CO by carbon in the melt is a secondary step.

Primary Step	$C + O_2 \rightarrow CO_2$	2)
Secondary Step	$CO_2 + C \rightarrow 2CO$	3)

The steady-state carbon contents of the melt are shown for the four coals in Table 4. The steady-state carbon content for lignite is only 0.3 wt% in contrast to 12% for anthracite. Thus, the lower the rank of the coal being gasified, the more reactive the carbon and the less free carbon in the bed necessary to promote CO production; hence, the time required to achieve steady state is shorter with lower rank coal.

TABLE 4

STEADY-STATE CARBON CONTENT OF MELT

Coal	Rank Number*	Steady-State Carbon Content of Melt (wt %)
Lignite	4-1	0.3
High-Volatile Bituminous Coal	2-5	2.4
Medium-Volatile Bituminous Coal	2-2	3.6
Anthracite	1-2	12.0

*The rank number shows the ASTM class number followed by the group number. In Class I, 1-1 is higher rank than 1-2, etc.

REFERENCES

1. A. L. Kohl, M. H. Slater, and K. J. Miller, "Status of the Molten Salt Coal Gasification Process," Proceedings of the Tenth Synthetic Pipeline Gas Symposium, Chicago, Illinois, October 30, 1978

2. A. L. Kohl, R. B. Harty, J. G. Johanson, and L. M. Naphthali, "Molten Salt Coal Gasification Process," Chem Eng Prog. 74 73 1978

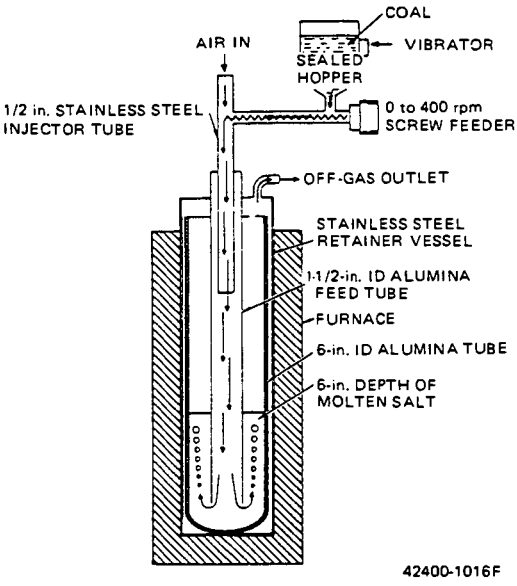

Figure 1. Bench-Scale Molten Salt Gasifier

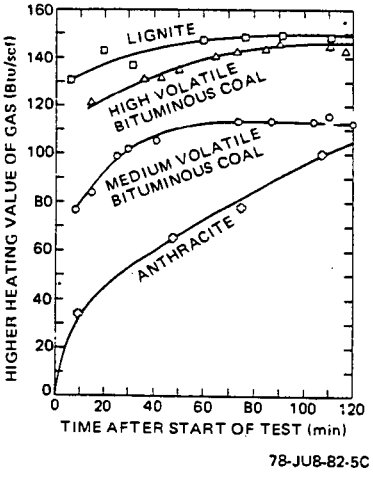

Figure 2. Change of Heating Value of Product Gas With Time for Different Coals

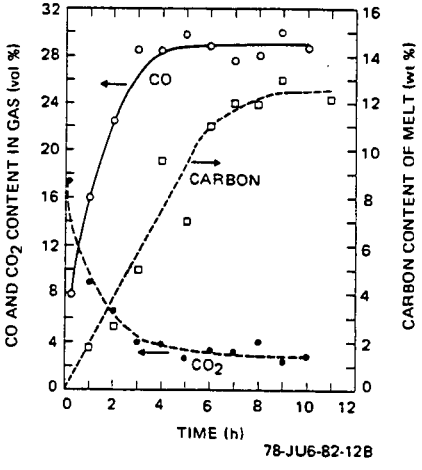

Figure 3. Effect of Carbon Content of Melt on CO and CO_2 Concentration in Gas

CATALYTIC COAL GASIFICATION-PART I: MECHANISM OF THE REACTION OF CO_2 WITH CHAR

By

AMIR ATTAR AND DANIEL C. BAKER
Department of Chemical Engineering
University of Houston
Houston, Texas 77004
December 1979

Catalytic coal gasification (CCG) can provide a competitive source of gas for domestic and industrial uses, consequently, CCG has been the subject of numerous studies. However, the mechanism of CCG, with catalysts like potassium carbonate is not clear, since no simple mechanism is known by which a solid can catalyze the rate of reaction of another solid.

Taylor and Neville (1921) reviewed the older literature on CCG and presented some rate data. More recently, Johnson (1976) and Cusumano et al. (1978) reviewed some of the modern literature on CCG. The thermodynamics and kinetics of gasification reactions were reviewed by von Fredersdorff and Elliot (1963).

Haynes et al. (1974) screened various materials as catalysts for coal gasification. They confirmed that alkali carbonates, like K_2CO_3 are very effective catalysts for coal gasification. Wilson et al. (1974) examined the effect of mixing nickel with alkali carbonates on the rate of gasification. They too found that alkali carbonates enhance the rate of gasification. Wilson et al. (1974) found that nickel that was added to the char, enhanced predominantly the methanation reaction of the gasification products, CO and H_2. Chauhan et al. (1977) examined the effect of incorporation of calcium and sodium on the rate of coal gasification. They also examined the effect of the particle size and the impregnation period of the coal on its rate of gasification. They found that small particles are consumed at faster rates than large particles and that the rate of gasification levels off after a given fraction of the coal has been gasified. Wilks et al. (1975) compared the time needed to gasify 90% of one char and two coals using various catalysts. They observed that impregnation of the coal with the catalyst is much more effective than adding the catalyst to the coal. The methane yield was the same whether a catalyst was added to the coal or not. Addition of 30% CO to steam suppressed the rate of gasification. A major study of various gasification catalysts and the rate of gasification has been conducted by Exxon Research and Engineering. Recently Nahas and Gallagher (1978) published data on the rate of CCG using K_2CO_3 and Vadovic and Eakman (1978) published a model for the rate of CCG. Tomita et al. (1977) added five minerals to coal and examined their effect on the rate of gasification. The results of Tomita et al. (1977) confirmed that all common minerals enhance to a limited extent the rate of coal gasification.

Since no simple mechanism is known by which one can explain the catalytic effect of one solid on the rate of reaction of another solid with a gas, we attempted to examine the mechanisms and rates of catalytic char gasification with different gases. Five possible rate enhancement modes were considered for the catalytic system char-K_2CO_3:

1. Catalysis by the chemical interaction of K_2CO_3 with oxygen functional groups in the char, and generation of more active sites.

2. Catalysis by generating a dipole due to electrical charges on the surface of the K_2CO_3.
3. Catalysis by the chemical interaction of K_2CO_3 with the gases, to yield more reactive gaseous species.
4. Catalysis by interference of the K_2CO_3 with the temperature field associated with the reacting char particle.
5. Catalysis by interference of the K_2CO_3 with the rate of adsorption of gases onto the char.

Mechanisms (1) and (3) attribute the catalytic effect to changes in the chemistry of the reaction, while mechanisms (2), (4), and (5) suggest physical effects as an explanation to the catalytic activity of K_2CO_3. Since K_2CO_3 enhances the rate of reactions of char with chemically different gases, e.g. CO_2, H_2O and H_2, one may expect the mechanisms of the catalysis to be insensitive to the nature of the gas. This observation tends to support catalytic mechanisms which rely more on changes in the physics of the reaction system. However, as will be demonstrated, the most likely catalytic effect relies on a synergist interaction between the chemistry and the physics of the catalytic system K_2CO_3-char.

The main reactions which are associated with char gasification are:

$$C + 2H_2 \rightleftarrows CH_4 \quad \text{slow below about } 650°C \qquad (1)$$

$$C + H_2O \rightleftarrows CO + H_2 \quad \text{fast above about } 500°C \qquad (2)$$

$$C + CO_2 \rightleftarrows 2CO \quad \text{fast above about } 500°C \qquad (3)$$

Two additional reactions which take place in a gasifier are the shift reaction:

$$CO + H_2O \rightleftarrows CO_2 + H_2 \qquad (4)$$

and the methanation of carbon monoxide:

$$CO + 3H_2 \rightarrow CH_4 + H_2O \qquad (5)$$

Figure 1 shows the Gibbs free energy (GFE), of the reactions vs. the temperature. The carbon used was graphite. Since the equilibrium constant, K, is related to the GFE by:

$$\Delta G° = -RT\ell nk \qquad (6)$$

it is obvious that gasification can proceed to CH_4 according to reaction 1 only at temperatures below about 838°K or 565°C. Reactions (2) and (3) can gasify graphite only at temperatures above 926°K (653°C) and 947°K (674°C) respectively. None of these three chemical reactions can be used to gasify graphite to any appreciable extent in the temperature range 565-653°C! Wile the rate of char gasification is expected to be different than that of graphite, the overall qualitative behavior may be similar.

Experimental

Figure 2 shows a schematic diagram of the experimental system. The system consists of five major parts:

1. A reactor
2. A gas chromatograph for gas analysis
3. A microprocessor-controlled pulse injector
4. A temperature monitor and programmer
5. A recorder and an interator.

Two types of reactors were used:

A. A microreactor with an optic fiber in it, which allowed examination of light emission from the surface of the sample (Figure 3).
B. A fixed-bed reactor, packed with char or treated char.

The system allows us to conduct isothermal and temperature-programmed tests, in addition to runs at different pressures. The operational range of temperature was 25-900°C and of pressures 0.1-0.5 Mpa. The system allows the injection of pulses of gas of variable sizes between 0.517 cm^3 and 10 cm^3. The range of temperature programming is 0-20°C/min. More detailed description of the system was published by Attar and Dupuis (1979).

During each run, a continuous stream of an inert gas was flowing through the reactor; as appropriate, a pulse of the reactive gas was injected into the reactor and gaseous products were obtained. The concentrations of CO, CO_2, H_2, H_2O, and CH_4 were determined using a thermal conductivity detector and a microprocessor-controlled integrator. Carbon monoxide and carbon dioxide were separated on a 200 cm x 0.3 cm column packed with 60-80 mesh Chromosorb® 105 at 65°C and with a nominal flowrate of 25 ml/min helium as a carrier gas. Methane and hydrogen were separated on a 200 cm x 0.3 cm column packed with 60-80 mesh molecular sieves 5 A at 80°C and with a nominal flowrate of 25 ml/min nitrogen as carrier.

A fixed sample of solid was placed in the reactor into which two thermocouples and an optic fiber were inserted. The radiation intensity coming from the reactor through the optic fiber was determined using a photomultiplier and an amplifier. The reactor internal temperature and a signal corresponding to the radiation intensity in the wavelength range of 200-750 nm were recorded vs. time. The photomultiplier produced a monotonically increasing signal relative to the radiation intensity which impinged on the optic fiber.

The fixed bed reactor consisted of 8 mm OD SS 316 tube packed with a known quantity of sample with a known particle size. Typically 30 cm length of tube were adequate.

Two types of analysis were done on the products of each pulse of reactive gas: analysis of the distribution of products by first separating them on a GC column, and analysis of the shape of the pulse of products as determined using a TC detector at the end of the fixed bed reactor.

The char was prepared from the 1.4 gm/cm^3 float fraction of Kentucky #9 coal. The coal was pyrolized at 806°C for 10 sec. The char was impregnated with solutions of the various catalysts and dried in vacuum at 70°C for 12 hours. Unless stated otherwise, the char particles used were smaller than 44 microns.

"Demineralization" of the char was done in a mixture of 2 vol. of concentrated HCl and 3 vol. water for 30 min at 40°C.

Silylation of the char was done by a 3:3:6 mixture of hexamethyldisilazane: trimethyl-chloro-silane in dry pyridine at 40°C for 30 min 10 ml of solution were used for each 5 gm char. The excess reagent was washed successively with pyridine and dry methanol and dried in vacuum oven for 12 hrs at 70°C.

When char reacts with CO_2

$$C + CO_2 \rightarrow 2CO \qquad (3)$$

two molecules of CO are obtained for each molecule of CO_2 which reacts. Therefore, the reliability of the experimental measurement can be checked by the closure of the material balance on the oxygen. Figure 4 shows the combined measured amounts of CO and CO_2 for pulses of fixed size which were injected at different reactor temperatures. The data show that the precision is excellent both in the case of graphite and char. The dimensionless standard deviations on the closure of the material balance on the oxygen are 1.1 and 2.6% respectively for the temperature range of 200-700°C. In this range of temperatures the rates of CO_2 to CO varied over several orders of magnitude. Larger error was obtained when slow desorption occurred, due to inconsistencies in the integration procedure of the GC peaks. However, in general, it was possible to close material balance on each pulse with 5% or better.

Preliminary Results and Discussion

An attempt was made to screen the various possible mechanisms relative to their influence on the rate of the gasification. The results of experiments that were conducted in order to prove or disprove each mechanism are presented and discussed individually.

Mechanism 1. Catalysis by increased site activity.

Although char is predominantly carbon, it has some oxygen and hydrogen. Part of the oxygen is present as adsorbed O_2, CO_2 and CO, however it is believed that some is bound as surface -OH and -COOH groups. Impregnation of char with K_2CO_3 using an aqueous solution produces much more active char than just adding K_2CO_3 (Wilks et al. 1975). This suggested that K^+ may replace the H^+ on the surface oxygen functions and thus produces more active surface dipole charges which adsorb gases like CO_2 more actively.

Test of Mechanism 1.

Many compounds are known which react selectively with oxygen functional groups. For example, a mixture of trimethyl-chloro-silane (TMCS) and hexamethyldisilazane (HMDS) reactions with OH groups as follows (Friedman et al. (1961)):

$$ROH + TMCS \xrightarrow[\text{pyridine}]{\text{dry}} ROSi \cdot (CH_3)_3 + HCl \qquad (7)$$

such a reaction blocks the oxygen site and makes it unavailable for exchange with K^+. Alkaline hydrolysis of the silicone compound yields inorganic silicates with OH groups NOT attached to the carbon.

$$ROSi \cdot (CH_3)_3 + 2H_2O \xrightarrow{[OH^-]} ROSi \cdot O(OH) + 3CH_4 \text{ (schematic)} \quad (8)$$

Samples of char were silylated according to reaction (7) and then impregnated with K_2CO_3. The rate of gasification with CO_2 of the silylated samples was slightly smaller than the rate of gasification of the non-silylated samples. Therefore, it was concluded that chemical interaction of K^+ with the oxygen functions is not the dominant catalytic mechanism.

Mechanism 2. Catalysis by solid-solid polarization.

Potassium carbonate, like many other salts, has negative surface charges. Since char is a good conductor, an electric dipole is created when K_2CO_3 touches char. It has been presumed that more active sites of high activity may be genreated by such a contact.

Test of Mechanism 2.

If the catalytic activity of K_2CO_3 was due to the dipolarization, one would expect every material with negative surface charges to have a similar catalytic effect to K_2CO_3. Since this is not observed experimentally it must be concluded that solid-solid dipolarization is not the dominant catalytic mechanism.

Mechanism 3. Catalysis by interaction between the K_2CO_3 and the gas which forms more reactive species.

It has been postulated that K_2CO_3 may interact with the gaseous molecules to form more reactive ones, which subsequently react with the char.

Test of Mechanism 3.

Potassium carbonate was found to catalyze the rate of reaction of char with many chemically and physically different gases. No products of binary interactions of activated species were found and it seems highly unplausible that the same solid will catalyze the formation of activated species from many different gases. Therefore, mechanism three has to be ruled out also. Additional data on this aspect were discussed by Thomas (1965).

Mechanism 4. Catalysis by the interaction of K_2CO_3 with the temperature field.

In ordinary gasification reactors the "reactor temperature" is measured and it is supposed that this temperature represents the reaction temperature. A catalytic effect is noted when higher rates of gasification of the solid are observed at the same MEASURED temperature. For the endothermic gasification reactions

$$C + CO_2 \rightarrow 2CO \qquad \Delta H \cong 40 \text{ kcal/mole} \qquad (3)$$

and

$$C + H_2O \rightarrow CO + H_2 \qquad \Delta H \cong 32 \text{ kcal/mole} \qquad (4)$$

heat has to be supplied to the char particle in order to maintain its gasification. If the rate of gasification is limited by the rate of heat transport, the temperature of the char, T_p, will be lower than the gas temperature, T_g or possibly the measured temperature, T_m. If K_2CO_3 impregnation enhances the rate of heat transport to the char, e.g. by absorbing more heat as radiation, one may conceive that conditions can exist, for which:

$$T_p < T_c < T_m \qquad (9)$$

The temperature of the char particles with catalyst, T_c, may effectively be larger than the temperature of the char with no catalyst, AT THE SAME MEASURED TEMPERATURE. This phenomenon will be recognized as "catalysis" since the rate of gasification is an increasing function of the temperature. The ratio of the rate of reaction of a particle with catalyst to that without one, r, will be approximately

$$r \cong \exp - \frac{E}{R}\left(\frac{1}{T_c} - \frac{1}{T_p}\right) > 1 \qquad (11)$$

Text of Mechanism 4.

Three tests were done to examine this mechanism:

A. The total radiation intensity in the reactor was measured using an optic fiber which was inserted into the char.

B. Pulses of CO_2 were injected into the reactor and the concentrations of CO_2 and CO were determined in the products. The approach function, ϕ_a, which measures how close the concentration of the gases approach equilibrium was plotted vs. the measured temperature, T_m

$$\phi_a = Y_{co}^2 \, P/Y_{co2} \qquad (12)$$

C. Calculations were made to estimate the possible effect of the rate of heat transport by radiation on the particle tempeature.

Figure 5 shows the radiation emitted from chars treated by various reagents vs. the measured temperature. The data shows that at the same measured temperature samples of char impregnated with more active catalysts emit less radiation than samples of char treated with less reactive catalysts. Based on this observation, it is tempting to assume that the effect of the K_2CO_3 is to enhance the rate of absorption of energy as radiation. Consequently, one would assume that the temperature of the K_2CO_3-treated char is larger than the temperature of the untreated char, at the same measured temperature. Since the reaction with CO_2 is endothermic, one must maintain that $T_p < T_c < T_m$.

Figure 6 shows the logarithm of the approach plotted vs. $10^3/T$ for graphite, untreated char and treated chars. The data show that larger approach is observed in the case of K_2CO_3-treated char than that which corresponds to graphite char, and to chars treated with $Ca(OH)_2$ and Na_2CO_3, all at the same reactor temperature.

Thermodynamics limits the value of the approach which can be obtained to the equilibrium value AT THE SAME TEMPERATURE. To explain the data, one must assume that either the char temperature is larger than the measured temperature, or that char has much larger activity than graphite and that equilibrium values derived based on graphite can not be applied to char. The char temperature can not be larger than the gas temperature because the gasification reaction is endothermic.

Two questions are addressed:

A. Under which circumstances the rate of heat transport may limit the rate of gasification by the endothermic reactions (2) and (3), and
B. Can the effect of heat transport by radiation be of sufficient magnitude to influence the temperature of the particle?

The answer to both problems is obtained using a simple steady-state energy balance on a coal particle.

Rate of heat transport by conduction + convection + Rate of heat transport by radiation

= Rate of absorption of heat by the reaction (13)

The complete mathematical analysis has been submitted for publication, the analysis shows that for particles of about 100 μ an increase in the rate of gasification by a factor of 1000-3000 will result in the rate of heat transfer limiting the rate of gasification. Heat transfer by radiation contributes 1-10% of the convection term near 700°C.

Mechanism 5. Catalysis by absorbing gas and retaining it near the surface of the char

Gas can be absorbed in a thin layer of coating present on the surface of solid supports. Thus, the system gas-solid will have a more "concentrated" gas-support interaction.

It is conceivable that if K_2CO_3 can dissolve CO_2, H_2O and H_2, then K_2CO_3 treatment of the char may result in larger surface concentrations of these gases and therefore in larger rates of gasification.

Test of Mechanism 5.

Packed beds of char with K_2CO_3 and without K_2CO_3 were prepared as described in the experimental section and used in the reactor. Pulses of gases were injected into the reactor and the pulses of products were analyzed. The conversion of each pulse, its shape and its retention in the

reactor were used to infer on the mechanism of the catalysis. The main conclusions from these tests are:

A. The pulses of gas are retained for a longer time in a reactor with treated-char relative to reactor with untreated char.

B. The shape of the pulses which came out of a reactor with treated char suggests that the gas disorbes from the K_2OC_3-treated char much slower than from the surface of untreated char. Figure 7 shows the forms of pulses of CO_2 injected to packed-bed reactors with char and with K_2CO_3-treated char at 650°C. The pulses coming out of the reactor with the K_2CO_3-treated char are flat and tailing. It takes as long as 10-20 minutes to completely desorb the pulse out. Figure 8 shows the shape of hydrogen pulses injected to the differential reactor at 700°C. Again, it is obvious that the residence time of H_2 on K_2CO_3-treated char is substantially longer than that on untreated char. Figure 9 shows the output signals from the gas chromatograph, when equal pulses of CO_2 were injected to columns packed with char and with K_2CO_3-treated char. The figure demonstrates three points: 1. more of the CO_2 is converted to CO when columns packed with K_2CO_3-treated char are used. 2. the CO_2 and the CO are retained on the K_2CO_3-treated char longer time than on the untreated char. 3. the pulses coming out of the K_2CO_3-treated char are tailing. These observations are consistent with mechanism five. The data show clearly that pulse of CO_2 stay in the reactor longer time when the reactor contains K_2CO_3-treated char, relative to when it contains untreated char. Silylation of char slightly reduces the residence time of pulses of CO_2 and the activity of the char. Treatment of silylated char with K_2CO_3 increases the activity of the char beyond that of untreated char, but not quite to the level of unsilylated char treated with K_2CO_3. Taylor and Neville (1921) observed that better catalysts absorb more CO_2 than poorer catalysts. However, they attributed the catalytic effect to the formation of surface carbon-oxygen complexes. Had surface complexes been formed, one would expect exchange of carbon from the gaseous carbon dioxide and the solid char. However, Yergey and Lampe (1974), who did tracer experiments using C^{13} on the gasification of char with $C^{13}O_2$ found that $C^{13}O$ and $C^{12}O$ evolve from the char simultaneously and at equal rates. These observations tend to support gasification mechanisms which do not permit exchange of carbon between the gas and the solid, or the formation of chemical bonds due to carbon-oxygen complexes.

Acknowledgement:

The authors wish to thank Dow Chemical Co. and Texas Energy Advisory Council for their generous support of this work.

References

1. Attar, A. and Dupuis, F., Ind. Eng. Chem., Proc. Des. and Dev., 18, 607-618 (1979).
2. Attar, A. and Robinson, R., submitted for publication.

3. Ayling, A. B., and Smith, I. W., Combust. and Flame., 18, 173-184 (1972).
4. Chauhan, S. P., Feldman, H. F., Stambaugh, E. P., and Oxley, J. H., Prep. Div. Fuel Chem., ACS, 22 (1) 38-52 (1977).
5. Cusumano, J. A., Dalla Betta, R. A., and Levy, R. B., Acad. Press., N.Y. 1978, Chapt. 10, p. 233.
6. Friedman, S., Kaufman, M. L., Steiner, W. A., and Wender, I., Fuel 40, 33-46 (1961).
7. Gardner, N., Samuels, E., and Wilks, K., P. 217-237 ("Coal Gasification", Adv. in Chem., Ser. 131, ACS, Washington (1974).
8. Haynes, W. P., Gasior, S. J., and Forney, A. J., p. 179-203, "Coal Gasification", Adv. in Chem., Ser. 131, ACS, Washington (1974).
9. Hill, F. B., and Wilhelm, R. H., AIChE J., 5 (41), 486-496 (1959).
10. Johnson, J. L., Catal. Rev. Sci. Eng., 14 (1), 131-152 (1976).
11. Nahas, N. C. and Gallagher, J. E., Jr., paper presented in the 19th Intersociety Energy Conversion Engineering Conference, Aug. 1978, San Diego, California.
12. Taylor, H. S. and Neville, H. A., J. Am. Chem. Soc. Soc., 43, 2055 (1921).
13. Thomas, J. M., p. 122-203 in "Chemistry and Physics of Carbon", Vol. 1, Walker, P. L., Jr., (ed)., Marcel Dekker, N. Y. (1965).
14. Tomita, A., Mahajan, O. P., and Walker, P. L. Jr., Prep. Div. Fuel Chem. ACS, 22 (1), 4-6 (1977).
15. Vadovic, C. J., and Eakman, J. M., Prep. Div. Fuel Chem., ACS, 23 (1978).
16. Von Fredersdorff and Elliot, M. A., Chap. 20 p. 892-1022, in "Chemistry of Coal Utilization", Lowry H. H. (ed) Suppl. vol., Wiley, H. Y. (1963).
17. Wilks, K. A., Gardner, N. C., and Angus, J. C., Prep. Div. Fuel Chem., ACS, 20 (3), 52-60 (1975).
18. Wilson, W. G., Sealock, L. J., Jr., Hoodmaker, F. C., Hoffman, R. W., Stinson, D. L., and Cox, J. L., p. 203-217 in "Coal Gasification", Adv. in Chem., Ser. 131, ACS, Washington (1974)
19. Yergey, A. L., and Lampe, F. W., Fuel 93, 280-281 (1974).

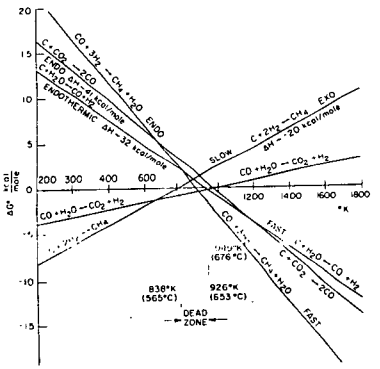

Fig. 1. Gibbs free energy of the main gasification reactions.

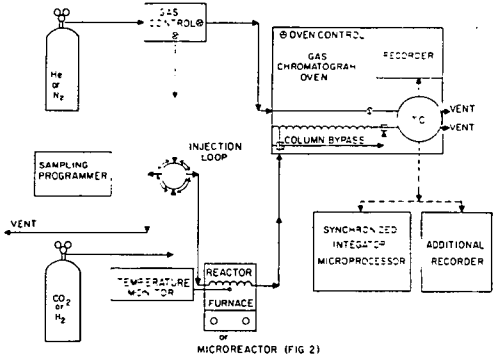

Fig. 2. Schematic diagram of the experimental system.

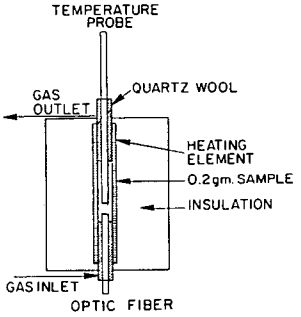

FIG.2 MICROREACTOR OPTION

Fig. 3. Microreactor with an optic fiber in it.

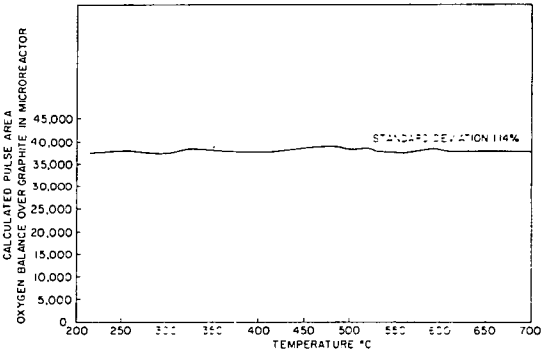

Fig. 4. Examination of the consistency of the results: closure of oxygen material balance.

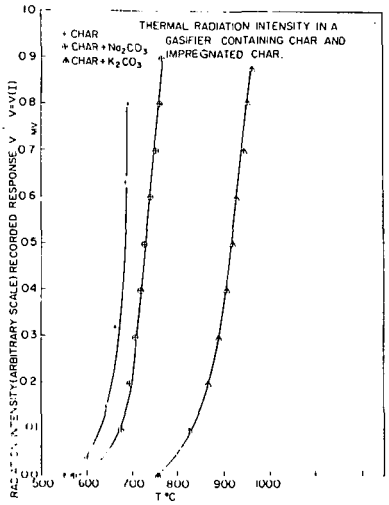

Fig. 5. The variation of the emission of light from the surface of char treated by various catalysis.

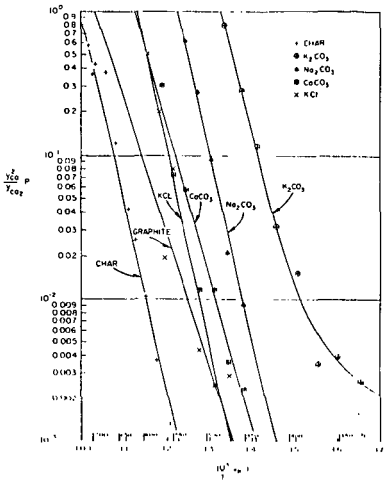

Fig. 6. The approach functions P_{Y^2CO}/Y_{CO_2} plotted vs. $10^3/T$ for chars treated by various catalysts.

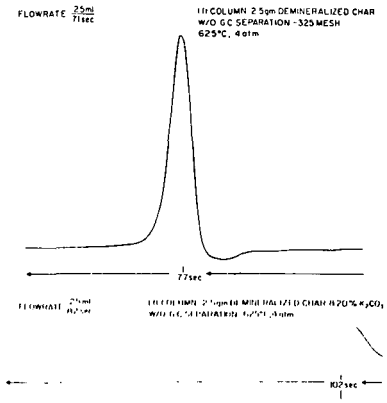

Fig. 7. The shape of pulses of CO_2 at the outlet of the packed bed reactor.

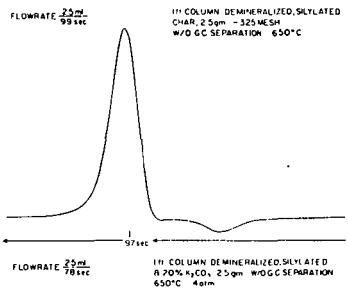

Fig. 8. The shape of pulses of CO_2 at the outlet of the packed bed.

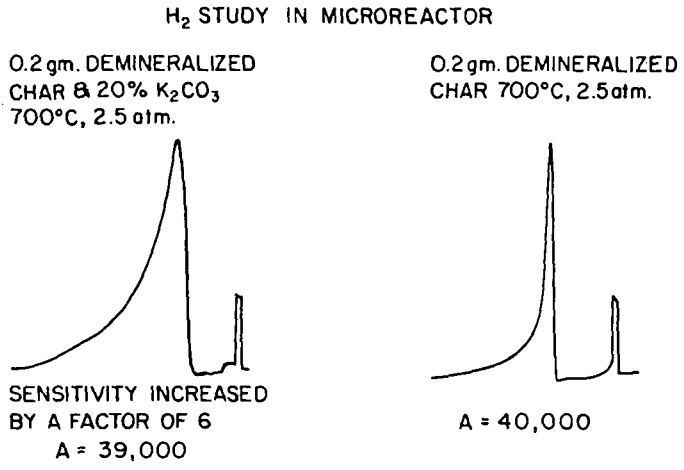

Fig. 9. The shape of pulses of H_2 at the outlet of the microreactor.

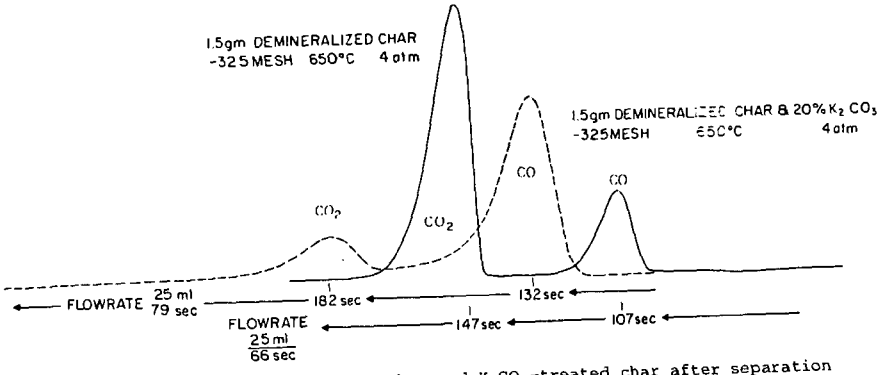

Fig. 10. Pulses of CO_2 from char and K_2CO_3-treated char after separation on the GC.

Char Reactivities and Their Relationship to Pore Characteristics

S. Katta and D. L. Keairns
Westinghouse R&D Center
Pittsburgh, PA 15235

INTRODUCTION

The study of char reactivities is fundamental to the design and performance evaluation of gasifiers for coal gasification. This investigation was undertaken in connection with the development of the Westinghouse coal gasification process. The objective of the study was to determine the reactivities of several chars and to examine the relationship between the reactivities and the pore surface areas or mean pore diameters. If char reactivities can be predicted from pore surface area or pore mean diameter, char characterization becomes simpler. This method can then be used as a screening technique to assess the performance of gasifiers.

A detailed experimental investigation on the rate of carbon-steam ($C-H_2O$) and carbon-carbon dioxide ($C-CO_2$) reactions with coke breeze was reported by Katta and Keairns (1). The reactivities of chars were used to predict gasification rates in several pilot plant tests by means of a gasification model.

The reactivity of carbonaceous material in a H_2O or CO_2 atmosphere depends on the rank of coal, the rate of heating, and the heat treatment temperature, all of which influence the pore characteristics. The pore structure and the chemical nature of the char control the reactivity in a H_2O, CO_2, or oxygen atmosphere. The reactivity of a material may not be the same in all these atmospheres since the mineral content influences each of these reactions to a different extent and the same pores are not involved in these reactions. Information from the literature indicates that a limited understanding has been gained on the influence of different parameters on the reactivities of chars.

In any coal gasification process much of the carbon conversion takes place through a $C-H_2O$ reaction. Hence, it is important to establish char reactivities in a steam atmosphere rather than in other atmospheres. A study of char reactivities in the atmospheres of H_2O, CO_2, oxygen, and hydrogen is important for a fundamental understanding of char behavior.

Jenkins et al. (2) studied the reactivities of various chars in air at 500°C as a function of heat treatment temperature, mineral content, and pore structure. They found that the chars became less reactive as the heat treatment temperature was increased, and that the magnitude of the effect depended on the type of char. They observed, also, that the

level of transitional porosity (estimated from nitrogen adsorption) increases the reactivity markedly since the ability of a gaseous reactant to reach the surface area in the micropores is enhanced. They concluded that the reactivity of chars prepared at the same temperature and heating rate is predominantly influenced by mineral matter and the rank of the parent coal.

The reactivities of several chars in a CO_2 atmosphere and the changes in pore structure with carbon conversion were investigated by Dutta et al. (3). They found that almost the entire surface area of chars seemed to be due to micropores smaller than 0.01 to 0.02 μm in diameter. They concluded that the reactivities were almost proportional to the surface areas occupied by pores above about 0.003 μm in diameter, suggesting that smaller pores are inaccessible to gaseous reactant. They derived a rate equation with a parameter that represents the change in available pore surface area with carbon conversion.

Johnson (4) conducted a comprehensive study on the effects of physical and chemical properties of chars on their reactivities. He concluded that the gasification of chars with hydrogen and steam-hydrogen (H_2O-H_2) mixtures occurs primarily on the surface within micropores which were defined as less than 5.5 nm in diameter.

EXPERIMENTAL WORK

The reactivities of various chars were determined at a temperature of 927°C and a pressure of 10 atmospheres in a steam-hydrogen-nitrogen (H_2O-H_2-N_2) atmosphere. Experiments were conducted in a reactor of 3.5 cm id and 30.5 cm height which was heated externally by an electric furnace. A sample of about 35 g of char of -1.0 + 0.25 mm size was placed on the distributor and fluidized by the gaseous mixture. Gas samples were taken for different inlet gas compositions, and the reaction rate was determined from the product gas composition and the estimated amount of carbon present in the bed at the time the sample was taken. At the end of the test, the bed material was weighed and the product gas line flushed to collect fines. The amount of fines collected in any run was very small. A detailed description of the apparatus and the experimental procedure are given in reference (1). The reaction data were analyzed on the basis of the rate equation derived from Ergun's model (5).

CHAR PREPARATION

Renton, Minnehaha, and Montour chars were prepared in the Westinghouse process development unit. Western Kentucky and Utah chars were obtained from FMC Corporation and Synthane char from the Synthane pilot plant.

SURFACE AREA MEASUREMENT

We degassed the char samples at 110°C for about four hours prior to measuring their surface areas, using carbon dioxide as the adsorbate at 298 K on a micromeritics Model 2100 surface area analyzer. An equilibration time of about 30 minutes was allowed for each adsorption point. The molecular area of CO_2 at 298 K was taken as 25.3 $\AA^2$.

The Dubinin-Polanyi equation (D-P equation) was used for the evaluation of surface areas of chars and is given below:

$$\log V_a = \log V_o - D \log^2 (P_o/P_2) \quad (1)$$

A plot of log V_a versus $\log^2 (P_o/P_2)$ yields the value of log V_o from which the specific surface area of the sample can be calculated. A value of 63.5 atm was used for the saturation vapor pressure of CO_2 at 298 K.

PORE VOLUME MEASUREMENT

Measurements on pore volume were made with a Micromeritics mercury penetration porosimeter Model 910 series. Pressures up to 17,000 psi were used in these measurements to cover a pore diameter range of 100 to 0.0104 μm.

RESULTS AND DISCUSSION

The following rate equation for the coke breeze-H_2O reaction had been obtained in a previous study (1):

$$r_2 = k_2/(1 + P_{H_2}/K_2 P_{H_2O}) \quad (2)$$

where r_2, k_2, and K_2 are the reaction rate per unit mass, min^{-1}, the reaction constant, and the equilibrium constant, respectively. k_2 and K_2 are given by

$$k_2 = 4.85 \times 10^6 \cdot \exp(-48{,}200/RT) \quad (3)$$

$$K_2 = 2.25 \times 10^6 \cdot \exp(-42{,}600/RT) \quad (4)$$

where T is the absolute temperature in K. The rate data were plotted with P_{H_2}/P_{H_2O} versus the inverse reaction rate to obtain the reaction rate parameters. The intercepts on the ordinate and the abscissa give the values of K_2 and $1/k_2$, respectively. Results for Renton, Minnehaha, FMC Western Kentucky, Synthane, Montour, and Utah chars are shown in Figures 1 to 6. The initial relative reactivities of various chars with reference to coke breeze are given in Table 1.

Table 1

RELATIVE REACTIVITIES OF CHARS

Char	Rate Constant, k_2, min^{-1}	Initial Relative Reactivity	Surface Area by CO_2 Adsorption	Mean Pore Diameter, μm
Coke Breeze	0.008	1.00	13.9	0.196
Minnehaha	0.08	9.88	85.2	0.066
Renton	0.02	2.47	199.8	0.033
Utah	0.081	10.13	126.8	0.036
FMC Western Kentucky	0.095	11.73	117.9	0.041
Synthane*	0.08	10.67	63.2	0.068
Montour	0.0195	2.44	23.3	0.161

*Reactivity evaluated at 32 percent carbon conversion.

The initial relative reactivities of the chars were plotted versus the pore surface areas determined by CO_2 adsorption and interpreted by Dubinin-Polanyi equation in Figure 7. If the data on Renton char is excluded, a correlation of these two variables can be obtained. In the absence of reactivity data, the relative reactivity can be estimated from CO_2 surface areas. This method, however, will probably be uncertain for some materials whose surface area develops primarily after significant conversion. Work on additional chars is recommended in order to improve the reliability of the method and to establish limitations.

The mean pore diameter of chars is calculated from the relation $\bar{D} = 4V/S_{CO_2}$, where V is the pore volume as measured by means of mercury porosimeter and S_{CO_2} is the surface area as measured from CO_2 adsorption. The relative char reactivities were plotted versus the mean pore diameter in Figure 8. A linear correlation was obtained by a regression analysis after excluding the data on Renton char. Use of this correlation requires the measurement of surface area and pore volume. Figures 7 and 8 indicate that more reactive chars have greater surface areas and smaller mean pore diameters than others, as would be expected.

SUMMARY

Relative reactivities of chars in a H_2O-N_2-H_2 atmosphere were measured in a laboratory fluidized bed. Results were analyzed on the basis of Ergun's rate equation, and the relative reactivities were calculated with reference to coke breeze. Surface areas of chars were obtained by means of CO_2 adsorption, and pore volumes were measured by means of mercury penetration porosimetry. A correlation can be identified between the relative reactivity versus the surface areas and the mean pore diameter for the limited number of chars investigated in the present study. Additional studies should be conducted to establish the range of validity with additional chars and drawbacks of this approach.

ACKNOWLEDGEMENTS

This work was performed as part of the Westinghouse coal gasification program under DOE contract EF-77-C-01-1514.

REFERENCES

1. Katta, S. and Keairns, D. L., Study of Kinetics of Carbon Gasification Reactions, submitted to I&EC Fundamentals for Publication (1980).

2. Jenkins, R. G., Nandi, S. P. and Walker, P. L., Jr., Fuel, 52, 288 (1973).

3. Dutta, S., Wen, C. Y. and Belt, R. J., Ind. Eng. Chem. Process Des. Dev., 16(1), 20-30 (1977).

4. Johnson, J. L., Presented at Symposium on Structure and Reactivity of Coal and Char, National ACS Meeting, Chicago (August, 1975).

5. Ergun, S., Bureau of Mines Bulletin 598, Washington, D.C. (1962)

NOMENCLATURE

D	a constant
$\bar{D}$	mean pore diameter of chars
k_2	rate constant of carbon-steam reaction, min^{-1} as defined by Ergun's rate equation
K_2	equilibrium constant of carbon-steam reaction as defined by Ergun's theory
P_{H_2}, P_{H_2O}	partial pressures of hydrogen and steam, respectively
P_o	saturation vapor pressure of adsorbate at adsorption temperature
r_2	initial rate per unit mass of carbon-steam reaction, (corresponds to a carbon conversion of zero) min^{-1}
S_{CO_2}	surface area of chars measured by CO_2 adsorption
T	absolute temperature of char bed, K
V	pore volume, cm^3/g
V_a	amount of CO_2 adsorbed at equilibrium pressure P_2
V_o	micropore capacity
X	fractional carbon conversion

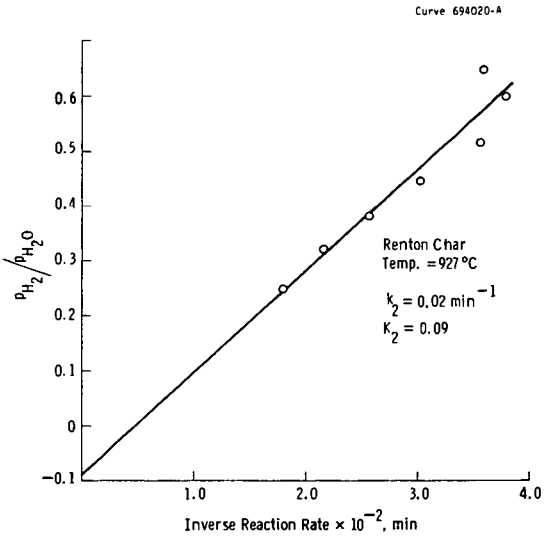

Figure 1 – Renton char – steam reaction

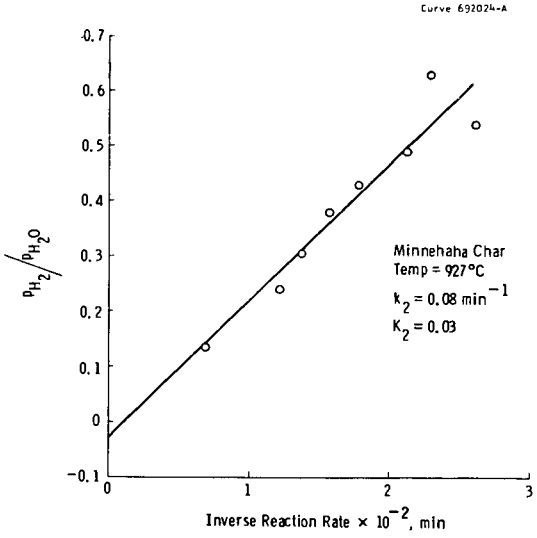

Figure 2 – Minnehaha char – steam reaction

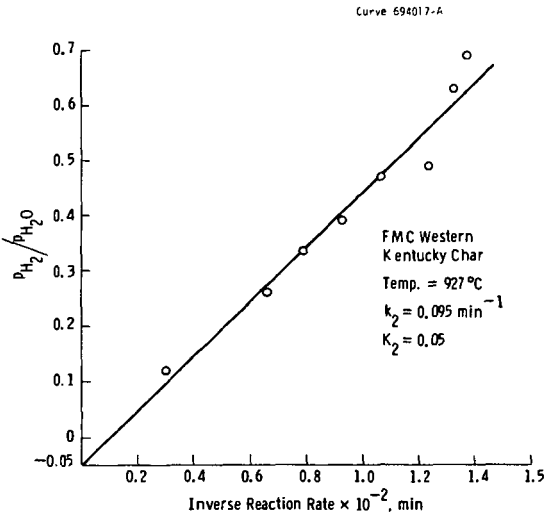

Figure 3 – FMC western Kentucky char – steam reaction

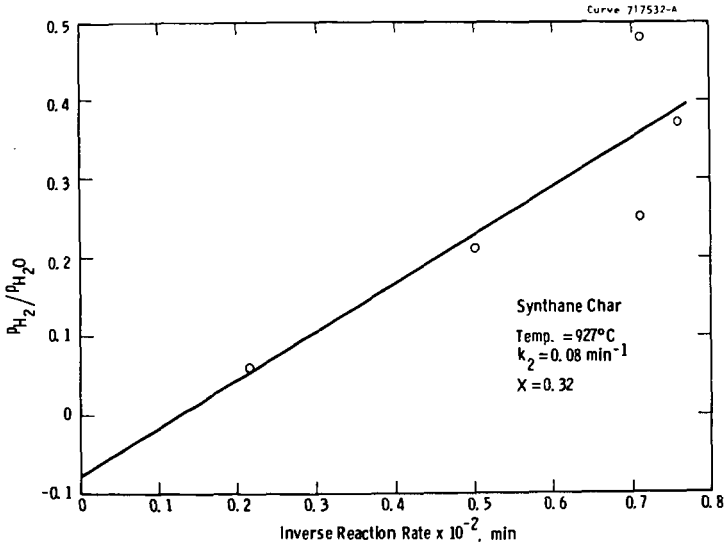

Figure 4 – Synthane char – steam reaction

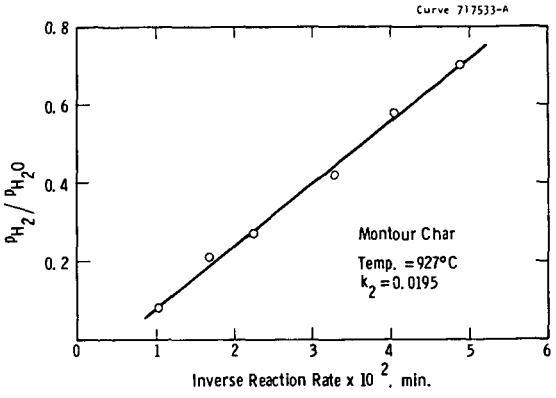

Figure 5 – Montour char – steam reaction

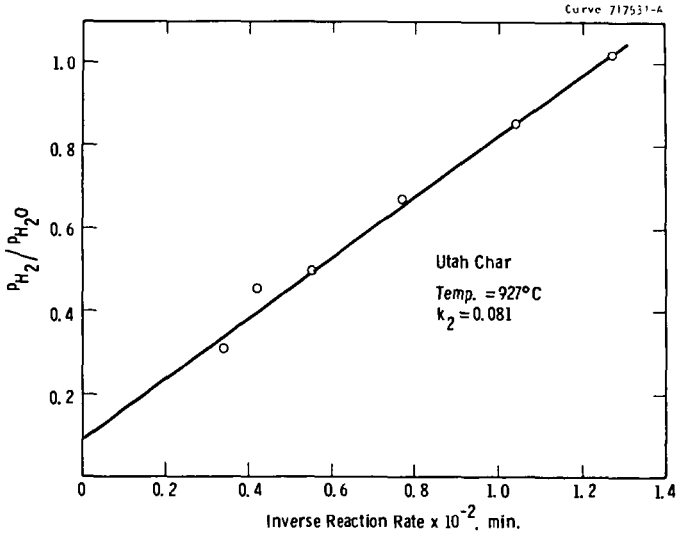

Figure 6 – Utah char – steam reaction

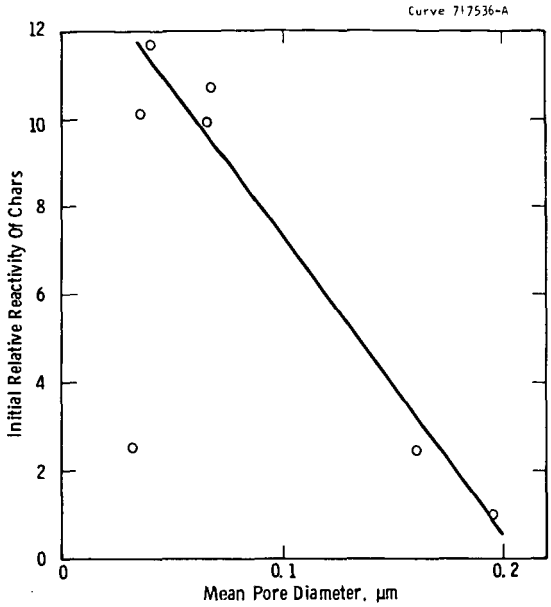

Figure 8 – Relationship between reactivity and mean pore diameter

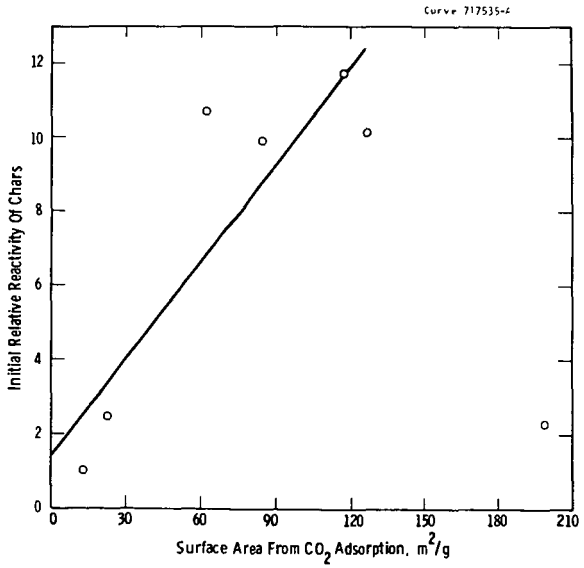

Figure 7 – Relationship between reactivity and surface area of chars

HYDROGENOLYSIS OF BENZENE AND ALKYLATED BENZENES OVER COAL CHARS

S. K. Gangwal and W. J. McMichael
Research Triangle Institute
P. O. Box 12194
Research Triangle Park, N. C. 27709

INTRODUCTION

The Research Triangle Institute (RTI) is conducting an experimental study to assess the environmental impacts of coal gasification and evaluate control technologies for the many potential pollutants that are formed during gasification. Pollutant generation behavior of 10 U.S. coals has been studied in a bench-scale gasifier under a variety of conditions (1-3). Process operating conditions such as continuous versus batch operation, fixed versus fluidized bed operation, temperature, coal type, pressure and particle size have been found to determine production behavior. Of major interest are the polycyclic aromatic hydrocarbons (PAH) and phenolic compounds.

Significant quantities of char or high ash solids are produced during coal gasification. One objective of this study was to determine the feasibility of using coal char as a catalyst to facilitate cracking of potential environmental pollutants. The authors are aware of only one previous study, which reported on decomposition of phenolics over lignite char (4). It was found that the presence of coal char greatly enhanced the decomposition of phenol. Virk, et al. (5) reviewed the literature on thermal hydrogenolysis of aromatic compounds. Benzene decomposition was slowest and anthracene decomposition was fastest among the various compounds studied (1 to 4 rings). No alkylated aromatics were reported upon, although various other studies (6-9) have been carried out on thermal hydrodealkylation of aromatics and phenols. In general, these studies agree with the mechanism originally proposed by Silsby and Sawyer (6) which results in a first order dependence of the rate on the concentration of the decomposing compound and half order dependence on hydrogen concentration with hydrogen dissociation at equilibrium. According to this mechanism, the cracking of alkylated aromatics and phenols seems to involve the benzene ring as an intermediate.

From the above discussion, it follows that benzene could serve as a model compound for comparing the catalytic hydrogenolysis potential of various coal chars. In addition to benzene, alkylated benzenes (toluene, ethylbenzene and o-xylene) were also chosen as model compounds for this study.

EXPERIMENTAL

The proximate and ultimate analysis of the char solids chosen for this study are shown in Table 1. The Wyoming subbituminous and the Illinois No.6 chars were produced by the steam-air gasification of the coals at 900°C and 200 psig in the RTI bench-scale gasifier. The Peabody char was obtained from Peabody Coal Company (Columbia, Tennessee) who prepared it by coking a Western Kentucky No.11 coal at 870 to 1090°C. For comparison, quartz and molecular sieve 4A were also used in the microreactor experiments. Representative samples of all materials were crushed and screened to 28 x 48 mesh. Microreactors were prepared as shown in Figure 1 with the volume of packing material being approximately 1 cm^3 and ranging in weight from 0.5 to 1.0 gram. A reactant gas containing 290 ppm benzene, 52.2 ppm toluene, 9.87 ppm ethylbenzene and 11.4 ppm o-xylene in nitrogen was used in all experiments. Hydrogen of high purity was blended with the reactant gas to obtain a hydrogen level of 50 percent. Details of the reactor flow system are shown in Figure 2. Gas residence time in the reactors ranged from approximately 0.25 to 0.5 seconds; and all experiments were carried out at slightly above atmospheric pressure. In the experiments utilizing coal chars the packed

TABLE 1. PROXIMATE AND ULTIMATE ANALYSIS OF CHARS

	Weight % As Received		
	Peabody Char	Illinois No.6 Char	Wyoming Subbituminous Char
Proximate			
Moisture	1.46	0.77	1.27
Volatile Matter	1.73	2.56	5.89
Fixed Carbon	84.61	39.94	36.03
Ash	12.20	56.73	56.81
Ultimate			
Carbon	82.34	39.61	40.53
Hydrogen	0.82	0.59	0.46
Nitrogen	1.17	0.72	0.44
Sulfur	2.06	1.56	0.48
Oxygen (by difference)	1.41	0.79	1.28

microreactor was conditioned overnight with the reactant gas-hydrogen mixture at 800°C. In the experiments utilizing quartz and molecular sieve packings and in the tests using an empty reactor conditioning was not carried out. This led to some interesting observations on the transient cracking activity. Reactor temperatures were varied from 500 to 800°C. Analysis of reactants and products were carried out by gas-liquid chromatography with an 8' x 1/8" stainless steel column containing Tris-1,2,3-cyanoethoxy propane on 80/100 mesh Chromosorb P operated with a helium carrier gas flow of 20 ml/min at 85°C oven temperature in a Perkin-Elmer 3920B gas chromatograph with a flame ioniziation detector; 1.0 ml samples were injected using a zero volume six-port stainless steel Carle valve, operated automatically with a valve actuator and a valve timer with a 16 minute cycle.

RESULTS AND DISCUSSION

In the present experimental study with benzene and three alkylated benzenes present in the feed gas, a full description of the kinetics would be extremely complex since so many possible parallel and series reactions can occur. To limit the complexity of the data analysis a simple first order decomposition of each component is assumed. This is probably reasonable for ethylbenzene and o-xylene, however, the assumption could lead to under-estimation of the benzene and toluene cracking rates since benzene and toluene production from ethylbenzene and o-xylene and benzene productionfrom toluene are ignored. Justification for the simplified analysis is that (1) the amount of ethylbenzene and o-xylene in comparison to benzene is small and should not contribute significantly to the apparent rate of benzene decomposition, (2) at high decomposition rates of benzene, ignoring benzene production from the other aromatics will result in small errors in the apparent rate of decomposition since the benzene concentration is almost six times that of any other component, and (3) an upper bound on the benzene decomposition rate can be estimated as discussed towards the end of this section.

In previous studies (4-9) of hydrocracking, hydrogenolysis or hydrodealkylation of aromatic compounds the data obtained are correlated using a first order rate with respect to the compound being decomposed and one-half order with respect to the hydrogen concentration. Since in all experiments of this study a constant hydrogen mole fraction was maintained and in large excesses, the rate can be

expressed in terms of a pseudo first order rate constant containing the hydrogen term. Assuming a plug flow reactor with negligible change in gas volume with extent of decomposition, the integrated material balance under isothermal conditions for the i^{th} component can be written as

$$k = \frac{1}{\tau} \ln \frac{C_{ii}}{C_{io}} \qquad 1)$$

where τ = space time, sec.

C_{ii}, C_{io} = inlet and outlet concentrations of the i^{th} species, g mole/cm^3.

k_2 = first order rate constant, sec^{-1}.

This equation was used to calculate the first order rate constants for all experiments in order that the relative activity of the packing material toward cracking of aromatics could be compared with the empty reactor activity and published homogeneous decomposition rates. For each packing material, rate constants were determined at a series of temperatures. Arrhenius plots of the first order rate constants for the individual compounds are shown in Figures 3 through 6 and are compared with existing literature data. Table 2 gives the least squares estimates of the pre-exponential factors and activation energies.

Examination of Figures 3 through 6 shows that the steady-state cracking activity obtained in the empty bed experiments is unusually high being on the order of 1 to 2 magnitudes greater than homogeneous first order constants reported in the literature. The empty bed experiments reported in this paper were carried out in reactors that had high surface to volume ratios (about 3-6 times those used in previous studies (4-11)). Also the activity appeared to increase rapidly with run time as seen in Figure 7. Apparently the surface of the stainless steel reactor is increasing in activity under the the reducing action of hydrogen and possibly carbon laydown (in some unknown form); and the activity reaches a steady-state value after extended time periods (on the order of 12-24 hours).

Comparing the steady-state empty bed constants to the first order rate constants associated with each char (which show no time dependent activity after overnight conditioning) it can be seen that the Wyoming and Illinois No.6 chars show enhanced cracking activity over the empty reactor. The Peabody char showed significantly lower activity and quartz had a lower initial activity than the empty bed demonstrating that the packing material blinded in part, the activity of the stainless steel reactor wall. Consequently the rate constants associated with the Wyoming and Illinois No.6 chars are significantly higher than the homogeneous rate constants and more than two orders of magnitude higher than the homogeneous rates reported previously in the literature. The higher activity of the Wyoming and Illinois chars over the Peabody char is likely to be due to their significantly higher ash contents, which are known to contain substantial quantities of silica and alumina.

Quartz was used in the microreactor for the purpose of comparison because it was initially thought that it would be relatively inert and would have a packed bed voidage similar to the chars. However, the initial activity of quartz showed rate constants at least an order of magnitude higher than homogeneous rate constants reported in the literature. Furthermore, the rate constants were observed to increase with run time at 748°C and over a 24 hour period the rate constants for benzene and toluene increased by an order of magnitude. The time dependent behavior of these constants are shown in Figure 7. The steady-state rate constants for benzene and toluene over quartz were 1.95 and 5.59 sec^{-1}, respectively. The initial rate constants for the decomposition of benzene and toluene over quartz were obtained by extrapolating the data by the method of Gangwal, et al.(12).

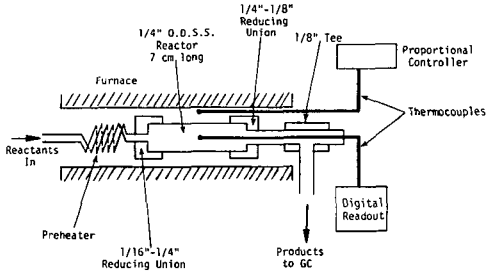

FIGURE 1. MICROREACTOR DETAILS.

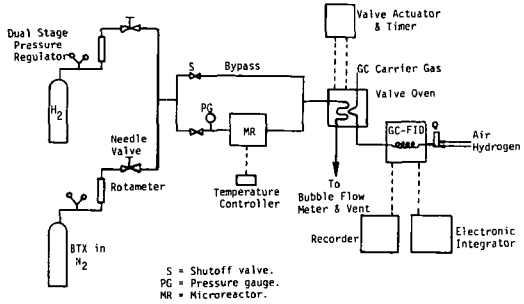

FIGURE 2. REACTOR SYSTEM SCHEMATIC.

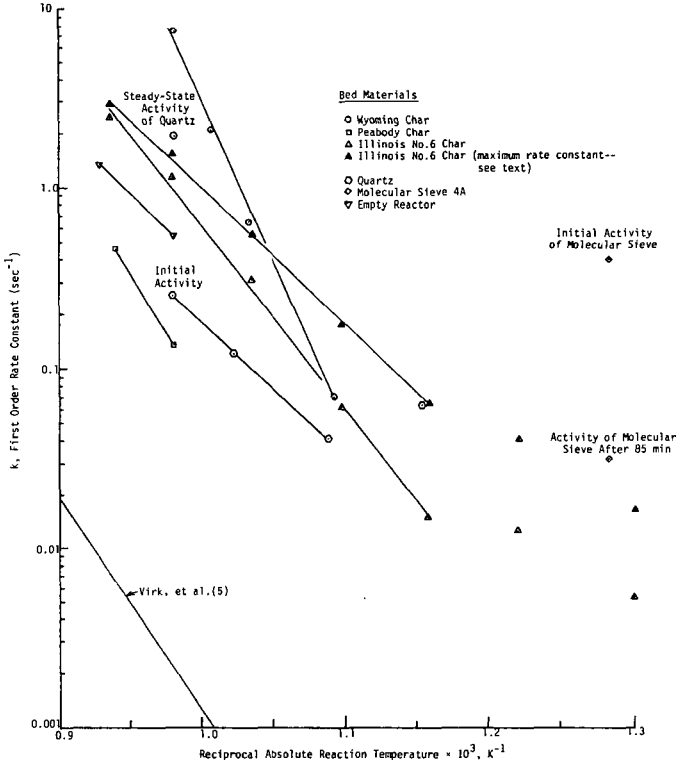

FIGURE 3. RATE CONSTANTS FOR BENZENE HYDROCRACKING.

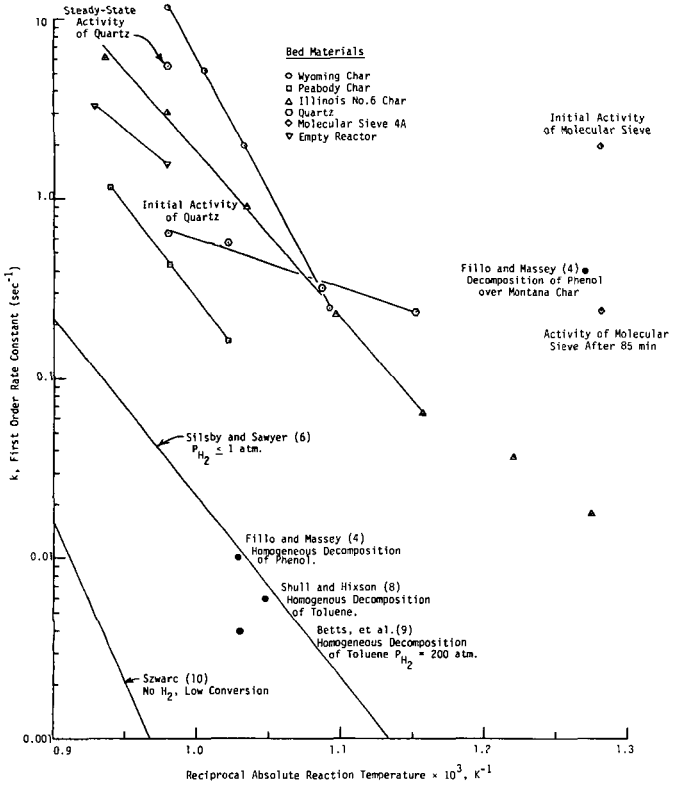

FIGURE 4. RATE CONSTANTS FOR TOLUENE HYDROCRACKING.

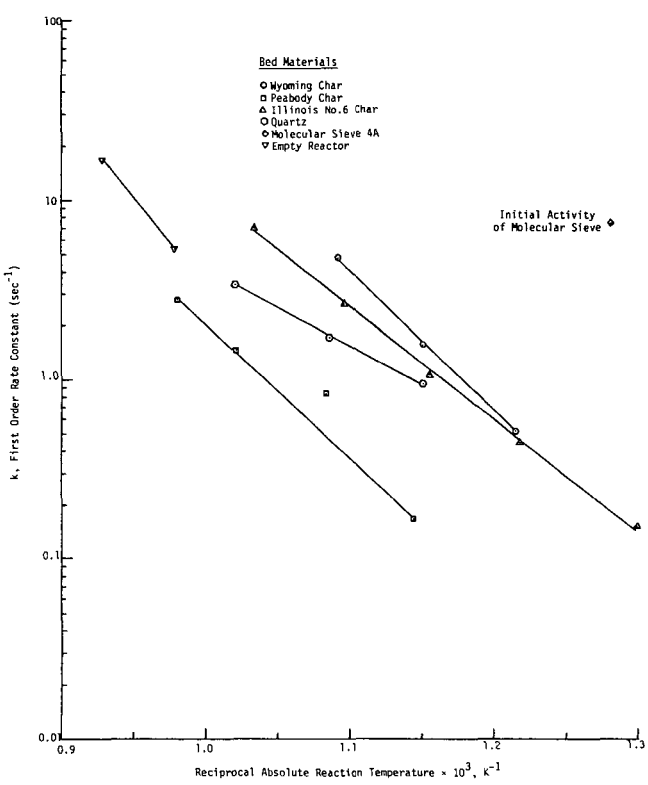

FIGURE 5. RATE CONSTANTS FOR ETHYLBENZENE HYDROCRACKING.

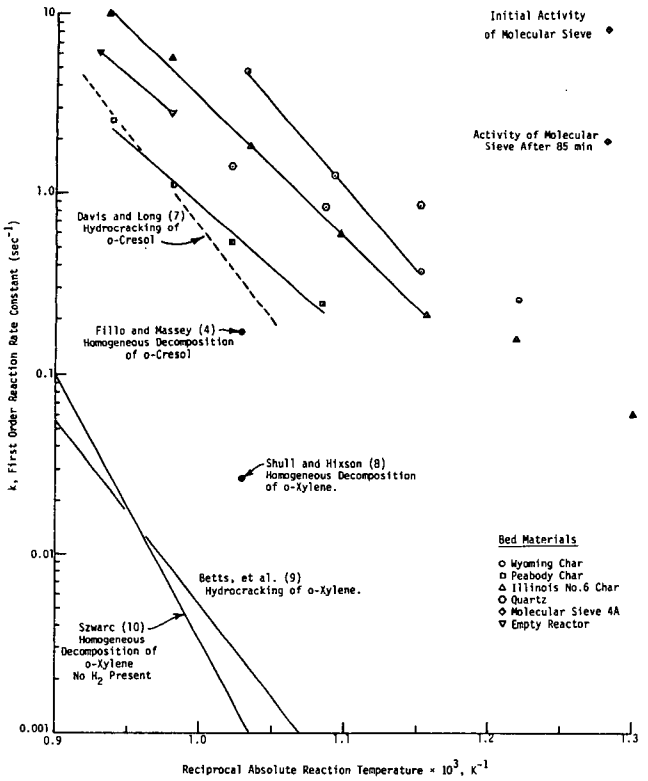

FIGURE 6. RATE CONSTANTS FOR O-XYLENE HYDROCRACKING.

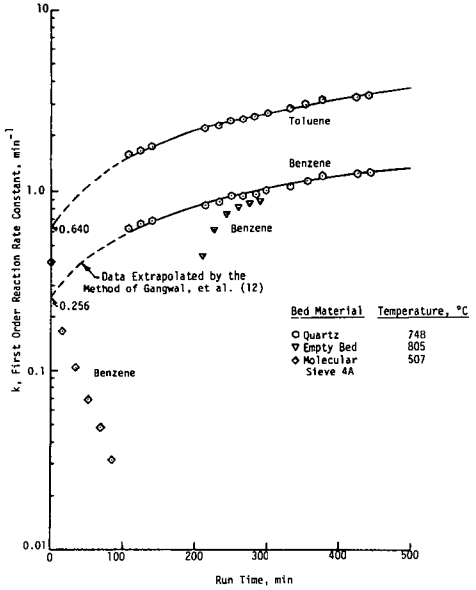

FIGURE 7. TIME DEPENDENT BEHAVIOR OF THE FIRST ORDER RATE CONSTANT.

TABLE 2. ARRHENIUS EQUATIONS FOR HYDROCRACKING

Compound	Material	Arrhenius Equations $k = \quad (sec)^{-1}$
Benzene	Wyoming Char	$1.71 \times 10^{18} \exp(-81290/RT)$
	Illinois No.6 Char+	$1.05 \times 10^{10} \exp(-46730/RT)$
	Peabody Char	$3.29 \times 10^{11} \exp(-57840/RT)$
	Quartz*	$4.61 \times 10^{6} \exp(-33920/RT)$
	Empty Reactor**	$3.38 \times 10^{7} \exp(-36510/RT)$
Toluene	Wyoming Char	$5.29 \times 10^{15} \exp(-68410/RT)$
	Illinois No.6 Char	$2.32 \times 10^{9} \exp(-41740/RT)$
	Peabody Char	$5.35 \times 10^{2} \exp(-47000/RT)$
	Quartz*	$2.98 \times 10^{2} \exp(-12360/RT)$
	Empty Reactor**	$7.21 \times 10^{6} \exp(-31250/RT)$
o-Xylene	Wyoming Char	$1.97 \times 10^{10} \exp(-42960/RT)$
	Illinois No.6 Char	$2.17 \times 10^{8} \exp(-35710/RT)$
	Peabody Char	$8.01 \times 10^{6} \exp(-31890/RT)$
	Quartz*	scatter
	Empty Reactor**	$1.75 \times 10^{7} \exp(-31830/RT)$
Ethylbenzene	Wyoming Char	$1.51 \times 10^{9} \exp(-34640/RT)$
	Illinois No.6 Char	$2.39 \times 10^{7} \exp(-29000/RT)$
	Peabody Char	$5.59 \times 10^{7} \exp(-34030/RT)$
	Quartz*	$8.05 \times 10^{4} \exp(-19610/RT)$
	Empty Reactor**	$2.06 \times 10^{10} \exp(-44830/RT)$

*Initial rate.
**Steady-state rate.
+Expression for maximum $k = 3.38 \times 10^{7} \exp(-36510/RT)$.

Material balances for carbon showed that carbon (in some form) was being deposited on the quartz over the 24 hour run period. It is possible that the deposited material was catalyzing the cracking of the benzene and toluene. After the 24 hour period at 748°C the temperature of the reactor was lowered to 650°C but no enhancement in activity over previous experiments at 650°C was observed, i.e., whatever was being formed at 748°C was not active at 650°C.

Molecular sieve 4A was also used as a packing material and showed very high initial cracking activity in comparison to the other packing materials investigated as can be seen in Figures 3 through 6. However, this activity quickly faded as can be seen in Figure 7, with coke deposits blocking the porous structure of the sieve being a probable deactivation mechanism.

Based on the data presented in Figures 3 through 6 the following additional observations can be made:

1. For a given volume of packing material and the same operating conditions the rate of cracking of the aromatic compounds is in the order

   ethylbenzene > o-xylene > toluene > benzene.

2. For a given aromatic compound and the same operating conditions with temperatures greater than 600°C, the activity of the char toward enhancing decomposition of compounds is in the order

   Wyoming char > Illinois No.6 char > Peabody char.

The theoretical activation energy for homogeneous hydrodealkylation of alkylated aromatics is 50 ± 5 kcal/mole, based on the hydrogen dissociation mechanism originally proposed by Silsby and Sawyer (6). The experimental values reported are generally 45-50 kcal/mole for toluene hydrodealkylation (6-9). However, the empty bed activation energy for toluene (Table 2) is significantly lower, i.e., 31 kcal/mole, substantiating in part that the catalytic nature of the stainless steel reactor may be responsible. Virk, et al. (5) report an activation energy of 52.6 kcal/mole for homogeneous hydrogenolysis of benzene. Again the empty bed activation energy for benzene is much lower. The heterogeneous hydrocracking reactions of benzene and toluene over the Wyoming char show significantly higher activation energies of 81 and 68 kcal/mole, respectively. The values are close to those reported by Szwarz (10) whose experiments were carried out in the absence of hydrogen. Thus the heterogeneous reaction may be proceeding by a mechanism which is entirely different from the homogeneous reaction. The Illinois and Peabody chars have activation energies associated with the decomposition of benzene and toluene which are considerably lower than those observed for the Wyoming char. One explanation for this is that the Wyoming char reaction rate is not limited by internal diffusion whereas the reaction rate for other chars might be. For an internal diffusion limited first order reaction the apparent activation energy is one-half of the true activation energy; this could explain in part the lower values observed for the Illinois and Peabody chars. This reasoning is supported by the experiments of Walker and coworkers (13-15) who have shown that low rank chars generally have an ample supply of feeder and transitional pores whereas bituminous and higher rank chars do not. The char samples used in this study have been sent to an outside testing laboratory for characterization of the pore structure and surface area. At the present time these results are not available; however, they will be reported at the presentation of this paper.

An upper bound on the benzene decomposition rate on Illinois No.6 char is shown in Figure 3 by the dark triangles. This is calculated assuming that benzene is an intermediate product from the cracking of the other aromatics present in the feed. When compared to the apparent rate (i.e., empty triangles) it can be seen that even higher rates of benzene decomposition exist if the assumption is true. The activation energy however is lower, i.e., 36.5 compared to 46.7 (see Table 2, footnote) and thus as the temperature increases the observed rate and the maximum possible rate approach each other.

The major gaseous product of decomposition of the aromatic compounds appeared to be light gases (probably mostly methane) although the GC column used in the experiment could not separate CH_4, C_2H_6 and C_2H_4. Much more methane was formed than could be accounted for by the removal of methyl groups from the alkylated benzene compounds. Also carbon balances showed that substantial quantities of the input carbon remained in the reactor. The only exception to this was in the case of the Wyoming char experiments run at 748°C and 800°C. In these cases carbon in the char also was converted to light gases (probably methane). The activation energy of this conversion was on the order of 104 kcal/g mole which corresponds to the temperature dependency of the equilibrium constant for hydrogen dissociation.

CONCLUSIONS

Based on the results obtained, it appears that coal-derived materials having high ash content show significant catalytic enhancement of the vapor

phase cracking of benzene and alkylated benzene compounds. It was found that the Wyoming subbituminous char showed significantly greater activity (as indicated by the first order reaction rate constants) than the Illinois and Peabody chars. The activity of the Peabody char was lower than the steady-state activity of the empty stainless steel reactor. The activity of stainless steel increased with time on stream to a steady-state activity that was an order of magnitude higher than the activity reported in the literature for the homogeneous decomposition of benzene and toluene.

ACKNOWLEDGEMENT

Support for this work from the U.S. Environmental Protection Agency, Fuel Process Branch, Research Triangle Park, N. C., under Grant No. R804979 is gratefully acknowledged.

REFERENCES

1. J. G. Cleland, et al., Pollutants from Synthetic Fuels Production: Facility Construction and Preliminary Tests. EPA-600/7-78-171, U.S. EPA, Research Triangle Park, N. C. (1978).
2. S. K. Gangwal, et al., Pollutants from Synthetic Fuels Production: Sampling and Analysis Methods for Coal Gasification. EPA-600/7-79-201, U.S. EPA, Research Triangle Park, N. C. (1979).
3. J. G. Cleland, et al., Pollutants from Synthetic Fuels Production: Coal Gasification Screening Tests. EPA-600/7-79-200, U.S. EPA, Research Triangle Park, N. C. (1979).
4. J. P. Fillo, and M. J. Massey, "Study of Phenolic Compound Decomposition under Synthane Gasifier Conditions," Final Report, EW-78-C-22-0208, Pittsburgh Energy Technology Center, October (1979).
5. P. S. Virk, L. E. Chambers, and H. N. Woebcke, "Thermal Hydrogasification of Aromatic Compounds," in Coal Gasification," L. G. Massey, ed., Adv. in Chem. Series 131, ACS, Washington, D. C. (1974).
6. R. J. Silsby, and E. W. Sawyer, "The Dealkylation of Alkyl Aromatic Hydrocarbons-I. The Kinetics and Mechanism of Toluene Decomposition in the Presence of Hydrogen," J. Appl. Chem., 6, 347 (1956).
7. G. A. Davies, and R. Long, "The Kinetics of the Thermal Hydrocracking of Cresols," J. Appl. Chem., 15, 117 (1965).
8. S. E. Shull, and A. N. Hixson, "Kinetics of Thermal Hydrodealkylation of Mesitylene, m-Xylene and Toluene," Ind. Eng. Chem., Proc. Des. Dev., 5 (2), 146 (1966).
9. W. K. Betts, F. Popper, and R. I. Silsky, "The Dealkylation of Alkyl Aromatic Hydrocarbons-II. The Dealkylation of Coal tar Naphthas," J. Appl. Chem., 7, 497, (1957).
10. M. Szwarc, "The C-H Bond Energy in Toluene and Xylenes," J. Chem. Phys., 16 (2), 128 (1948).
11. B. W. Jones, and M. B. Neuworth, "Thermal Cracking of Alkyl Phenols," Ind. Eng. Chem., 44 (12), 2872 (1952).
12. S. K. Gangwal, J. Fathikalaji and G. B. Wills, "Breaks in Behavior of a Tungsten-Oxide on Silica Catalyst in Propylene Disproportionation," Ind. Eng. Chem. Product Res. Dev., 16 (3), 23 (1977).
13. Linares-Salano, A., O. P. Mahajan, and P. L. Walker, Jr., "Reactivity of Heat Treated Coals in Steam," Fuel, 58, 327 (1979).
14. Hippo, E., and P. L. Walker, Jr., "Reactivities of Heat-Treated Coals in Carbon Dioxide at 900°C," Fuel, 54, 245 (1975).
15. Jenkins, R. G., S. P. Nandi, and P. L. Walker, Jr., "Reactivities of Heat-Treated Coals in Air at 500°C," Fuel, 52, 288 (1973).

MODEL STRUCTURE FOR A BITUMINOUS COAL

L. A. Heredy

Energy Systems Group
Rockwell International Corporation
8900 De Soto Avenue
Canoga Park, California 91304

I. Wender

Office of Advanced Research and Technology
Office of Fossil Energy
Department of Energy
Washington, DC 20545

Studies on coal genesis and investigations of the chemical constitution of coal indicate that bituminous coal has a macromolecular structure in which a large number of basic units of condensed ring structures are connected by aliphatic and heteroatom bridges. Various aromatic and heterocyclic structures have been identified as constituents of the coal, and several research data suggest the presence of hydroaromatic rings.

Because of the complexity of the coal structure, it is very difficult to present a concise summary of the available structural information. One of the approaches, which has been used to summarize and to illustrate the main chemical structural features of coal, is the construction of "model coal molecules." Although many details of model coal structures are necessarily qualitative in nature and need to be updated as new research data become available, the derivation and construction of model molecular structures for coal serve an important purpose because they help the coal researcher to summarize and evaluate the consistency of experimental data from a structural viewpoint and to identify key areas where more research is needed.

An important application of model structures was reported by van Krevelen (1), who proposed formulae for the aromatic constituents of coals at different stages of coalification. More recently, Given (2), Wiser (3), and Gibson (4) have proposed model molecular structures for high-volatile bituminous coals of approximately 82 to 83% C content. While there are significant differences among these proposed structures, several of their basic features are similar: they all contain relatively small condensed aromatic ring systems, consisting on the average of two to four condensed rings; flourene- and phenanthrene-type condensed aromatic rings predominate; the nonaromatic part of the molecule consists mostly of hydroaromatic rings; and there are few alkyl (mainly methyl) groups.

The large amount of new structural information that has been obtained in recent years on bituminous coals warrants an updating of model coal structures. One of the most important coal structural properties, the carbon aromaticity, has been determined directly by solid-state carbon-13 NMR spectroscopy using ^{1}H-^{13}C cross-polarization (5,6) and magic-angle spinning (7,8). The average size of condensed aromatic structures in high-volatile bituminous coals has been estimated on the basis of investigations of coal extracts (9,10). A new oxidative degradation technique has been developed to investigate the aliphatic structures in coal (11). Many additional new data have been forthcoming about a variety of subjects dealing with coal structural research, such as the distribution of oxygen in bituminous coal among different functional groups, the characterization of heterocyclic compounds in coal extracts, and the detailed structural characterization of coal extracts and coal liquefaction products.

The research that has been carried out on the structural characterization of coal extracts and coal hydrogenation products is of particular interest. Although the structural features of these products differ in various degrees from those of the parent coal, structural investigations with such materials can be conducted with greater accuracy because their solubility allows the application of a number of separation and analytical techniques that cannot be used with coal. The structural characterization of these materials generally consists of solvent and

chromatographic fractionation, followed by ultimate analysis, high-resolution proton and carbon-13 NMR spectrosocpy, molecular weight, and phenolic-OH measurements of the fractions. Two recent structural studies of this type have been used for the derivation of model molecular structures. Bartle et al. (10) carried out the structural analysis of extracts obtained from high-volatile bituminous coal by supercritical-toluene extraction at 400°C. It was concluded that one of the extracts, which represents 27% of the coal, contains small aromatic units held together by methylene, heteroatom, and biphenyl linkages. Approximatley 30% of the available sites of the aromatic skeleton are occupied by alkyl and naphthenic groups. Farcasiu (12) investigated the structure of coal liquids produced by the Solvent Refined Coal Process. The proposed average structure of one of the major fractions ("polar aromatics") consists of a benzofuran ring which has a phenyl and a naphthyl group as substituents. In other fractions the presence of benzene, benzofuran, and condensed hydroaromatic rings is indicated.

The model coal molecule described in this paper is presented with the following objectives: (1) to incorporate into the model new structural information that has become available in recent years, (2) to derive additional input data for the model molecule by means of a mathematical analysis, and (3) to test the model by comparing the experimentally observed behavior of a high-volatile bituminous coal in a number of chemical reactions with the expected behavior of the model molecule in the same reactions.

Experimental Input Data

The composition of a vitrain concentrate from a typical high-volatile bituminous coal was selected for this study because many basic research data are available in the literature for coals of this rank.

Input data included the elemental composition, the aromaticity of the coal, the structural formulae of the aromatic constituents, and the distribution of the heteroatoms among the different functional groups. The elemental composition and the general formula of the coal are shown in Table 1. The general formula was calculated for a unit containing 100 carbon atoms, corresponding to a "molecular weight" of about 1450. This molecular weight is, of course, arbitrary; as indicated in Figure 1, this "molecule" is connected to other parts of a larger structure (linkages-P).

TABLE 1

CHARACTERIZATION OF HIGH-VOLATILE BITUMINOUS COAL USED IN MODEL STRUCTURE STUDIES

Elemental Composition (dmmf basis)	(wt %)	(atom %)
C	83.2	53.1
H	5.5	42.0
O	7.7	3.7
N	1.1	0.6
S (org.)	2.5	0.6
Total	100.0	100.0

General Formula (100 C basis): $C_{100}H_{79}O_7NS$

Carbon Aromaticity: $f_a = 0.70$

The value of the carbon aromaticity (f_a) of coals of 82 to 83% C content has been measured by a number of different methods. Dryden (13) found a value of f_a = 0.66 using infrared and high-resolution proton-NMR spectroscopic measurements made with a coal of 82.5% C content and with extracts of the same coal. Work by Heredy et al. (14,15), based on acid-catalyzed depolymerization of a high-volatile bituminous coal and the high-resolution proton-NMR spectra of the depolymerization products, gave f_a = 0.65. Retcofsky (9) found f_a = 0.73 by investigating coal extracts using high-resolution proton-NMR spectroscopy. The investigation of a solid coal by Vanderhard and Retcofsky (5) using cross-polarization carbon-13 NMR spectroscopy gave f_a = 0.76. The average of these values (f_a = 0.70) was used in this work.

The aromatic structures used in the construction of the model molecule are shown in Figure 2. They were selected on the basis of the following experimental information. Dryden (13) estimated that the average number of condensed rings in the aromatic part of the structure of high-volatile bituminous coal with C = 82.5% was less than three. Retcofsky (9), as well as Heredy et al. (14,15), estimated that in the same type of coal the average number of condensed rings in the aromatic part of the structure was about three. Naphthalene and phenanthrene were selected as specific condensed aromatic structures for use in the construction of the model molecule because these compounds were found frequently in coal extracts (16). With regard to the selection of specific heterocyclic constituents, the findings of Kessler et al. (16) and Sternberg et al. (17) were used. It has been shown (16) that a sizeable fraction of the organic sulfur in the coal is in benzothiophene-type structures, and much of the oxygen is in benzofuran- or dibenzofuran-type structures. Carbazole has been identified (17) as one of the nitrogen-containing aromatic structures in coal hydrogenation products.

The following distribution was used for the oxygen among the different structural positions. Of the seven oxygen atoms in the model molecule, four were located in phenolic-OH groups on the basis of the work of Friedman et al. (18). One oxygen atom was located in an aromatic ether linkage on the basis of data published by Ignasiak and Gawlak (19), and one was located in a dibenzofuran structure as discussed before (16). It was assumed that one oxygen atom was in a cyclic aliphatic ether structure.

The five constituent aromatic structures of the model molecule are interconnected by five bridges. One of the bridges is the aromatic ether linkage mentioned in the previous paragraphs; the other four are aliphatic hydrocarbon structures.

Mathematical Analysis

No independent experimental data were used to obtain the structural characteristics of the nonaromatic part of the model molecule. This information was derived from the general formula of the model molecule and the structural formulae of the aromatic constituents of the model molecule (Figure 2) using a mathematical analysis. A method applied by Whitehurst et al. (20) was used as the basis for developing this analysis. The complete analysis will be presented in a more detailed report.

In essence, the analysis involves the construction of a matrix. The vertical columns list a series of aromatic H contents for the aromatic part of the molecule (corresponding to different degrees of aromatic substitution). The horizontal lines list different types of aliphatic and hydroaromatic substituents that can be attached to the aromatic part of the model molecule (aliphatic chains, single or condensed hydroaromatic rings - Figure 3). Both the percentage of aromatic hydrogen content of the aromatic part of the model molecule and the structural configuration of the nonaromatic part of the model molecule can be expressed in terms of the

number of positions that can be substituted in the aromatic and in the nonaromatic parts of the model molecule, respectively. Matching those aromatic hydrogen contents and aliphatic structural types in the matrix, which can accept the same number of substituents, identifies the percentage of aromatic hydrogen content of the model molecule as well as the aliphatic/hydroaromatic structural configuration.

When the procedure described in the previous paragraph is carried out using the input data given in Table 1 and Figures 2 and 3, it is found that the best match of aromatic and aliphatic substitutions is obtained at an aromatic H content of about 30%. Furthermore, the analysis indicates that most of the nonaromatic structures are composed of hydroaromatic rings of the types of Structures 4, 7, and 8 (Figure 3). On the basis of this analysis, hydroaromatic structures of these types were used to construct the nonaromatic part of the model molecule. The proposed structure of the model molecule is shown in Figure 1. The distribution of carbon, hydrogen, and heteroatoms among different structural positions in the model molecule is shown in Table 2.

TABLE 2

CHARACTERISTICS OF THE MODEL COAL MOLECULE

				Hydroaromatic Ring							
		Aromatic		Alpha		Beta		Other Alpha Aliphatic		Phenolic OH	
Element	Total No. of Atoms	No.	%	No.	%	No.	%	No.	%	No.	%
Hydrogen	79	23	29.1	21	26.6	20	25.3	11	13.9	4	5.1
Carbon	100	70	70.0	13	13.0	12	12.0	5	5.0	-	-

		Aromatic Ether		Heterocyclic						Phenolic OH	
		No.	%	No.	%					No.	%
Oxygen	7	1	14.3	2	28.6				-	4	57.1
Nitrogen	1	-	-	1	100.0				-	-	-
Sulfur	1	-	-	1	100.0				-	-	-

Evaluation of Chemical Reactions

It is of interest to compare the expected behavior of the model molecule in some of the chemical reactions which have been used to investigate bituminous coals with the experimentally observed behavior of high-volatile bituminous coals.

A large fraction of the hydrogen atoms, 41 of the 79 in the model molecule, are in hydroaromatic structures. Of these, 24 hydrogen atoms would be expected to evolve as hydrogen gas under the catalytic dehydrogenation conditions used by Reggel et al. (21). The experimentally obtained number for vitrain concentrates of 82.5 to 84.0% C content was 23 to 30 H atoms evolved per 100 carbon atoms.

The expected effect of reduction of the model molecule with lithium-ethylenediamine was estimated by using experimental data obtained on the reduction of a variety of organic compounds by Reggel et al. (22). It was estimated that the model molecule would take up 24 H atoms. The experimentally obtained number for vitrain concentrates of 82.5 to 84.0% C contents was the addition of 21 to 22 H atoms per 100 C atoms (22).

The expected reactivity of the model molecule in phenol-BF_3-catalyzed depolymerization can be evaluated (23). The bonds on both sides of the CH_2-bridge would break because they are bonded to reactive aromatic sites on a phenanthrene and on a OH-activated phenanthrene ring, respectively. Furthermore, the bond between the OH-activated phenanthrene ring and the -CH_2-CH-group of the hydroaromatic ring would break. These interactions would release and solubilize the phenanthrothiophene-based fragment from the rest of the molecule. The yield of this depolymerization product would be 27%. Heredy et al. obtained a net phenol-soluble depolymerized product yield of 29% in a phenol-BF_3-catalyzed depolymerization experiment using a coal of 82.4% C content (14,15).

The treatment of the model molecule with a reagent mixture consisting of trifluoroacetic acid, hydrogen peroxide, and sulfuric acid would give a mixture of carboxylic acids (11). The principal low molecular weight products would be acetic acid and succinic acid, formed in a ratio of 3 to 8 on a hydrogen basis from the oxidation of the methyl group and the two -CH_2-CH_2-groups. The actual testing of high-volatile bituminous coals by Deno et al. (11) showed that these two acids are the predominant products with an acetic acid to succinic acid ratio of about 1 to 3.

In summary, a model chemical structure was derived for a high-volatile bituminous coal of 83% C content, using the elemental composition, the distribution of heteroatoms among different functional groups, the carbon aromaticity, and the formulae of the constituent aromatic structures as input data. A mathematical method was used to calculate the value of the hydrogen aromaticity and to derive the formulae of the nonaromatic constituents of the model structure.

The experimentally observed behavior of bituminous coal vitrains in a number of chemical reactions was compared with the expected behavior of the model structure in the same reactions. The following chemical reactions of coal were examined: catalytic dehydrogenation in boiling phenanthridine using palladium catalyst; reduction with lithium-ethylenediamine; acid-catalyzed depolymerization using phenol-boron trifluoride catalyst; and oxidation with a mixture of trifluoroacetic acid, hydrogen peroxide, and sulfuric acid. Good agreement was found for all of these reactions between the experimentally obtained product distributions from vitrain and the product distributions that would be expected under similar conditions from the model structure.

REFERENCES

1. D. W. van Krevelen, Coal, Elsevies Publishing Company (1961) pp 433-480

2. P. H. Given, Fuel, 39, 147 (1960)

3. W. H. Wiser, Proc. EPRI Conference on Coal Catalysis, Santa Monica, California (1973)

4. J. Gibson, The Constitution of Coal and Its Relevance to Coal Conversion Processes, The Robens Coal Science Lecture, BCURA, London (1977)

5. D. L. Vanderhart and H. L. Retcofsky, Fuel, 55, 202 (1976)

6. A. Pines and D. E. Wemmer, Symposium on New Analytical Methods, 175th ACS Meeting, Fuel Chem. Div. Paper No. 39 (1978)

7. K. W. Zilm, R. J. Pugmire, D. M. Grant, R. E. Wood, and W. H. Wiser, Fuel, 58, 11 (1979)

8. V. J. Bartuska, G. E. Mociel, and F. P. Miknis, Symposium on New Analytical Methods, 175th ACS Meeting, Fuel Chem. Div. Paper No. 40 (1978)

9. H. L. Retcofsky, Applied Spectroscopy, 31, 116 (1977)

10. K. D. Bartel, W. R. Ladner, T. G. Martin, C. E. Snape, and D. F. Williams, Fuel, 58, 413 (1979)

11. N. C. Deno, B. A. Greigger, and S. G. Stroud, Fuel, 57, 455 (1978)

12. M. Farcasiu, Fuel, 56, 9 (1977)

13. I. G. C. Dryden, Coal, in Kirk-Othmer's Encyclopedia of Chemical Technology, Volume 5, John Wiley and Sons, Inc. (1964) pp 640-641

14. L. A. Heredy, A. E. Kostyo, and M. B. Neuworth, Fuel, 44, 125 (1965)

15. L. A. Heredy, A. E. Kostyo, and M. B. Neuworth, Coal Science, Advances in Chemistry Series, 55, 493 (1966)

16. T. Kessler, R. Raymond, and A. G. Sharkey, Jr., Fuel, 48, 197 (1969)

17. H. W. Sternberg, R. Raymond, and F. K. Schweighardt, Science, 188, 49 (1975)

18. S. Friedman, M. L. Kaufman, W. A. Steiner, and I. Wender, Fuel, 40, 33 (1961)

19. B. S. Ignasiak and M. Gawlak, Fuel, 56, 216 (1977)

20. D. D. Whitehurst, M. Farcasiu, T. O. Mitchell, and J. J. Dickert, Jr., Nature and Origin of Asphaltenes in Processed Coals, Section 7, 1977 Annual Report, EPRI AF-480

21. L. Reggel, I. Wender, and R. Raymond, "Catalytic Dehydrogenation of Coal. III. Hydrogen Evolution as a Function of Rank," Fuel, 47, 373-89 (1968)

22. L. Reggel, C. Zahn, I. Wender, and R. Raymond, "Reduction of Coal by Lithium-Ethylenediamine and Reaction of Model Compounds with Metal-Amine Systems," Bureau of Mines Bulletin 615 (1965)

23. L. A. Heredy, Preprints, ACS Div. Fuel Chem., 24, No. 1, 142 (1979)

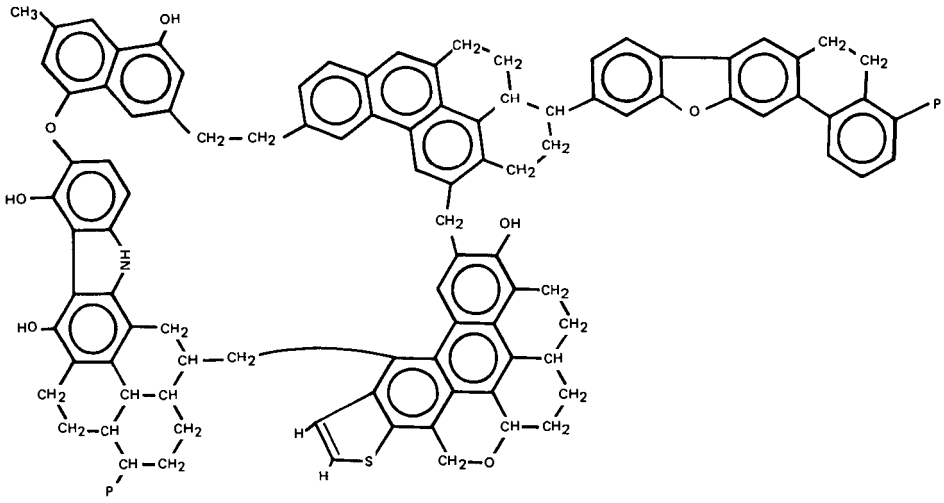

Figure 1. Proposed Structure of the Model Coal Molecule

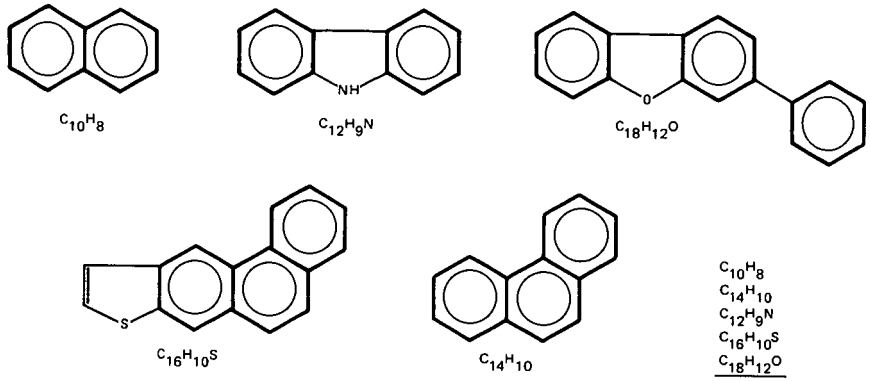

Figure 2. Aromatic Constituents of the Model Molecule

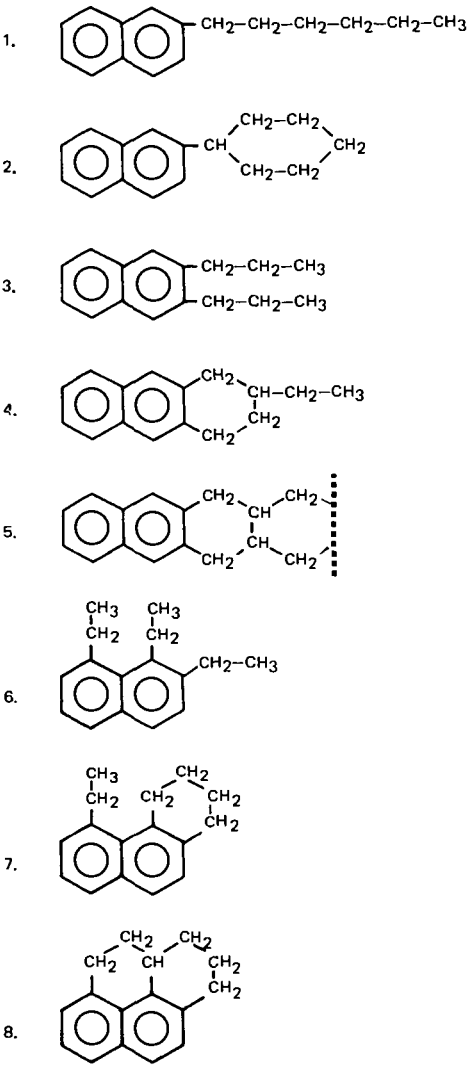

Figure 3. Basic Configurations of C_6 Aliphatic Structures

THE APPLICATION OF FOURIER TRANSFORM INFRARED SPECTROSCOPY TO THE CHARACTERIZATION OF COAL STRUCTURE

Paul C. Painter and R. W. Snyder

Materials Science and Engineering Department
Steidle Building
The Pennsylvania State University
University Park, PA 16802

INTRODUCTION

Infrared spectroscopy is an important and widely used analytical tool for determining the structure of organic materials. Most of the fundamental work on applying this technique to coal characterization was performed in the 1950's and 1960's and has been reviewed in a number of articles (1-4). These studies were limited by two major problems. First, coal absorbs strongly in the infrared so that in conventional dispersive instruments only a weak signal reaches the detector, producing relatively poor spectra. Second, the overlap and superposition of the absorption bands of such complex multicomponent systems result in spectra consisting of broad features with little fine structure, so that only a general, mainly qualitative, identification of a few functional groups has so far been possible.

The introduction of computerized Fourier transform infrared spectrometers opens up new possibilities for the spectroscopic characterization of coal and coal derived liquids. There are several advantages of FTIR compared to dispersive instruments, discussed in detail in a number of reviews (5-7). Essentially, the use of an interferometer rather than a system of gratings and slits results in a higher energy throughput to the detector. This, coupled with the ability of such internally calibrated computerized systems to co-add a large number of interferograms, results in markedly superior spectra, particularly in the energy limiting situations encountered in coal studies. The resulting multiplexed spectrum can then be scale-expanded by the computer to display subtle features without undue interference from background noise. However, in coal studies it has been our experience that the most significant results can be obtained by applying the types of computer routines that have recently become associated with FTIR, particularly spectral subtraction and least squares curve fitting. In fact, the first application of FTIR to the characterization of coal in this laboratory depended more on such computer manipulations than on the enhanced sensitivity of these instruments. Methods for the complete analysis of the major mineral components present in coal have been developed (8-11). We have also applied FTIR to a number of problems concerning the organic structure of coal, including studies of solvent refined coal (12) and the changes that occur upon carbonization (13) and oxidation (14,15). In this communication we will initially discuss the application of recently introduced FTIR computer routines to the quantitative determination of species present in coal, both inorganic and organic. We will then conclude by considering the utility of these methods in determining variations in structure as a function of position in a seam.

RECENT DEVELOPMENTS IN THE ANALYSIS OF MINERAL MATTER IN COAL BY FTIR

Recent work in this laboratory has demonstrated that FTIR offers considerable potential for quantitatively determining the major mineral components present in coal or, more precisely, present in the low temperature ash (LTA)(8-11).

Essentially, the procedure consists of the successive subtraction of the spectra of mineral "standards" from the spectrum of the LTA. As the bands of the most prevalent or most highly absorbing minerals are removed, those of the weakly absorbing or less prevalent components are revealed, allowing a more complete and accurate analysis. It was found that all major components (those constituting at least 3-4% by weight) could be determined, providing that appropriate mineral "standards" are available.

Despite the obvious potential and advantages of the FTIR method, there are still major problems. Perhaps the most critical of these is the availability of suitable standards. This problem is particularly acute in the analysis of clays, but not one unique to FTIR since other methods also rely on standards for calibration of band and line intensities. One solution to this problem that is particularly suited to FTIR is the compilation of an extensive mineral library, because spectra of these materials can be routinely and conveniently stored on disk or magnetic tape and recalled at any future time. We are in the process of building such a library, but it is already apparent that we have in some respects substituted one problem for another. How do we choose the "correct" or most appropriate standard for a particular analysis? For example, we have kaolinite samples from different geographic localities that differ subtly in their spectra according to parameters such as degree of crystallinity. Finally, even if by luck or judgement we choose an appropriate mineral spectrum for a particular analysis, the accuracy of the FTIR method is limited by the essentially subjective judgement of when bands have been exactly subtracted from a spectrum. Such errors are not large for major components having strong well resolved bands, but can become critical in determining low concentrations of certain species. We believe that the application of least squares curve fitting programs, first described by Koenig and co-workers (16), offer at least a partial solution.

The utility of the method is best illustrated by a simple example. Figure 1 compares the FTIR spectra of three individual clays. Also included is the spectrum of a mixture of these three clays, which (as noted above) is extremely difficult to quantitatively analyze by other methods. The least squares program was then asked to fit the spectra of seven standards to the spectrum of the mixture. We deliberately included spectra of mineral standards that we knew were not contained in the snythetic mixture in order to test the utility and accuracy of the procedure. The results are shown in Table 1 and the resulting "composite" spectrum is compared to that of the original mixture in Figure 2. The composite spectrum was constructed by adding the spectra of the components weighted according to the parameters determined in the least squares analysis. Not only did the program pick the correct clays in spite of the similarity in their spectra, but also was able to distinguish between two kaolinites from different origins. This latter result was somewhat of a surprise because the spectra of the two kaolinites are extremely similar, as can be seen from Figure 3, differing only slightly in the relative intensities of one or two bands. In addition to quickly and conveniently "picking" the right components, the program also gave directly a quantitative measure of the clays present that is in very good agreement with the weighed quantities. (This direct measure was possible because we normalized all spectra by dividing them by a number equal to the weight of material in the KBr pellet.) The analysis can be improved by then rejecting all components with minor and negative contributions to the fit. Clearly, if we are examining a low temperature ash we would then have to check that we were not eliminating a true minor component by subtracting the spectrum of the major components from that of the ash (using the subtraction parameters also determined by the least squares fit program).

In applying this technique to the analysis of an LTA we use the least squares curve-fitting procedure to first pick the "best" standards from a given set. As in the analysis of the simple mixtures we can then reject those mineral spectra that have negative subtraction coefficients (but not necessarily those with the small positive contributions) and repeat the fit. The least squares coefficients, (corresponding to the subtraction parameters) determined by this final analysis are then a quantitative measure of the contribution of each mineral. Finally, a check on the accuracy of the results can be obtained by sequentially subtracting the spectrum of each component. This ensures that minor components have not been inadvertently ignored.

Although this procedure sounds tedious, these tasks are in fact performed rou-

tinely and quickly by the FTIR mini-computer. As an example we will consider the results of the analysis of the LTA of an Illinois #6 coal, as presented in Table 2. The percentage weight fraction figures were taken directly from the solution vector. Two clays were determined to have a negative contribution, one of them to our initial surprise was the Illinois kaolinite. Our preconceptions were that an Illinois kaolinite would be the best standards for an analysis of an Illinois coal. However, the fundamental difference in these two standards is probably the degree of crystallinity (11). Consequently, the kaolinite in this sample appears to have a degree of cyrstallinity that is better approximated by the Georgia kaolinite. The least squares fit was repeated after the removal of the Illinois kaolinite and illite spectra from the refinement. These results are also presented in Table 2 where they are compared to the results taken from traditional infrared and x-ray methods. It can be seen that there is good agreement for those minerals determined by both techniques. However, traditional procedures were not capable of accurately determining clays, whereas the FTIR method does provide what appears to be a reasonable analysis of these materials.

We did not determine pyrite by FTIR because this mineral does not have absorption bands in the spectral range (1500-500 cm^{-1}) used in this study. This mineral can be routinely determined by FTIR techniques in the far infrared region (8). Nevertheless, the amount of material unaccounted for by the FTIR analysis is of the same order of magnitude as the concentration of pyrite determined by x-ray diffraction, strongly suggesting that by extending the spectral range of the analysis a complete determination of the major mineral components of this coal is possible. We believe the potential of this and other programs (factor analysis, etc.) for solving the problems presented by the determination of mineral matter in coal are only now being realized, but it is apparent that a good analysis of all major components can already be performed using FTIR.

THE QUANTITATIVE DETERMINATION OF HYDROXYL FUNCTIONAL GROUPS IN COAL

We are in the process of developing techniques to quantitatively determine functional groups present in coal. As an example we will consider the determination of -OH groups. The O-H stretching mode appears near 3400 cm^{-1} in the spectra of coal. However, direct measurements of the intensity of this band cannot be used to determine such groups. A major problem is that the alkali halides used in sample preparation absorb water, which absorbs strongly in this spectral range. Some of the absorbed water appear to be in a bound state since it has been reported that heating to about 300°C is required for complete removal. Furthermore, coals also contain absorbed water in amounts that appear to vary according to rank and other parameters. Finally, the success of applying spectral subtraction and other procedures associated with FTIR leads us to believe that the best method for determining functional groups, particularly those containing oxygen, will prove to be a combination of chemical and FTIR procedures. For example, the infrared spectrum of a coal from Arizona is compared to the spectrum of the same sample subsequent to acetylation in Figure 4. Bands due to acetyl groups are clearly visible but it would be a difficult task to use these bands to determine the number of acetyl groups introduced and hence the number of O-H groups that have been reacted. Although suitable model compounds are available to obtain the extinction coefficients of the characteristic C=O, CH_3 and C-O bands near 1765, 1370 and 1200 cm^{-1} respectively, there is a major problem in measuring the intensity of these bands using traditional infrared methods because of overlap with the absorption bands of the coal. However, with FTIR we can subtract the spectrum of the unreacted material from that of the reacted to give the difference spectrum also shown in Figure 4. It can be seen that the characteristic acetyl bands are now relatively well resolved and it is a straightforward task to draw an appropriate baseline and measure peak heights or even make integrated absorption measurements. A plot of peak heights vs. concentration of coal in the KBr pellet is shown in Figure 5. The slope of these lines is equal to the extinction coefficient of the

acetyl absorption under consideration multiplied by the concentration of such groups in the coal. This latter parameter has been determined by measurements using other techniques. Consequently, this calibration allows us to use the results of this study in determining the concentration OH groups in other coals.

Acetylation usually only allows a determination of total OH content and does not allow a discrimination between phenolic and alkyl OH groups. However, using FTIR these two types of functional groups can be distinguished. Acetylation of coal OH groups leads to ester formation;

$$\text{COAL} - \text{OH} + \text{CH}_3\text{COOH} \rightarrow \text{COAL} - \text{O} - \overset{\overset{\text{O}}{\|}}{\text{C}} - \text{CH}_3$$

Alkyl esters normally absorb between 1720 and 1740 cm^{-1}. However, when an electron withdrawing group such as an aromatic entity is attached to the single bonded oxygen this band is shifted to about 1770 cm^{-1}. The strong absorption near 1765 cm^{-1} in the difference spectrum shown in Figure 4 can therefore be assigned to acetyl groups that have reacted with phenolic OH, while the weaker shoulder near 1725 cm^{-1} can be assigned to acetyl groups that have reacted with alkyl OH groups. We are presently investigating the use of least squares curve resolving techniques in order to obtain a measure of the relative proportions of these groups, but the potential for making such measurements is clearly outstanding.

VARIATIONS ON A SEAM

The variation in coal composition according to position in a seam is a problem not only in the use of this fuel in conversion processes but also in fundamental research aimed at the elucidation of structure. FTIR is particularly sensitive to small differences in materials through the use of spectral subtraction and other computer routines. We have recently examined channel samples along an exploration adit through a Canadian coking coal (14). It was determined that samples from the mouth and end of the adit showed extensive oxidation, as measured by free swelling index, while samples from near the center showed lower degrees of oxidation and still had good coking properties. The infrared spectra of several stations along the adit are shown in Figure 6. The spectra are similar and the only discernable difference involves the intensity of a shoulder near 1690 cm^{-1}, which has a minimum near the center of the seam. We subtracted the spectrum of a sample from the center of the adit (70 ft) from the spectra of samples near the extremities in order to detect in more detail the chemical differences. Scale expanded difference spectra obtained by subtracting the spectrum of the 70 ft station from that of the 30 ft and 40 ft stations and the 110 ft and 125 ft stations are shown in Figure 7. These stations represent the center, mouth and end of the adit respectively. It is apparent that there are four prominent bands in the 1500 and 1800 cm^{-1} region of the spectrum. Band assignments are listed in Table 3. Perhaps the most surprising is the presence of a strong band near 1585 cm^{-1} characteristic of a COO^- group.

These results suggested that carbonyl and carboxyl groups were the major products of oxidation and the principal difference in these samples, according to position in the seam. This interpretation is in disagreement with other oxidation studies which have relied on chemical methods to determine groups formed upon oxidation. However, these latter studies have usually involved oxidation of a sample under laboratory conditions. There is the possibility that the C=O groups detected in this FTIR study were due to some sort of natural variability. Consequently, we applied FTIR to the characterization of coal oxidized in the laboratory. The infrared spectrum of an unoxidized coal is compared to the spectrum of the same sample oxidized for a short time at elevated temperature (about 150°C) in Figure 8. It can be seen that the major difference in the two spectra is the appearance of a shoulder near 1695 cm^{-1} in the spectrum of the oxidized sample. Figure 8 also shows the difference spectrum obtained by subtracting

the spectrum of the unoxidized sample from that of the oxidized. The criteria used to determine the "correct" degree of subtraction was the elimination of the kaolinite bands at 1035 and 1010 cm^{-1}, since this clay should be relatively unaffected by low-temperature oxidation. It can be seen that this subtraction results in the elimination of the aromatic C-H stretching mode near 3050 cm^{-1} and the aromatic C-H out-of-plane bending mode between 700 and 900 cm^{-1}. This is to be expected in that direct oxidative attack of the aromatic nuclei is unlikely under the oxidation conditions used in this study and confirms the choice of kaolinite bands as a subtraction standard.

In contrast to the aromatic C-H bands, the aliphatic C-H stretching modes near 2900 cm^{-1} appear negative, or below the baseline, demonstrating a loss in CH_2 groups upon oxidation. This observation is not particularly novel, as methylene groups in the benzylic position are well known to be sensitive to oxidation and are probably the initial site of oxidative attack. However, the difference spectrum reveals new detail in the 1700 to 1500 cm^{-1} region of the spectrum. The 1695 cm^{-1} band, which appeared as a weak shoulder in the original spectrum of the oxidized coal, is now resolved as a separate band. Furthermore, a prominent new band near 1575 cm^{-1} is now revealed in the difference spectrum. This band is not detectable in the original spectrum. The 1695 cm^{-1} absorption is probably due to an aryl alkyl ketone while the 1575 cm^{-1} mode can be assigned to an ionized carboxyl group COO^-. Clearly, at this initial stage of the oxidation these bands represent the major products of oxidation. Weak, broad residual absorption between 1200 and 1300 cm^{-1} in the difference spectrum could possible be due to C-O bonds, as in phenols or ethers, but we would be hard pressed to identify any separately resolved bands assignable to functional groups of this type. Nevertheless, bands that can be assigned to such groups do appear at higher levels of oxidation. For example, Figure 9 compares the infrared spectrum of a coal sample, oxidized to give 6.7% oxygen uptake, to the spectrum of the unoxidized sample. The difference spectrum, obtained using the same subtraction criteria described above, is also shown in this figure. A prominent difference band can now be observed near 1200 cm^{-1} bands. In addition, a weak shoulder near 1765 cm^{-1} can now be resolved. This band can be assigned to an ester (see Table 3).

These spectral changes closely parallel those observed in a previous study of the variation in oxidation of coal according to position in a seam, discussed above. Consequently, the formation of carbonyl and carboxyl groups is apparently a general phenomenon during oxidation. This conclusion contradicts the results of some chemical methods of characterizing oxidation products, where no change in carboxyl or carbonyl content was detected and it was proposed that ether cross links are central to loss of swelling behavior.

CONCLUSIONS

The results reviewed above clearly demonstrate the potential of FTIR for investigating coal structure. By applying a least squares curve fitting program and spectral subtraction methods it is possible to quantitatively determine the major mineral species present in a coal. These methods are also a sensitive probe of changes in organic structure. We have illustrated their application to the determination of hydroxyl functional groups and the formation of carbonyl and carboxyl groups during oxidation.

REFERENCES

1. Dryden, I. G. C. in 'The chemistry of coal utilization' (H.H. Lowry, Ed.) Suppl. Vol. John Wiley and Sons, New York, p. 232 (1963).
2. Speight, J. B. Applied Spectroscopy Reviews (ed. E. G. Brame, Jr.) 5, 211 (1971).
3. Speight, J. G. in 'Analytical Methods for Coal and Coal Products', (C. Karr, Jr. ed.), volume II, 75 (1978), Academic Press.

4. Brown, J. K. J. Chem. Soc. 744 (1955).
5. Griffiths, P. R. Chemical Infrared Fourier Transform Spectroscopy, 1975, John Wiley and Sons, New York.
6. Koenig, J. L., Applied Spectroscopy, 1975, 29, 293.
7. Coleman, M. M. and Painter, P. C., J. Macromol. Sci. Revs. Macromol. Chem. C16(2), 197 (1978).
8. Painter, P. C., Coleman, M. M., Jenkins, R. G., Whang, P. W. and Walker, P. L., Jr., Fuel, 57, 337 (1978).
9. Painter, P. C., Coleman, M. M., Jenkins, R. G. and Walker, P. L., Jr., Fuel, 57, 125 (1978).
10. Painter, P. C., Snyder, R. W., Youtcheff, J., Given, P. H., Gong, H. and Suhr, N., Fuel (in press).
11. Painter, P. C., Snyder, R. W., Stepusin, S. and Davis, A. Applied Spectroscopy (submitted).
12. Painter, P. C. and Coleman, M. M., Fuel, Vol. 58, 301 (1979).
13. Painter, P. C., Yamada, Y., Jenkins, R. G., Coleman, M. M., and Walker, P.L., Jr., Fuel, Vol. 58, 293 (1979).
14. Painter, P. C., Snyder, R. W., Pearson, D. E. and Kwong, J., Fuel (in press).
15. Painter, P. C., Coleman, M. M., Snyder, R. W., Mahajan, O., Kamatsu, M., and Walker, P. L., Jr., Fuel (accepted for publication).
16. Antoon, M. H., Koenig, J. H and Koenig, J. L. Applied Spectroscopy 31, 518 (1977).

TABLE 1

ANALYSIS OF MINERAL MIXTURE BY LEAST SQUARES FTIR.

Mineral	Wt. Fraction As Prepared (%)	Initial Least Squares FTIR Analysis	Final Least Squares FTIR Analysis
Kaolinite (Illinois)	50	47	46
Kaolinite (Georgia)	0	-0.3	0
Illite	0	3	0
Montmorillonite	25	31	24
Mica/Montmorillonite	25	29	30
Quartz	0	-9	0
Calcite	0	-0.2	0

TABLE 2

ANALYSIS OF LOW TEMPERATURE ASH

(ILLINOIS #6 COAL, 'ROUND ROBIN' SAMPLE)

Mineral	Wt. Fraction By FTIR Least Squares Analysis I	Wt. Fraction By FTIR Least Squares Analysis 2	Wt. Fraction By X-ray And Conventional IR Methods %
Kaolinite (Illinois)	-12	0	13.5
Kaolinite (Georgia)	20	13	
Quartz	24	25	20
Calcite	6	7	6
Pyrite	N/D	N/D	20
Montmorillonite	21	18	N/D
Mica/Montmorillonite	16	9	
Illite	-6	0	
TOTAL	69%	72%	59.5%
UNACCOUNTED FOR	31%	28%	40.5%

N/D - not determined.

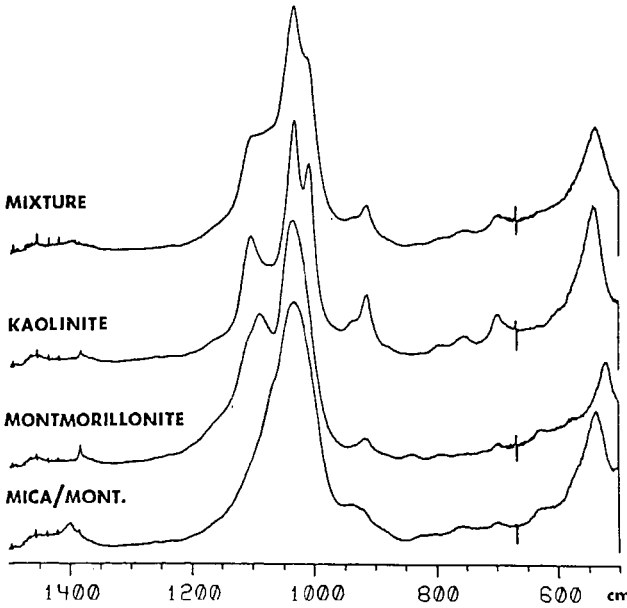

Figure 1: Scale expanded FTIR spectra in the range 500-1500 cm^{-1} of three clays, mica-montmorillonite, montmorillonite and kaolinite. The spectrum shown at the top is that of 1:1:2 mixture by weight of the three clays respectively.

TABLE 3

BAND ASSIGNMENTS FOR THE INFRARED SPECTRA OF COALS

ALIPHATIC AND AROMATIC GROUPS		OXYGEN CONTAINING FUNCTIONAL GROUPS	
Wave Number cm^{-1}	ASSIGNMENT	Wave Number cm^{-1}	Assignment
		3300	Hydrogen Bonded
3030	Aromatic C-H		
2950 sh	CH_3		
2920 } 2850 }	Aliphatic -CH CH_2 and CH_3		
		1835	C = O, Anhydride
		1775-1765	C = O, Ester with Electron withdrawing group attached to single bonded oxygen 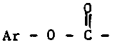
		1735	C = O, Ester
		1690-1720	C = O, Ketone, Aldehyde and, -COOH
		1650-1630	C = O Highly Conjugated 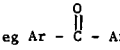
1600	Aromatic Ring Stretch	Approx. 1600	Highly Conjugated Hydrogen Bonded C = O
		1560-1590	Carboxyl Group in Salt Form $-COO^-$
1490 sh	Aromatic Ring Stretch		
1450	CH_2 and CH_3 Bend Possibility of Some Aromatic Ring Modes		
1375	CH_3 Groups		
		1330 to 1110	C-O Stretch and O-H Bend in Phenoxy Structures, Ethers.
		1100-1000	Aliphatic Ethers, Alcohols.
900-700	Aromatic C-H out-of-plane bending modes		
860	Isolated Aromatic H		
833 (Weak)	1,4 Substituted Aromatic Groups		
815	Isolated H and/or 2 Neighboring H		
750	1,2 Substituted ie 4 Neighboring H		

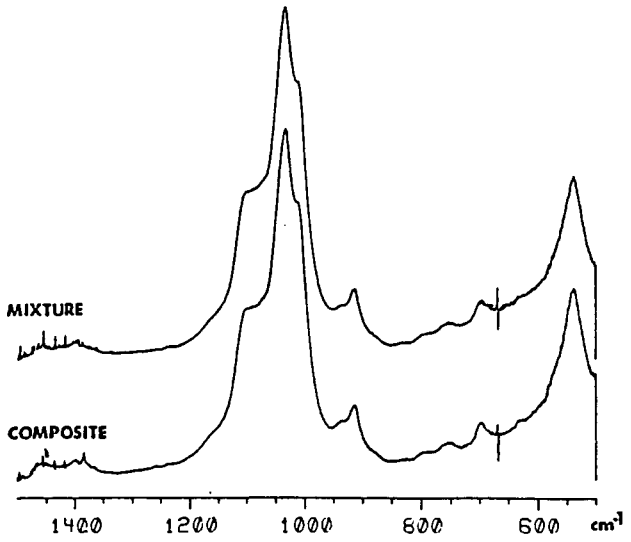

Figure 2: Scale expanded FTIR spectra in the range 500-1500 cm^{-1}.

Top: Mineral mixture of mica/montmorillonite, montmorillonite and kaolinite (1:1:2 by weight).
Bottom: Composite spectrum synthesized from the least squares fitting program.

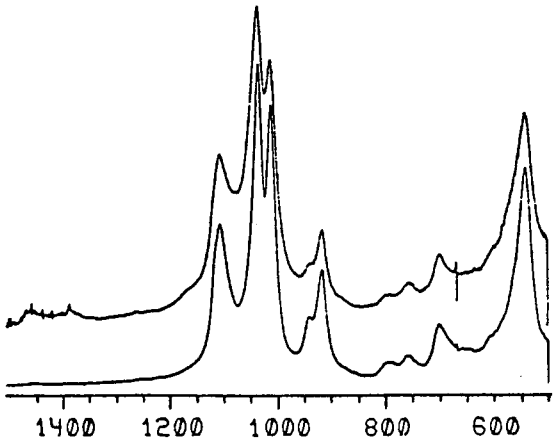

Figure 3: FTIR spectra in the range 500-1500 cm^{-1} of kaolinite standards

Top: Illinois.
Bottom: Georgia.

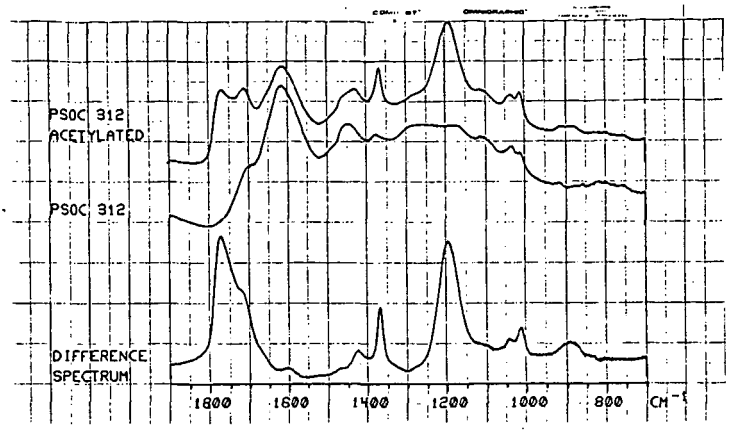

Figure 4: Top: FTIR Spectrum of acetylated coal
Middle: FTIR spectrum of original coal (PSOC 312)
Bottom: Difference spectrum

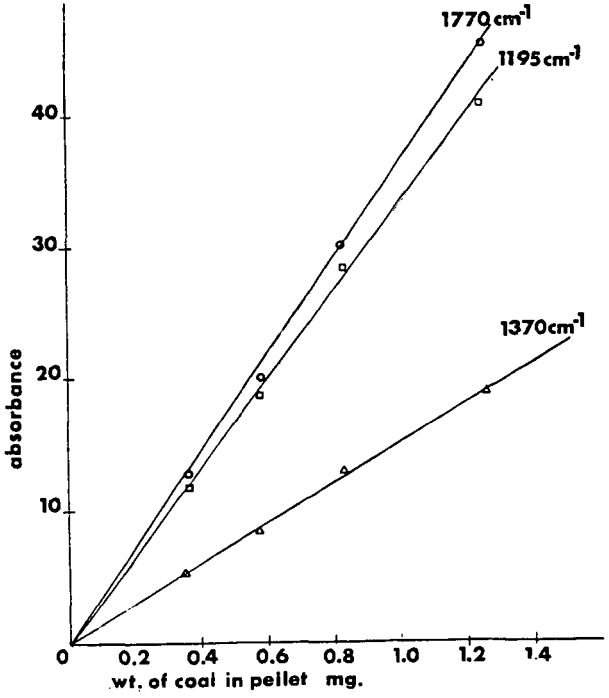

Figure 5: Plot of peak height of 1765; 1370 or 1195 cm^{-1} bands vs. concentration of coal in KBr pellet. (Measurements made on difference spectra)

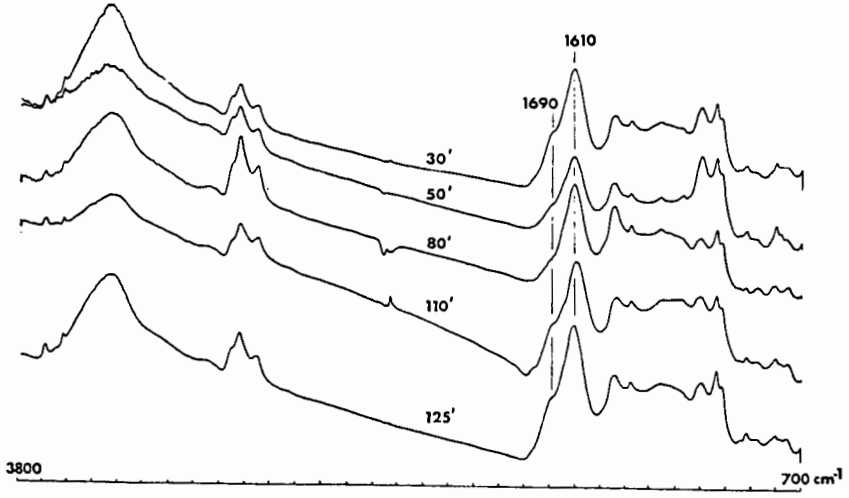

Figure 6: Infrared spectra of selected coal samples from stations along the seam.

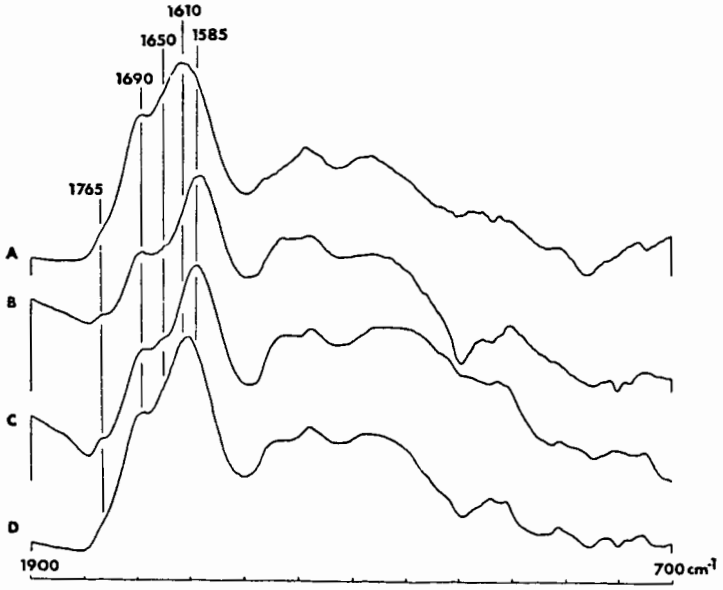

Figure 7: Difference spectra obtained by subtracting spectrum of coal from 70 ft. station from spectra of coals from A. 30 ft., B. 40 ft., C. 110 ft., and D. 125 ft.

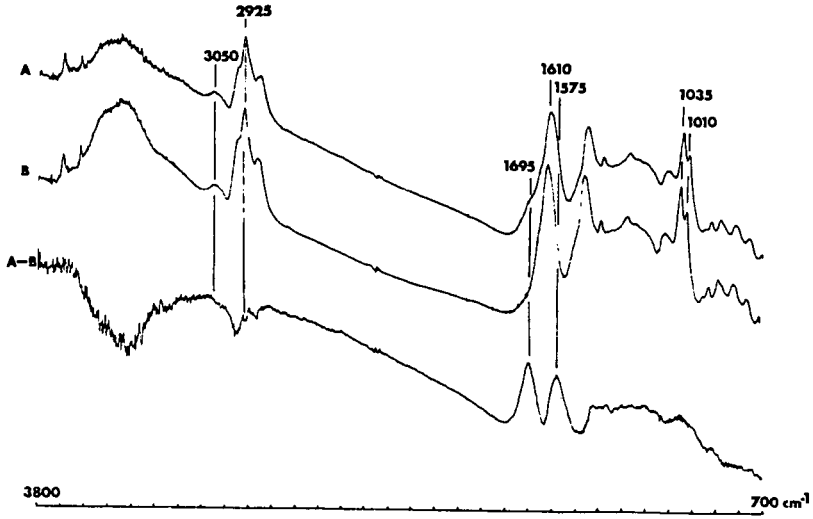

Figure 8: FTIR spectra in the range 700-3800 cm^{-1}.
A. Coal sample slightly oxidized at 150°C.
B. Unoxidized coal.
A-B. Difference spectrum.

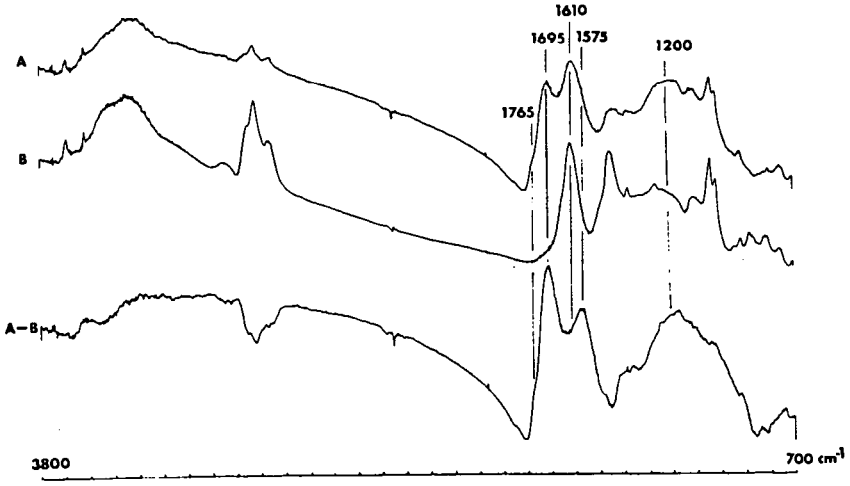

Figure 9: FTIR spectra in the range 700-3800 cm^{-1}.
A. Oxidized coal (6.7% O_2 uptake).
B. Unoxidized coal.
A-B. Difference spectrum.

THE NATURE AND COMPOSITION OF COAL HUMIC ACIDS

Swadesh Raj

Ebasco Services Incorporated, Two World Trade Center, New York, NY 10046

During the early stages of coalification the chemical substances in the decayed organs of higher plants are condensed into the humic acid-like substances. Classical theories of coal formation do not show characteristics of condensation product formed from the complex mixture of parent substances. These humic acid-like substances are ill defined substances of diverse origin and their composition is unknown. Although it has been known for many years that mild oxidation of bituminous coals yields humic acid-like material[1]. Reagents such as potassium permanganate, hydrogen peroxide and aqueous nitric acid have been used in the previous work[2]. The reagent selected here was aqueous performic acid which was generated by a reversible reaction between anhydrous formic acid and hydrogen peroxide. The mildness of the conditions, the speed of reaction and its simplicity were the factors for the reagent selection.

In this paper results are presented on humic acids which are extracted from thirty-eight different oxidized coals. Correlation equations are developed to predict the humic acid yields for coals of various origin. Elemental analyses of oxidized and parent coal are compared. Efforts are made to analyze changes in the amount and composition of mineral matter resulting from the chemical reaction. Petrographic changes as a result of oxidation is also studied. NaOH - soluble and insoluble materials are analyzed using FTIR. Infrared spectra of coals, humic acids and residues are interpreted and discussed.

EXPERIMENTAL PROCEDURE

The dried samples of coals (-80 mesh size) were dispersed in anhydrous formic acid (99 percent) (50 ml for 5 gms of each). The 30 percent hydrogen peroxide was then added, 2 ml at a time, at such a rate that the temperature rose to about 50°C. The mixture was then allowed to cool to room temperature for the next 24 hours with constant stirring. It was then filtered and the solid washed with water.

The dry residue, oxidized coal was then extracted with 1N NaOH in a stream of nitrogen gas at room temperature for another period of 24 hours with constant stirring. The insoluble residue was removed by centrifugation, washed and dried. The washings and NaOH soluble portion were collected and acidified to pH 1 and left overnight. The acid insoluble portion settled and most of the supernatent was siphoned from the precipitate. The precipitate was centrifuged and washed to about pH 5. Both the solids (NaOH soluble and insoluble) were dried in a vacuum oven at approximately 80°C for about 24 hours and analyzed on a Nicolet FTIR. KBr pellets of coals were prepared by mixing 1 mg of dry, finely ground sample with 300 mg of KBr.

Approximations were made of the mineral contents by determining (a) the high-temperature ash yields of humic acids and NaOH insolubles, (b) the yields of ash from the same materials in an oxygen-plasma low-temperature asher (LTA). Ultimate analysis of the oxidized products were obtained from the Commercial Testing and Engineering Co, Inc. Maceral analysis of oxidized product was done by coal petrography technique.

EXPERIMENTAL RESULTS

There is some difficulty in expressing the data on a completely sound basis, because of the complications introduced by the presence of mineral matter. There is a loss in weight of the mineral matter during oxidation. The mineral matter contents of coal and oxidized product are different. Neither the dmmf nor the mineral containing analyses can usefully be compared when expressed as percentages.

In Table 1 the weights of constituents in the sample taken for reaction are compared with their weights in the oxidized product. The losses shown for C, H, N in Table 1 contain no assumptions and are as good as the raw analytical data. Obviously there are uncertainties in the weights of organic sulfur and mineral matter, and hence in oxygen by difference. The results indicate that about 8-20 percent of the carbon and 0-15 percent of the hydrogen in the original coal is lost during the oxidation. The weight of oxygen is increased by 120-170 percent, and it appears to have doubled. It is clear that the data are not very satisfactory in this case. They should be considered qualitative in nature, nevertheless the data generated is first of its kind where efforts are made to interpret the data analytically for products of a chemical reaction of coals that considers the changes in the amount and composition of mineral matter resulting from the reaction.

The extraction of humic acids with sodium hydroxide is likely to disrupt partially the structure of the clay minerals and solubilize some material, which will not necessarily be completely reprecipitated by HCl with the humic acid. The sum of the LTA values for the humic acid and NaOH insolubles usually exceeded the mineral matter content of the coal by a considerable margin, suggesting that clay structures had been drastically altered. The sum of the high-temperature ashes bore a variable relation to the mineral matter content of the coal. In Figure 1 the yields of humic acids are expressed on the dry ash-free basis as a fraction of dmmf coal taken and are plotted against dmmf carbon contents. A tendency for the humic acid to increase with rank exists. The coals from Eastern Province tended to give the higher yields because this Province contains coals that in general are of higher rank than those of other Provinces. Regression analyses developed from the data showed that results for coals could be expressed by the equation.

$$\text{humic acid yield} = 3.15 \times \%C - 183$$

where the correlation coefficient is 0.95 for Rocky Mountain Province, 0.56 for Eastern Province and 0.22 for Interior Province coals. A correlation coefficient of 0.75 was found when all the data were used with respect to the Province of origin and can be expressed as

$$\text{humic acid yield} = 2.91 \times \%C - 163$$

As stated above, the hydrogen peroxide was added at such a rate as to limit the temperature rise due to the exothermic reaction. With Eastern coals the peroxide had to be added more slowly than with coals from the other Provinces, in order to avoid exceeding the temperature limit. It follows that the reaction with Eastern coals is more exothermic than with other coals.

Petrographic examination of the oxidized product do indicate that vitrinite had been greatly altered in appearance while sporinite and the inert macerals changed little or not at all. The apparently unaltered macerals could still be

recognized as such in the NaOH - insoluble materials which contain most of the inorganic material of the oxidized coal. The humic acid production arises from the vitrinite maceral which contain very minute quantities of mineral matter. Both of these materials (NaOH - insoluble and soluble) are analyzed by Nicolet FTIR and compared with that of coals.

The FTIR obtains spectra in digital form. The correction for the mineral matter and moisture is made[3,4]. The infrared spectra for the humic acids, NaOH - insoluble residue and coals are shown in Figures 2 to 4. Spectra obtained from coals and humic acids show a close similarity in the absorptions associated with the various C-H bonds and skeletal vibrations. Generally, the conclusions drawn from the absence of bands from the absorption spectrum are by no means less valuable than the information furnished by the existing bands. It is generally believed that coal contains no, or very few, C=O groups, isolated C=C and C≡C bands are absent. Aliphatic CH, CH_2 and CH_3 on the other hand do occur, as well as aromatic ring systems. -C-O- or C-O-C bands and associated OH and NH bands are probably also present.

DISCUSSION AND CONCLUSION

Infrared spectra of coals and humic acids demonstrate a very close similarity. The spectra from humic acids also resemble the spectra from coal tar[3], suggesting that the humic acids are the monomers derived due to the coal oxidation. Ash analysis and infrared analysis show that most of the organic matter ends up in the NaOH soluble part while most of the inorganic matter goes into the NaOH insoluble material.

Humic acid formation have been referred[5] earlier to "Regenerated Ulmins." This assumption needs further evidence. During the oxidation of coal, considerable oxygen enters the bonds of the coal molecule. Most of the vitrinites were greatly altered in appearance while sporinite and the inert macerals were changed little or not at all. The apparently unaltered macerals could still be recognized as such in the NaOH - insoluble material. The infrared spectra of NaOH - insoluble material looks like char, but the corrected spectra for the NaOH insoluble material show the absorption pattern similar to parent coal suggesting that the organic matter in that part is still highly polymerized similar to coal.

In all cases, the aliphatic C-H vibrations at 2850-2950 cm^{-1} are sharp, and the other C-H vibrations at 1450-1480 cm^{-1} and at 1375-1380 are there. Absorption near 1375 cm^{-1} is due to vibrations of the methyl group. When gem-dimethyl groups (ie, two methyl groups on the same carbon atom) are present, this band splits into a closely spaced doublet. Such splitting was observed in few spectra but not of an equal intensity. The aromatic absorption near 1600 cm^{-1} are very intense. Correlation of the magnitudes of the 1600 cm^{-1} peak with the hydroxyl content of a variety of coal, humic acid and even of the NaOH - insoluble material indicate that hydroxyl, in the form of phenolic hydroxyl contributes strongly to the peak.

Absorption due to C=O is very strong in all cases. These were at variable frequencies in the range 1660-1740 cm^{-1}, most often 1700-1730 cm^{-1}. The spectra of coals of bituminous rank do not show carbonyl absorption in the usual region (1660-1760 cm^{-1}). This absorption is quite clear in humic acids and entirely due to the presence of carboxyl groups which has been the result of oxidation.

A peculiar feature of the spectra is the ubiquity of absorption close to 1260 cm^{-1}. It is not quite intense but usually showed a multiplicity of peaks in the range 1250-1300 cm^{-1}. Primary and secondary alcohols, and phenols, may absorb in this region. Aromatic ethers also absorb here. The absorption appears to be due to some kind of C-O vibration, and such vibrations are often accompanied by other vibrations in the range 1000-1200 cm^{-1}. Indeed, bands were found at 1020-1030, 1070-1080 and 1170-1190 cm^{-1}. The striking point is that if any absorption in the region 1000-1300 cm^{-1} that was observed, was in the narrow ranges specified. This seems to suggest that a number of structural elements containing oxygen were widespread in coals and coal humic acids and differ surprisingly little from coal to coal.

A parallel situation is found with regard to another ubiquitous band in the range 795-820 cm^{-1}. This band is sharp in the spectra and sometimes intense. Weaker bands at higher frequencies (near 400-1000 cm^{-1}) were also seen.

The bending vibrations of aromatic C-H bonds are found near 870 cm^{-1} region, and their frequencies are used to identify substitution patterns in the benzene ring. Thus compounds with substituents in the 1, 4- or 1, 2, 3, 4-positions have an absorption near 830 cm^{-1} ($\pm$30 cm^{-1}), while 1, 2, 3-trisubstituted compounds absorb near 780 cm^{-1} ($\pm$20 cm^{-1}). Absorption near 750 cm^{-1} is ($\pm$20 cm^{-1}) characteristic of 1, 2-disubstituted compounds. No single pattern of substitution shows bands near both 750 and 830 cm^{-1}. The intensities of these bands is variable with pure compounds, but is often high. Weak shoulder is seen at 3030 cm^{-1} (aromatic C-H stretching) and the weak band near 1600 cm^{-1} (aromatic ring skeletal vibration?). No firm answer can be given, but probably the intensities are sufficiently consistent, since in pure aromatic compounds the 1600 cm^{-1} bond is sometimes quite weak. Sharp absorption at 1600 cm^{-1} in the spectra is due to -OH substitution on the aromatic ring[3,6].

The striking observation is that if these bands are present in a spectrum, they are always close to the same frequencies, and absorptions corresponding to other benzene substitution patterns than those mentioned are not seen at all. The implication is, once more, that certain structural elements or skeletons are of very frequent occurrence and differ surprisingly little from coal to coal which is in agreement with the other related published works[7,8].

ACKNOWLEDGMENT

The help extended by Dr P Solomon for obtaining the IR spectra is greatly appreciated.

REFERENCES

1. Given, P H, Fuel (39), 463 (1960)

2. Lowry, H H, Chemistry of Coal Utilization Supplement Volume, John Wiley and Sons Inc, New York (1963)

3. Solomon, P R, Conference on "Coal Combustion Technology and Emission Control" California Institute of Technology, Pasadena, CA, February 5-7 (1979)

4. Painter, et al, Fuel (57) 124 (1978)

5. Francis, W, in "Coal" pp 523, 533, Second Edition, (1961)

6. Fujii, S, O'Sawa, Y, and Sugimura, H, Fuel (49) 68 (1970)

7. Raj, S, ACS Division of Fuel Chemistry Preprints, 178th Meeting, (24) (1979)

8. Raj, S, IInd International Coal Utilization Conference on Coal Technology, Houston, Texas November 1979

Figure 1
YIELDS OF HUMIC ACIDS AS FUNCTION OF CARBON CONTENTS OF COALS

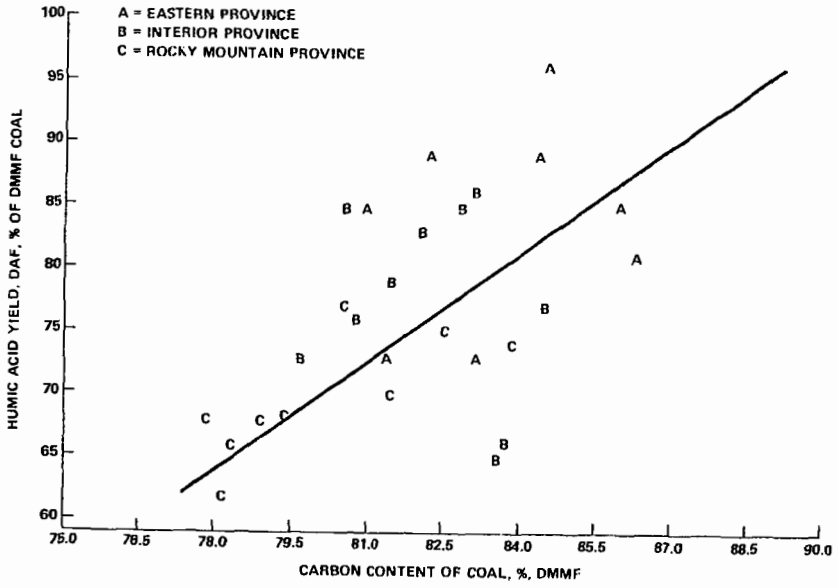

Table 1

Changes in Weight of Elementary Constituents Resulting from Performic Acid Oxidation

(The Figures Shown are Weights in Grams)

	PSOC 221 (HVA, Kentucky)			PSOC 278 (HVA, Ohio)		
	Original	Oxidized	Δ	Original	Oxidized	Δ
Whole Sample	5.037	4.870	-0.167	5.097	4.986	-0.111
C	3.763	3.140	-0.623	3.156	2.842	-0.314
H	0.289	0.250	-0.039	0.244	0.216	-0.028
N	0.073	0.065	-0.008	0.067	0.044	-0.023
S	0.102	0.082	-0.020	0.104	0.104	0
O (by diff.)	0.440	1.195	+0.755	0.352	0.961	+0.609
MM	0.343	0.140	-0.203	1.174	0.818	-0.356

	PSOC 284 (HVA, Illinois)			PSOC 314 (HVA, Utah)		
	Original	Oxidized	Δ	Original	Oxidized	Δ
Whole Sample	5.049	4.855	-0.194	5.032	4.769	-0.263
C	3.162	2.881	-0.281	3.625	2.914	-0.711
H	0.220	0.220	0	0.270	0.245	-0.025
N	0.070	0.054	-0.016	0.074	0.058	-0.016
S	0.058	0.058	0	0.030	0.025	-0.005
O (by diff.)	0.274	0.669	+0.395	0.451	1.019	+0.568
MM	1.266	0.975	-0.291	0.581	0.508	-0.073

Figure 2
INFRARED SPECTRA OF VARIOUS STAGES OF A COAL[3]

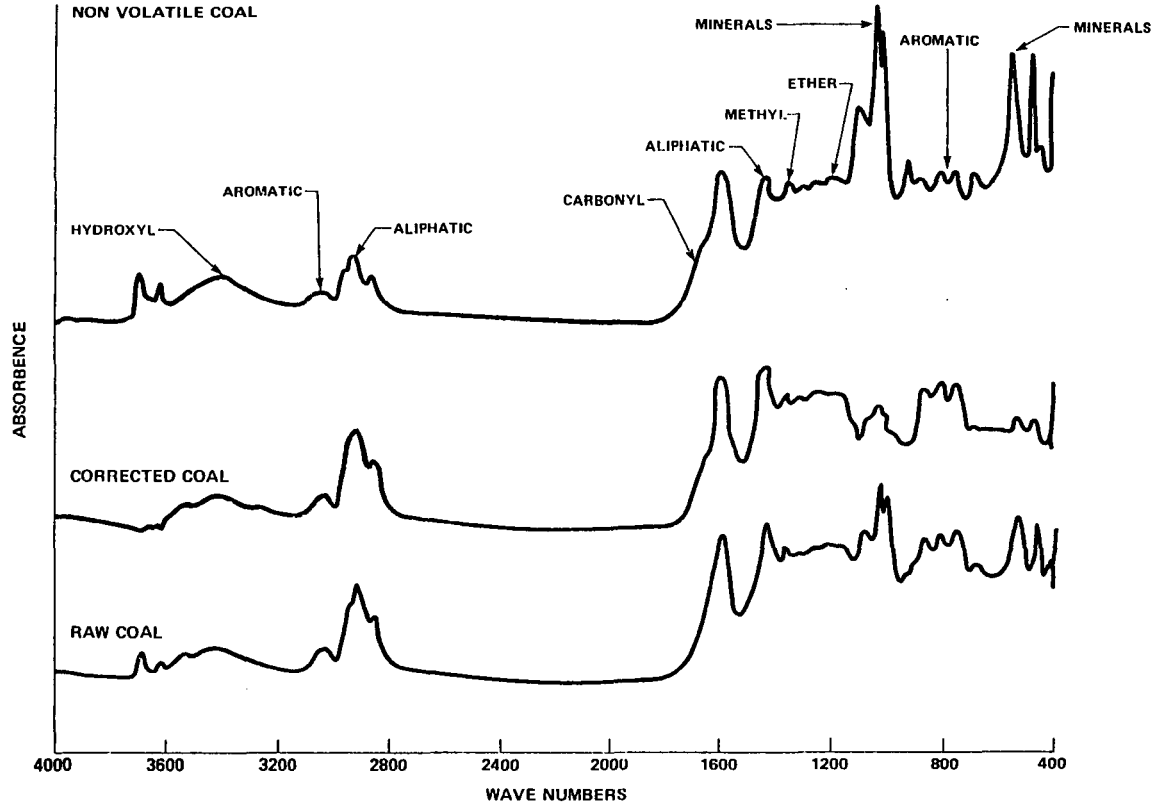

Figure 3
INFRARED SPECTRA OF (A) TEXAS LIGNITE (B) PSOC 168[3]

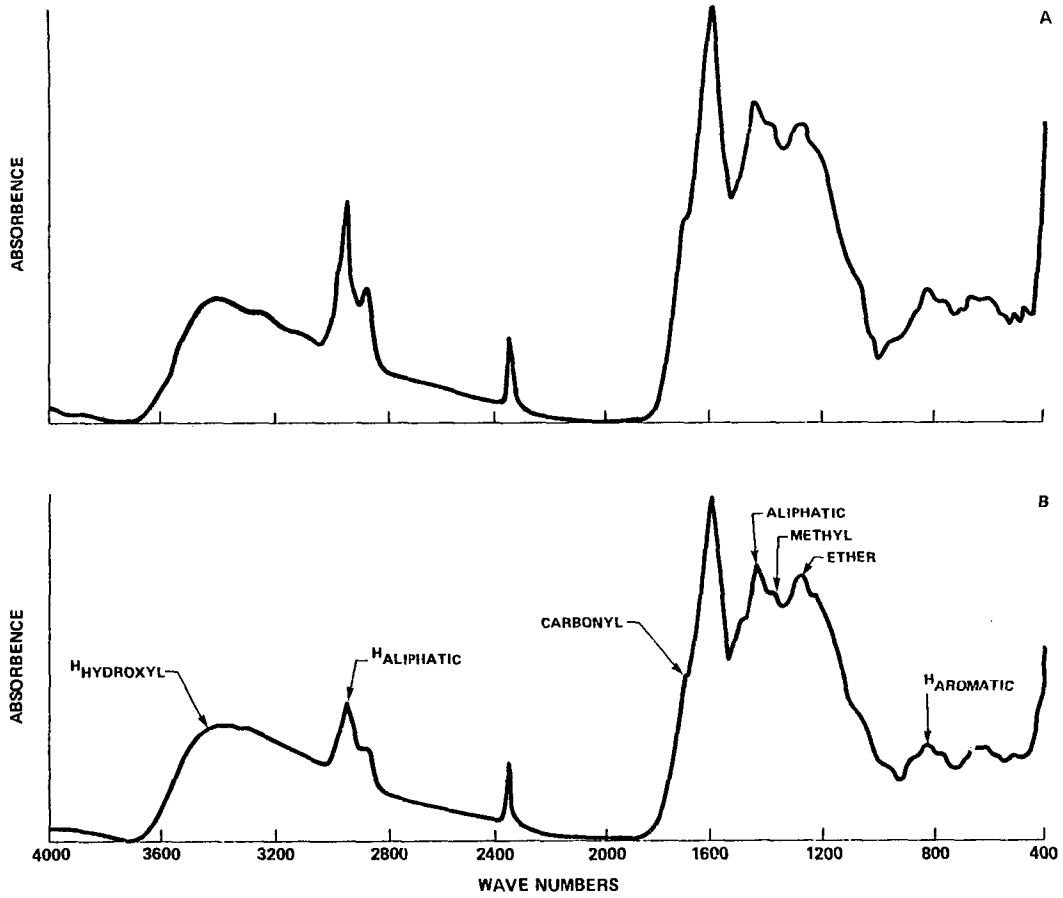

Figure 4
INFRARED SPECTRA OF (A) PSOC 282 HUMIC ACID, (B) PSOC 221 HUMIC ACID, (C) PSOC 295 HUMIC ACID, AND (D) PSOC 295 NaOH-INSOLUBLE

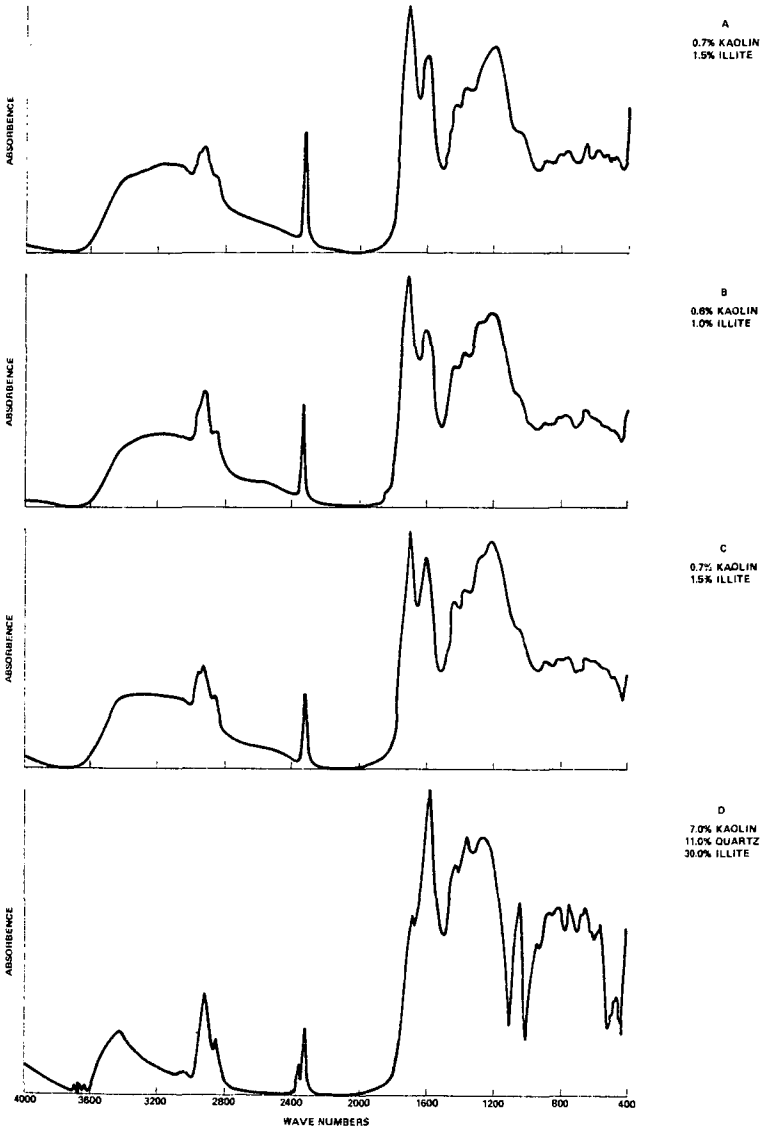

INSIGHTS INTO THE CHEMICAL STRUCTURE OF COAL FROM THE NATURE OF EXTRACTS

W.R. Ladner, T.G. Martin and C.E. Snape

National Coal Board, Coal Research Establishment,
Stoke Orchard, Cheltenham, Glos., GL52 4RZ, England.

K.D. Bartle

Department of Physical Chemistry, University of Leeds,
Leeds, LS2 9JT, England.

ABSTRACT

As part of a National Coal Board programme aimed at deriving transport fuels and chemical feedstocks, the chemical structure of extracts from coals of varying rank are being studied. This information helps to give an insight into the structures of the original coals. Supercritical gas extraction yields, with little degradation, large quantities of material (20-50% d.a.f. coal), which may be compared with products obtained by: (a) a less mild process employing hydrogen-donor solvents such as hydrogenated anthracene oil, and (b) simple solvent extraction. The molecular weight range of the extracts (300-2000) makes separation by solvent fractionation and adsorption chromatography, followed by examination by NMR spectroscopy, the most appropriate analytical methods for their structural characterisation. The SCG and solvent extracts consist of small aromatic clusters joined by methylene and heteroatom bridges. The aliphatic constituents are principally alkyl groups for which chain length decreases with increasing rank, so that aromaticity correspondingly increases from 40-80%. The main chemical structures present in the various extracts are independent of extraction conditions. This, taken with the significantly different MW distributions, allows important conclusions to be drawn as to the nature of the fragments present in the original coals.

1. *INTRODUCTION*

Investigations into the organic chemical structure of coals can broadly be divided into three groups:

(i) physical methods, for example infra-red spectroscopy (1) and solid state ^{13}C NMR (2), which can be used to obtain information about the chemical groupings;

(ii) chemical methods, for example oxidation (3) and depolymerisation using boron trifluoride and phenol (4), which give information about the size of aromatic clusters and about substituents and linking groups in the coal molecule;

(iii) characterisation of extracts, for example the structural analysis of extracts obtained in high yields can be used to deduce information about the parent coals.

The Coal Research Establishment of the National Coal Board is currently developing two coal liquefaction processes. These involve the extraction of coal with (a) supercritical gas (SCG) at temperatures up to 720 K and pressures of about 200 bar (5-7) and (b) coal-derived hydrogen-donor solvents (HDS) at temperatures around 670 K, but at pressures close to ambient (7). The extracts obtained from both processes are then hydrocracked and further reformed to the

desired liquid products. SCG extraction with aromatic solvent yields up to 50% d.a.f. coal as tractable homogeneous extract together with reactive char. The extract is produced by mild thermolysis of the coal and is volatilised by the presence of an SCG (8). HDS extraction removes up to 90% of the organic part of the coal by a mechanism thought to involve stabilisation of the free radicals formed by hydrogen donation from the solvent (9).

Moderate conditions are experienced by coals in both processes so that extensive breakdown and reformation of coal molecular structures during extraction is unlikely to occur, although limited thermolysis and chemical bond cleavage must be taking place for the bulk of the coal to become soluble in the solvent media. However, rapid removal of molecular fragments from the extraction zone in the gas extraction process and stabilisation of radical species by hydrogen donation in the HDS process (9) probably prevent the occurrence of reformation, recombination and further degradation reactions. Therefore, the structures of molecules released and recovered as extract may well be representative of the molecular building blocks of the original coals.

Conversion of extracts to more valuable low boiling oils has necessitated a study of their molecular structures and advantage has been taken of these investigations together with some structural studies conducted on coal extracts prepared by simple solvent extraction to make some predictions about the molecular structures of parent coals.

2. EXPERIMENTAL AND RESULTS

2.1 Coals and Their Extraction

In this investigation seven coals were used (three bituminous, one perhydrous and three lignitic) and the yields of the extracts prepared from these are shown in Figure 1. For convenience of presentation, the bituminous coals and lignites have been labelled 1, 2 and 3. Soxhlet extractions were performed with toluene and pyridine for periods between 25 and 250 hours. SCG extractions were carried out semi-continuously with toluene and other aromatic solvents at temperatures between 620 and 690 K (10). Bituminous coal 1 was also extracted with hydrogenated anthracene oil (HDS) at 670 K.

2.2 Fractionation of Extracts and Analyses

The extracts were separated into benzene insolubles (BI), asphaltenes and n-pentane solubles (n-PS) fractions (10). In some cases the n-PS fraction was further fractionated by silica-gel adsorption chromatography into paraffins, aromatics (low phenolic -OH content) and polars (high phenolic -OH content). Some BI fractions were silylated (11) to render them soluble in tetrahydrofuran and chloroform for molecular weight determinations and NMR spectroscopy respectively. Silylation was especially valuable in view of the large BI fractions in many of the extracts (see Figure 1).

Most fractions were subjected to ultimate, MW and phenolic -OH analyses. Number average MWs were determined isopiestically using an Hitachi-Perkin-Elmer 115 instrument. Phenolic -OH contents were measured by enthalpimetric titration. Some typical results for these analyses are given in Table 1.

2.3 Spectroscopy

^{1}H NMR spectra were obtained at 60 MHz using an Hitachi-Perkin-Elmer R24B instrument with chloroform-d and pyridine-d_5 as solvents. Figure 2 shows the ^{1}H NMR spectra of the asphaltenes from the HDS extract of bituminous coal 1 and of the SCG extracts of bituminous coal 3, perhydrous coal and lignite 1.

Fourier transform ^{13}C NMR spectra were obtained at 45 MHz using a Bruker WH 180WB instrument with chloroform-d as solvent. Chromium acetylacetonate was added to the samples and gated decoupling was employed to obtain reliable quantitative data (12). Figure 3 shows the ^{13}C NMR spectra of the asphaltenes from the HDS extract of bituminous coal 1 and of the SCG extracts of bituminous coal 3, the polars from SCG extract of perhydrous coal and the aromatics from SCG extract of lignite 3.

2.4 Structural Analysis Scheme

The distribution of hydrogen types determined by ^{1}H NMR, as shown in Figure 2, has been combined with elemental and phenolic -OH analyses and MW to give the numbers of the various atoms or groups in the average molecule; these have then been used to derived the structural parameters defined in Table 2.

The number of aliphatic carbon atoms (C_{al}) was obtained using the assumed atomic H/C ratios (a,b,c and d) for the different aliphatic environments measured by ^{1}H NMR. These were chosen by consideration of the groups contributing to the bands in the ^{1}H NMR spectra. For example, since only methyl groups contribute to the $H_{,3}$ band, d = 3 and similarly, since mainly methylene groups contribute to the $H_{,2}$ band, a = 2. The choice of values of b and c was more difficult since they were found to be dependent on coal rank, both methylene and methyl groups being major contributors to the $H_{,2}$ and $H_{,3}$ bands. Therefore, b and c were chosen to give C_{al} and f_a (aromaticity) values consistent with the direct measurement of these parameters by ^{13}C NMR.

Values of the structural parameters for a selection of the asphaltenes, BI and aromatic fractions of typical extracts are given in Table 3. The structural parameters have been used to construct representative structures for some of the asphaltenes and these are given in Figure 4. Where necessary, more than one structure has been given so that a better fit is achieved with the calculated structural parameters. The structures illustrated must, of course, be considered as averages of the many species present in each fraction.

3. DISCUSSION ON COAL EXTRACTS

3.1 Yields and Molecular Weights

The results of extraction and fractionation given in Figure 1 are not comprehensive, but present a range of values for the processes under investigation. Comparison of the compositions of the various extracts is of considerable interest since they are derived by using widely varying degrees of extraction severity from coals with markedly different characteristics.

Extraction of coals with toluene gave very small yields of soluble materials (5% d.a.f. coals) while pyridine gave much larger yields (up to 20% d.a.f. coal), which increased with increasing coal rank. These findings are in agreement with those of previous investigators (13,14).

Extraction with toluene and with pyridine is likely to involve only solvation of low MW molecules trapped in the coal matrix and some disruption (particularly with pyridine) of hydrogen bonds with consequent release of materials of higher MW and polarity. Thus the pyridine extract of bituminous coal 3 contains a large proportion of BI of MW about 1500.

At temperatures between 620 and 690 K, SCG extraction of bituminous coals yielded quantities of BI comparable to those obtained by pyridine extraction. The quantities of these BIs increased with increasing extraction temperature.

The large proportions of benzene soluble fractions always present in SCG extracts indicate that, apart from simple solvation and hydrogen bond breaking, some thermolysis of chemical bonds may have occurred, although little gas was generated during extraction.

In HDS extraction the material obtained in excess of that released by SCG extraction is largely benzene insoluble with a MW 2000. Such high MW material is too involatile to be dissolved in supercritical solvents.

For the lignites, the overall picture is somewhat similar to that of the bituminous coals except that both pyridine and SCG extraction gave much smaller quantities of BI material (MW 1000). No BIs were obtained by SCG extraction of lignite 3 at 610 K, but at 690 K a small amount (5% d.a.f. coal) was produced. These findings imply that MW distributions are a function of coal rank.

The perhydrous coal yielded four times more BIs by SCG extraction than by pyridine extraction, but the MWs of both fractions are close to 2000. This suggests that the large quantities of both benzene soluble (30% d.a.f. coal) and BI (20%) material could be produced from the perhydrous coal by mild thermolysis of, for example, long alkyl bridging groups between aromatic nuclei and that the high MW benzene insoluble material is more structurally amenable to dissolution in the SCG than are the BIs from bituminous coal.

3.2 Elemental and Functional Group Analyses

Table 1 shows that for all the extracts, the solvent separation procedure has given fractions with decreasing H/C ratio and increasing heteroatom content going from n-PS to BI material. Silica gel adsorption chromatography of PS yielded aromatic fractions which contain little phenolic -OH.

The overall H/C ratios of the extracts from the lignites and perhydrous coal are significantly higher than those of the bituminous coals. The extracts from lignites generally have much larger heteroatom contents than those from the bituminous and perhydrous coals. The heteroatom contents of all the pyridine and SCG extracts of bituminous and perhydrous coals are similar to those of the parent coals. For the SCG extracts of bituminous coals H/C varies little as the temperature is increased from 620 to 690 K. However, the SCG extract of lignite 3 shows a significant decrease in heteroatom content at 690 K which suggests that a number of the heteroatoms are in structures, such as carbonyl and aliphatic ethers, which are easily cracked. The heteroatom contents of the HDS extracts of the bituminous coals are slightly less than those of the parent coals and also of the corresponding SCG extracts; this implies that the digestion conditions have resulted in some chemical cleavage of bonds containing heteroatoms.

Table 1 indicates that acidic hydroxyl groups generally account for approximately 65% of the oxygen in the bituminous and perhydrous coal extracts, while acidic hydroxyl (i.e. phenolic and carboxyl) groups account for well under half the total oxygen in most of the pyridine and 610 K SCG extract fractions of lignite.

3.3 NMR Spectra

The NMR spectra show that the extracts of bituminous coals (Figures 2a and b, 3a and b) contain fewer aliphatic groups than the extracts of lignite (Figures 2c and 3c), the ^{1}H spectra of the former containing much more prominent H bands. The sharp bands at 1.3 ppm in the ^{1}H spectra and at 29.7 ppm in the ^{13}C spectra of the lignite and perhydrous coal extracts are attributed to methylene groups in alkyl side chains containing at least 8 carbon atoms (15).

The bands between 1.5 and 2.0 ppm in the ^{1}H spectra of the HDS bituminous coal and lignite extracts indicate the presence of hydroaromatic groups. These groups probably result from hydrogen transfer reactions occurring in the former case, but in the latter they possibly originate from the parent coal. A comparison of the ^{13}C spectra shows that the SCG extract of bituminous coal contains a greater proportion of bands between 18 and 22.5 ppm; these are largely attributed to methyl groups (15).

In the ^{13}C spectra of the HDS and SCG extracts of bituminous coal (Figures 3a and b), the intensity of the C_{AR}-O band between 148 and 168 ppm, together with the absence of carbonyl resonances between 170 and 210 ppm, indicate that virtually all the non-phenolic oxygen is present in aromatic ether groups.

3.4 Extract Structures

The structural parameters (Table 3) and the average structures (Figure 4) highlight the differences in the chemical nature of the various extracts. The aliphatic carbon contents of the lignite and perhydrous coal extracts are significantly larger than those of the bituminous coal extracts, but methyl is the main constituent in all the extracts. As previously described, long alkyl side chains are prominent in the extracts of the lignites and perhydrous coal, occurring mainly in the low MW fractions. The average alkyl chain length (CL) for extracts of the lignites and the perhydrous coal is between 2.5-4 and decreases to 2 for those from the bituminous coals. The overall aliphatic H/C ratio is approximately 2 for all the extracts, except those obtained with pyridine and by SCG extraction of the bituminous coals where the ratio is 2.5 because of a greater proportion of methyl. For all extracts decreases with increasing MW.

The degree of condensation for the lignite SCG extracts (dC = 0.73-0.82) indicates that the aromatic nuclei consist mainly of single rings. The dCs for the SCG extracts of the perhydrous and bituminous coals (0.6-0.7) are characteristic of 1-3 ring aromatic nuclei in the molecules. For the bituminous coals, little variation occurs, either in the nature and content of alkyl groups, or in the degree of condensation of aromatic nuclei between simple solvent and SCG extracts. The aromatic structure of the HDS extract is slightly more condensed than those of the solvent and SCG extracts.

4. CONCLUSIONS ON ORGANIC COAL STRUCTURES

The determinations of the structural characteristics of extracts representing large proportions of the organic matter in the coals from which they were derived make it reasonable to draw conclusions about the molecular constitution of the coals themselves. Arguably the thermal treatments used in the two NCB extraction processes will cause some cleavage of less stable molecular bonds. However, the extraction temperatures used are only around 670 K and the molecular fragments once formed are either volatilised by the SCG and removed or stabilised by the presence of hydrogen-donor species. Furthermore, it has been shown that the structures of SCG extracts of bituminous coal are similar to those of the corresponding solvent extracts.

Results of this structural study indicate an increase in aromaticity of the extracts (0.4-0.8) with increase of coal rank which is consistent with extensive data for coals (16). Further, the average sizes of aromatic clusters in the extracts are in general agreement with published work on these types of coal. For example, Hayatsu et al (17) found that alkaline cupric oxide oxidation of lignites produced mainly single ring aromatic carboxylic acids, while bituminous coals gave substantially 2 and 3 ring derivatives.

The indications from our work are that coals consist of aromatic ring clusters of varying sizes and degrees of condensation, depending on coal rank, interlinked by simple molecular bridge systems and by hydrogen bonding. This evidence contrasts with some of the earlier data which suggested that hydroaromatics and, in particular, adamantyl groups (18,19) are major contributors to coal structure. There is certainly no evidence of adamantyl groups being present in our coal extracts. Such structures would give rise to broad bands in the ^{1}H NMR spectra between 1.0 and 2.0 ppm, probably centred at 1.5-1.7 ppm (20), and not the sharp bands centred at 1.3 ppm as observed in Figure 2. Apart from simple bridge systems, alkyl groups must account for the majority of aliphatic carbon present in the coals used. Simple bridge systems, such as methylene, were deduced by Heredy et al (4) from the products obtained by depolymerisation of coal with phenol and boron trifluoride.

Information on the structure of the parent coals may be obtained from the molecular weight data for various extract fractions. Extracts from all of the coals contain large quantities of benzene soluble material released by mild thermolysis at temperatures between 620 and 690 K. The quantities yielded represent a far greater proportion of low (600) MW material than was previously thought to be present in the coals on the basis of results from simple solvent extraction and low temperature carbonisation. If extensive thermolytic degradation of the basic coal structure has not occurred during extraction, then this benzene soluble material must be representative of lower MW structural units in the coals.

The BIs from the SCG extracts of the lignites and perhydrous coals are predominantly of high MW (2000). Those from pyridine and HDS extracts of the bituminous coals are similar, being 1500 and 2000 respectively. However, the fact that no BI material was obtained by low temperature (610 K) SCG extraction of lignite supports the view that coalification processes involve reduction in molecular size of unit structures brought about mainly by loss of large alkyl side chains with aromatisation procedures accounting for increasing size of ring clusters (21).

5. ACKNOWLEDGEMENT

We thank the National Coal Board for permission to publish this paper. The views expressed are those of the authors and not necessarily those of the Board.

6. REFERENCES

1. Brown, J.K., J. Chem. Soc., 744 (1955).
2. Maciel, G.E., Bartuska, V.J. and Miknis, F.P., Fuel, 58, 391 (1979).
3. Hayatsu, R., Scott, G., Moore, L.D. and Studier, M.H., Nature, 257, 378 (1978).
4. Heredy, L.A., Kostyo, A.E. and Neuworth, M.B., Fuel, 43, 414 (1964).
5. Maddocks, R.R. and Gibson, J., CEP, 59, June 1977.
6. Whitehead, J.C. and Williams, D.F., J. Inst. Fuel, 48, 182 (1975).
7. Davies, G.O., Chem. Ind., 560 (1978).
8. Paul, P.F.M. and Wise, W.S., "The Principles of Gas Extraction", Mills and Boon, London, 1971.
9. Neavel, R.C., Fuel, 55, 237 (1976).
10. Bartle, K.D., Ladner, W.R., Martin, T.G., Snape, C.E. and Williams, D.F., Fuel, 58, 413 (1979).
11. Snape, C.E. and Bartle, K.D., Fuel, 58, 898 (1979).
12. Ladner, W.R. and Snape, C.E., Fuel, 57, 656 (1978).

13. Wise, W.S., "Solvent Treatment of Coal", Mills and Boon, London, 1971.
14. Lahage, P. and Decroocq, D., Revue de l'Institut Francais du Petrole, 31, 99 (1976).
15. Snape, C.E., Ladner, W.R. and Bartle, K.D., Anal. Chem., 51, 2189 (1979).
16. Van Krevelen, D.W., "Coal - Its Formation and Constitution", Elsevier, Amsterdam, 1961.
17. Hayatsu, R., Winans, R.E., Scott, R.G., Moore, L.P. and Studier, M.H., Fuel, 57, 541 (1978).
18. Farcasiu, M., ACS Div. Fuel Chem., 24(1), 121 (1979).
19. Chakrabatty, S.K., World Conf. of Future Sources of Organic Raw Materials, Toronto, July 1979.
20. Podehradska, J., Hajek, M. and Hala, S., Collect. Czech Chem. Commun., 43, 250 (1978).
21. Camier, R.J. and Sieman, S.R., Fuel, 58, 67 (1979).

TABLE 1 - Analyses of Typical Extract Fractions

	Bituminous Coal						Perhydrous Coal			Lignite					
	HDS 1		SCG 2 620 K Ar	SCG 3 670 K		Py 3	SCG 690 K			SCG 1 690 K		SCG 2 610 K Ar	SCG 3		
	As	BI		As	BI	BI	n-PS	As	BI	As	BI		610 K Ar	690 K As	690 K BI *
% C	86.1	84.5	88.4	82.2	80.5	76.7	86.2	83.2	82.5	80.2	77.5	84.0	79.8	79.7	79.2
% H	6.5	5.5	8.4	6.6	5.8	5.3	10.0	7.3	6.6	7.4	5.5	9.6	9.9	6.7	5.5
% O	5.1	6.6	2.1	8.6	10.5	12.2	4.1	8.5	8.8	10.4	12.9	N.D.	N.D.	9.0	17.0
% N+S	2.2	2.7	N.D.	2.4	2.7	3.1	N.D.	N.D.	N.D.	N.D.	N.D.	4.4	10.4	4.3	5.6
% -OH	5.0	4.2	0.8	6.2	7.0	6.2	1.7	5.7	5.8	5.6	4.2	N.D.	N.D.	5.6	3.1
MW	610	2030	310	430	720	1500	490	780	2090	690	1750	275	250	620	1860
H/C Ratio	0.90	0.78	1.13	0.96	0.86	0.82	1.38	1.04	0.96	1.10	0.85	1.36	1.48	1.0	0.83

Key: Py = Pyridine SCG = Supercritical gas HDS = Hydrogen-donor solvent
As = Asphaltenes BI = Benzene insolubles Ar = Aromatic fraction of n-pentane solubles
n-PS = n-pentane solubles

N.D. = Not determined

* = Analysis corrected for ash

TABLE 2 - Definitions of Structural Parameters

Structural Parameter	Definition
No. of aliphatic carbon atoms, C_{al}	$\frac{H_{\alpha,2}}{a} + \frac{H_{\gamma}}{b} + \frac{H_{\beta}}{c} + \frac{H_{\gamma}}{d}$
Aromaticity, f_a	$\frac{C - C_{al}}{C}$
Degree of alkyl substitution,	$\frac{\frac{H_{\alpha}}{b}}{H_{AR,OH} + \frac{H_{\alpha}}{b}}$
Average alkyl chain length, CL	$\frac{C_{al} - H_{\alpha,2}}{\frac{H_{\alpha}}{b}}$
Degree of condensation, dC	$\frac{H_{AR,OH} + \frac{H_{\alpha}}{b} + 2(\frac{H_{\alpha,2}}{a} + \text{non-phenolic O+N+S})}{(C - C_{al}) + (\frac{H_{\alpha,2}}{a} + \text{non-phenolic O+N+S})}$
Aliphatic $\frac{H}{C}$ ratio	$\frac{H}{C} \times \frac{\text{aliphatic hydrogen}}{H \text{ (from } ^1H \text{ NMR)}} \times \frac{C}{\text{aliphatic carbon (from } ^{13}C \text{ NMR)}}$

TABLE 3 - Structural Parameters for Typical Extract Fractions

Structural Parameter	Bituminous Coal						Perhydrous Coal		Lignite				
	HDS 1		SCG 2 620 K	SCG 3 670 K		Py 3	SCG 690 K		SCG 1 690 K		SCG 2 610 K	SCG 3	
	As	BI	Ar	As	BI	BI	As	BI	As	BI	Ar	610 K Ar	690 K As
C_{al}	12.5	31.7	7.5	7.7	9.9	20.6	21.0	46.9	18.7	31.8	9.7	9.8	14.1
f_a	0.71 (0.70)	0.78 [0.79]	0.67	0.74 (0.74)	0.80	0.79 [0.79]	0.61 (0.60-0.64)	0.67	0.60	0.72	0.50	0.42	0.66
σ	0.27	0.22	0.32	0.24	0.21	0.23	0.37	0.30	0.37	0.29	0.32	0.30	0.34
CL	2.4	2.3	2.0	1.9	1.6	1.9	2.7	2.7	2.7	2.5	3.1	5.4	2.1
dc	0.58	0.62	0.66	0.69	0.74	0.70	0.66	0.70	0.79	0.73	0.95	N.D.	0.82
Aliphatic H/C ratio	2.0	2.2	N.D.	2.5	N.D.	2.6	N.D.	N.D.	N.D.	N.D.	2.1	2.1	N.D.

Key: ( ) = direct values from ^{13}C NMR

[ ] = direct values from ^{13}C NMR of silylated benzene insolubles

Py = pyridine
SCG = supercritical gas
HDS = hydrogen-donor solvent

As = asphaltenes
BI = benzene insolubles
Ar = aromatic fraction of n-pentane solubles

N.D. = not determined

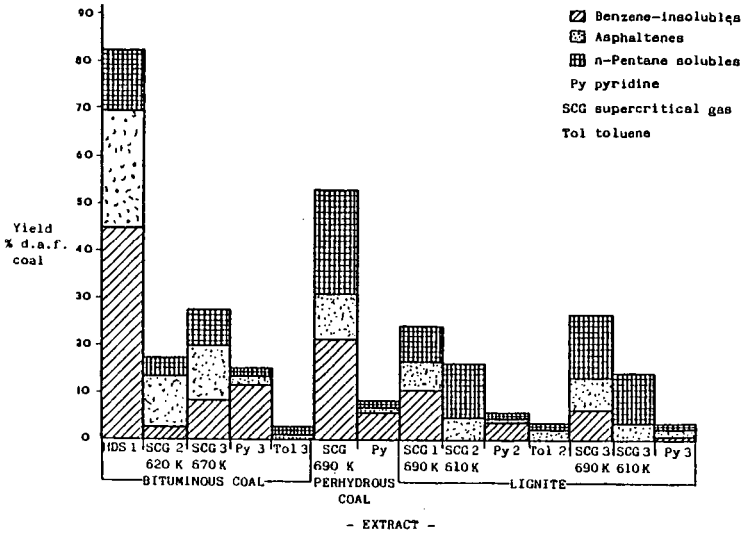

Figure 1 Some Yields of Extracts and their Solvent Fractions

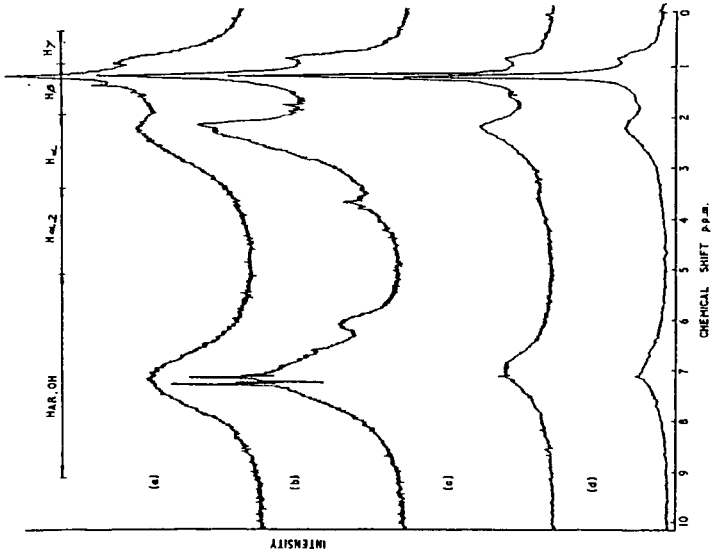

Figure 2 ^{1}H NMR Spectra of Asphaltenes from (a) HDS Extract of Bituminous Coal 1 and SCG Extracts of (b) Bituminous Coal 3, (c) Perhydrous Coal and (d) Lignite 1

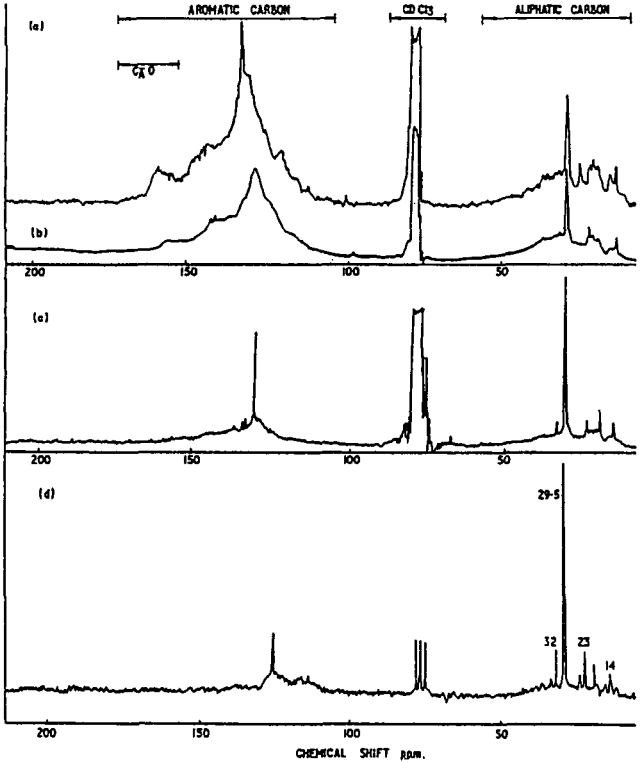

Figure 3 ^{13}C NMR Spectra of (a) Asphaltenes from SCG Extract of Bituminous Coal 3, (b) Asphaltenes from HDS Extract of Bituminous Coal 1, (c) Polars from SCG Extract of Perhydrous Coal and (d) Aromatics from SCG Extract (610 K) of Lignite 3

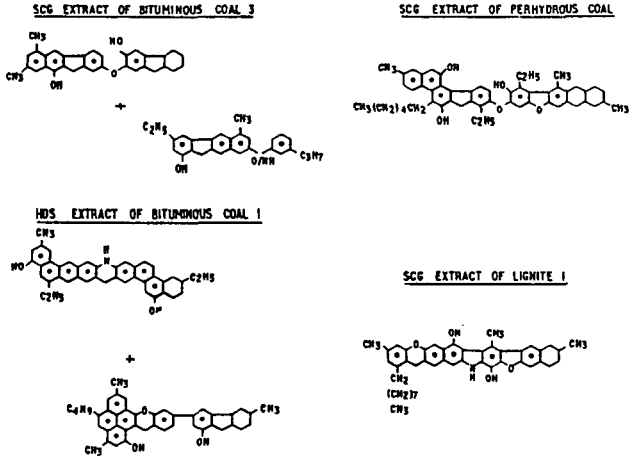

Figure 4 Average Structures for Some Asphaltene Fractions

AN INVESTIGATION OF THE OXYGEN AND NITROGEN GROUPS IN SUPERCRITICAL GAS EXTRACTS OF COAL BY NMR

T.G. Martin and C.E. Snape

National Coal Board, Coal Research Establishment
Stoke Orchard, Cheltenham, Glos., GL52 4RZ, England.

K.D. Bartle

Department of Physical Chemistry, University of Leeds
Leeds, LS2 9JT, England.

ABSTRACT

In the liquefaction processes under development by the National Coal Board coal extracts, including supercritical gas extracts, are subjected to catalytic hydrocracking. Thus, characterisation of heteroatoms in these extracts is important for identifying species which may give rise to catalyst poisoning. NMR methods are described for nitrogen and oxygen group determinations. Hydroxyl groups in extracts may be completely silylated so that they can be estimated from the $OSi(CH_3)_3$ band in the ^1H NMR spectrum. The solubility of benzene-insoluble fractions is also significantly increased by silylation so that they can be easily studied by NMR. The ^{19}F nucleus provides a magnetic label for hydroxyl via reagents such as hexafluoroacetone, and may allow identification of different environments for such groups. ^{13}C NMR is suitable for characterising non-phenolic oxygen groups, since the resonances of carbon in carbonyl and aromatic ether groups are well separated. Basic nitrogen can be studied by ^1H and ^{19}F NMR via hydrogen-bonding interactions with model phenols such as 2,6-xylenol and p-fluorophenol. For neutral nitrogen, labelling with ^{19}F, using e.g. trifluoroacetyl imidazole, shows promise.

1. INTRODUCTION

Supercritical gas (SCG) extraction of coal with aromatic solvents, such as toluene, at temperatures around 690 K and pressures of about 200 bar (1) gives up to 50% d.a.f. coal as a homogeneous extract, which is then subjected to catalytic hydrocracking to produce liquid products. Characterisation of heteroatoms in the extract is important in helping to identify species which may contribute to catalyst poisoning.

Established titrimetric methods for hydroxyl group (2,3) and basic nitrogen group (4,5) determinations are of great value in structural characterisation of extracts. There are, however, no established procedures for the measurement of non-hydroxylic functions or neutral nitrogen functions. We describe here our attempts to compliment and extend existing functional group methods by utilising the NMR spectroscopic methods which are summarised in Table 1. Hydroxyl groups have been determined by ^1H and ^{19}F spectroscopy following derivatisation with trimethylsilyl (groups) and adduction with hexafluoroacetone (HFA). Non-hydroxyl groups have been determined directly from ^{13}C NMR spectroscopy. Basic nitrogen groups have been estimated from their interaction with 2,6-xylenol by observing the changes in the -OH chemical shift. Preliminary results using an alternative ^{19}F NMR method with p-fluorophenol have been obtained. Derivatisation with trifluoroacetyl imidazole, which acts as an ^{19}F magnetic label, is under investigation as a possible route for estimating neutral nitrogen directly.

2. EXPERIMENTAL

The SCG extracts were fractionated by solvent separation and silica gel adsorption chromatography, as previously described (6). Asphaltenes and methylated asphaltenes (prepared by the method used by Liotta (7)) were separated by Sternberg's acid/base procedure (8). Silylation of the extract fractions was carried out as previously (9), and HFA adducts of some asphaltene fractions were prepared by bubbling the gas into ethyl acetate solutions (10). Also, trifluoroacetyl esters of carbazole and indole were prepared by warming at 80°C in pyridine with trifluoroacetyl imidazole for 30 minutes.

^{1}H NMR spectra were obtained at 60 and 220 MHz using Perkin-Elmer R24B and R34 instruments respectively. For the ^{1}H NMR studies of basic nitrogen, silylated extract fractions were added to 0.2 molar 2,6-xylenol in carbon tetrachloride, and changes in the hydroxyl chemical shift were observed. ^{13}C NMR spectra were obtained at 45 MHz in chloroform-d using a Bruker WH 180WB instrument under experimental conditions which have been shown to yield quantitative data (11). ^{19}F NMR spectra were obtained at 84.6 MHz using a Bruker WH90 instrument; furfuryl alcohol was used as an external standard for determination of -OH contents from the spectra of HFA adducts. The procedure described by Gurka and Taft (12) was followed for studying basic nitrogen using 0.01 molar p-fluorophenol where p-fluoroanisole is employed as an internal standard.

Basic nitrogen contents were also determined by non-aqueous potentiometric titration (4,5) and acidic hydroxyl contents were measured by enthalpimetric titration (3,6). Gas chromatographic analysis was carried out on the trifluoroacetyl esters of indole and carbazole.

3. RESULTS AND DISCUSSION

3.1 Hydroxyl Oxygen

The hydroxyl contents determined from the intensity of the $-OSi(CH_3)_3$ band in the ^{1}H NMR spectra of extract fractions were in reasonable agreement with the values obtained by enthalpimetric titration (see Table 2), indicating that all the hydroxyl groups in the extracts have been silylated. In addition, silylation gives a significant enhancement of extract solubility (9). The presence of non-acidic (alcoholic) hydroxyl groups was discounted since there was no evidence of $-OCH_2$ resonances in the ^{13}C NMR spectra. Figure 1 is the ^{1}H NMR spectrum of the silylated benzene-insolubles from an SCG extract of bituminous coal. It shows that the $-OSi(CH_3)_3$ band, which is well separated from the other aliphatic resonances, has a maximum at 0.3 ppm with a broad shoulder extending to -1 ppm indicative of the presence of both unhindered (meta- and para-substituted) and hindered (ortho-substituted) phenolic groups (13). Unlike the spectra of Synthoil products (14), no splitting of the $-OSi(CH_3)_3$ band was observed at 220 MHz. The two sharp peaks between 0 and 0.2 ppm are attributable to a little hexamethyldisiloxane (hydrolysis product) and silylating reagent (hexamethyldisilazane). Methylation (7) and acetylation (15) are alternatives to silylation for measurement of hydroxyl groups, but both these methods have much longer preparation times (1 day) than silylation (1-2 hours). Also, there is an overlap of $-OCH_3$ resonances with ring-joining methylene resonances between 3.4 and 4.2 ppm in coal extracts (6).

Silylation, which gives a reliable measure of the total hydroxyl content, provides little information on the distribution of hydroxyl groups. On the other hand, HFA adducts considerably less than half the total number of hydroxyl groups (see Table 2), but gives a good separation in the ^{19}F NMR spectra between hindered and unhindered phenolic hydroxyl groups. The evidence

obtained so far suggests that there are similar numbers of hindered and unhindered groups in an asphaltene SCG extract fraction of a bituminous coal.

3.2 Non-Hydroxyl Oxygen

^{13}C NMR spectroscopy is particularly useful for assessing the environments of non-hydroxyl groups because the resonances due to carbonyl groups, which lie between 170 and 210 ppm, are well separated from those due to aromatic ethers (148-168 ppm) and aliphatic ethers (55-70 ppm) (16), although the resonances of aromatic ether groups partially overlap with those of phenolic hydroxyl groups (148-158 ppm). Figure 2 shows that no carbonyl and aliphatic ether resonances are discernible in the spectrum of the asphaltene fraction of an SCG extract of bituminous coal, but the distinct band between 158 and 168 ppm is solely attributed to aromatic ether groups. From silylation and integration of the C_{AR}-O band between 148 and 168 ppm, the aromatic ether groups were estimated to account for 30% of the total oxygen content in SCG extracts of bituminous coal.

3.3 Basic Nitrogen

The changes observed in the position of the hydroxyl band in the ^{1}H NMR spectrum of 0.2 molar 2,6-xylenol when (a) model compounds and (b) silylated coal extracts were added are shown in Table 3. Linear plots of the concentration of the basic species against shift in the spectrum were found up to a concentration of about 0.15 molar of the basic species and the values shown in Table 3 were taken from those graphs. A similar correlation was found by Tewari et al (17) who used o-phenyl phenol, but in the present work 2,6-xylenol was preferred because it gives a sharp hydroxyl resonance in CCl_4. The hydroxyl chemical shift of 2,6-xylenol on its own remains constant at 4.3 ppm for concentrations 0.2 molar, which indicates that hydrogen bonding of 2,6-xylenol itself ceases to be significant at these concentrations. For the SCG extract fractions prior silylation was required to prevent exchange of hydroxyl hydrogen between the extract and 2,6-xylenol.

The results of the studies on model compounds (Table 3) show that little change in chemical shift for non-basic species, such as dibenzofuran and indole occurs while changes between 0.8 and 1.2 ppm/0.1 mole were obtained for alkyl substituted pyridines and quinolines. The changes in hydroxyl chemical shift generally increased with increasing degree of alkyl substitution and it is thought that di- and trisubstituted pyridines are the most realistic models for basic nitrogen environments in SCG extracts. The changes in chemical shift were found to vary greatly for the silylated SCG extract fractions and an encouraging correlation, shown in Figure 3, was obtained with basic nitrogen contents determined by non-aqueous potentiometric titration.

In an alternative approach, ^{19}F NMR was utilised and preliminary results obtained with 0.01 molar p-fluorophenol suggest that some correlation may exist between the ^{19}F chemical shift titration curves obtained for silylated SCG extract fraction and basic nitrogen content. For model bases, the change in ^{19}F chemical shift reaches a maximum value, e.g. 2.5 ppm for pyridine, when large concentrations (0.4 molar) have been added. However, for extract fractions, this maximum value cannot be measured directly because of their limited solubility in CCl_4, and therefore information has to be derived from the titration curves obtained for low (0.2 molar) extract concentrations.

To isolate basic fractions for the studies described above, Sternberg's acid/base procedure (8) was employed for the asphaltenes of a bituminous coal SCG extract. This gave 60% bases which is significantly larger than the amounts thought to be present by the -OH chemical shift method (30%) and by

non-aqueous potentiometric titration (20%). The analysis of the base-hydrochloride salt suggested that not every molecule contained a basic nitrogen group. To help to resolve this issue, methylated asphaltenes were separated by the same acid/base procedure, but only 20% of bases was obtained, indicating that the acid/base procedure is inappropriate for SCG extracts of bituminous coals, probably due to the relatively low basic nitrogen contents and high phenolic hydroxyl contents.

3.4 Non-Basic Nitrogen

Recently, trifluoroacetyl derivatives of indole and carbazole (50% yield) have been prepared with trifluoroacetyl chloride (18). This is an important development since most non-basic nitrogen in extracts of bituminous coal is thought to be in the form of aromatic secondary amines. In the present work, we found that 90% of indole and carbazole can be derivatised using trifluoroacetyl imidazole. In an attempt to measure non-basic nitrogen in SCG extracts, methylation prior to esterification with this reagent and detection by ^{19}F NMR is being carried out.

4. CONCLUSIONS

The results of this investigation demonstrate that NMR methods (^{1}H, ^{13}C, ^{19}F) offer viable alternatives to existing titration techniques for determining phenolic hydroxyl and basic nitrogen in coal extracts and provide ways for the direct measurement of non-hydroxyl and non-basic nitrogen groups.

5. ACKNOWLEDGEMENTS

The authors wish to thank the European Coal and Steel Community for financial support, Mr. M.P. Mendoza for carrying out basic nitrogen and acidic hydroxyl determinations and the National Coal Board for permission to publish this paper. The views expressed are those of the authors and not necessarily those of the Board.

6. REFERENCES

1. Whitehead, J.C. and Williams, D.F., J. Inst. Fuel, 48, 182 (1975).
2. Blom, L., Edelhausen, L. and van Krevelen, D.W., Fuel, 36, 135 (1957).
3. Vaughan, G.A. and Swithenbank, J.J., Analyst, 95, 891 (1970).
4. Moore, R.T., McCutchan, P. and Young, D.A., Anal. Chem., 23, 1639 (1951).
5. Darlage, L.J., Finkbone, H.N., King, S.J., Ghosal, J. and Bailey, M.E., Fuel, 57, 479 (1978).
6. Bartle, K.D., Ladner, W.R., Martin, T.G., Snape, C.E. and Williams, D.F., Fuel, 58, 413 (1979).
7. Liotta, R., Fuel, 58, 724 (1979).
8. Sternberg, H.W., Science, 188, 49 (1975).
9. Snape, C.E. and Bartle, K.D., Fuel, 58, 898 (1979).
10. Leader, G.R., Anal. Chem., 45, 1700 (1973).
11. Ladner, W.R. and Snape, C.E., Fuel, 57, 656 (1978).
12. Gurka, D. and Taft, R.W., J.A.C.S., 91, 4794 (1969).
13. Schwager, I. and Yen, T.F., Fuel, 58, 219 (1979).
14. Schweighardt, F.K., Retcofsky, H.L., Friedman, S. and Hough, M., Anal. Chem., 50, 368 (1978).
15. Baltisberger, R.J., Patel, K.M., Stenberg, V.I. and Woolsey, N.F., ACS, Div. Fuel Chem., 51(2), 310 (1979).
16. Snape, C.E., Ladner, W.R. and Bartle, K.D., Anal. Chem., 51, 2189 (1979).
17. Tewari, K.C., Kan, N., Susco, D.M. and Li, N.C., Anal. Chem., 51, 182 (1979).
18. Dorn, H.C., Szabo, P., Koller, K. and Glass, T., ACS, Div. Fuel Chem., 51(2), 309 (1979).

Table 1 Summary of NMR Methods for Heteroatoms

Group	NMR Nucleus	Method
Hydroxyl oxygen	^{1}H ^{19}F	Silylation Adduction with hexafluoroacetone
Non-hydroxyl oxygen	^{13}C	Observation of ^{13}C chemical shifts
Basic nitrogen	^{1}H ^{19}F	Observation of change in hydroxyl chemical shift of 0.2 molar 2,6-xylenol Observation of change in chemical shift of 0.01 molar p-fluorophenol
Neutral nitrogen	^{19}F	Esterification with trifluoroacetyl imidazole

Table 2 Hydroxyl Contents of SCG Extract Fractions

Fraction	% Hydroxyl		
	Enthalpimetry	Silylation	HFA Adduction
Asphaltenes, bituminous coal	6.3	6.3	1.4
Benzene-insolubles, bituminous coal	6.6	7.2	N.D.
Acid asphaltenes, bituminous coal	6.0	5.3	N.D.
Asphaltenes, perhydrous coal	4.7	4.6	N.D.

N.D. = Not Determined

Table 3 Hydroxyl Chemical Shift Changes of 0.2 molar 2,6-xylenol on the Addition of 0.1 moles of (a) model compounds and (b) silylated SCG extract fractions

Model Compound (a)	Chemical Shift Change ppm (from 4.3 ppm)	Silylated SCG Extract Fraction (b)	Chemical Shift Change ppm (from 4.3 ppm)
Indole	0.02	Bituminous coal	
Dibenzofuran	0.02		
Anisole	0.02	Aromatic fraction, n-pentane solubles	0.05
Tetrahydrofuran	0.15		
Quinoline	0.87	Polar fraction, n-pentane solubles	0.24
Pyridine	0.82		
2-methyl pyridine	0.96	Asphaltenes	0.35
3-methyl pyridine	1.10		
4-methyl pyridine	1.00	Perhydrous coal	
2-ethyl pyridine	0.85		
4-ethyl pyridine	0.85	Asphaltenes	0.35
2,3-dimethyl pyridine	1.00		
2,5-dimethyl pyridine	0.97	Lignite	
2,6-dimethyl pyridine	0.90		
3.4-dimethyl pyridine	1.08	Asphaltenes	1.2
2,4,6-trimethyl pyridine	1.16		
4-methyl quinoline	1.16		

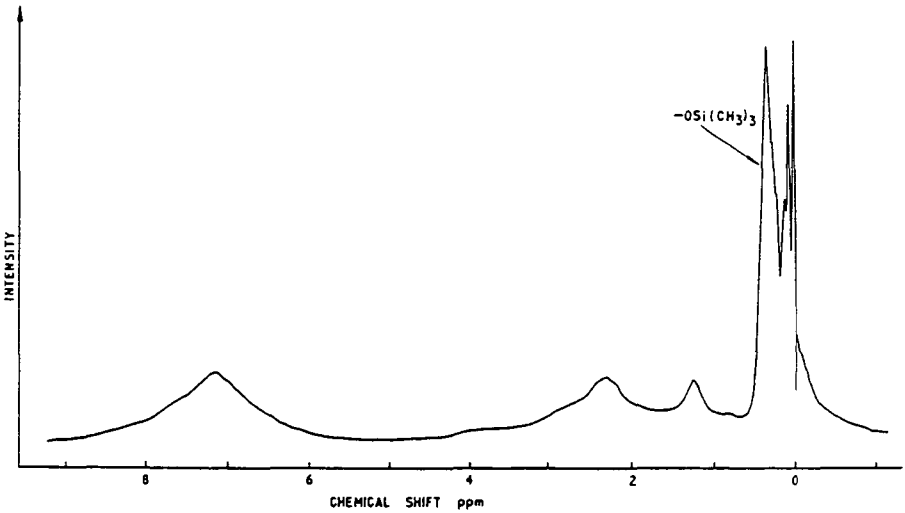

FIGURE 1. ^1H NMR SPECTRUM OF SILYLATED BENZENE INSOLUBLES FROM SCG EXTRACT.

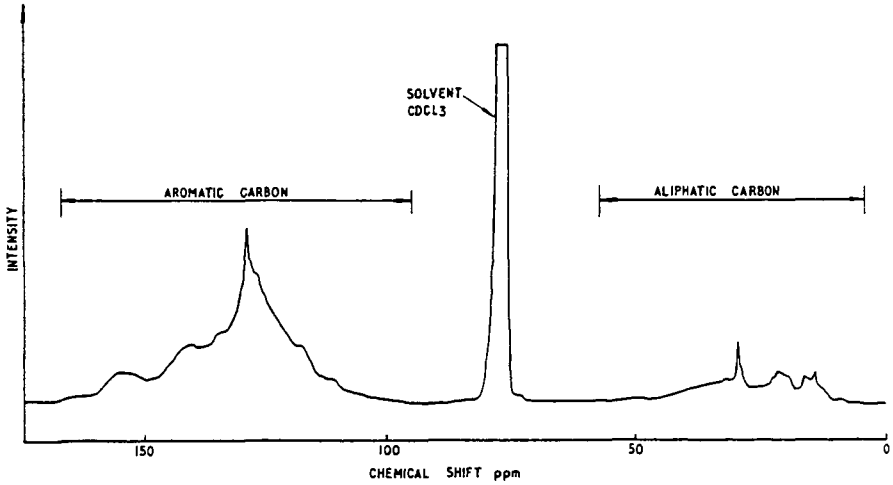

FIGURE 2. ^{13}C NMR SPECTRUM OF ASPHALTENES FROM SCG EXTRACT.

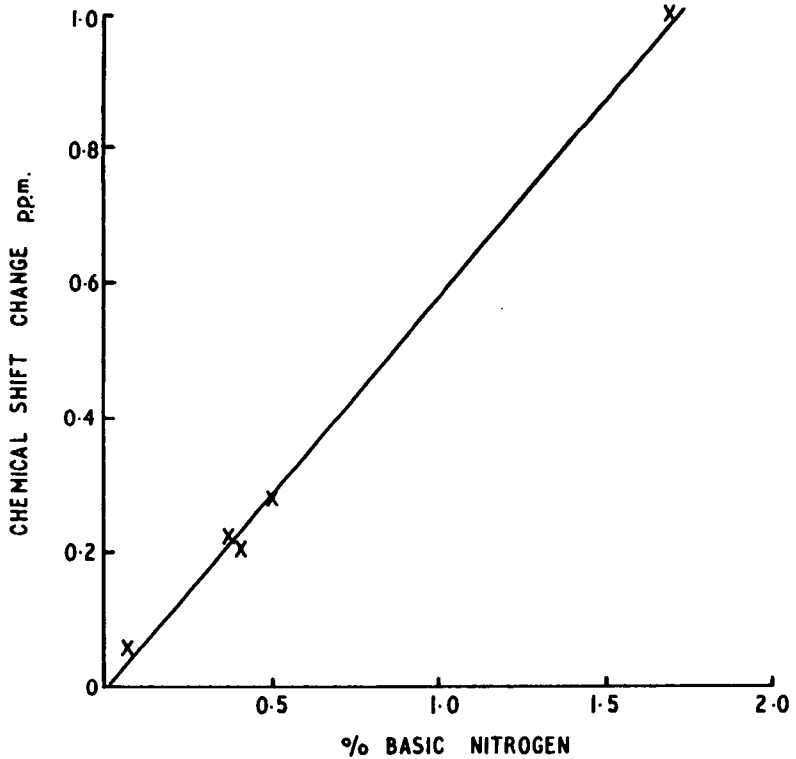

FIGURE 3. PLOT OF HYDROXYL CHEMICAL SHIFT CHANGES FOR 0·2 MOLAR 2,6 XYLENOL ON ADDITION OF 50mg SAMPLE vs % BASIC NITROGEN FOR SCG EXTRACT FRACTIONS.

MEASUREMENT OF THE REACTIVITY OF A KENTUCKY 9 AND 11 COAL USING A MICROAUTOCLAVE

Shuji Mori and Burtron H. Davis

University of Kentucky, Institute for Mining and Minerals Research
Iron Works Pike P.O. Box 13015, Lexington, KY 40583

The liquefaction reactivity of Kentucky #9 and #11 coal was measured in a micro-autoclave. The conversions were carried out using a tetralin solvent and 2000 psig hydrogen pressure. The noncatalytic conversion, based on pyridine extraction, exhibited a maximum at less than 15 minutes reaction time; reaction times longer than 15 minutes resulted in conversion lower than 90-95% maximum conversion. The catalytic and noncatalytic conversions showed contrasting behavior at reaction times longer than 15 minutes. The conversion continued to increase with time when a cobalt-molybdena catalyst was and secondary reactions caused the "apparent conversion" to decline at reaction times greater than 15 mintues. The noncatalytic reactivity at the maximum conversion depends on the length of time the coal is presoaked in the tetralin solvent; presoaking at room temperature for four days results in a conversion that is about 5% greater than the conversion obtained after only a two hour presoaking.

INTRODUCTION

Attempts have been made to correlate the liquefaction reactivity of coals to the carbon content (1,2), with the petrography (3,4) or with the "reactive maceral" content (5,6). Also, experimental difficulties (7-9) have limited the data available for short reaction times.

Diffusion is usually not a problem for reaction in a conventional batch autoclave with vigorous agitation, but the heatup period is long for such a system and it is difficult to assess the influence of slow heatup on short time coal conversion experiments.

In the present work, a small glass lined reactor capable of a rapid heatup was used to measure the noncatalytic and catalytic coal conversions at short reaction times.

EXPERIMENTAL

Samples of Kentucky No. 9 and No. 11 were ground to -60 mesh and to 16-36 mesh, respectively. The ultimate and proximate analytical data for these materials are given in Table 1.

The reactor, illustrated in Figure 1, was fabricated from 316 SS. A glass liner of about 10cc volume was placed in the reactor. The reactor was attached to a manifold with a pressure gauge and a valve. A thermowell of 1.59mm o.d. (1/16" O.D.) extended into the liquid contained in the reactor.

Approximately 1.5gr of a Kentucky No. 9 coal was mixed with 1.5gr of ground ceramic material as a filler (16-36 mesh); the solids were slurried with approximately 6gr of test value. For the noncatalytic reaction with Kentucky No. 11 coal was approximately 3gr of the coal mixed with 6gr of tetralin. For the catalytic run approximately 1.5gr of Kentucky No. 11 and the same amount of a prereduced Co/Mo catalyst (American Cyanamid HDS-1442-A, 1/16" extrudate) were mixed with approximately 6gr of tetraline. All of the reaction was initiated at 3.45×10^6 N/M^2 (500 psig) hydrogen pressure.

The reactor was immersed to the "nut" top in a fluidized sand bath (Tecam Model SLB-2) at 435^{o}C. The bath temperature decreased slightly when the reactor was introduced, but the temperature was restored to 435^{o}C within approximately one-half minute by manual adjustments of the heater control, and was maintained at 435 $\pm$ 2^{o}C thereafter. Reactor pressure was recorded at one-minute intervals

and temperatures of the reactor and the sand bath were recorded continuously. At the end of the reaction period the reactor was quickly immersed in a cold sand bath for a period of one minute, then quenched in cold water. No mechanical agitation was applied to the reactor or its contents during reaction.

The reactor contents were transferred to a dry, weighed Soxhlet extraction thimble with the aid of pyridine and Sochlet extraction with hot pyridine (150 ml total) was carried out under an atmosphere of nitrogen for a period of 42 hours. Pyridine was replaced with methanol and extraction was continued for six hours, after which the thimble and its contents were dried overnight in a vacuum desiccator over calcium chloride. Drying of the extraction residue was continued in a vacuum oven at 60°C and was considered to be completed when the weight loss between successive four-hour drying periods less than 10mg. Conversion calculations are based on weights of residues and are given on a moisture-ash-free basis.

In the course of this work it became evident that the methanol extraction step did not remove all of the pyridine from the pyridine insolubles and that some pyridine was strongly retained by the residues at 60°C (vacuum). Thorough removal of pyridine could be accomplished at 150°C (vacuum) but the resulting weight losses were too small to change calculated conversions significantly or alter interpretations given below.

RESULTS AND DISCUSSION

For a Kentucky No. 9 coal, the conversion depends on the reaction temperature as shown in Figure 2. The conversion, in the absence of a catalyst, reached a maximum in 10 to 15 minutes and slowly decreased for longer reaction times due to the pyridine-insoluble "coke" formation. Such conversions at 15 minutes are shown in Figure 1 as a function of temperature between 350° and 500°C. Above 450°C, coking is so severe at the reaction time that the coal conversion, based on pyridine-insoluble, appears to be quite low.

Preliminary work indicated that the length of coal presoaking time in the tetralin solvent prior to reaction may alter the maximum conversion. The influence of room temperature presoaking of the coal sample in tetralin was determined for periods varying from two hours to two weeks. The maximum conversion for a 15-minute retention time was three to four percent lower for the two hour presoaking than for soaking for one day or longer (Figure 3). In the other runs in this report a presoaking of 24 hours was employed.

The conversion with and without a catalyst is presented in Figure 4. For the noncatalytic conversion of the Kentucky No. 9 coal at 435°C, a maximum conversion of about 90% is obtained after a reaction time of 10 to 15 minutes. The reproducibility of the conversion for duplicate runs at each retention time was better than ± 1.5%. At reaction times greater than 15 mintues, the conversion shows a gradual decrease. This conversion decline appears to be due to the formation of "pryidine insoluble coke." Petrographic analysis of the residue from the pyridine extraction confirmed the presence of coke at the later reaction times. Some investigators have reported a similar maximum (10) while others have not observed the maximum (11).

The Kentucky No. 9 coal was obtained as a -60 mesh powder. In order to prevent compaction of the coal particles due to settling, the coal was mixed with ceramic particles 16-36 mesh. The larger particle size Kentucky No. 11 coal was run without the ceramic material. The use of the larger coal particles, as well as the ebullating bed agitation due to the initial heating of the bottom of the tall, narrow, reactor, enabled us to obtain reproducible conversion without mechanical agitation.

The temperature dependence of the noncatalytic conversion of a Kentucky No. 11 coal was presented in Figure 2. The conversion at the 15-minute reaction times was nearly the same in the temperature range 400-450°C and this conversion is represented in Figure 4 by the symbol ⊗. The maximum conversion, based on pyridine solubles, is the same for the Kentucky No. 9 and No. 11 coal; however,

many more coals must be converted to verify whether this is generally the case.

The catalytic conversion of a coal should be more rapid than the noncatalytic conversion. However, the observed fifteen minute catalytic conversion is lower than the noncatalytic conversion. The catalytic conversion also differs from the noncatalytic conversion at longer reaction times since the catalytic conversion continues to increase whereas the noncatalytic conversion decreased with longer reaction times.

The catalytic conversion is more difficult to explain than the noncatalytic conversion. One complication is due to chemical changes in the catalyst during the reaction period. In the present runs the catalyst was prereduced at 500°C and transferred to the reactor in a dry box. However, the catalyst is sulfided to some extent during the reaction period. The catalyst used for the 60 minute run contained, after the Sochlet extraction, one wt.% sulfur. However, this amount of sulfur can account for only a small fraction of the lower conversion observed at the 15 minute reaction time. One possibility is that "coke" deposits on the Co-Mo/Al_2O_3 catalyst are responsible for apparent low conversion much the same as observed in the run with Kentucky No. 9 coal with the ceramic material. The catalyst may cause coke deposition more rapidly than the ceramic material since the catalytic conversion is higher at all times than the noncatalytic conversion at 60 minutes with ceramic material present. In addition, the "coke" on the catalytic material appears to be slowly hydrogenated to yield gaseous and liquid products at higher conversions as the reaction time increases.

There are a number of possibilities to explain why the catalytic conversion is lower than the noncatalytic conversion at early reaction times. Another reason for this may be due to a rapid catalytic conversion to secondary products compared to the conversion of coal to primary products. Since these catalytic conversions of primary liquid products are hydrogen consuming, it is possible that the hydrogen donor solvent (and/or hydrogen) is depleted to the point where the primary coal liquefaction is hindered because of lower hydrogen concentration.

TABLE 1

ULTIMATE AND PROXIMATE ANALYSIS

PROXIMATE ANALYSIS (WT.%)	KY-9 COAL[a]	KY-11 COAL[b]
Moisture	1.7	6.47[c]
Ash	10.9	9.81
VM	42.1	38.4
FC	45.3	45.7
ULTIMATE ANALYSIS (WT.%)		
C	66.5	66.89
H	4.9	4.63
N	0.9	0.54
S	4.3	3.11

[a]Calorific value, 12,230 BTU/lb.

[b]Calorific value, 12,310 BTU/lb.

[c]As received basis.

The SRC conversion data in Figure 5 was obtained in the Wilsonville, Alabama 6 ton/day demonstration plant (10) and the H-coal data was obtained in the 3 ton/day PDU at Hydrocarbon Research, Incorporated (11). The conversion, compared on a hydrogen consumption basis, is lower for the runs without a catalyst than when a catalyst was used. The conversions in both runs were based on pyridine soluble materials. Thus, it appears that the data obtained in the microautoclave show the same trend as obtained in the much larger reactors.

REFERENCES

1. Storch, H.H., L.L. Fisher and G.C. Sprunk, "Hydrogenation and Liquefaction of Coal," U.S. Bureau of Mines, 1941, Tech. Paper 622.
2. Fisher, C.H., G.C. Sprunk, A. Eisner, H.J. O'Donnel, "Hydrogenation and Liquefaction of Coal," U.S. Bureau of Mines, 1942, Tech. Prog. Report 642.
3. Stopes, M.C., Roy. Soc. London, Proceedings, Series B, 1919, V, 90.
4. Storch, H.H., Industrial and Engineering Chemistry, 1937, 29, No. 12, 1376.
5. Given, P.H., D.C. Cronauer, W. Spackman, H.L. Lovell, A. Davis and B. Biswas, Fuel 1975, 54, 34.
6. Given, P.H., D.C. Cronauer, W. Spackman, H.L. Lovell, A. Davis and B. Biswas, Fuel 1975, 54, 40.
7. Given, P.H., W. Spackman, A. Davis, P.L. Walker, H.L. Lovell and M. Coleman, "The Relation of Coal Characteristics to Liquefaction Behavior," 1976, FE 2494-1.
8. Given, P.H., W. Spackman, A. Davis, P.L. Walker, H.L. Lovell and M. Coleman 1977, FE 2494-2.
9. Schall, J., "Compilation and Assessment of SRC Experience: Data Book," 1979, EPRI AF-1019.
10. Weber, W.H., J.W. Roberts, G.B. Vsnick, B.H. Cottle, Jr., C.T. Harwell, W.R. Hollenack, C.R. Mcllwain, A.K. Rao, C.G. Churchman, F.L. Pate and G. Haider, EPRI AF-918, Nov., (1978), page 191.
11. H-Coal Integrated Pilot Plant, Phase 1, Final Report, Vol. II, July (1977).

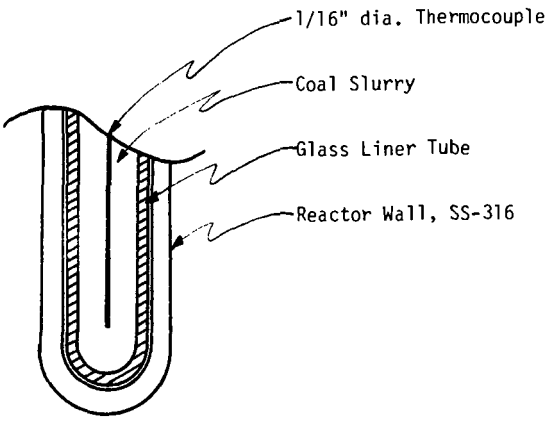

Figure 1. A schematic drawing of the bottom portion of the microautoclave reactor.

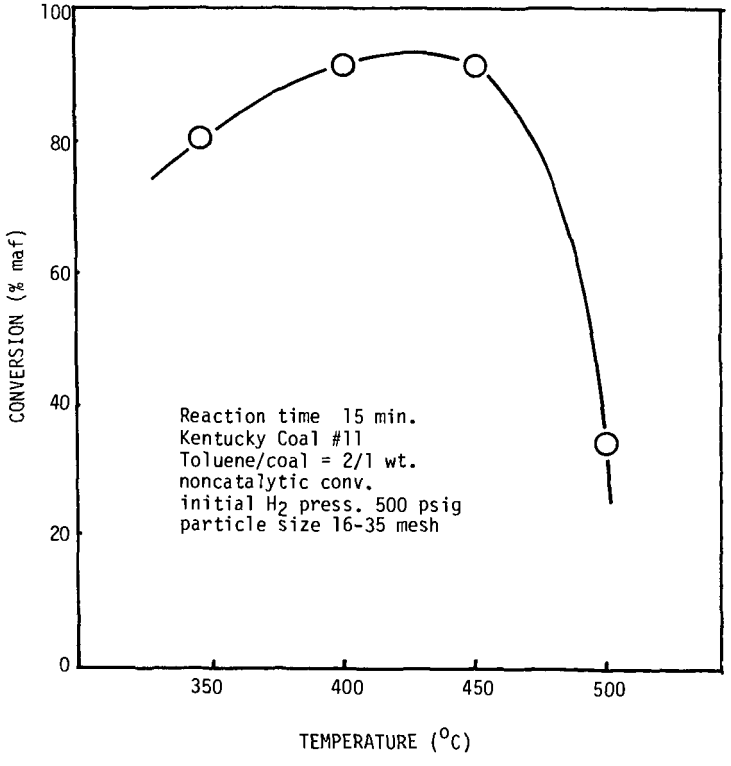

Figure 2. The dependence on the conversion for the noncatalytic reaction at fifteen minutes reaction time.

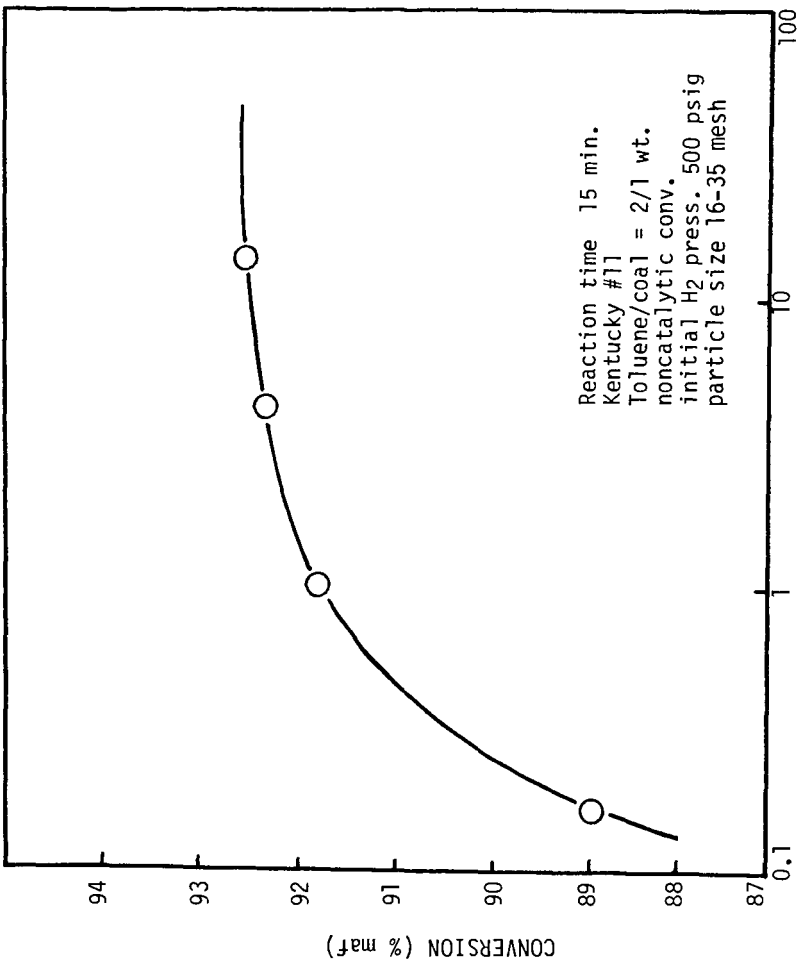

Figure 3. The effect of presoaking on the noncatalytic conversion.

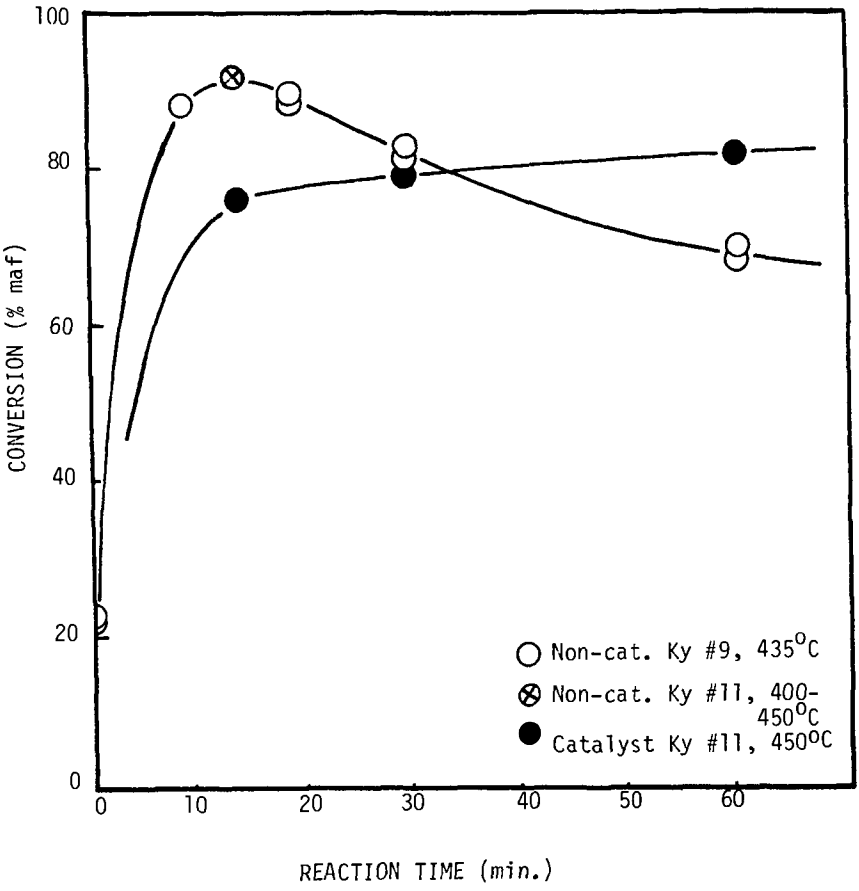

Figure 4. The time dependency of the conversion with and without catalyst.

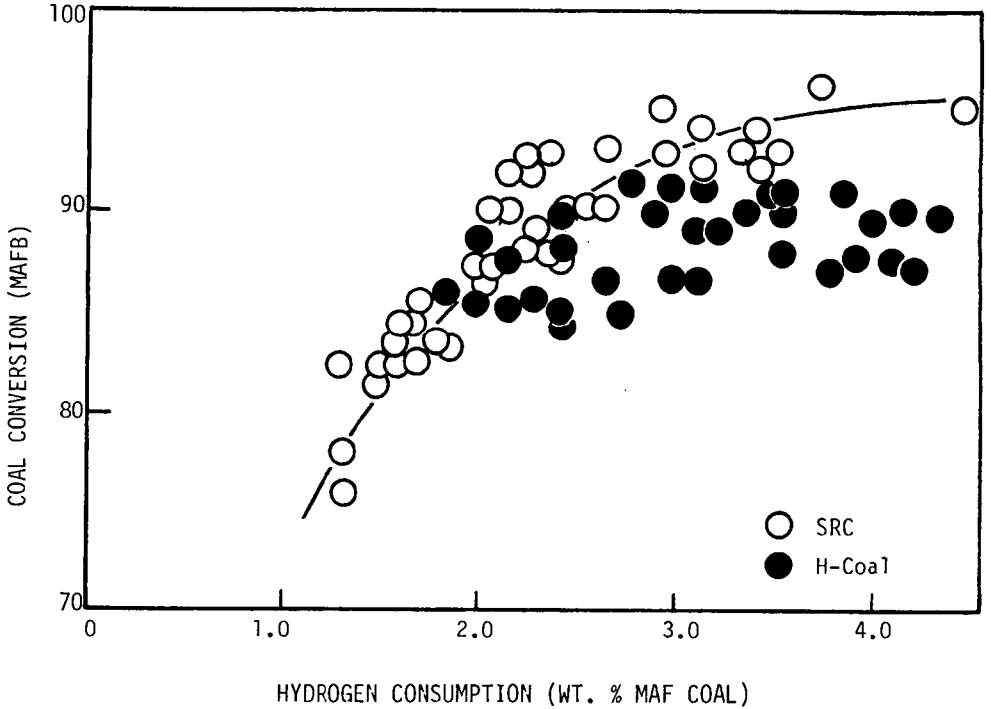

Figure 5. A comparison of the conversion of Illinois #6 coal with and without a catalyst in 3-6 ton/day size reactors in the SRC-I and H-Coal processes.

KINETICS AND MECHANISMS OF THE HYDROLIQUEFACTION OF COAL: ILLINOIS NO. 6, BURNING STAR COAL IN SRC-II HEAVY DISTILLATE*

M. G. Thomas and T. C. Bickel

Sandia National Laboratories, Albuquerque, NM 87185

Introduction

Four major industrial processes are currently being applied to coal liquefaction at the demonstration level, H-Coal[1], Exxon Donor Solvent (EDS)[2], Solvent Refined Coal I (SRC-I) and Solvent Refined Coal II (SRC-II)[3]. One of the reasons for parallel development of these processes is the lack of basic understanding of the reaction mechanisms, activation energies, and rates of reaction of coal liquefaction. We have begun a multifaceted program to delineate information on a number of coal-solvent combinations in order to develop a process kinetic model for coal liquefaction that will better enable process designers to make sound technical decisions.[4]

The present study has been conducted to obtain rates of reaction and activation energies for one coal--Illinois No. 6, Burning Star high volatile bituminous coal--and one solvent--coal-process derived SRC-II Heavy Distillate (450-850°F distillation range). Coal to solvent ratio, reaction time, temperature, and pressure are variables in a parametric study between 275°C and 475°C. Two different types of reactors were employed, a microreactor system for screening and a continuous flow reactor for the derivation of kinetic data. No attempt to generalize the results is made; although the autors believe that the descriptions contained are applicable to other systems. Generalizations will be attempted as the overall study continues.

Experimental

Illinois No. 6, Burning Star Mine coal was used in all experiments. The coal was ground to -45 mesh and riffled into 1 gallon containers. Proximate and ultimate analyses are provided in Table I. The liquefaction solvent used was untreated SRC-II heavy distillate received from the Ft. Lewis, Washington Pilot Plant. Elemental analysis, gravity, and boiling range is provided in Table II. Although the solvent was a 450-850°F cut, it contained ∿ 5-10% pentane insoluble material. The solvent was received in 55 gallon drums, rolled, and transferred to 5 gallon cans from where it was sampled.

Microreactors were used to study the initial dissolution of coal and the effects of solvent/coal ratio on conversion. The microreactors have a total volume of ∿ 20 cm^3, and are designed to operate between 0-2000 psi hydrogen and 25-500°C. The total mass of the reactors is 0.6 Kg. A Tecann fluidized bed sand bath is used for rapid reactor heating and provides a 2-2.5 minute heat-up time. A water quench provides a 90 sec quench between 400° and 50°C. Wrist-action shaking, ∿ 300 cpm, with a 2-inch stroke, is used for mixing. Mass balances are routinely within 1% based upon total reactor charge.

Data for the rates of reaction and activation energies were obtained using a non-recycle continuous flow tubular reactor, Figure 1. The reactor consists of 4 independently heated stages (.203" ID helical coils) and was operated isothermally at 400°, 425°, 450°, and 475°C,

* This work supported by the U.S. Department of Energy.

Table I. Proximate and Ultimate Analysis of Illinois No. 6 Burning Star Coal

Proximate Analysis	Wt %
Moisture	3.41
Ash	10.39
Volatile	36.70
Fixed Carbon	49.50

Ultimate Analysis	Wt %
Moisture	3.41
Carbon	69.90
Hydrogen	4.59
Nitrogen	1.15
Chlorine	0.07
Sulfur	3.06
Ash	10.39
Oxygen (diff)	9.43
	100.00

Sulfur Form	Wt %
Pyritic	1.11
Sulfide	0.09
Organic (diff)	1.86
Total Sulfur	3.06

Table II. Analysis of SRC-II Heavy Distillate

Ash (%)	0.05	
Carbon (%)	89.8	
Hydrogen (%)	7.6	
Nitrogen (%)	1.4	
Sulfur (%)	0.4	
Oxygen (%)	1.8	
Pentane Insols	6%	
Distillate Yield	86.5	850°F

at coal plus solvent mass flowrates of 0.7 to 6 lb/h, hydrogen pressure of 2000 psi, and gas flowrates of 10-200 MSCF per ton of coal. Reaction temperatures are predicted to be attained within 6.5 ft of the reactor inlet and the total length of the reactor was varied between 10-83.5 ft. Liquid and gas samples are obtained separately at atmospheric pressure. Data reported are obtained from analyses of samples withdrawn at steady state conditions; i.e., after 1.5 h at fixed reactor operating conditions. The coal derived products, obtained at the conclusions of the runs, were extracted exhaustively into pentane-soluble (oil), benzene-soluble pentane-insoluble (asphaltene), THF-soluble benzene-insoluble (preasphaltene), and THF-insoluble (inorganics + IOM) fractions. Elemental analyses were provided

by Huffman Laboratories. Viscosities were measured with a Brookfield model LVT viscometer. Gas samples were obtained at all conditions and analyzed with an HP 5840 gas chromatograph equipped with a TC detector. The columns are teflon-lined aluminum packed with 800-100 mesh Poropak Q.[5]

Results and Discussion

In order to establish a kinetic model for coal liquefaction, we have endeavored to determine a stepwise reaction mechanism. The proposed first step is the dissolution of coal. Data from microreactor runs in the temperature range 275°-375°C--below typical liquefaction temperatures--are presented in Table III. There is a small solubility of coal in the solvent at low temperatures, and marked increases at temperatures between 275°C and 350°C. Equilibrium in terms of gas make and solubility are attained rapidly. Up to 350°C, the SRC-II solvent is depleted. Solvent is a reactant with coal.[4] The stoichiometry of the coal-solvent reaction can be estimated by weight loss of solvent and net THF sols. Based upon these data, it appears that the reaction can be represented as

$$1\ \text{Coal} + 3\ \text{Solvent} \rightarrow 3\ \text{Preasphaltene}.$$

This stoichiometry is also consistent with published values for molecular weights of solvent (250), preasphaltene (1000), and coal (2250)[6]. The stoichiometry and approximate molecular weights establish a mass balance for the initial dissolution step. It is also seen that it is primarily the pentane insoluble fraction of the initial solvent--the heavier, more functional portion--that reacts with coal in this initial reaction.

The second reaction step appears to be the decomposition of preasphaltene. In a recent study, reactions of preasphaltene and asphaltene obtained from liquefaction experiments with another Illinois No. 6 coal, River King, were shown to react thermally

$$\left.\begin{array}{l}\text{Preasphaltene} \rightarrow \text{Asphaltene} \\ \text{Asphaltene} \rightarrow \text{Oil.}^{7}\end{array}\right\} \begin{array}{l}400\text{-}425°\text{C} \\ 10\text{-}15\ \text{minutes}\end{array}$$

Both coal-derived substrates appear to react in a series reaction path, ultimately producing oil. Thus, the mechanistic reaction path used for subsequent kinetic analysis is

$$\text{Coal} + \text{Solvent} \xrightarrow{1.} \text{Preasphaltene} \xrightarrow{2.} \text{Asphaltene} \longrightarrow \text{Oil}$$

Although the production of gas accompanies each step, the primary gas production occurs at short time and is primarily (in terms of mass) associated with coal.

Kinetics Treatment

The coal liquefaction reaction kinetics were determined using data from a non-recycle continuous tubular flow reactor (Figure 1). The reaction mechanisms were the result of the microreactor experiments previously described. The scale-up to the continuous flow reactor is necessary for reaction kinetics in order for industrial application of the results because the microreactor eliminated aspects of the overall reaction scheme such as hydrogen mass transfer, and multiphase flow regimes, and mixing.

Table III. Microreactor Data from Liquefaction Runs Between 275-375°C

Run No.	Run Parameters		Gas Make		Liquid Product, Wt				Conversion	
	Temp °C	Time	CO_2	C_1-C_4	PreA	THF Insols	Asph	Oil	Toluene	THF
1	275	6.5 min	1.49	-	.36	2.3	-	-	-	15
2	300	6.5 min	1.25	-	.50	2.1	.46	4.7	-7	24
3	300	26 min	1.85	.04	.59	2.1	.31	5.0	-1	24
4	325	6.5 min	1.32	.03	.47	1.7	.48	5.2	15	40
5	325	26 min	1.83	.09	.60	1.6	.38	5.2	11	44
6	350	6.5 min	1.84	.17	.65	1.5	.61	5.1	16	44
7	375	6.5 min	2.30	.47	.92	1.2	-	-	-	61
8	375	26 min	2.72	1.29	.90	1.0	-	-	-	70
9	Blank	-	-	-	0	2.67	.58	4.8	-	-

Because of the complicated multiphase flow in the reactor, we are unable (at this time) to quantitatively determine the residence time of each reactant phase in the reactor. As a consequence, reaction times are expressed as space time, θ, i.e.,

$$\theta = \frac{\text{Volume of Reactor}}{\text{Coal/Solvent Slurry Mass Flowrate}} \left(\frac{ft^3\text{-hr}}{lb_m}\right)$$

It is possible to determine the activation energy of the various liquefaction reactions, but the pre-exponential multiplier (frequency factor) in the Arrhenius type rate constant will be a function of the spacetime and therefore is questionable when used in other reactor systems.

The data obtained using the flow reactor were analyzed as previously described. The product slate from the reactor was found to be independent of the gas flowrate over the range used (10-200 MSCF/ton coal). Thus, hydrogen transfer from the vapor phase to the liquid phase was insignificant for this work and was eliminated from the further consideration. The kinetic parameters were estimated using a non-linear minimization algorithm (Powell's conjugate gradient method[8]) in conjunction with a Runga Khulta 7/8 numerical integrator. Based upon the reaction mechanism and stoichiometry determined from the microreactors, a component mass balance can be written for the system:

$$\frac{d[C]}{dt} = -0.8\ k_1[C][S] + k_2[P] - k_7[C] \qquad 1)$$

$$\frac{d[P]}{dt} = k_1[C][S] - k_2[P] - k_3[P] + k_4[A][S] \qquad 2)$$

$$\frac{d[A]}{dt} = 0.8\ k_3[P] - 0.8\ k_4[A][S] - k_5[A] + k_6[S]^3 \qquad 3)$$

$$\frac{d[S]}{dt} = -0.2\ k_1[C][S] + 0.2\ k_3[P] - 0.2\ k_4[A][S] + k_5[A] - k_6[S]^3 \qquad 4)$$

$$\frac{d[G]}{dt} = k_7[C] \qquad 5)$$

where: [C] = weight fraction in whole liquid product (WLP) of coal

[P] = weight fraction in WLP of preasphaltene

[A] = weight fraction in WLP of asphaltene

[S] = weight fraction in WLP of solvent

[G] = weight fraction gas (C_1-C_4, CO, CO_2, H_2S)

t = space time (hr ft^3/lb_m)

k_1-k_7 = Arrhenius rate constants.

The reaction rate constants k_1-k_7 were determined numerically using the data obtained from the tubular flow reactor at a given reactor isothermal operating condition (i.e., Figure 2 as an example). For a given set of k_1-k_7, the concentration profiles as a function of space time of [C], [P], [A], [S], and [G] can be obtained by numerically integrating the mass balance equation (eqns 1-5) using the concentration profiles. By using the deviation between the calculated and experimental concentration profiles as the objective function of an unconstrained minimization algorithm, e.g.,

$$\text{minimize } f(k_1,k_2,\ldots,k_7) = \sum_{j=1}^{n}\sum_{i=1}^{m} \text{abs } \frac{(C^*_{ij} - C_j(t_i))}{\bar{C}_i}$$

$$\bar{C}_i = \begin{cases} C^*_{ij} \text{ if } C^*_{ij} \geq 1.0 \times 10^{-6} \\ 1 \text{ otherwise} \end{cases}$$

where: C^*_{ij} = weight fraction of component j at space time t_i

$C_j(t_i)$ = calculated weight fraction of component j at time t_i

n = number of components (n = 5)

m = number of experimental data points

an optimal set of reaction rate constants k_1-k_7 can be obtained. The technique in effect chooses the best set of k_1-k_7 in order that the deviation between the experimental and calculated concentration profiles is minimized. A set of optimal reaction rate constants is obtained for each isothermal reactor data set. Shown in Figure 2 are the experimental data and the calculated concentration profiles of the

coal, preasphaltene, asphaltene, solvent, and gas components obtained during the 450°C isothermal reactor run. Here, agreement between the experimental data and the predicted concentrations is within experimental precision, ± 2% absolute. The treatment considers isothermal conditions and the initial preasphaltene and IOM concentrations are extrapolated from tubing reactor experiments. Activation energies for the series reactions are presented in Table IV.

Table IV. Activation Energies for Selected Liquefaction Reactions

Activation Energies	Reaction
15	Preasphaltene → Asphaltene
21	Asphaltene → Oil
32	Coal → Preasphaltene

Activation energies are obtained from an Arrhenius treatment of rate constants obtained at four temperatures, 400, 425, 450, and 475°C. The treatment of the entirety of these data is beyond the scope of this presentation and can be found elsewhere.[9]

Summary

We have shown that the liquefaction of Illinois No. 6 Burning Star coal in SRC-II Heavy Distillate procedes via a series reaction:

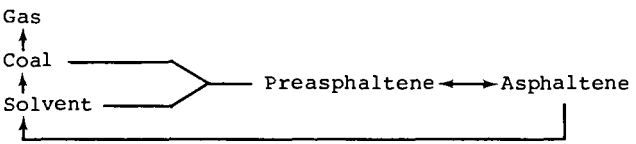

From parametric studies in tubing reactors and a continuous tubular flow reactor, we have calculated stoichiometries, rate constants, and activation energies. The stoichiometries for the reaction at 450°C were

Coal + 3 Solvent → Preasphaltene

Preasphaltene → 2 Asphaltene

Asphaltene → 3 Oil

Activation energies for the preasphaltene and asphaltene conversions are 15 and 21 Kcal/mole, respectively.

References

1. Comolli, A. G., Bernard, R. R., and Johanson, E. S., "Advances in H-Coal," Proceedings of the 14th Intersociety Energy Conversion Engineering Conference, Vol. 1, pp. 815-820, August 5-10, 1979.

2. Epperly, W. R., Schutter, R. T., "Donor Solvent Coal Liquefaction Process," Coal Processing Technology, Vol. V, AIChE, 1979.

3. Schmid, B. K., and Jackson, D. M., "Liquid and Solid Fuels by Recycle SRC," Coal Processing Technology, Vol. V, AIChE, 1979.

4. Thomas, M. G., Traeger, R. K., "A Low Temperature Reaction Path for Coal Liquefaction," Preprints of the National ACS Meeting, Div. of Fuel, Vol. 24, No. 3, September 1979.

5. Thomas, M. G., Noles, G. T., "Sandia Fossil Fuel Analytical Laboratory," Sandia National Laboratories Report SAND-78-0088, April 1978.

6. Sternberg, H. W., Raymond, R., and Schweighard, F. K., Science, 188, 49 (1975).

7. Thomas, M. G., Sample, D. G., Floyd, J. L., "Selectivity of Catalysts Toward Coal-Derived Products," submitted to FUEL, January 1980.

8. Himmelblau, D. M., Applied Non-linear Programming, McGraw-Hill, New York, 1972.

9. Thomas, M. G., Bickel, T. C., "The Kinetics and Reaction Mechanisms in Coal Liquefaction," manuscript in preparation.

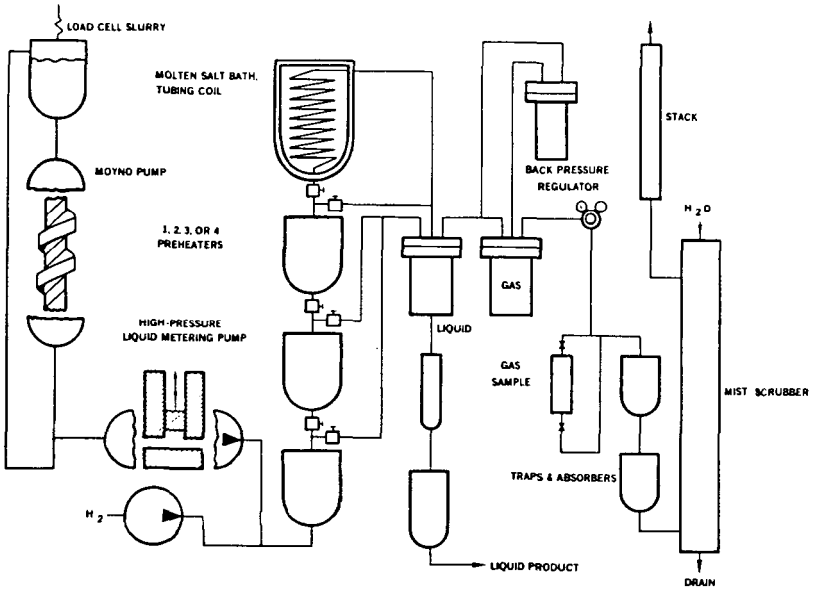

Figure 1. Continuous Coal Liquefaction Reactor

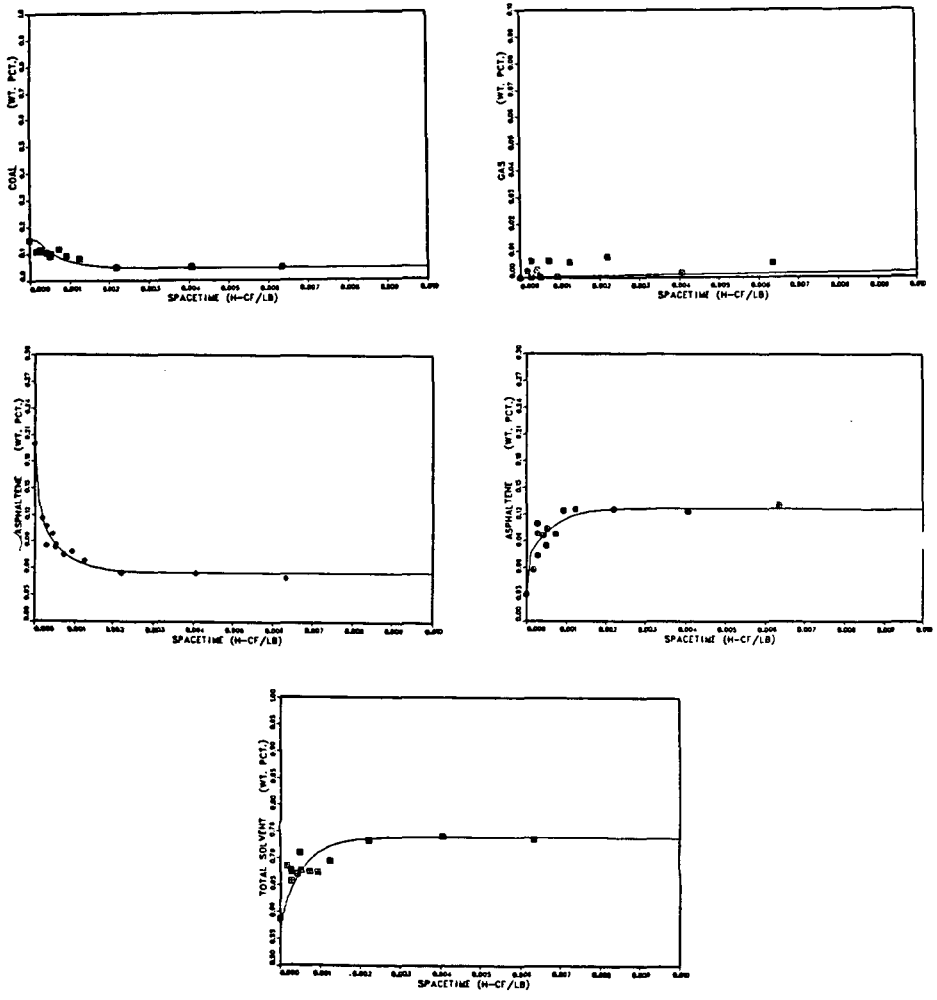

Figure 2. Experimental data and model predictions of Concentrations as a function of time.

Chemical Changes In Coal Liquefaction

N. C. Deno, Kenneth W. Curry, J. Edward Cwynar, A. Daniel Jones, Robert D. Minard, Thomas Potter, Walter G. Rakitsky, and Karen Wagner

Department of Chemistry, Pennsylvania State University, University Park, PA 16802

Mobil Research and Development Corp. supplied five coals and their soluble and insoluble fractions after 3 mins solvent refining and their soluble fraction after 90 mins solvent refining. All samples were oxidatively degraded with CF_3CO_3H-H_2SO_4. The major effects of solvent refining on molecular structure were the large increases in arylmethyl, arylphenyl, and total aromatic material.

Liquefaction (solvent refining) of coal involves thermolysis of benzyl-oxygen and/or benzyl-benzyl bonds as the first step in the depolymerization. This view derives from NMR studies[1], studies with model compounds[1,2], and oxidative degradations with $Na_2Cr_2O_7$[3] and CF_3CO_3H[4]. The oxidative degradations with CF_3CO_3H are now extended to five new coals. Products have been determined from the original coal, the soluble and insoluble fraction after 3 mins. and the soluble fraction after 90 mins. The data are summarized in Tables 1 and 2.

The best method for determining the amount of arymethyl groups in coals is from the yield of acetic acid formed in oxidative degradation with CF_3CO_3H-H_2SO_4[4-6]. The data from this method are shown in Table 1. The following observations and interpretations are made.

1. A sharp increase in arylmethyl accompanies liquefaction in all five coals and in two coals which were studied earlier[4]. This increase is the result of thermal cleavage to benzyl radicals and abstraction of hydrogen atoms by the benzyl radicals to form arylmethyl.

2. All five coals give about the same percentage increase in arylmethyl after 90 mins of solvent refining, but not after 3 mins. This indicates that benzyl radicals form from more than one type of structure. Arylmethyl formation is 87-99% complete in the last three coals in Table 1 after 3 mins whereas it is only 33% and 50% complete in the first two coals. Based on studies of model compounds[1,2], it is attractive to ascribe arylmethyl formation in 3 mins to cleavage of benzyl ethers and slower cleavage to bibenzyl structures. Despite the obvious oversimplification, this is the best estimate as yet of the relative amounts of C-O and C-C cleavage. It is also direct evidence for bibenzyl structures in PSOC 372 and 330 and the first direct evidence for such structures in any coal.

3. It might have been expected that the more arylmethyl, the more cleavage, and the more SRC. In fact the opposite is shown in Table 1. The conflict would be resolved if coal liquefaction depended more on certain critical cleavages and the conversion of a 3-dimensional polymer to a 1-dimensional polymer than on the total amount of cleavage and the extent of depolymerization.

4. The amount of arylmethyl in the residue (3 min) is about the same as in the original coal. This indicates that arylmethyls do not play any role in liquefaction as expected.

5. No higher homologs of acetic acid were observed indicating the absence of arylalkyls above methyl.

The data in Table 2 show that biaryl structures are rare or absent in the original coals but appear in significant quantity on liquefaction. The foremost evidence for this are the changes in yields of benzoic acid (column 136). This product was not observed from any of the five coals, but it was an important product from SRC (solvent refined coal). Model studies have shown that benzoic acid forms from biphenyl and other biaryls in which one of the phenyl rings is unsubstituted. It does not form from alkylbenzenes, a variety of polyaromatics, and many other model compounds[5,6].

There are three other products in Table 2 whose appearance or increase indicate biaryl structures. These are benzene-1,4-dicarboxylic acid (194b), benzene-1,3-dicarboxylic acid (194c), and benzene-1,3,5-tricarboxylic acid (310b). All have non-adjacent carboxyl groups. These are more characteristic of biaryl structures in contrast to fused aromatics which form products with adjacent (1,2) carboxyls.

We interpret the appearance of simple phenyl substituents to the reductive removal of the heteroatom in benzthiophenes, benzfurans, and possibly benzpyrroles. If one of the benz rings is unsubstituted, such a reductive hydrogenolysis would create a simple phenyl group attached to the remaining polymer by a biphenyl type of bond. While phenyl groups would also be generated by hydrogenolysis of fluorenes, fluorenes are expected to be stable under the conditions of liquefaction.

On the basis of oxidative degradations of Illinois no. 6 and Wyodak coals before and after liquefaction, it was concluded that the aromatic structure increases on liquefaction[4]. The evidence was an increase in phthalic (benzene-1,2-dicarboxylic) acid, which is the dominant product from most polyaromatic systems[5].

The increase in aromatic structure is also shown by certain lactones which are minor products from oxidation of a variety of polyaromatic hydrocarbons[5]. They appear from oxidation of the solvent refined samples but not from the original coals (Table 4).

Oxidation of coals with 40% HNO_3 at 60° provides a reliable method for determining the amounts and lengths of linear alkane chains in coals by converting such chains to linear diacids of two less carbons[7]. As expected, the amounts and lengths showed no change on solvent refining on Illinois no. 6 Monterey coal.

Illinois no. 6 Monterey coal and Wyodak coal showed marked decreases in the yields of succinic acid after solvent refining[4]. This was interpreted as showing a marked decrease in dihydrophenanthrene structures. This decrease in succinic acid product is not shown by the five coals in Table 2. It is possible that dihydroaromatic structures donate hydrogen to benzyl radicals but are regenerated by transfer of hydrogen from solvent to the coal polymer.

ACKNOWLEDGEMENT

We are grateful for support for this work from EPRI (Electric Power Research Institute) and DOE (U.S. Department of Energy). We are also grateful to

Dr. Duayne D. Whitehurst of Mobil Research and Development Corporation for supplying the samples of coals and solvent refining coals.

EXPERIMENTAL

The samples were kindly provided by Dr. D. D. Whitehurst of Mobile Research and Development Corporation. The parent coals were bituminous and had been originally obtained from the Penn State Coal Base and carry their code number.

The procedure for oxidation with CF_3CO_3H-H_2SO_4 is identical to that reported earlier[5]. The analysis and conversion to methyl esters was modified as follows.

The acetic acid was determined from the proton magnetic resonance spectrum of the filtered reaction mixture. The area of the acetic acid peak was compared to the area of the peak of a weighed amount of DSS as originally described[6]. This method is preferable to the distillation method[5] providing line broadening is not too severe.

The isolation of the methyl esters has been made more quantitative by modifying the procedure for isolation. The removal of volatile material and the conversion to methyl esters was unchanged[5]. After esterification with BF_3 in methanol, 100 cm^3 of saturated aqueous NaCl was added and the mixture extracted with three 35 cm^3 portions of CH_2Cl_2. The combined CH_2Cl_2extracts were washed with 100 $cm^3$of 3% $NaHCO_3$ followed by washing with saturated aq. NaCl. A weighed amount of acetophenone was added as an internal standard. The solution was dried over $MgSO_4$. The responses to the detector in the gas chromatogram were calculated from effective carbon numbers as before[5].

REFERENCES

1. Whitehurst, D. D., Mitchell, T. O., Farcasiu, M., and Dickert, J. J., Jr., "The Nature and Origin of Asphaltenes in Processed Coals," EPRI Report AF-480, Second Annual Report under Project RP-410-1, July 1977

2. Hayatsu, r., Winans, R. E., Scott, R. G., Moore, L. P., and Studier, M. H. in Organic Chemistry of Coal, Am. Chem. Soc. Symposium Series No. 71, J.W. Larsen, ed., 1978

3. Benjamin, B. M., Raaen, V. F., Maupin, P. H., Brown, L. L., and Collins, C. J. Fuel 1978, 57, 269

4. Deno, N., Greigger, B. A., Jones, A. D., Rakitsky, W. G., Whitehurst, D. D., and Mitchell, T. O. Fuel, in press

5. Deno, N., Curry, K. W., Greigger, B. A., Jones, A. D., Rakitsky, W. G., Smith, K. A., Wagner, K., and Minard, R. D. Fuel, in press

6. Deno, N., Greigger, B. A., and Stroud, S. G. Fuel 1978, 57, 455

7. Deno, N., Curry, K. W., Jones, A. D., Keegan, K. R., Rakitsky, W.G., Richter, C. A., and Minard, R. D. Fuel, submitted

Table 1 Yields of acetic acid from oxidative degradations with CF_3CO_3H-H_2SO_4

Name	Penn State coal base number[a]				
	372 Kentucky Imboden	330 Penn. Middle Kittaning	256 Penn. Lower Freeport	312 Arizona Red	405 Oklahoma Lower Hartshorne
% liquified[a] (3 min)	79	70	65	51	25
% C (maf)	85.9	83.5	88.2	78.4	89.8
rank	HVA	HVB	med. vol.	HVC	low vol.
	Yield of acetic acid (meq. per g of maf)[b]				
parent coal	0.44	0.33	0.31	0.42	0.31
SRC (3 min)	0.77	0.74	1.05	1.46	1.51
SRC (90 min)	1.45	1.15	1.06	1.60	1.69
residue (3 min)	0.33	0.41	0.27	0.27	0.24

[a] Samples and liquefaction data were supplied by D. D. Whitehurst, Mobil Research and Development Corp.

[b] The percentages of moisture (m) and ash (a) are available from the Penn State Coal Base computer printouts. The SRC samples had negligible moisture or ash. In calculating the yields of acetic acid from the residue, it was assumed that all of the ash in the coal was retained in the residue in correcting to a maf (moisture and ash free) basis.

Table 2 Absolute yields (mg per g maf) of products[a] from oxidative degradations with CF_3CO_3H-H_2SO_4

MW of methyl ester	132	146	136	204	218a	218b	194a	194b	194c	276	252a	252b	310a	310b
PSOC-372														
coal	17.7	4.9	---	1.2	0.7	4.3	---	---	---	1.3	3.3	---	2.1	---
SRC (3 m)	10.5	3.7	2.3	0.5	0.7	5.6	---	0.9	0.7	2.0	2.0	0.8	0.9	0.1
SRC (90 m)	13.7	6.8	3.5	0.6	0.5	7.2	---	2.4	1.3	2.0	6.7	2.4	2.4	0.4
res (3 m)	7.6	0.7	0.6	0.3	0.7	1.6	1.0	0.4	0.4	0.2	2.8	---	1.7	0.3
PSOC-330														
coal	21.0	6.1	---	1.2	0.9	2.3	---	0.2	0.2	1.5	1.5	---	1.6	---
SRC (3 m)	18.4	6.8	6.1	1.0	0.4	10.0	---	2.4	---	2.6	6.0	---	1.7	0.2
SRC (90 m)	2.5	7.1	7.1	0.1	0.7	2.8	7.7	4.9	3.2	3.0	9.3	0.1	4.4	1.0
res (3 m)	5.1	4.2	1.5	0.1	0.3	0.6	0.5	0.4	0.4	0.6	2.2	---	1.9	0.7
PSOC-256														
coal	18.7	3.9	---	1.1	0.6	1.6	0.2	0.5	0.4	0.9	3.2	---	2.2	---
SRC (3 m)	6.8	6.2	5.9	0.1	0.8	0.7	2.0	1.9	1.9	2.7	9.3	0.2	5.3	0.7
SRC (90 m)	5.8	8.4	6.6	0.4	1.0	10.2	3.2	3.3	2.3	3.5	12.0	0.1	0.5	1.1
res (3 m)	12.5	3.1	2.3	1.0	0.2	2.4	1.7	0.8	0.6	1.6	7.1	---	2.9	0.5
PSOC-312														
coal	13.8	4.9	---	2.0	1.8	10.7	---	---	0.5	2.8	2.5	0.2	1.1	0.2
SRC (3 m)	6.7	12.8	5.9	1.6	0.8	10.4	---	3.3	---	2.8	3.9	1.3	0.9	0.2
SRC (90 m)	11.7	14.3	4.8	0.3	1.8	6.7	---	2.6	3.1	3.3	8.2	0.1	2.8	0.4
res (3 m)	14.8	3.4	1.6	1.2	0.6	4.9	0.7	0.5	0.7	1.6	3.3	0.2	2.3	0.5
PSOC-405														
coal	7.9	2.4	---	0.6	0.1	2.5	1.3	0.9	0.5	0.8	2.5	0.2	1.0	0.3
SRC (3 m)	3.5	10.7	5.8	0.2	1.4	5.2	2.8	3.6	2.7	2.6	7.2	0.2	4.5	0.6
SRC (90 m)	0.9	9.1	5.3	0.3	1.8	1.3	4.0	6.9	---	3.6	9.1	0.2	2.9	0.4
res (3 m)	10.9	3.9	2.4	0.2	0.5	2.8	2.5	1.6	1.8	3.6	10.0	---	6.1	1.1

[a]Identified in Table 3.

Table 3 Identification of products in Table 2

MW of methyl ester	Relative GC ret. time	Name of corresponding acid (X is COOH)
132	3.20	malonic acid (XCH_2X)
146	4.60	succinic acid (XCH_2CH_2X)
136	5.15	benzoic acid
204	9.23	1,1,2-ethanetricarboxylic acid
218a	10.54	1,2,3-propanetricarboxylic acid
218b	10.97	oxiranetricarboxylic acid
194a	11.10	benzene-1,2-dicarboxylic acid
194b	11.33	benzene-1,4-dicarboxylic acid
194c	11.58	benzene-1,3-dicarboxylic acid
276	14.33	oxiranetetracarboxylic acid
252a	15.79	benzene-1,2,4-tricarboxylic acid
252b	16.14	benzene-1,3,5-tricarboxylic acid
310a	19.18	benzene-1,2,4,5-tetracarboxylic acid
310b	19.50	benzene-1,2,3,5-tetracarboxylic acid

Table 4 Absolute yields (mg per g maf) of selected minor products from oxidative degradations with CF_3CO_3H-H_2SO_4

	MW of products containing N					MW of lactones								
	209	239	253	297	311	192	250b	250c	250d	250e	264	308a	308b	322
PSOC-372														
coal	---	---	0.4	0.4	0.4	---	---	---	---	0.1	---	0.4	0.3	---
SRC (3 m)	0.2	---	---	0.4	---	0.2	---	0.2	0.2	---	---	0.3	tr	---
SRC (90 m)	0.3	---	---	---	---	0.8	0.5	0.5	0.7	0.1	---	0.6	0.3	---
res (3 m)	0.1	0.5	---	0.4	---	---	---	0.1	---	---	---	---	---	---
PSOC-330														
coal	---	0.1	0.2	0.4	0.5	---	---	---	---	---	---	0.3	0.4	---
SRC (3 m)	---	---	---	---	---	0.2	0.2	0.2	0.2	---	---	0.5	0.3	---
SRC (90 m)	0.3	0.3	---	0.7	---	0.2	0.5	0.5	0.3	0.7	0.3	0.7	1.0	0.4
res (3 m)	---	0.2	---	---	---	---	---	---	0.2	0.5	---	---	0.7	---
PSOC-256														
coal	---	0.1	0.3	0.6	0.2	---	---	---	---	0.2	---	0.1	0.3	---
SRC (3 m)	---	0.4	---	1.1	---	---	0.7	0.3	0.1	0.6	---	0.2	0.7	---
SRC (90 m)	0.2	---	---	---	---	0.3	0.5	0.4	0.5	0.3	---	1.3	1.0	---
res (3 m)	---	0.2	---	0.3	---	---	---	---	---	---	---	0.3	---	---
PSOC-312														
coal	---	---	---	0.3	---	---	---	---	---	0.1	---	0.4	0.4	---
SRC (3 m)	---	---	---	---	---	0.4	0.5	0.8	0.3	0.2	---	0.3	---	---
SRC (90 m)	0.3	---	---	---	---	0.3	0.4	0.2	0.4	0.2	0.2	0.6	0.4	0.2
res (3 m)	0.2	0.1	---	0.7	---	---	---	0.1	---	---	---	---	0.4	---
PSOC-405														
coal	---	---	---	0.1	---	---	tr	tr	---	tr	---	0.1	tr	---
SRC (3 m)	---	0.6	---	1.8	---	0.2	0.4	0.2	---	0.6	0.2	0.4	0.2	0.2
SRC (90 m)	0.6	0.5	---	3.4	---	0.8	0.9	0.2	0.3	1.1	---	0.2	0.2	0.4
res (3 m)	0.4	0.9	---	3.1	---	---	---	0.9	---	---	---	---	0.4	---

Table 4 (continued)

[a]The following identifications (somewhat speculative) are based on MW from chemical ionization mass spectra, the number of carbonyls from the MW of the CD_3OH ester, and fragmentation in electron impact mass spectra. The MW's in the Table are of the methyl esters and the following names are of the corresponding carboxylic acids: 209, 3-carboxypyridine-2-acetic acid; 239, pyridine-2,x,y-tricarboxylic acid (the 2-COOH does not esterify); 253, pyridine-3,4,5-tricarboxylic acid; 297, pyridine-2,3,4,5-tetracarboxylic acid (the 2-COOH does not esterify); 311, a pyridinetetracarboxylic acid.

The lactones (named as the corresponding hydroxy acid) were as follows: 192, 2'-carboxyphenyl-2-hydroxyacetic acid (a major product from naphthalene); 250b-e, analogs of 192 with an additional carboxyl on the benzene ring (one at each of the four positions); 264, 2'-carboxyphenyl-3-hydroxypropanoic acid; 308a and b, analogs of 192 with two carboxyl groups on the benzene ring; 322, the analog of 264 with an additional carboxyl group on the benzene ring.

SOLUBILIZATION OF COALS BY NON-REDUCTIVE ALKYLATION IN LIQUID AMMONIA

M. Gawlak, N. Cyr, D. Carson and B. Ignasiak

Alberta Research Council
11315 - 87 Avenue
Edmonton, Alberta, Canada

In a previous communication we reported that a major portion of a low rank vitrinite (80.8% C, daf) could be converted to chloroform soluble products by non-reductive ethylation in liquid ammonia (1). This paper presents the results of our more in-depth studies on non-reductive alkylation of five Cretaceous and two Carboniferous coals. To assist in understanding of the chemical aspects of the non-reductive alkylation, which has been only marginally explored in organic chemistry, a considerable amount of work was carried out on alkylation of various model compounds.

Experimental

The particle size of coal samples was reduced to below 300 mesh and, prior to reaction, the samples were dried in vacuo (13 pascals) at 70°C. The reaction was conducted under protective cover of oxygen-free helium in 150 ml of vigorously stirred liquid ammonia containing sodium and potassium amides generated "in situ" by action of anhydrous ferric chloride (0.8-1.0 g) on metallic sodium (3.0 g) and potassium (3.0 g). Precautions were taken to ensure that a complete conversion of metals to the respective amides took place prior to addition of coal sample. The mixture was stirred for six hours. 100 ml of anhydrous ethyl ether was added and the contents were alkylated with 2.05 molar excess (on the combined alkali metals) of the desired alkyl bromide. Solvents and excess alkyl bromide evaporated overnight. The contents were acidified with 5 N hydrochloric acid, the product was washed thoroughly with cold water, extracted overnight with refluxing water and dried. Three successive ethylations were carried out on each sample of coal.

Alkylation of model compounds was carried out under similar conditions except that smaller quantities of ammonia (70-80 ml), ferric chloride (0.5 g), sodium (1.7 g) and potassium (1.7 g) were used. The amount of substrate was always the same (0.028 M). Reaction product was recovered either by filtration (solids), or by extraction with organic solvent (chloroform or ether). Products were analysed by GC, GC-MS and NMR spectroscopy.

Proton and C-13 spectra of soluble products (alkylated coals and model compounds) were recorded in $CDCl_3$ using Brueker WP-80 apparatus. For C-13 NMR spectra signal accumulation was necessary. C-13 spectra of solid coals were recorded in the Laboratories of the National Research Council, Ottawa, using a Brueker CXP-180 spectrometer and cross polarization-magic angle spinning technique.

Number average molecular weights of coal extracts and of their subfractions were determined in pyridine using Corona-Wescan vapour pressure osmometer and concentrations 1-20 g/Kg.

GPC fractionation was carried out on column of Sephadex LH-60, an hydroxypropylated dextran gel, 80 cm in length and 2.5 cm in diameter using chloroform as solvent.

Results and Discussion

Alkylation of Coals. The information regarding the origin and rank of coals tested and the results of alkylation studies conducted on these coals is summarized in Table 1. The number of alkyl groups introduced into coal varied from 7 to 18 per 100 original carbon atoms. The carboniferous coals tested in these studies appeared to be more susceptible to solubilization than their Cretaceous counterparts. Alkylation took place on both oxygen and carbon atoms. Depending on coal, the ratio of alkylated oxygen to alkylated carbon atoms varied from 0 (coal #5) to approximately 0.5 (coals #1, 2 and 3).

Long chain alkyl groups, n-butyl and n-hexyl, seem to alkylate hydroxyl groups more efficiently than short chain, ethyl groups. There is a residual level of hydroxyl groups which defies ethylation. No simple relationship exists between the number of alkyls introduced and the degree of solubilization.

Non-reductive alkylation of coal #7 led to high conversion of this coal to chloroform soluble product. Extraction of a small sample (0.5 g) of triply ethylated coal resulted in 63% solubility. However, when larger sample (10 g) was similarly extracted, the solubility was lowered to 48.1%. Essentially the same total solubility (49.6%) was obtained when ethylation was alternated with extraction after each of the three ethylation steps. Such experimental sequence will be referred to in this text as alternate ethylations 1, 2 and 3.

Number average molecular weights of fractions solubilized by either method are similar: 1260 for triply ethylated coal, and 1140, 1300 and 1250 for soluble parts of alternate ethylations 1, 2 and 3 respectively.

Gel permeation chromatography of solubilized fraction of triply ethylated coal showed that 8.7% of sample had molecular weight of 15,440; 11.2% - 10,430; 10.4% - 5,740; 12.3% - 2,570; 35.2% - 910 to 1,040; 10.4% - 875; 2.6% - 580; and 9% of sample was not recovered from the column, even after the polarity of chloroform was increased by addition of 1% ethanol.

NMR Spectra. NMR spectra of untreated solid coal #7 and of its solubilized fractions are reproduced in Figures 1-4. Comparison of

the aliphatic region of C-13 spectra of our fractions with C-13 spectra of solid coal, coal liquids and coal extracts published in literature (2, 3, 4) is made in Table 2. The most consistent and intense line is that at 29-30 ppm. Absorption bands at 9, 12 and 14 ppm are strong in the fractions of ethylated coal. These bands are associated with the methyl carbons of the introduced ethyl groups. This was proven conclusively by ethylation with D_5-ethyl bromide, which led to disappearance of these bands (Figure 3) together with elimination of much of the underlying hump in the 25-35 ppm region (methylene absorptions β to an aromatic ring; ref 5).

Noticeable difference between the C-13 spectra of non-reductively solubilized coal and the spectra of fractions resulting from other methods of solubilization is the C-13 line at 46 ppm. Absorption band approximating this frequency is seen in the spectrum of solid coal of Zilm and co-workers (3). It is also present in coal #7. The environment responsible for this absorption was lost in other methods of solubilization but was preserved in our alternatively ethylated samples. The intensity of this spectral line increases progressively for solubilized fractions of alternate ethylations from 1 to 3. This strengthening of absorption at 46 ppm seems to be associated with a weakening signal at 29 ppm. Another relevant observation is that the line at 46 ppm is absent in triply ethylated coal. It also disappeared on second ethylation of soluble product from alternate ethylation 1. The above spectral observations could be interpreted in terms of changes in C-13 chemical shifts occurring on alkylation of structural unit of coal of a 9,10-dihydrophenanthrene (DHP) type.

Secondary carbons in 9 and 10 positions of 9,10-DHP absorb at 29 ppm. On ethylation, when both hydroaromatic carbons are transformed into tertiary carbon atoms (-CHR-CHR-) their C-13 absorption shifts to 46 ppm. Under conditions of exhaustive ethylation (triple ethylation of the same coal sample, and second ethylation of solubles of alternate ethylation 1) the easily accessible sites do not exist any more. The more difficult tertiary environments are then substituted which leads to disappearance of the spectral line at 46 ppm.

Ethylation of Model Compounds. Eight model compounds (adamantane, indan, dibenzyl, diphenylmethane, 9,10-dihydrophenanthrene, 9,10-dihydroanthracene, fluorene and acenaphthene) were ethylated under the conditions of non-reductive alkylation of coal. GC-MS and NMR analyses of the products provided information on relative reactivity of hydrogen atoms in these compounds (Table 3). Hydrogen atoms in polycyclic condensed network of adamantane are unreactive. Negligible monoethylation (0.1%) occurred in indan. Ethylation of dibenzyl was low, and that of 9,10-DHP only moderate. Activation of methylene group by two phenyl rings makes the hydrogen quite reactive in liquid ammonia. Activation by phenyl ring and an olefinic bond as in indene (an impurity in indan) is also effective. Hydrogen atoms in 9 and 10 positions of dihydroanthracene and in 9 position of fluorene substitute very readily.

Acenaphthene produced a puzzle: all of it reacted to give multiple isomers of di-, tri-, tetra-, and even penta-ethylated compounds. Ten major and at least twenty minor components resulted. Work on their identification is now in progress.

The C-13 spectra of ethylated coal and of some of the model compounds have absorption lines upfield to 8.4 ppm. These are the absorption lines of the methyl carbons δ to an aromatic ring. The presently known upfield absorption limit for the δ methyl groups extends only to about 10 ppm (6). In addition to 8.5 band in the ethylated coals, the high field absorption was observed for the methyl carbon in diethyldiphenylmethane (8.4 ppm), 9,9,10,10-tetraethyl-9,10-dihydroanthracene (8.6 ppm) and 9,9-diethylfluorene (8.5 ppm). C-13 absorption in the region of 46 ppm was observed for 9,10-diethyl-9,10-dihydrophenanthrene (46.3 ppm); 9,10-diethyl-9,-10-dihydroanthracene (48.4 ppm) and in 1-ethyl-1,2-diphenylethane (carbon 1-49.9 ppm; carbon 2-43.6 ppm).

Acknowledgement

The authors express their thanks to Dr. J. Ripmeester of the National Research Council of Canada for recording of the spectra of samples of solid coal, and for his valuable discussion.

Literature Cited

1. Ignasiak, B.; Carson, D.; Gawlak, M. Fuel, 1979, 58, 833.
2. Fisher, P.; Stadelhofer, J. W.; Zander, M. Fuel, 1978, 57, 345.
3. Zilm, K. W.; Pugmire, R. J.; Grant, D. M.; Wood, R. E.; Wiser, W. H. Fuel, 1979, 58, 11.
4. Pugmire, R. J.; Grant, D. M.; Zilm, K. W.; Anderson, L. L.; Oblad, A. G.: Wood, R. E. Fuel, 1977, 56, 295.
5. Stothers, J. B., "Carbon-13 NMR Spectroscopy", Organic Chemistry Monograph Series vol. 24; Academic Press, 1972, p. 97.
6. Yosuke Maekawa; Tadashi Yoshida; Yuji Yoshida Fuel, 1979, 58, 864.

Table 1. Summary of the Alkylation Data

Coal No.	Origin	%C, daf	Alkyl group used	Solubility, wt%daf		OH groups/100 C atoms			Alkyl groups/100 C atoms after each alkylation calculated from:						Final no.* of alkyl groups on:	
				initial	after 3 alkylations	initial	after alkyln 1	after alkyln 3	ΔW			%H			C	O
	CRETACEOUS COALS															
1.	Saskatchewan	73.9	ethyl	2.9	24.5	6.6	4.3	2.8	7.0	9.1	11.8	7.4	-	14.8	9.5	3.8
2.	Alberta	77.7	ethyl	3.0	33.2	5.5	-	1.7	8.6	15.9	17.8	5.4	6.4	7.5	8.8	3.8
			n-propyl		33.0	5.5	2.1	1.4	7.7	11.4	13.1	8.0	11.7	14.3	9.6	4.1
			i-propyl		30.7	5.5	3.1	2.8	5.6	7.9	9.7	4.7	-	8.2	6.2	2.7
			n-butyl		38.5	5.5	3.2	1.2	9.0	11.5	12.7	6.3	9.5	12.2	8.1	4.3
			n-hexyl		35.7	5.5	-	0.3	11.7	13.6	15.0	9.0	14.0	16.9	10.7	5.2
3.	British Columbia	80.6	ethyl	3.6	25.9	4.8	-	1.4	6.3	8.7	10.5	4.4	6.2	7.3	5.5	3.4
4.	Alberta	86.8	ethyl	3.6	28.0	1.1	0.4	0.4	5.9	7.7	9.0	4.2	6.0	7.0	7.3	0.7
5.	British Columbia	88.8	ethyl	3.8	28.9	0.3	0.3	0.3	5.8	7.9	9.5	8.1	-	12.5	11.0	0
	CARBONIFEROUS COALS															
6.	West Virginia	83.2	ethyl	6.3	39.0	2.3	1.6	0.9	11.7	13.0	14.4	5.6	-	12.6	12.1	1.4
7.	Freeport seam	87.3	ethyl	3.2	63.6	1.1	0.7	0.5	5.1	7.5	8.4	4.1	-	7.3	7.2	0.6

*per 100C atoms, using the average of ΔW and %H after three alkylations

Table 2. Aliphatic Region of C-13 NMR Spectra of Coals and Some Coal Derived Products

Sample	Chemical Shifts, ppm from TMS														
coal #7 (solid)	-46-43*					-30**				-19-			-14-11-		
coal (solid) (3)	-44-					-29-				-20-15-					
coal extract (2)		37.8		32.4	30.2	29.8	23.1	21.5	19.1			14.2			
(2)				31.9		29.7	22.7	21.4	19.8			14.1			
coal liquid (3)			33			29		22	20	17	15				
coal liquid (4)					31	30		22			15				
triply ethyl[d] #7		37		32		29.5	22.5	21.5				-14-12-9-			
triply D_5-ethyl[d] #7	43	37		32		29.7	23	21.5	19			14			
alt.ethylation 1	46	37	33	32		29	23	22	19		15	14	-9-		
alt.ethylation 2	46			32	31	29		22			15	14	-8.5-		
alt.ethylation 3	46					29	28	22			15	14	12-9-		
alt. ethylation 1 ethylated again			-33-			29		-22-			-15-14-12-8.5				

*-43-indicates a broad band with a maximum, for example, at 43

**underline indicates a high intensity absorption

Table 3. Summary Information on Ethylation of Model Compounds

Model Compound	Molar Ratio*	% Conversion	Aliphatic C-13 nmr shifts of originally present C modified by ethylation			introduced ethyl	
			C	CH	CH_2	CH_2	CH_3
Adamantane	1.07	NR**					
Indan	1.07	99.9 NR 0.1 mono-					
Dibenzyl	1.07	98 NR 2 mono-		49.9	43.6	28.4	12.0
Diphenyl-methane	2.14	93.6 mono- 6.4 di-		53.4	-	28.6 29.4	12.8 8.4
9,10-Di-hydrophenan-threne	1.07	66.7 NR 24.7 mono- 8.6 di-	- -	40.2 46.3	33.6 -	26.2 27.9	12.0 12.2
9,10-Di-hydroanthra-cene	1.07	53.4 di- 24.3 tri- 22.3 tetra-	-	48.3	-	35.2	13.3 8.6
Fluorene	2.14	100 di-	56.2	-	-	32.8	8.5

* moles of combined alkali metals to moles of hydrogen on α carbon to an aromatic ring

** NR - no reaction

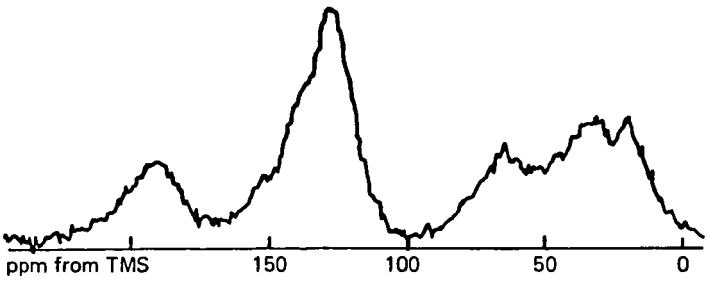

Figure 1. C-13 nmr spectrum of solid coal no. 7.

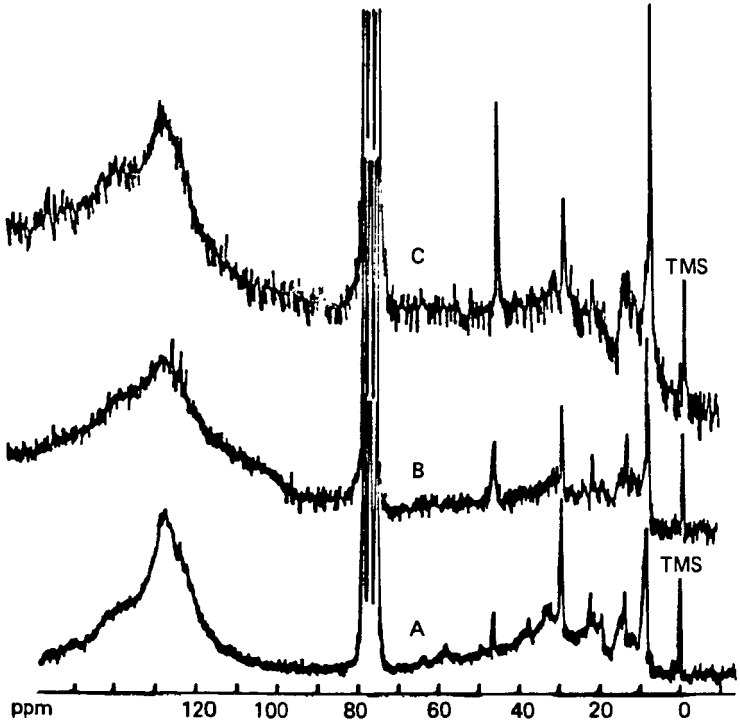

Figure 2. C-13 nmr spectra of solubilized coal no. 7 after: A-first alternate ethylation; B-second alternate ethylation; C-third alternate ethylation.

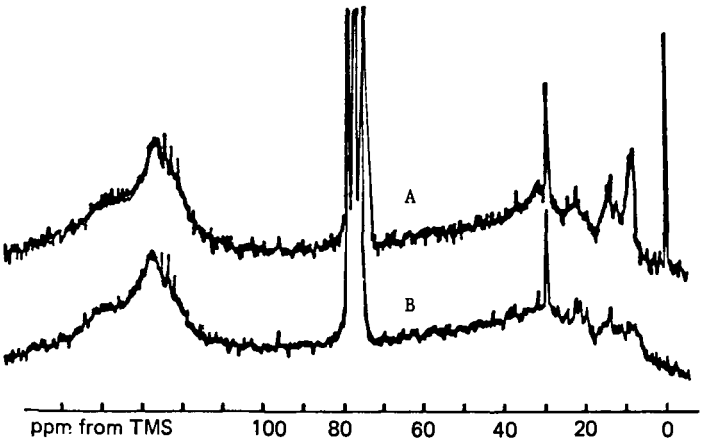

Figure 3. C-13 nmr spectra of solubilized coal no. 7 after: A-triple ethylation; B-triple D_5-ethylation.

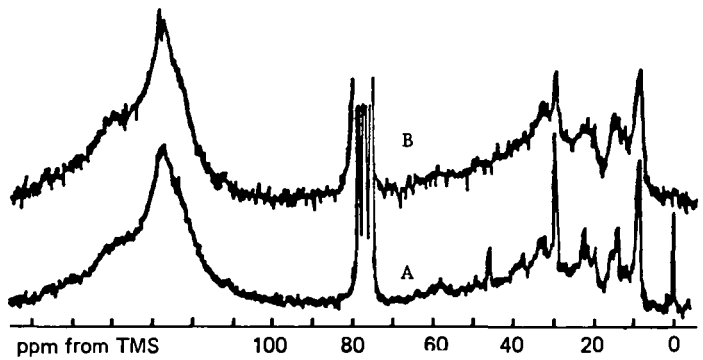

Figure 4. C-13 nmr spectra of solubilized coal no. 7 after: A-first alternate ethylation; B-sample A ethylated once more.

Reactions of Three Double Ring Heteroaromatic Model Coal Compounds in Excess Tetralin

R.G. Mallinson, K.C. Chao, and R.A. Greenkorn

School of Chemical Engineering
Purdue University
West Lafayette, Indiana 47907

INTRODUCTION

The liquefaction of coal is one of the ways needed for extending liquid fuel supplies. In order to better utilize these resources through modelling and optimization of processes, a fundamental understanding about the nature of the chemical and physical changes taking place is necessary. One of the major processes now under development involves a donor solvent to help transfer hydrogen to the coal. Recently more and more effort has been devoted to the understanding of the chemistry of reactions between the solvent and model coal compounds which contain structural similarities to coal moieties (1,2,3,4,5,6,7).

This study investigates the reaction rates of three heteroaromatic compounds; benzothiophene (I), indole (II), and benzofuran (III), in excess tetralin.

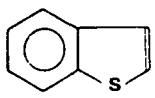

(I)

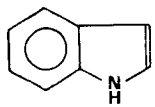

(II)

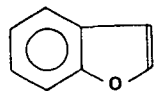

(III)

Temperatures from 400 to 450°C are used with a pressure of 1500 psig in a batch microreactor without hydrogen gas. The reactions of tetralin in the absence of acceptor compounds have also been examined. The major reactions for all of the systems have been modelled as first or second order reactions which give rise to a coupled nonlinear system of equations which is solved numerically.

EXPERIMENTAL

The batch microreactor system is depicted in Figure 1. The reactor is a 9/16 inch tee made of 316 stainless steel by Autoclave Engineers. To this are fitted reducers which allow the use of 1/8 inch tubing for inlet and exit lines. The actual lines to the reactor are 1/16 inch O.D. tubing with an I.D. of 0.005 inches. Pieces of 1/8 inch tubing are fitted over the 1/16 inch tubing at the ends to couple them to the aforementioned reducers, and the inlet and exit valves. The reactor volume is 4.1 milliliters. A fluidized bed sandbath with an external controller maintains the reactor temperature to within $\pm$ 0.5°C of the desired value. The reactor remains in the bath at all times and is charged from a manually operated piston displacement pump. The operating pressure for all experiments is 1500 psig which is sufficiently high to suppress vaporization of reaction products. The pressure is generated by the pump, rather than by gas pressure. The basic procedure to charge a sample to the reactor is to first evacuate the reactor through valves C and B (Figure 1). Then, after valve C is closed, the reactor is charged with the appropriate volume of fluid from the pump sufficient to achieve a pressure of 1500 psig after thermal equilibrium is reached. The temperature initially drops 30 to 35°C upon charging, but recovers to within about 3°C in about one minute. After the temperature has recovered and the operating pressure reached, valve D is shut. At the end of the reaction period the sample is discharged through valve E from which it expands and condenses into a trap. After the sample has cooled, a nitrogen

purge displaces the sample into a sample vial. The reactor is evacuated and is then ready for another sample.

The chemicals used in this study were all purchased from Aldrich Chemical Company. The purity of all reactants was at least 99%. Tetralin was redistilled to 99.8 percent purity with naphthalene the only observed impurity.

Analyses are made by gas liquid chromatography. A Hewlett Packard 5710A G.C. with thermal conductivity detector is used. Two types of liquid phases are used, Apiezon L for a boiling point separation and Bentone 34 for a π bond separation, both supported on chromasorb W packing. Quantification of the samples is accomplished with a Columbia Scientific CSI-208 digital integrator. Further details of this work are available elsewhere (6).

RESULTS AND DISCUSSION

Tetralin. We have studied the decomposition of tetralin by itself in order to establish "baseline" reaction rates. Temperatures of 400 and 450°C have been used. The two major reactions are:

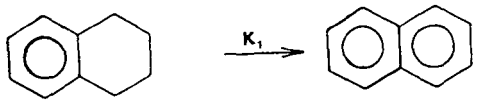

1)

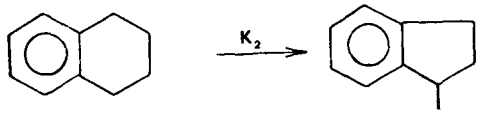

2)

At 450°C a small amount of indan is also observed along with trace amounts of benzene, toluene, and ethylbenzene. These products are as expected from the literature (5). Reactions 1 and 2 are modelled as first order in tetralin. The rate constants and activation energies are listed in Table 1. Figures 2, 3 and 4 show the data (points) with the curves generated by the models:

$$\frac{d[TET]}{dt} = -(K_1+k_2)[TET] \qquad 3)$$

$$\frac{d[NAPTH]}{dt} = k_1[TET] \qquad 4)$$

$$\frac{d[MEI]}{dt} - k_2[TET] \qquad 5)$$

where: [TET] = mole fraction tetralin

[NAPTH] = mole fraction naphthalene

[MEI] = mole fraction methylindan

It can be seen that the model fits the data well. A zero order model was found to give a worse fit of the data.

Benzothiophene in tetralin. Benzothiophene with an initial mole fraction of 0.10 in tetralin was reacted at 400, 425, and 450°C. The major product was dihydrobenzothiophene. At 450°C toluene and ethylbenzene appeared in small amounts. These two products appeared in equimolar amounts with a rate that increased with time, indicative of a secondary product. They reached a concentration of 0.63 mole

percent at the maximum reaction time of 120 minutes. Benjamin et.al. (1) also found toluene and ethylbenzene as well as benzene as products from benzothiophene reacted in excess tetralin at 400°C for 18 hours. It thus appears that benzothiophene desulfurized thermally.

Based on the observed reactions of benzothiophene the proposed model is:

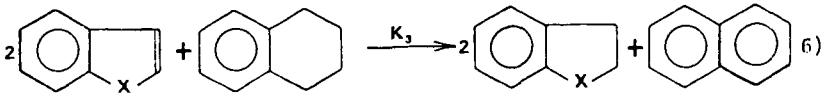

6)

The stoichiometry requires that two moles of benzothiophene react with one mole of tetralin in order to balance the hydrogen. This is written as a net reaction. We have made the steady state assumption for dihydronaphthalene to simplify the rate expression from the reactions:

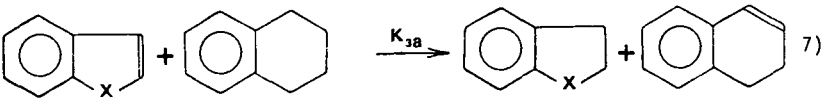

7)

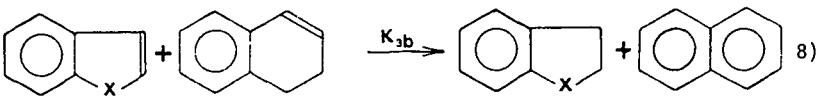

8)

Dihydronaphthalene is observed in very small amounts (<0.05 mole percent) throughout all of the reactions. This implies that k_{3a} is rate determining and is what is determined as k_3 from reaction 6. The rate equations for reactions 1, 2 and 6 are:

$$\frac{d[ACCEPT]}{dt} = -2k_3[ACCEPT][TET] \qquad 9)$$

$$\frac{d[TET]}{dt} = -\{k_1+k_2+k_3[ACCEPT]\}[TET] \qquad 10)$$

$$\frac{d[NAPTH]}{dt} = \{k_1+k_3[ACCEPT]\}[TET] \qquad 11)$$

where: [ACCEPT] = mole fraction of acceptor

Here [ACCEPT] is used to represent the acceptor species concentration generally since the same model is used for the indole reactions to be described subsequently. Reaction 2 is not altered so equation 5 remains unchanged. For convenience, concentrations are expressed in mole fractions. The units of all rate constants are then inverse minutes. The use of mole fractions requires the assumption of a constant molar volume for the reaction mixture. The system of equations 5,9,10, and 11 are coupled and nonlinear. A computer program (6) utilizing a Marquardt optimization scheme was used for parameter estimation. The results for the benzothiophene reaction system are shown in Figures 5 through 8 where the curves represent the model and the points represent the data. It can be seen that the data is well represented by the model at all three temperatures. The rate constants and activation energies are given in Table 2. A comparative discussion of the rates and activation energies between the different reacting systems is postponed until all of the results have been presented. We do point out now that k_1 and k_2 are always determined from the data of the particular reaction system rather than being held constant at the values determined for tetralin.

Indole in tetralin. Indole was reacted in tetralin with an initial indole mole fraction of 0.128. The reaction was run at 425 and 450°C. The major product was indoline (2,3-dihydroindole). At 450°C small amounts of o-ethylaniline and o-methylaniline (o-toluidine) were observed. Figure 9 shows the indole concentration versus time at the two temperatures. The model again fits the data well, and the model also represents the tetralin, naphthalene, and methylindan concentrations well at both temperatures. The rate constants and activation energies are given in Table 3.

Benzofuran in tetralin. The initial mole fraction of benzofuran in tetralin was 0.10. The reactions were run at 400 and 450°C. The reaction was very fast at 450°C with a half life of 25 minutes. Unlike the previous two acceptors, the hydrogenated acceptor, 2,3-dihydrobenzofuran, was not observed. At 450°C the major products were o-ethylphenol and o-methylphenol (o-cresol). At 400°C, however, only small amounts of these two products were observed. Since dihydrobenzofuran was not observed it was not clear whether it was an unstable intermediate or whether the reaction proceeded through another chemical route. An experiment was conducted with 5 mole percent dihydrobenzofuran in excess tetralin at 425°C to help elucidate the pathway. The same products (alkylphenols) were formed, and the rate was comparable to that of the reaction of benzofuran (eg; not instantaneously). An additional note is that benzofuran was formed from the dihydrobenzofuran. Thus it seems that the reaction of benzofuran is different from its sulfur and nitrogen analogs. It was found that the model used for the previous two acceptor compounds represented poorly the benzofuran concentration at 400°C, but not so poorly at 450°C. At both temperatures the model fittings of methylindan, naphthalene and tetralin were good. Evidently a non-hydrogen transferring reaction is dominant at 400°C. To account for this different reaction a first order decomposition model is used:

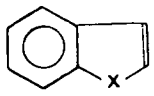

$$\xrightarrow{K_4} \text{PRODUCTS} \qquad 12)$$

The kinetic equation is then:

$$\frac{d[\text{Benzofuran}]}{dt} = -k_4[\text{Benzofuran}] \qquad 13)$$

Equations 3,4, and 5 are then used for tetralin, naphthalene and methylindan concentrations respectively. Table 4 shows the values for k_1, k_2, and k_4 along with the activation energies. Figure 10 shows the predicted benzofuran concentration for reaction 12 and the data. The fit of the data is good, much better at 400°C than for the hydrogen transfer model and no worse at 450°C. The predictions for tetralin, naphthalene, and methylindan are also as good for this model as with the hydrogen transfer model at both temperatures.

Comparative discussion. Figure 11 summarizes the result of the acceptor reaction models. It can be seen that benzothiophene and indole react at similar rates while benzofuran reacts at a significantly higher rate. The activation energies range from 30.0 to 51.2 kcal/gmole with benzothiophene exhibiting the largest temperature effect, with indole and benzofuran considerably less.

The end products of the three reactions indicate that only benzothiophene loses its heteroatom, producing alkylbenzenes. Indole and benzofuran produce the corresponding anilines and phenols. The products of the benzothiophene reaction and the stability of anilines and phenols under the type of reaction conditions as in this study is confirmed by the literature (1).

The kinetics of reaction 4 (production of naphthalene via tetralin decomposition that is not due to acceptor reactions) is summarized in Figure 12. The activation energy for this reaction with no acceptor present is 27.9 kcal/gmole, lower than in any of the acceptor systems. The rates are also lowest for the non-acceptor system,

by a significant amount. The benzothiophene and indole systems have similar rates with activation energies of 38.7 and 60.1 kcal/gmole, respectively. Originally it was planned to not optimize the rate constants for reactions 1 and 2, but to keep them constant at the values determined from the non-acceptor tetralin decomposition run. The variation in the rate has been observed previously (2) with changes in acceptor or solvent components, and we also noted changes in the methylindan rates, despite its model independence from the acceptor reaction. The values of k_1's and E_a's are in the range of values previously reported for reaction 4 (2) except that the E_a = 60.1 kcal/gmole for indole is significantly higher.

Figure 13 summarizes the results of the reaction producing methylindan. The rate constants are very similar to those in (2) again, although with less variation than those of (2). The activation energies range from 46.9 kcal/gmole for tetralin decomposition, to 57.0 kcal/gmole for benzothiophene. The activation energies are significantly higher in this study than in (2). As previously noted, the variation in k's is evidently due to the effect of the acceptor. Possibly the acceptor acts as an "initiator" by enhancing hydrogen abstraction from the solvent. Once the tetralin free radical is formed it can give up another hydrogen to form dihydronaphthalene or rearrange to form a more stable methylindan free radical and then accept a hydrogen atom back.

REFERENCES

1. Benjamin, B.M., Raaen, V.F., Maupin, P.H., Brown, L.L., Collins, C.J., Fuel, 57, 269 (1978).
2. Cronauer, D.C., Jewell, D.M., Shah, Y.T., Kueser, K.A., Ind. Eng. Chem. Fundam., 17, 4, 291 (1978).
3. Cronauer, D.C., Jewell, D.M., Shah, Y.T., Modi, R.J., Ind. Eng. Chem. Fundam., 18, 2, 153 (1979).
4. Cronauer, D.C., Jewell, D.M., Shah, Y.T., Modi, R.J., Seshadri, K.S., Ind. Eng. Chem. Fundam., 18, 4, 368 (1979).
5. Hooper, R.J., Battaerd, H.A.J., Evans, D.G., Fuel, 58, 132 (1979).
6. Mallinson, R.G., M.S. Thesis, Purdue University (1979).
7. Whitehurst, D.D., Farcasiu, M., Mitchell, T.O., EPRI Annual Report No. AF-480, RP-410-1, (July 1977).

Table 1. Rate Constants and Activation Energies for Tetralin Blank Run

	400°C	450°C	E_a(Kcal/gmole)
$k_1(min^{-1})$	2.89×10^{-5}	1.23×10^{-4}	27.9
$k_2(min^{-1})$	5.66×10^{-5}	6.46×10^{-4}	46.9

Table 2. Rate Constants and Activation Energies for Benzothiophene Run

	400°C	425°C	450°C	E_a(Kcal/gmole)
$k_1(min^{-1})$	2.79×10^{-6}	1.41×10^{-4}	3.70×10^{-4}	38.7
$k_2(min^{-1})$	7.00×10^{-5}	3.86×10^{-4}	1.34×10^{-3}	57.0
$k_3(min^{-1})$	1.991×10^{-4}	7.4×10^{-4}	2.81×10^{-3}	51.2

Table 3. Rate Constants and Activation Energies for Indole Run

	425°C	450°C	E_a(Kcal/gmole)
$k_1(min^{-1})$	1.17×10^{-4}	5.18×10^{-4}	60.1
$k_2(min^{-1})$	3.84×10^{-4}	1.44×10^{-3}	53.4
$k_3(min^{-1})$	1.08×10^{-3}	2.43×10^{-3}	32.7

Table 4. Rate Constants and Activation Energies for Benzofuran Run

	400°C	450°C	E_a(Kcal/gmole)
$k_1(min^{-1})$	1.64×10^{-4}	1.55×10^{-3}	43.6
$k_2(min^{-1})$	1.24×10^{-4}	1.82×10^{-3}	52.2
$k_4(min^{-1})$	5.93×10^{-3}	2.78×10^{-2}	30.0

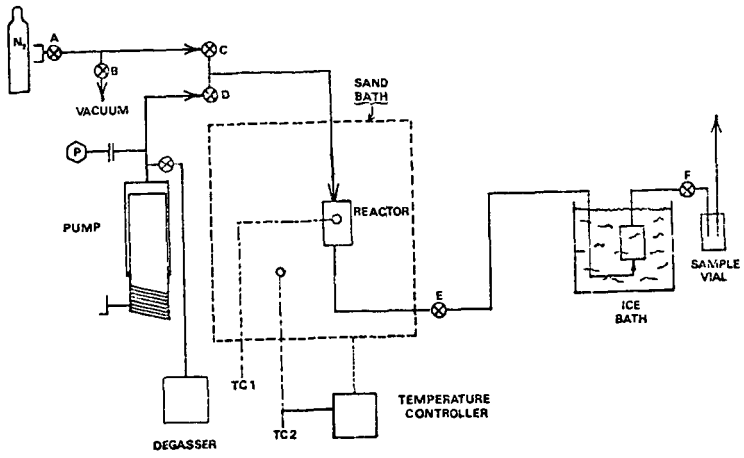

Figure 1. Experimental Microreactor System

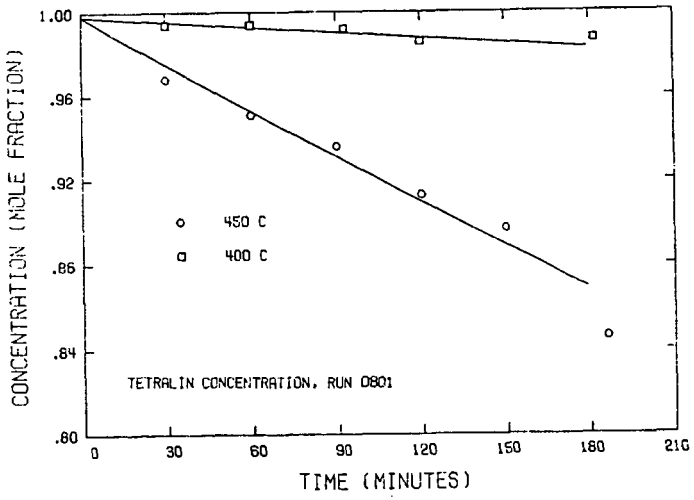

Figure 2. Tetralin Composition in Tetralin Blank Run

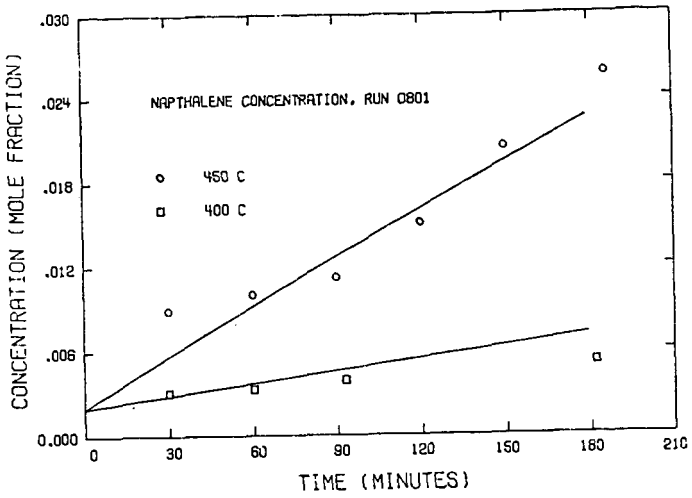

Figure 3. Naphthalene Composition in Tetralin Blank Run

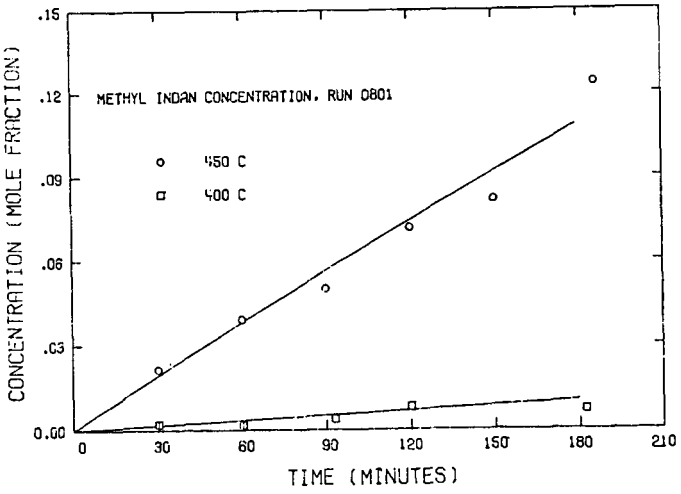

Figure 4. Methylindan Composition in Tetralin Blank Run

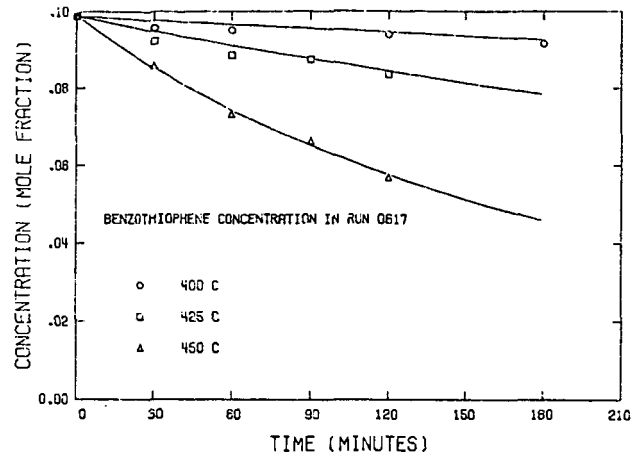

Figure 5. Benzothiophene Composition in Benzothiophene Run

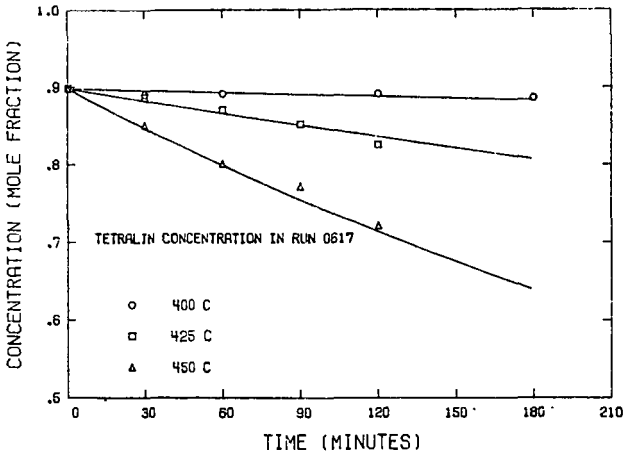

Figure 6. Tetralin Composition in Benzothiophene Run

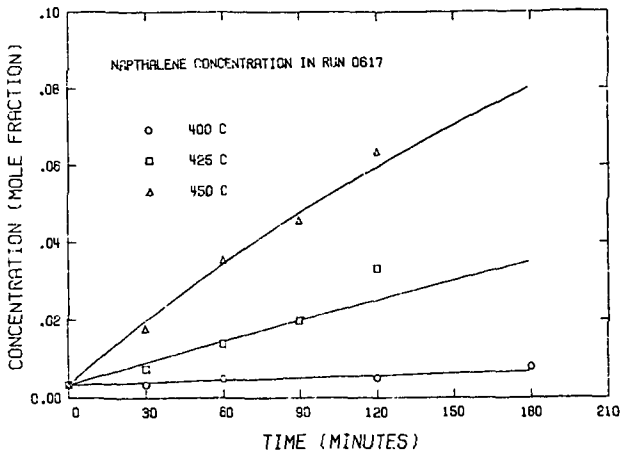

Figure 7. Naphthalene Composition in Benzothiophene Run

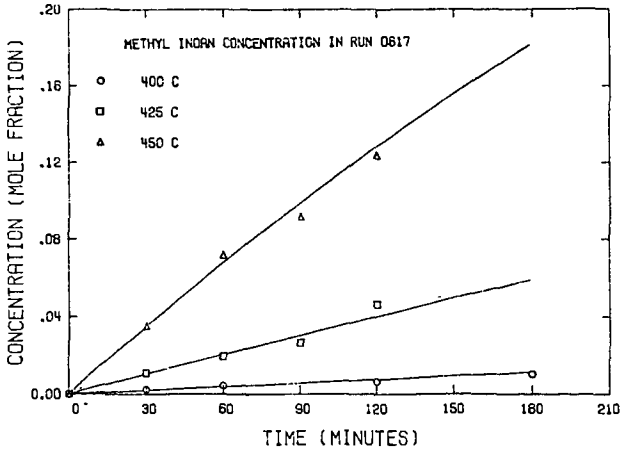

Figure 8. Methylindan Composition in Benzothiophene Run

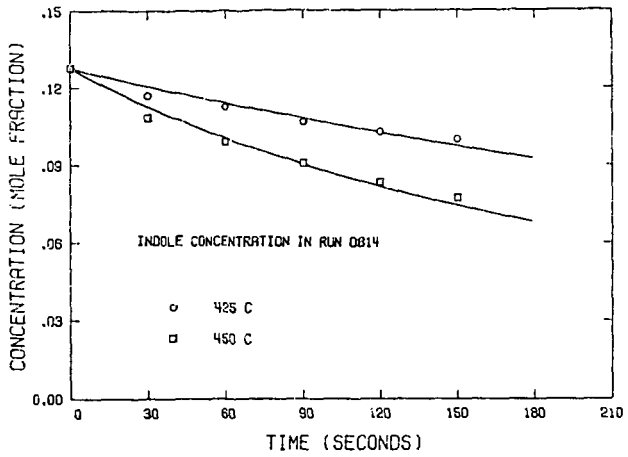

Figure 9. Indole Composition in Indole Run

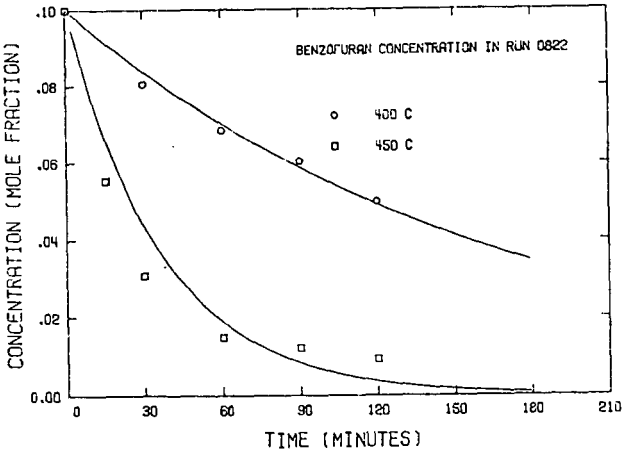

Figure 10. Benzofuran Composition in Benzofuran Run

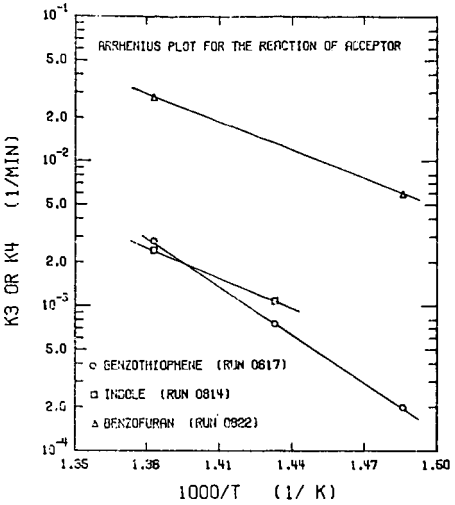

Figure 11. Arrhenius Plot for Acceptor Reaction Model

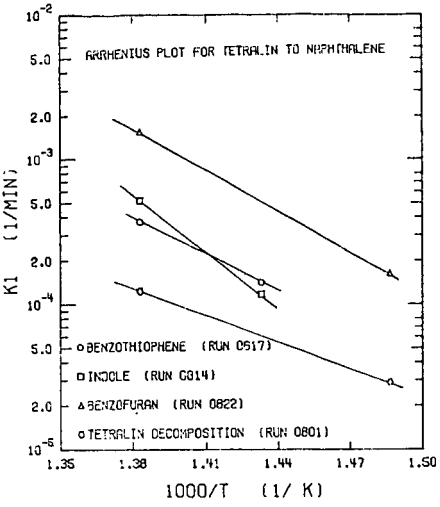

Figure 12. Arrhenius Plot for Reaction of Tetralin to Naphthalene

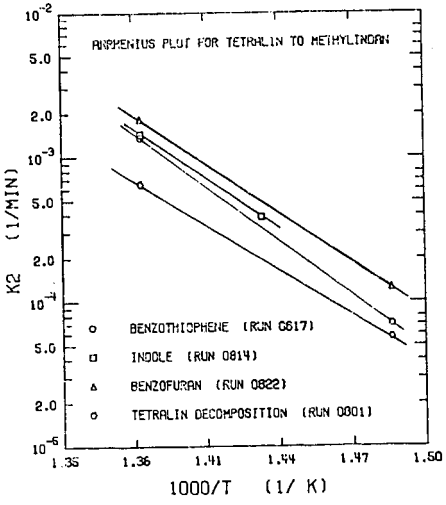

Figure 13. Arrhenius Plot for Reaction of Tetralin to Methylindan

HYDROGEN TRANSFER FROM ALCOHOL DONORS TO AROMATIC SUBSTRATES

M.J. Garry and P.S. Virk

Department of Chemical Engineering
Massachusetts Institute of Technology
Cambridge, MA 02139

Introduction:

The use of alcohols in coal liquefaction by donor solvents dates to the earliest works (1) wherein the tetralin donor used also contained phenol and cresol additives; chemically similar mixtures have been used more recently (2,3) to simulate commercial donor solvents. Alcohols have also directly been employed as hydrogen donors for coal liquefaction, in which application isopropanol, cyclohexanol and o-cyclohexylphenol have proven effective (4), whereas t-butanol is ineffective (5). The mechanism of hydrogen transfer from alcohol donors to coal is obscure. However, free radical types of mechanisms, such as recently proposed (6,7) for coal liquefaction, seem especially unsatisfactory because the essential step would have to involve abstraction of a relatively strongly bonded hydrogen in the alcohol by a coal fragment radical formed from homolysis of a weak bond in the coal.

The present work was motivated by a hypothesis (8,9) that coal liquefaction may entail concerted, pericyclic reaction paths. In this context, hydrogen transfer from an alcohol donor, such as isopropanol, to a coal acceptor, such as phenanthrene, may be viewed as a six electron [4e($\sigma\sigma$) + 2e(Π)] group transfer reaction:

(RO)

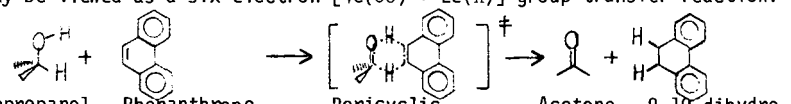

Isopropanol 4e($\sigma\sigma$) Donor | Phenanthrene 2e(Π) Acceptor | Pericyclic Transition State | Acetone | 9,10 dihydrophenanthrene

According to the Woodward-Hoffmann (10) rules for orbital symmetry conservation, reaction (RO) would be thermally allowed for supra-supra stereochemistry, which is sterically favorable.

Pursuit of our hydrogen transfer hypothesis suggested exploration of a grid comprising two alcohol donors, namely cyclohexanol and ortho-cyclohexylphenol, and two aromatic acceptors, namely phenanthrene and anthracene. Of these substrates, the cyclohexanol is a 4e($\sigma\sigma$) donor akin to isopropanol while the o-cyclohexylphenol is a 6e($\sigma\Pi\sigma$) donor of the contrary orbital symmetry. Similarly, the phenanthrene, a 2e(Π) acceptor, has orbital symmetry opposite to anthracene which is a 4e($\Pi\Pi$) acceptor. In the 2 x 2 matrix of thermal reactions between these donor-acceptor pairs, combinations with a total of (4n+2)e should theoretically (10) be allowed in supra-supra stereochemistry while those with a total of (4n)e should be forbidden in supra-supra but allowed in supra-antara stereochemistry. Such differences should be manifest, and hence experimentally discernible, in the respective reaction kinetics. Figure 1 illustrates these principles of orbital symmetry conservation for the present hydrogen transfer reactions. Experimental results obtained to date with the cyclohexanol donor are reported in this paper.

Experimental:

All experiments were conducted in stainless steel batch reactors with an

internal volume of 0.503 cm^3; the reactors were immersed in a salt bath for times ranging from 0.16 to 12 hours at temperatures from 300 to 425°C. Heating and cooling times were calculated to be insignificant compared with reaction times. Experiments conducted in an argon atmosphere, when compared with reactions in air, indicated no effect of atmosphere on reaction rate. Vapor-liquid equilibrium calculations were used to ensure that >95% of the reactants remained in the liquid phase at all times. Upon reaction and subsequent quenching, the products were dissolved in solvent--toluene for anthracene reactions, carbon tetrachloride for phenanthrene reactions--and analyzed on an HP 5720 gas chromatograph. Product identification was based on G.C. coinjection techniques as well as nmr spectra. Material balance closure was effected in all experiments, and particular care was taken to effect a hydrogen transfer balance. Thus, we define a ratio H of the mols of hydrogen donated, h_d, as measured by appearance of dehydrogenated donor, to the mols of hydrogen accepted, h_a, as measured by the appearance of hydrogenated acceptor; in all cases $H = (h_d/h_a) = 1.00 \pm 0.08$. The chemicals used were all of purity > 99.5% as received; the anthracene and phenanthrene substrates were further purified and assayed to ensure that the content of the related dihydro compound was below detection limits, i.e., < 0.05%.

Results.

Preliminary investigation of reaction pathways revealed that three types of reactions occurred. First, the hydrogen transfer reaction, our primary objective, which is symbolically represented by:

(R1) D + A → DD + HA

D, A, DD, and HA are respectively the donor, acceptor, dehydrogenated donor and hydrogenated acceptor; the initial (donor/acceptor) ratio is termed S. Second, the hydrogenated acceptor HA could, in general, revert to the original acceptor:

(R2) HA → A

This usually occurred by elimination of molecular hydrogen but disproprotionation, with formation of a further hydrogenated form of HA, was also possible. Third, the donor D could react by paths other than (1), typically suffering pyrolytic decomposition:

(R3) D → products

In the present work, D = cyclohexanol (CHL), A = either anthracene (ANT) or phenanthrene (PHE), DD = cyclohexanone (CHN), and HA = either dihydroanthracene (DHA) or dihydrophenanthrene (DHP). The experimental grid constructed to examine the preceding pathways is shown in Table 1, which indicates substrate(s), diluent, and reaction conditions of temperature, time and concentration for each of five sets of reactions.

Broadly, the experimental results showed that hydrogen transfer, (R1), was by far the major reaction in all circumstances. Reversion of hydrogenated acceptor, (R2), was usually small relative to (R1) but occurred to an appreciable extent at the higher temperatures and holding times. Donor decomposition, (R3), was always negligible relative to (R1) at $T \leq 400$ C. Thus, in deriving the desired kinetic parameters for (R1), the experimental data could directly be treated as if (R1) were the only reaction occurring; corrections for (R2), which were small, allowed more refined parameters to be obtained for (R1) while corrections for (R3) were so small as to be neglible. The kinetic analyses employed are summarized in Table 2.

Data for hydrogen transfer from cyclohexanol to anthracene at T = 375 C are presented in Figure 2, which essentially displays anthracene conversion x vs time for various initial donor/acceptor ratios, $15.4 > S > 0.25$. The ordinate of Figure 2 is a function of conversion chosen to test the presumed second order form of (R1), as suggested by Case 1 of Table 2. Following a typical set of data, say S = 15.4 (squares), the ordinate, starting from the origin, increases with increasing time, linearly at low times, $t < 2$ hr, but with decreasing slope thereafter, eventually becoming constant, independent of time, for $t > 6$ hr. Physically, the initial linear portion represents the kinetics of the forward reaction (R1) alone, while the long-time asymptote of constant conversion represents an approach to equilbrium. It is noteworthy that the initial slopes are much the same for all S, directly yielding $k_1 = 5.6 \times 10^{-6}$ l/mol s independent of substrate proportions, which supports the second order kinetics presumed for (R1). It is also interesting that the asymptotic long-time conversions available at each of S = 1 and S = 15.4 both lead to apparent equilibrium constants $K_{app} = [X^2/(1-X)(S-X)] \sim 0.02$.

Refined rate constants, derived from the initial slope data of Figure 2 after taking account of all other reactions, are displayed in Figure 3 on co-ordinates of $\log_{10}k_1$ vs $\log_{10}S$. It can be seen that $\log_{10}k_1 = -5.25 \pm 0.07$ over $-0.6 < \log_{10}S < 1.2$, i.e. a variation in $\log_{10}k$ of about 0.1 unit over 1.8 decades of substrate proportions ranging on either side of stochiometric. The observed invariance of k relative to S confirms that the cyclohexanol-anthracene hydrogen transfer reaction follows second order kinetics at T = 375 C.

Having established the order, and hence being assured of a meaningful bimolecular rate constant k_1, the hydrogen transfer reaction kinetics were explored over the temperature range from 300-400 C at a fixed S = 4. An Arrhenius plot of these results is presented in Figure 4, using coordinates of $\log_{10}k_1$ vs θ^{-1}, where $\theta^{-1} = (10^3/4.573\ T$ in Kelvins) is an inverse temperature scale; it should be noted that an Arrhenius relation of form $\log_{10}k = \log_{10}A - E^*/\theta$, where A is the pre-exponential factor with units of k and E^* is the activation energy in kcal/mol, will yield a straight line on Figure 4 with slope $\Delta\log_{10}k/\Delta\theta^{-1} = -E^*$. Data for the cyclohexanol-anthracene reaction (circles in Figure 4) show $\log_{10}k_1$ linearly related to θ^{-1} over nearly two decades of the ordinate. The best fit then yielded the hitherto unknown Arrhenius parameters, $\log_{10}A(\ell/\text{mol s}) = 6.0 \pm 0.2$ and E^* (kcal/mol) = 33.1 ± 0.6, which were our goal.

Hydrogen transfer from cyclohexanol to phenanthrene, set 2 in Table 1, was investigated in a manner exactly analogous to that described for cyclohexanol-anthracene in Figures 2, 3, and 4, and similar conclusions could be drawn. Thus, for cyclohexanol-phenanthrene, at T = 400 C, plots akin to the earlier Figure 2 for initial donor/acceptor ratios $8 > S > 0.125$ yielded initial slopes independent of S, with $k_1 \sim 0.65 \times 10^{-6}$ ℓ/mol s. Also, asymptotic long-time conversions led to $k_{app} \sim 0.15 \times 10^{-3}$ at each of S = 4, 1, and 0.125. A further plot of $\log_{10}k_1$ vs $\log_{10}S$, shown in Figure 3, yielded $\log_{10}k_1 = -6.2 \pm 0.2$ over the range $-0.9 < \log_{10}S < 0.9$, affirming the relative invariance of k to substrate proportions and showing the hydrogen-transfer kinetics to be second order. Finally, cyclohexanol-phenanthrene hydrogen transfer rate constants were derived at temperatures from 375-425 C at fixed S = 4. These results, plotted in Figure 4 (squares), yield Arrhenius parameters $\log_{10}A(\ell/\text{mol S}) = 7.6 \pm 0.6$ and E^* (kcal/mol) = 42.5 ± 3.5. Since the data for cyclohexanol-phenanthrene span only a single decade of $\log_{10}k_1$, the corresponding Arrhenius parameters are subject to rather more uncertainty than in the case of cyclohexanol-anthracene.

Reversion of the hydrogenated acceptor to the original acceptor, general reaction (R2), was studied at the conditions indicated for entries 3 and 4 in Table 1, using dihydroanthracene (DHA) and dihydrophenanthrene (DHP) substrates with decalin

diluent, which latter was inert. In general, reversion occurred by two parallel pathways, namely hydrogen elimination (R2') and disproportionation (R2"), of the form:

$$\text{(R2')} \quad HA \xrightarrow{k_2'} A + H_2$$

$$\text{(R2")} \quad 2HA \xrightarrow{k_2"} A + JA$$

where all symbols have their earlier meaning and JA is a more hydrogenated form of the acceptor, e.g. tetrahydroanthracene.

Experiments with DHA substrate at T = 375 C revealed that with neat substrate, 4.0 M, the initial rates of (R2') and (R2") were of comparable magnitudes. With increasing dilution, however, the initial rates of (R2") decreased relative to (R2') until, at the lowest substrate concentration of 0.2 M, (R2") was negligible relative to (R2'). Further, examination of the kinetics showed (R2') to be strictly first order in DHA with $k_2' = (27 \pm 2) \times 10^{-6}$ s^{-1} at initial substrate concentrations from 0.23 to 4.3 mol/liter; reaction (R2") was approximately second order at initial concentrations from 0.9 to 4.3 mol/liter, where it could be measured, yielding $k_2" = (37 \pm 11) \times 10^{-6}$ ℓ/mol s. Additional experiments with neat DHA over the temperature range 325-400 C provided Arrhenius parameters $\log_{10}A(s^{-1}) = 12.5 \pm 0.6$ and E* (kcal/mol) = 50.8 ± 0.8 for the first order DHA reversion rate constant k_2'; these experiments also yielded data for (R2") but corresponding Arrhenius parameters are yet unavailable, pending confirmation of the reaction order.

Experiments with DHP substrate showed (R2') to be the only reversion pathway, with (R2") undetectable. At T = 425 C, the reaction was strictly first order with $k_2' = (34 \pm 2) \times 10^{-6}$ s^{-1} at initial substrate concentrations from 0.22 to 4.0 mol/liter. Arrhenius parameters for DHP reversion over the temperature range 375-420 C were $\log_{10}A(s^{-1}) = 12.6 \pm 0.3$ and E* (kcal/mol) = 58.1 ± 0.8.

Relating the reversion experiments (R2) to the hydrogen transfer experiments (R1), it should be noted that in the latter reaction, the hydrogenated acceptor initially appears at infinite dilution. Thus, of the two reversion pathways, (R2') and (R2"), which are respectively first and second order, (R2') makes much the more significant contribution. Analytically, the overall reversion rate constant $k_2 = k_2' + k_2"[HA] \rightarrow k_2'$ as $[HA] \rightarrow 0$. The cyclohexanol-anthracene series of experiments further confirmed this inference in that the tetrahydroanthracene product symptomatic of (R2") was not detected at times < 2 hr. The rate data obtained for (R2') thus adequately accounted for the reversion reaction (R2) in the present study.

Finally, in regard to the donor decomposition reaction (R3), set 5 in Table 1, the cyclohexanol alone was substantially stable at T ≤ 400 C, with fractional decompositions < 0.03 in 4 hr. At T = 425 C cyclohexanol decomposition, initially to cyclohexanone, became appreciable, with a pseudo first order rate constant $k_3 \sim 20 \times 10^{-6}$ s^{-1}. In processing the hydrogen transfer data, corrections for (R3) were always negligible.

Discussion:

Kinetic data for hydrogen transfer reactions between alcohol donors and aromatic acceptors have not hitherto been reported, precluding comparisons with earlier work. However, the experimental evidence can reasonably be interpreted in favor of a concerted reaction mechanism. Both the hydrogen transfer reactions studied exhibited second order kinetics, being first order in each of the donor and acceptor. This is a necessary condition that must be fulfilled for (R2) to be considered

bimolecular, as written. Further, the Arrhenius parameters ($\log_{10}$A(ℓ/mol s), E*(kcal/mol)) were respectively for CHL-ANT (6.0, 33.1) and for CHL-PHE (7.6, 42.5). Of these the $\log_{10}$A $\sim$ 6.8 ± 0.8 represent activation entropies ΔS^{+} (cal/mol K) = -31.7 ± 3.7 which are large and negative and of much the same magnitude reported (11,12) for Diels-Alder reaction which is well known to be a concerted cyclo-addition (10). There is evidently close steric similarity between the pericyclic transition state of our hydrogen transfer reaction, as shown in the prototype (RO), and the transition state for cyclo-addition. The observed activation energies E*(kcal/mol) = 38 ± 5 cannot independently be interpreted, though their magnitudes are entirely comparable to values known for allowed hydrogen shifts (13), which involve similar orbital interactions.

While the thermochemistry of the present hydrogen transfer reactions is not well known, estimates (14) suggest (ΔS^{o}_{r}(cal/molK), ΔH^{o}_{r}(kcal/mol) for CHL-ANT ($\sim$ 0, $\sim$ 0) and for CHL-PHE ($\sim$ 0, +5); i.e. the reactions are virtually thermoneutral. Consequently, invoking microscopic reversibility, Arrhenius parameters for the reverse hydrogen transfer reactions should be quite similar to those obtained for the forward reactions. In regard to thermochemistry it is also worth noting that the present experiments led to apparent equilibrium constructs of order 10^{-2} for CHL-ANT and 0.15 x 10^{-3} for CHL-PHE at T = 400 C. These cannot be directly interpreted for want of activity coefficient data but their ratio should depend solely on the differences between the entropies and enthalpies of hydrogenation of the acceptors. Estimates (14) of (ΔH^{o}_{f},S^{o}) for each of ANT, DHA, PHE, DHP lead, at T = 400 C, to the theoretical ratio K(CHL-ANT)/K(CHL-PHE) $\sim$ 60 which is of the order of the experimentally observed ratio K_{app}(CHL-ANT/K_{app}(CHL-PHE) $\sim$ 70.

It is interesting to compare the present hydrogen transfer from cyclohexanol with that from Δ^{1}-dialin, a hydrocarbon donor of the same orbital symmetry. Comparable experiments reported elsewhere (15) yielded ($\log_{10}$A(ℓ/mol s), E*(kcal/mol)) = (6.1, 31.0) for the Δ^{1}-dialin-phenanthrene system; $\log_{10}$A is similar to that obtained in the present work for CHL-PHE while the activation energy is lower by an amount comparable to the reduction in the enthalpy of reaction, in rough agreement with the Evans-Polanyi principle.

The reversion reactions (R2) also merit brief discussion inasmuch as kinetic data have not hitherto been reported for hydrogen elimination from either of the DHA or DHP substrates studied in this work. The general reaction (R2') has literature precedent, the case HA = 1,4 cyclohexadiene, A = benzene having been studied (13,16) in the gas phase and found to be unimolecular with Arrhenius parameters ($\log_{10}$A (s^{-1}), E*(kcal/mol)) = (12.4, 43.8); the reaction mechanism has been interpreted (10) as a concerted thermally-allowed 6e suprafacial group transfer. In the present study, (R2') with HA = DHA was strictly unimolecular with Arrhenius parameters ($\log_{10}$A,E*) = (12.6, 50.8). Since there is a clear stereo-electronic analogy between hydrogen elimination from 1,4 cyclohexadiene and that from 9,10-dihydroanthracene, the analogous kinetic data can be taken to imply that the latter reaction is also a 6e pericyclic group transfer. The case of (R2') with HA = DHP which is unimolecular with ($\log_{10}$A,E*) = (12.6, 58.1) is not yet directly amenable to theoretical interpretation. According to the Woodward-Hoffman rules (10), this hydrogen elimination is thermally allowed with antara-supra stereochemistry and without further stereochemical information it is not obvious whether the higher E* relative to DHA represents a stereochemical demand or an orbital symmetry barrier. However, it is interesting that in regard to hydrogen elimination, DHP is more refractory than DHA to essentially the same extent that 1,3 cyclohexadiene (17) is more refractory than 1,4 cyclohexadiene (16).

Finally it is worth noting that with present system of donors and acceptors,

the hydrogen transfer from donor to acceptor was appreciably faster than either hydrogenated acceptor reversion or donor decomposition. This is evidently desirable in the context of actual coal liquefaction operations. Further studies, with appropriate coal-related model donors and acceptors, which thus elucidate the pathways for hydrogen transfer could be practially useful in suggesting donors and processing conditions for the optimal deployment of hydrogen during direct liquefaction.

Conclusions:

1. Hydrogen transfer reactions between cyclohexanol (CHL) donor and each of anthracene (ANT) and phenanthrene (PHE) acceptors have been studied in the liquid phase at temperatures from 300 to 425 C, times from 0.16 to 12.0 hr and initial donor/acceptor ratios of 0.125 to 15.4.

2. In addition to the desired hydrogen transfer reaction (R1), two other pathways were observed, namely, (R2) reversion of the hydrogenated acceptor to original acceptor by way of both hydrogen elimination (R2') and disproportionation (R2"); and (R3) pyrolytic donor decomposition. The kinetics of (R2) and (R3) were also investigated and it was found that (R2) was small and (R3) negligible relative to (R1).

3. The hydrogen transfer reactions were bimolecular, being of order one in each of donor and acceptor. Arrhenius parameters ($\log_{10}$A(ℓ/mol s), E*(kcal/mol)) were respectively for CHL-ANT (6.0 ± 0.2, 33.1 ± 0.6) and for CHL-PHE (7.6 ± 0.6, 42.5 ± 3.5).

4. The observed molecularity and Arrhenius parameters suggest a concerted pericyclic mechanism for the hydrogen transfer with a relatively tight transition state akin to that well known for Diels-Alder cycloaddition.

5. Hydrogen elimination from dihydroanthracene (DHA) and dihydrophenthrene (DHP) liquids was studied at temperatures from 300 to 450 C, times from 0.16 to 10.0 hrs and substrate concentration ranges of 0.2 to 4.0 mol/liter.

6. The hydrogen elimination reactions were strictly unimolecular. Arrhenius parameters ($\log_{10}$A(s^{-1}), E*(kcal/mol) were respectively for DHA (12.6 ± 0.6, 50.8 ± 0.8) and for DHP (12.6 ± 0.3, 58.1 ± 0.8).

7. The observed hydrogen elimination from DHA to ANT is strikingly analogous to thatfrom 1,4 cyclohexadiene to benzene and suggests a similar concerted pericyclic group transfer reaction.

Acknowledgement:

This work was supported by U.S. D.O.E. seed funds administered by the M.I.T. Energy Laboratory.

References:

1. Pott, A. and Broche, H., Glückauf 69 903 (1933).

2. Whitehurst, D.D.: "Asphaltenes in Processed Coals," Annual Report EPRI-AF-480 (1977) and references therein.

3. Ruberto, R.G., Cronaner, D.C., Jewell, D.M., and Seshadri, K.S., Fuel 56 25 (1977).

4. Curran, G.P., Struck, R.T., and Gorin, E., Ind. & Eng. Chem. Proc. Des. & Dev. 6 (2) 166 (1967).

5. Ross, D.S., and Blessing, J.E., ACS Div. of Fuel Chem. Preprints 22 (2) 208 (1977).

6. Neavel, R.C., Fuel 55 161 (1976).

7. Whitehurst, D.D., ACS Symposium Series 71 1 (1978).

8. Virk, P.S. "Pericyclic Pathways in 1,2-Diphenylethane Decomposition", Fuel 58, 149 (1979).

9. Virk, P.S., ACS Div. of Fuel Chem. Preprints 24 (2), 000 (1979).

10. Woodward, R.B., and Hoffmann, R.: "The Conservation of Orbital Symmetry", Verlag Chemie GmbH, Weinheim (1970). Pericyclic reaction terminology defined in this text is used in the present paper.

11. Wasserman, A.: "Diels-Alder Reactions", Elsevier Publ. Co., Amsterdam (1965).

12. Sauer, J., Angew. Chem. Intnl. 6 (1) 14 (1967).

13. Frey, H.M. and Walsh, R., Chem. Rev. 69 103 (1969).

14. Shaw, R., Golden, D.M., and Benson, S.W., J. Phys. Chem. 81 1716 (1977).

15. Bass, D.H., and Virk, P.S.: "Hydrogen Transfer from Dialin Donors", paper presented to the Div. of Fuel Chem., ACS Houston Meeting (1980).

16. Benson, S.W., and Shaw, R., Trans. Faraday Soc. 63 985 (1967).

17. Benson, S.W., and Shaw, R., J. Am. Chem. Soc. 89 5351 (1967).

Table 1. Reaction Conditions.

Set	Substrates	Diluent	Reaction Conditions: Temperature C	Time hr	Concentration S or M
1	CHL + ANT	None	300-400	0.16-12.	0.25-16.
2	CHL + PHE	None	350-425	0.25-10.	0.25-8.0
3	DHA	DEC	300-400	0.16-10.	0.25-4.0(Neat)
4	DHP	DEC	375-450	0.25-12.	0.25-4.0(Neat)
5	CHL	None	325-425	0.25-10.0	4.0 ± 0.2

Notes: Compound abbreviations are as follows:
CHL - cyclohexanol ANT - anthracene PHE - phenanthrene
DEC - decalin DHA - 9,10 dihydroanthracene DHP - 9,10 dihydrophenanthrene

S = initial substrate ratio CHL/ANT or CHL/PHE (sets 1 and 2).
M = concentration, mol/liter of DHA, DHP or CHL (sets 3, 4, and 5).

Table 2. Kinetic Analyses

Reactions: (R1) $D + A \xrightarrow{k_1} DD + HA$
(R2) $HA \xrightarrow{k_2} A + H_2$

Differential Equation: $d(HA)/dt = k_1(D)(A) - k_2(HA)$

Constraints: $t = 0$: $(D/A)_0 = S$; $(HA/A)_0 = 0$
$t > 0$: $A_0 = A + HA$

Solutions:
Case 1. $k_2 = 0$, all S.

$$\frac{1}{A_0(S-1)} \ln\left[\frac{1 - (X/S)}{1 - X}\right] = k_1 t \quad ; \quad X = 1 - (A/A_0) = (HA/A_0)$$

Case 2. $k_2 > 0$, $S > 1$

$$\frac{1}{A_0 S(1+k_2/k_1 SA_0)} \ln\left[\frac{1}{(1-X(1+k_2/k_1 SA_0)}\right] = k_1 t$$

Case 3. $k_2 > 0$, $S < 1$

$$\ln\left[\frac{k_1 SA_0 \exp(-k_1 A_0 t)}{k_1 SA_0 \exp(-k_1 A_0 t) - k_2 X}\right] = k_2 t$$

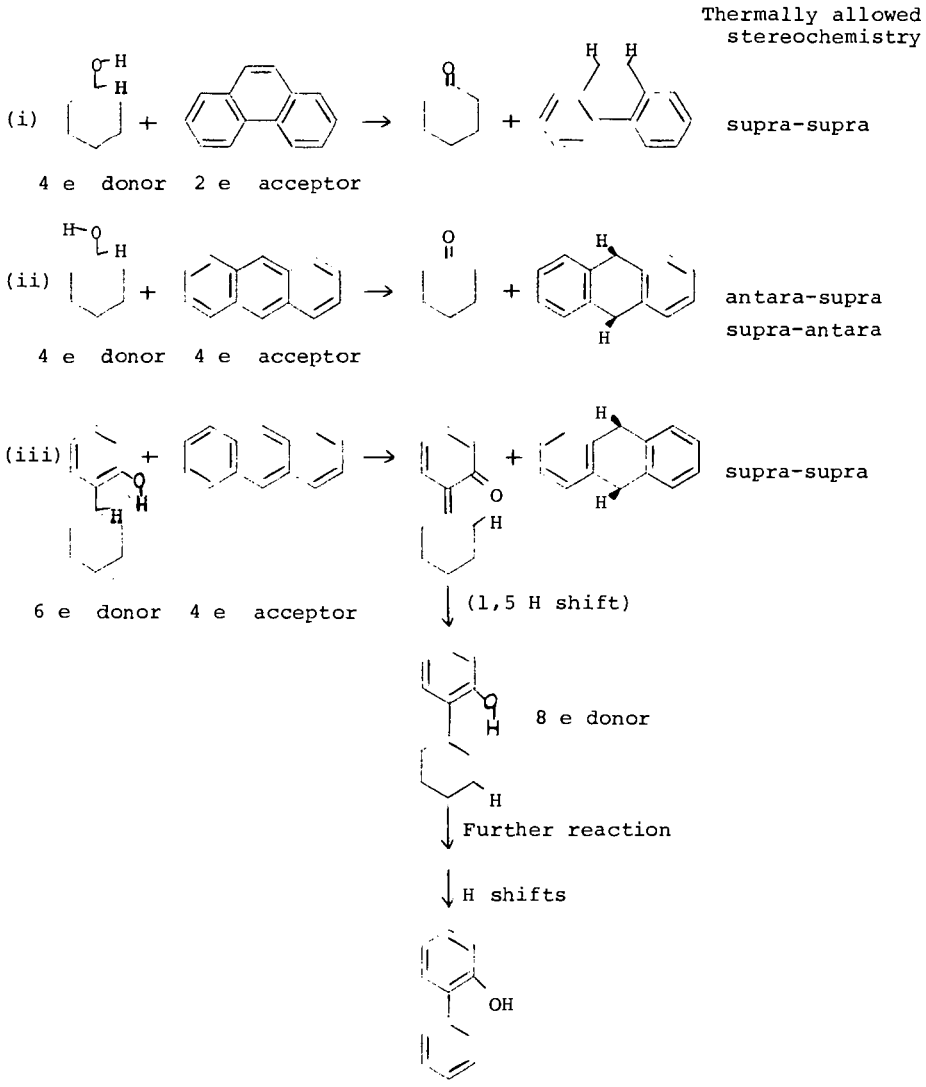

Figure 1. Orbital symmetry conservation in hydrogen transfer.

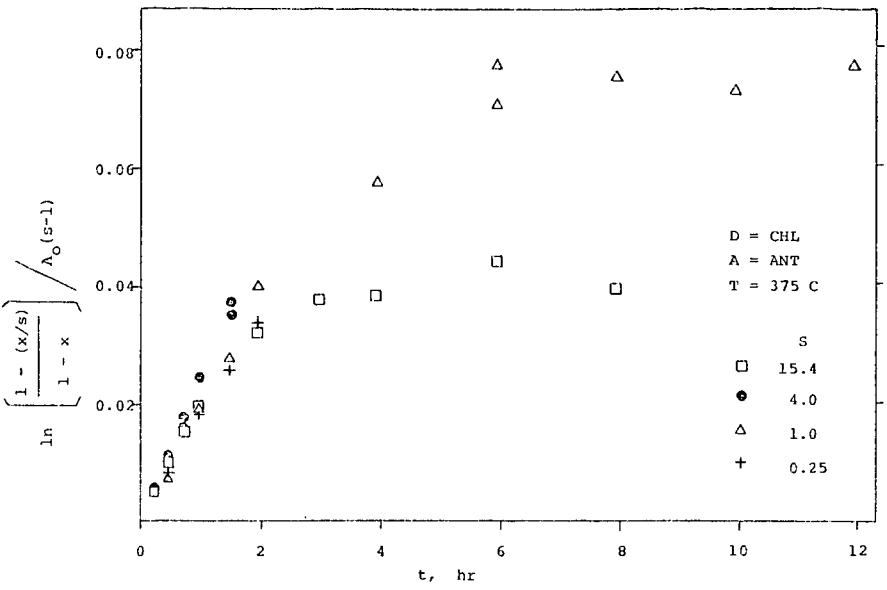

Figure 2. Hydrogen transfer kinetics: Conversion versus time.

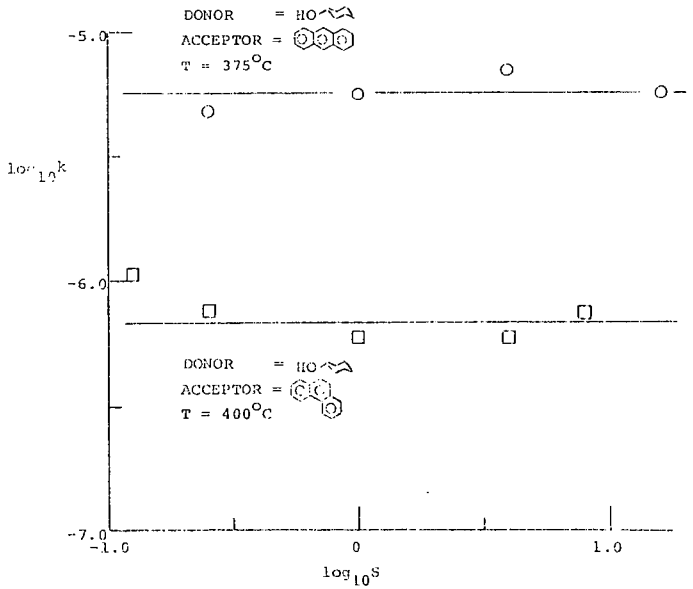

Figure 3. Hydrogen transfer kinetics:
Effect of (donor/acceptor) ratio.

Figure 4. Hydrogen transfer kinetics: Arrhenius plot.

REACTION: D + A → DD + HA

DONOR = HO- 

ACCEPTOR	$\log_{10}A$	E^*
○ 	6.0 ±0.2	33.1 ±0.6
□ 	7.6 ±0.6	42.5 ±3.5

SULFUR REMOVAL FROM COAL CHAR USING " CONVERT-REMOVE" TECHNOLOGY

ANN BAUGH TIPTON

OCCIDENTAL RESEARCH CORPORATION,
P.O. BOX 19601,
IRVINE, CALIFORNIA 92713

BACKGROUND

The reactivity of the organic sulfur in coal and char continues to be the major challenge to finding an economical method to produce a compliance boiler fuel, i.e., to remove ninety percent of the sulfur from run-of-mine coal prior to combustion.

Two recent studies, one by Contos, Frankel and McCandless(1) and another by Attar and Dupuis(2), offer clues to what will be needed in an improved method to meet these goals for coal desulfurization. The study by Contos, et al., described the economic and technical strengths of existing processes for chemical coal cleaning. The study concludes, "Chemical Coal Cleaning Processes can remove as much as 95 to 99 percent of pyritic sulfur and up to about 40 percent of the organic sulfur from run-of-mine coal." The comparison of the major processes from this study is shown in Table 1.

Table 1

COMPARISON OF MAJOR CHEMICAL COAL CLEANING PROCESSES*

	Max. % Removal		Product Cost
Process	Pyrite	Organic S	$/Ton
Magnex	90	0	40.70
Syracuse	50-70	0	37.00
Meyers	90-95	0	43.40
Ledgemont	90-95	0	46.90
DOE	95	40	51.60
GE	-	75% Total -	41.80
Battelle	95	25-50	55.90
JPL	90	70	46.00
IGT	95	85	65.80
KVB	95	40	47.50
Arco	95	"some"	46.00-58.00

* Ref. (1)

With the exception of IGT, all of the processes in Table 1 which remove organic sulfur rely on oxidizing agents. The evidence seems quite convincing that the most difficult to remove organic sulfur is not reactive to oxidizing agents. This, in turn, leads us to pursue reducing agents.

Recent research by Attar and Dupuis(2) offers evidence for the capability of reducing agents for organic sulfur removal. Attar *et al.* used strong reducing agents with catalyst at temperatures up to 400°C as a method to identify and quantify organic sulfur groups in coal. Attar *et al.* found that almost half of the organic sulfur in high sulfur bituminous coals did not react under their test conditions. Attar and Dupuis conclude, "An upper bound exists on the maximum portion of the organic sulfur than can be removed without the complete destruction of the coal matrix."

These studies, then, point to a coal desulfurization method which uses reducing agents at temperatures which destruct the coal matrix. The technology to be reported is one such approach to the problem. The conventional approach which incorporates these features is hydrodesulfurization (HDS). This is used in the IGT process listed in Table 1 with the highest product cost of all, $66/ton, and before that was the major step in the Clean Coke Process. HDS uses very high hydrogen to solids ratios to remove sulfur. An example of HDS with char is shown in Figure 1. Here, almost 200,000 SCF H_2/ton was required to take 2.4% sulfur to 0.7% sulfur. In this example, even with large volumes of hydrogen, a compliance fuel was not produced. The main chemical reaction which controls the sulfur removal in HDS and demands the high hydrogen capacity is the equilibrium reaction between ferrous sulfide and hydrogen,

$$FeS + H_2 = Fe + H_2S. \qquad \text{Eq. (1)}$$

At 800°C, the concentration of hydrogen sulfide in hydrogen would have to be less than 2000 ppm before this reaction would proceed forward. To keep the hydrogen sulfide dilute enough for sulfur removal to occur requires 125,000 SCF of hydrogen per ton of coal to remove one percent of sulfur.

CHEMISTRY OF THE "CONVERT-REMOVE" TECHNOLOGY

The "Convert-Remove" technology uses two types of treatment steps to produce a low sulfur product. The Convert step is concerned with lowering the organic sulfur while the Remove step only affects inorganic sulfur.

THE CONVERT STEP

The chemistry of the Convert step includes two reactions. First, hydrogen, reacts with organic sulfur (RS) to form hydrogen sulfide,

$$RS + H_2 = R' + H_2S. \qquad \text{Eq. (2)}$$

Next, the hydrogen sulfide is free to react with in-situ sulfur scavengers to form inorganic sulfides because the hydrogen to solids ratio is low,

$$FeO + H_2S = FeS + H_2O. \qquad \text{Eq. (3)}$$

The overall result of hydrogen treatment is the conversion of organic sulfur to inorganic sulfur with total sulfur remaining constant. This is in extreme contrast to the conventional approach to hydrogen treatment (HDS) where much higher hydrogen to solids ratios are used and sulfur is removed.

THE REMOVE STEP

The removal of the inorganic sulfide sulfur could be accomplished in a number of ways, e.g., acid leach(3), oxidation. However, we have chosen an approach which regenerates the sulfur scavengers, i.e., steam displacement using the reverse of the reaction by which it was formed,

$$FeS + H_2O = FeO + H_2S. \qquad \text{Eq. (4)}$$

While high flow rates of steam are now required to sweep out the hydrogen sulfide to maintain removal, very little water is actually consumed - probably no more than a gallon per ton of char.

EXPERIMENTAL

Two laboratory batch reactor systems are used for desulfurization studies. Figure 2 shows the schematic diagram of the reactor setup. One of the reactor

systems is equipped with two gas chromotographs for on-line gas analysis. One gas chromatograph (a Perkin Elmer Sigma 1) is used to monitor hydrocarbons and fixed gas composition in steam and hydrogen treatments of solids. The sulfur species such as H_2S, SO_2, COS, CH_3SH, CH_3SCH_3, CH_3SSCH_3 and CS_2 of the gas stream are measured by a Tracor gas chromatograph with a Hall detector.

The high sulfur chars used in the experiments reported in the next section were produced in a bench scale entrained flow reactor using an air-nitrogen mixture as carrier gas. Pulverized West Kentucky No. 9 seam coal (Hamilton Mine) at 1075°F for 0.69 sec. with 3% oxygen for decaking was used to produce the coal char.

RESULTS

The strength of the "Convert-Remove" technology comes from the discovery that repetition of short cycles of the two treatment steps is more effective for sulfur removal than is a single two-step cycle with long treatment times. Also we find that when an initial coal devolatilization step has produced a char with a high sulfide sulfur content, an initial Remove treatment step prior to the "Convert-Remove" cycle will produce a lower sulfur product. The results which established these effects are given in Table 2.

Table 2

CONVERT (C) AND REMOVE (R) TREATMENT STEPS

CHAR DESULFURIZATION RESULTS

Process Steps	Total Sulfur	Sulfide Sulfur	Organic Sulfur	SCF H2 Ton	$lbSO_2$ MMBTU
Coal	2.75	0.04	1.74	--	4.2
Starting Char	2.42	0.59	1.73	--	4.2
CR	0.64	0.13	0.43	76,800	1.1
RCR	0.49	0.03	0.37	76,800	0.9
CRCR	0.34	0.04	0.29	153,600	0.6
CRCRCR	0.23	0.05	0.13	230,400	0.4
CCCRRR	0.46	0.18	0.18	230,400	0.8
Starting Char	2.48	0.80	1.59	--	4.3
CR	0.94	0.34	0.52	12,800	1.6
CCRRR	0.50	0.10	0.27	25,600	0.7
CRCR	0.43	0.14	0.22	25,600	0.5
RCRCR	0.27	0.11	0.09	25,600	0.4

In the first series of tests, high volumes of hydrogen were used. In the second series, we reduced the hydrogen volume by an order of magnitude. For an initial Convert treatment we have found that volumes as low as 1000 SCF/ton are effective. The results are shown in Figure 3.

The technology has also been tested on a Wyoming sub-bituminous coal and a "Flash Pyrolysis" char (4) from this coal. The results of these tests are shown in Table 3. These data give strong support to our mechanism for organic sulfur removal via an in-situ sulfur scavenger. All treatment times - 5, 10, 15, or 30 min. - with hydrogen produced identical results. The sulfide sulfur capacity of this material is quickly saturated by the hydrogen treatment. Until this sulfide sulfur is removed with steam, the residual organic sulfur is unreactive to the hydrogen. The three step RCR treatment is marginal for ninety percent removal, while the five step RCRCR treatment accomplished almost complete removal.

Table 3

"CONVERT - REMOVE" TREATMENTS OF

WYOMING SUB-BITUMINOUS COAL AND CHAR

	Flash Pyrolysis Char			Coal		
Treatment*	Total Sulfur	Sulfide Sulfur	Organic Sulfur	Total Sulfur	Sulfide Sulfur	Organic Sulfur
Feed Coal	0.79	0	0.63	0.72	0.02	0.61
Char	0.54	0.06	0.41	-	-	-
C(5)	0.64	0.13	0.49	0.74	0.18	0.48
C(10)	0.65	0.11	0.51	0.68	0.19	0.40
C(15)	0.58	0.15	0.40	0.59	0.19	0.32
C(30)	0.64	0.14	0.47	0.74	0.21	0.46
R(15)	0.36	0	0.34	0.55	0.04	0.46
R(30)	0.35	0	0.32	0.53	0.06	0.40
RCR	0.11	0.03	0.06	0.16	0.04	0.08
RCRCR	0.03	0.01	0	0.07	0.04	0

* C-10 min., R-30 min. unless given in parenthesis

A side benefit of the "Convert-Remove" technology is the removal of nitrogen. The nitrogen contents of the coals, chars, and desulfurized chars are given in Table 4.

Table 4

"CONVERT - REMOVE" TREATMENT

ALSO TAKES OUT HALF OF THE COAL NITROGEN

	% N (Dry Basis)		
Coal Description	Feed Coal	Char	Desulfurized Char
W. Ky. No. 9 Seam	1.55	1.65	0.77
Wyoming Sub-bituminous	1.24	1.33	0.64

For both the bituminous and sub-bituminous coals about half of the nitrogen was removed.

CHAR REACTIVITY

Reactivity of char to both combustion and desulfurization is important to the utilization of the "Convert-Remove" technology. All of the chars tested in our program were devolatilized in an entrained flow reactor with high heating rates, short resistance time and moderate temperature using ORC's "Flash Pyrolysis" technology (4). Such conditions have been shown to be ideal for producing reactive chars (5,6,7,8). Essenhigh (5,6) found that a gasification char had equivalent reactivity to combustion as coal, while a COED char produced with lower heating rates and longer residence times had a much lower reactivity. Walker (7,8) in studying reactivity of chars to gasification, found that both rapid heating and low temperature air oxidation of caking coals enhance the reactivity of the chars produced.

We have found that less sulfur is removed by direct "Convert-Remove" treatment of a decaked high sulfur bituminous coal than is removed from char. However, the same level of sulfur removal is found for sub-bituminous coal and char. Consequently when caking high sulfur coals are to be desulfurized, an initial coal devolatilization treatment which produces a reactive char, e.g., partial gasification or decaking and rapid pyrolysis, will be needed. Recovery of the volatilized coal fraction will be important to good economics for any coal feed.

CONCLUSION

The "Convert-Remove" technology is effective in removing ninety percent or more of the sulfur in a reactive char from high sulfur bituminous coals and in sub-bituminous coals or chars.

REFERENCES

1. Contos, G.Y., Frankel, I.F., McCandless, L.C., "Assessment of Coal Cleaning Technology: An evaluation of Chemical Coal Cleaning Processess," EPA-600/7-78-173A, PB-189493/9WE, August 1978.

2. Attar, A. and Dupuis, F., "Data on the Distribution of Organic Sulfur Functional Groups in Coal," Preprints of Division of Fuel Chemistry, ACS, 24 (1), 166 (1979).

3. Tipton, A.B., "Improved Hydrodesulfurization of Coal Char by Acid Leach," ACS Symposium Series, No. 64, 280 (1977).

4. Che, S.C., Duraiswamy, K., Knell, E.W., and Lee, C.K., "Flash Pyrolysis Coal Liquefaction Process Development," Occidental Research Corporation Final Report to the U.S. Department of Energy, Fe-2244-26, April 1979.

5. Essenhigh, R.H. and Csaba, J., Ninth Symposium (Internation) on Combustion, p. 111, Academic Press, 1963.

6. Cogoli, J.G., Gray, D. and Essenhigh, R.H., "Flame Stabilization of Low Volatile Fuels," Combustion Science and Technology, 16, 165, (1977).

7. Ashu, J.T., Nsakala, N.Y., Mahajan, O.P. and Walker Jr., P.L., "Enhancement of Char Reactivity by Rapid Heating of Precusor Coal," Fuel, 57, 250 (1978).

8. Mahajan, O.P., Komatsu, M. and Walker Jr., P.L., "Low Temperation Air Oxidation of Caking Coals, I. Effects on Subsequent Reactivity of Chars Produced," Fuel, to be published.

Figure 2

Laboratory Batch Reactor for "Convert-Remove" Treatment

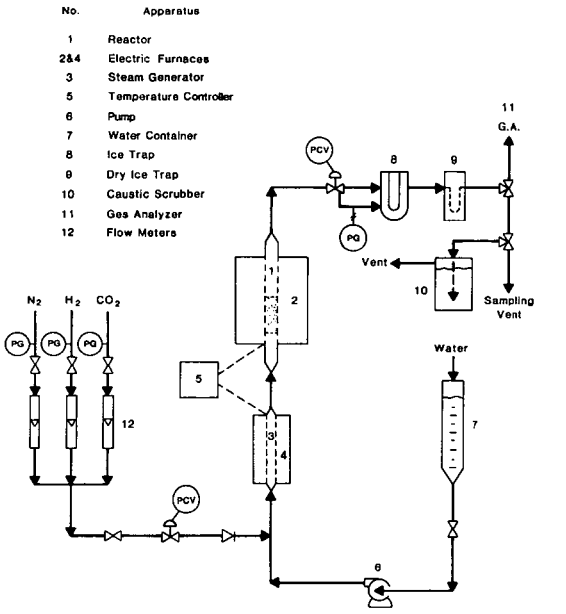

4645

Figure 1

Hydrodesulfurization Requires High Hydrogen Capacity

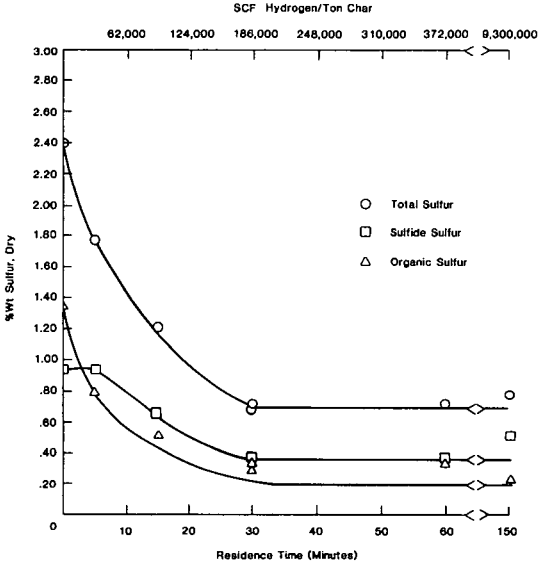

2899

Figure 3
Convert Treatment Uses Low Hydrogen Volumes

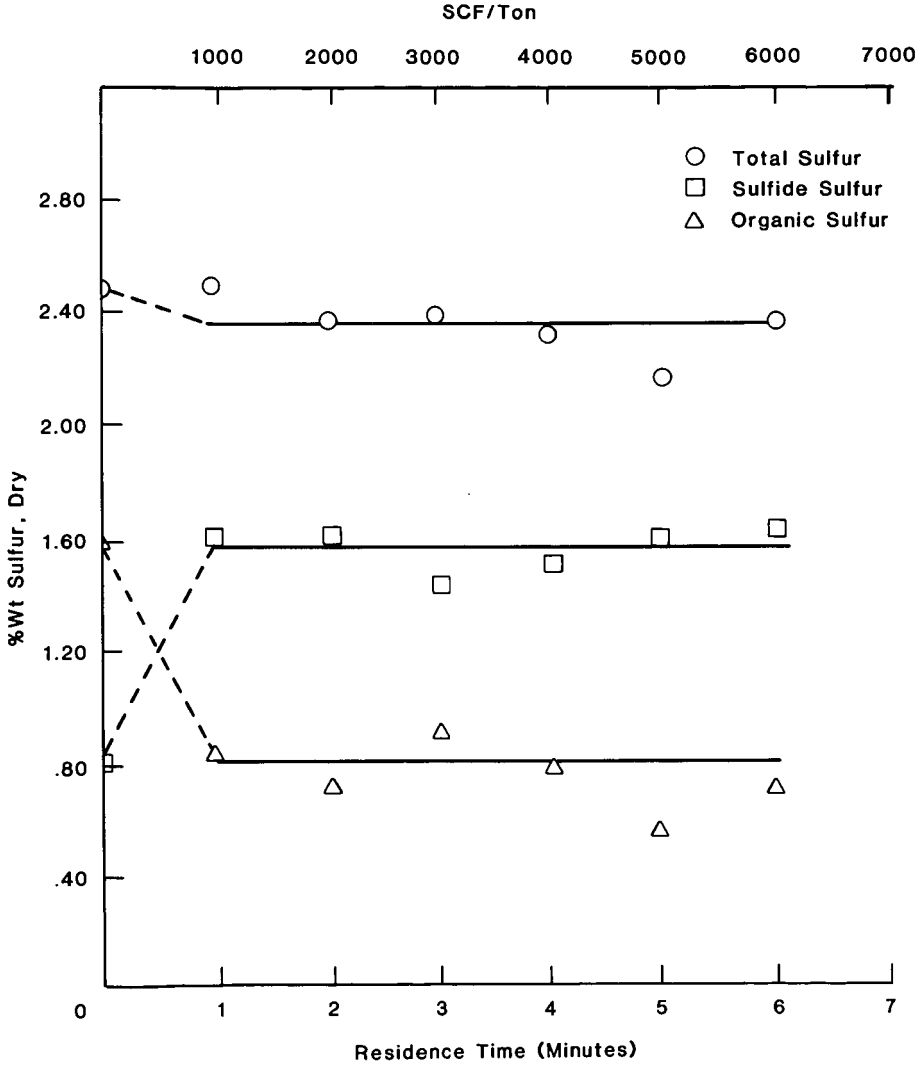

PYROLYSIS OF THE POLYMER COAL: STRUCTURE AND KINETICS

BY

AMIR ATTAR AND GREGORY G. HENDRICKSON

DEPARTMENT OF CHEMICAL ENGINEERING
UNIVERSITY OF HOUSTON
HOUSTON, TEXAS 77004

1. INTRODUCTION

A kinetic model which predicts the rate of formation of gaseous products produced during coal pyrolysis has been developed. The basis assumptions of the kinetic model are similar to those of Attar (1) for the kinetics of coal liquefaction in a hydrogen donor solvent. The main assumption is that different coals consist of the same organic functional groups and that the differences between coals are due to the different concentrations of the functional groups. The functional groups most important in forming gaseous products are hydroaromatic hydrogen, methyl groups, ethyl groups and oxygen functionalities, i.e., carboxyl groups, carbonyl groups, phenols and ether linkages. The products of coal pyrolysis are to a large extent determined by the initial concentration of each of the above mentioned functionalities.

The chemistry and thermodynamics of functional group reactions in coal are, to a first-order approximation, independent of the particular coal (2). It is also plausible to assume that the reaction rate of each functional group is independent of the particular coal and only dependent upon the regent, the reactive group and the temperature. Thus the kinetic parameters, the activation energy and the frequency factor, are assumed to be independent of the particular coal. Arrhenius dependence of the rate constants are assumed.

The rate of product generation appears to be controlled by thermal decomposition of the coal (3), thus the rate of chemical reaction is assumed to be the controlling rate. Mass transfer effects have been neglected. The bond breaking process has been assumed to proceed by a free radical mechanism for which the steady state assumption can be applied. The free radicals can then form stable products by combination reactions with other radicals or by hydrogen abstraction reactions. Secondary reactions, other than the water-shift reaction, have been neglected. The water-shift reaction has been assumed to proceed to equilibrium.

The kinetic model incorporates all of the above assumptions into a set of rate equations for the transformations of the various functional groups. Isothermal

kinetics or a constant heating rate can be used. The rate expressions are integrated numerically using a semi-implicit third order Runge-Kutta method with the initial functional group distribution in a coal as the boundary condition. After each integration step, the water-shift reaction is shifted to equilibrium.

2. KINETIC MODEL

The kinetic model which has been developed is based on the premise that free radicals are released from the coal matrix and then undergo combination reactions or hydrogen abstraction reactions to form stable products. The free radicals which are released from the coal matrix include hydrogen atoms, methyl groups and ethyl groups. Each of these radicals is released from the coal matrix according to the first-order reaction

$$S - R \rightarrow S\cdot + R\cdot$$

where $S\cdot$ is the radical remaining in the solid phase to later take place in tar forming or char forming reactions and $R\cdot$ is either $H\cdot$, $\cdot CH_3$ or $\cdot C_2H_5$. Once formed, the free radicals can either undergo a second-order combination reaction of the type

$$R_i\cdot + R\cdot_j \rightarrow R_iR_j$$

where i and j refer to any of the above mentioned radicals and R_iR_j is the stable product, or they can abstract hydrogen from the coal matrix to result in the stable product RH. The hydrogen abstraction reaction is a second-order reaction of the type.

$$R\cdot + S'H \rightarrow S'\cdot + RH$$

The reactions involving free radicals can produce the gaseous products H_2, CH_4, C_2H_6, C_3H_8 and C_4H_{10}. Once a stable product is formed, cracking reactions to form lower molecular weight products are not assumed to occur. This assumption is approximately correct in that the components most likely to crack, i.e., C_3H_8 and C_4H_{10}, are produced only in minor quantities. Ethylene production is assumed to occur as a resulted of the unimolecular decomposition of ethyl radicals according to the reaction

$$\cdot C_2H_5 \rightarrow C_2H_4 + H\cdot$$

Other reactions which must be considered involve oxygen functional groups. The oxygen functional groups are responsible for the formation of CO_2, CO and H_2O. Carbon dioxide is assumed to occur due to decarboxylation reactions involving carboxyl groups. Carbon monoxide is assumed to be formed from two sources. The low temperature peak is thought to result from elimination of quinonic-carbonyl groups. The higher temperature peak is thought to result from the cleavage of ether linkages. Water formation is due to reactions involving phenol groups. Each of these products is assumed to be formed according to first-order kinetics.

Finally, the gas phase reaction

$$H_2O + CO \rightleftharpoons CO_2 + H_2$$

must be considered. This reaction has been shown to be approximately in equilibrium in the products from coal pyrolysis (4,5) and is the only "secondary" reaction considered in the kinetic model. After each integration step the product composition is shifted to equilibrium values for the above reaction. The water-shift reaction is the "tie" between the effective rate of production of each of the products involved and the actual rate of production of each of these products.

3. MATHEMATICAL DEVELOPMENT

As previously mentioned, the rate of formation of $H^{\cdot}$, $\cdot CH_3$, $\cdot C_2H_5$, CO_2, CO and H_2O is assumed to be described by first-order kinetics. The rate of formation of each of these species can thus be described by the equations

$$\frac{dR_i}{dt} = k_i (S\text{-}R)_i$$

where R_i is the "gas" phase concentration of the i-th species and $(S\text{-}R)_i$ is the concentration of that species remaining attached to the coal matrix. When R_i is $H^{\cdot}$, $\cdot CH_3$ or $\cdot C_2H_5$ the radical can be stabilized by combination reactions with other radicals or by hydrogen abstraction reactions. Both of the above reactions are assumed to follow second-order kinetics with the exception of two hydrogen atoms combining to form molecular hydrogen which requires a third body for stabilization of the product. Thus the rate of formation of stable products is described by equations 3.2 through 3.7.

$$\frac{d(H_2)}{dt} = k_1 (H^{\cdot})^2 (M) + k_2 (H^{\cdot})\ S\text{-}H \qquad 3.2$$

$$\frac{d(CH_4)}{dt} = k_3 (H^{\cdot}) (\cdot CH_3) + k_4 (\cdot CH_3) (S\text{-}H) \qquad 3.3$$

$$\frac{d(C_2H_6)}{dt} = k_5 (\cdot CH_3)^2 + k_7 (\cdot C_2H_5) (H^{\cdot}) + k_8 (\cdot C_2H_5) (S\text{-}H) \qquad 3.4$$

$$\frac{d(C_3H_8)}{dt} = k_6 (\cdot CH_3) (\cdot CH_3) (\cdot C_2H_5) \qquad 3.5$$

$$\frac{d(C_4H_{10})}{dt} = k_9 (\cdot C_2H_5)^2 \qquad 3.6$$

$$\frac{d(C_2H_4)}{dt} = k_{10} (\cdot C_2H_5) \qquad 3.7$$

In equations 3.2 - 3.7 the radical combination reactions occur with no activation energies. Hydrogen abstration rate constants and the ethyl decomposition rate constant assume Arrhenius behavior. The rate constants associated with equations 3.1 - 3.7 are listed in Tables 3.1 - 3.3. Along with

the rate constants associated with the functional group transformations are activation energies for the decomposition reactions of the polymers assumed to characterize the bond breaking process involved in the functional group transformations.

In order to integrate the given rate equations the radical concentrations must be available. The radical concentrations have been obtained with radical balances and the assumption that the steady-state approximation is valid.

According to Benson (6), the steady-state assumption has been shown to be valid if the total radical concentration is negligible compared to the reactant and product concentrations. The radical concentrations are usually negligible in the integration procedure which has been incorporated. The utility of the steady-state assumption is that it converts differential equations into algebraic equations which can then be solved for the radical concentrations. The radical balances are presented in equations 3.8 - 3.10.

$$\frac{d(H\cdot)}{dt} = \frac{d(S-H)}{dt} - 2k_1 (H\cdot)^2 (M) - k_2 (H\cdot) (S-H) - k_3 (\cdot CH_3) (H\cdot) - k_7 (\cdot C_2H_5) (H\cdot) + k_{10} (\cdot C_2H_5) = 0 \qquad 3.8$$

$$\frac{d(\cdot CH_3)}{dt} = \frac{d(S-CH_3)}{dt} - k_3 (\cdot CH_3)(H\cdot) - k_4 (\cdot CH_3) (S-H) - 2k_5 (\cdot CH_3)^2 - k_6 (\cdot CH_3) (\cdot C_2H_5) = 0 \qquad 3.9$$

$$d(\cdot C_2H_5) = d(S-C_2H_5) - k_6 (\cdot CH_3) (\cdot C_2H_5) - k_7 (\cdot C_2H_5) (H\cdot) - k_8 (\cdot C_2H_5) (S-H) - 2k_9 (\cdot C_2H_5)^2 - k_{10} (\cdot C_2H_5) = 0 \qquad 3.10$$

In the kinetic model the radical balances are solved by successive approximations until a solution is obtained within allowable error.

Table 3.1

Functional Group Decomposition Rate Constants

Functional Group	A(sec^{-1})	E(kcal/mole)
-H	73.0	25.0
$-CH_3$	16.7	18.0
C_2H_5	16.7×10^6	31.4
-COOH	550.0	19.5
-C=O	55.0	18.0
-O-	2500.0	30.2
-OH	1.05×10^{15}	

Model Compound	E(kcal/mole)	Reference
Tetralin (-H)	22.0	11
Polybenzyl ($-CH_3$)	53.0	12
Polyacrylic Acid (1-COOH)	27.0	13
Poly (2,6-dimethyl-1,4-phenylene ether)(OH)	57.0	14

Table 3.2

Radial Reaction Rate Constants

Reaction	k(cc/mole sec)	Reference
$H\cdot + H\cdot + M \rightarrow H_2 + M$	8.9×10^{15}*	15
$\cdot CH_3 + H\cdot \rightarrow CH_4$	6.0×10^{12}	16
$\cdot CH_3 + \cdot CH_3 \rightarrow$	3.16×10^{13}	17
$\cdot CH_3 + \cdot C_2H_8$	2.51×10^{12}	18
$\cdot C_2H_5 + H\cdot \rightarrow C_2H_6$	3.63×10^{12}	17
$\cdot C_2H_5 + \cdot C_2H_5 \rightarrow C_4H_{10}$	1.0×10^{13}	18
$\cdot C_2H_5 \rightarrow C_2H_4 + H\cdot$	$k = 2.7 \times 10^{14} \exp(-40{,}900/RT)\,sec^{-1}$	19

Table 3.3

Hydrogen Abstraction Reactions Rate Constants

Reaction	log A(cc/mole sec)	E(kal/mole)	Reference
$H\cdot + S\text{-}H \rightarrow H_2 + S\cdot$	10.61	5.4	20
$\cdot CH_3 + S\text{-}H \rightarrow CH_4 + S\cdot$	10.61	8.0	estimated
$\cdot C_2H_5 + S\text{-}H \rightarrow C_2H_6 + S\cdot$	13.5	4.4	estimated

4. RESULTS

The concentrations of the various gaseous products produced during coal pyrolysis and the rate of formation of these gases can be obtained by employing the kinetic model previously described. The results of modeling the prolysis of two typical coals are described in this section. In both cases, the results from the kinetic model have been compared to experimental data obtained from the literature. The published data is that of Campbell and Stephens (7) and Makino and Toda (8,9).

Campbell and Stephens (7) pyrolyzed Wyodak subbituminous coal at temperatures between 110° and 1000°C. A constant heating rate of 3.33°C/mm was used to heat a sample weighing 50 gm and consisting of particles sized between 10 mesh and 6 mesh. Argon was used as a carrier gas to sweep the gaseous products to a mass spectrometer for quantitative determination of the product composition. Experimentally obtained gas evolution curves are compared with the curves obtained from the kinetic model in Figures 1-4. A material balance is presented in Table 4.1. The experimental carbon dioxide yield was estimated by graphical integration of the experimental rate of evolution curve.

It is interesting to compare the initial functional group distribution with the calculated gaseous yield. It can be seen that all of the methyl groups go into the formation of methane and all of the ethyl groups form ethane. Radical combination reactions other than with hydrogen are negligible. Also, if enough hydrogen is subtracted from the initial hydrogen concentration to account for methane and ethane formation, the yield of molecular hydrogen would be 61.3 cm^3/gm compared to the calculated yield of 98.9 cm^3/gm. This apparent discrepancy, along with the observation that more carbon dioxide is in the products than there is carboxyl groups in the feed is the result of the water-shift reaction. For this case, the overall effect of the water-shift reaction is a shift in the direction

$$H_2O + CO \rightarrow CO_2 + H_2$$

It should be noted that all of the calculated water yield is formed from the phenols. If some moisture is initially present and the water-shift reaction proceeds in the same direction as before, the calculated hydrogen yield could be made to approach the experimental yield.

The methane and ethane yields are presented in Figure 1. It can be seen that first-order kinetics do not adequately describe the rate of methane formation, especially at the tail end of the rate curve. This observation is in agreement with Fitzgerald and Van Krevelen (10) who said that the rate of methane formation does not decrease as rapidly as predicted by first-order kinetics. Based on kinetic arguments, they postulated a second source of methane to be the reaction

$$C(s) + 2H_2 \rightarrow CH_4$$

The second methane source which is postulated here is the rupture of alicyclic rings. Methane has been shown to be produced upon the pyrolysis of tetralin (11), thus alicyclic rings are known to be able to form methane upon pyrolysis.

Table 4.1

Characterization of Wyodak Subbituminous Coal

Coal Composition		Gaseous Equivalent of the Initial Functional Group Distribution		Gaseous Yield (cm^3/gm)		
Component	Wt.%	Group	Conc.(cm3/gm)	Component	Experimental	Model
C	66.76	-H	196.4	H_2	124.8	98.9
H	5.25	$-CH_3$	67.2	CH_4	67.2	67.2
O	16.99	$-C_2H_5$	6.6	C_2H_6	6.63	6.6
N	1.11	-COOH	18.2	CO_2	48	54.9
S	0.74	C =O	26.1	CO	45.9	63.6
		-O-	73.1	H_2O	---	66.8
		-OH	101.9			

The rupture of alicyclic rings should be more important in lower ranked coals since the concentration alicyclic ring is postulated to decrease with an increase in rank.

A comparison between calculated and experimental volatilization yields for an anthracite are illustrated in Figures 5-8. Makino and Toda (8,9) used a flow-type high pressure reactor and a constant heating rate of 3.3° C/min up to a final temperature of 900°C in their experiments. A constant flowrate of helium was used to sweep gaseous products out of the reactor and into a high speed chromatograph for analysis. Argon was used as a carrier gas in separate experiments for the determination of hydrogen. The experimental curves reproduced herein were obtained by graphical integration of experimental rate curves. An estimated 10-15% error in the calculated yields is possible. A material balance is included in Table 4.2.

Table 4.2

Characterization of Omine Anthracite

Coal Composition		Gaseous Equilvalent of the Initial Functional Group Distribution				
Component	Wt.%	Group	Conc.(cm^3/gm)	Component	Experimental	Model
C	93.2	-H	150.1	H_2	138.7	71.8
H	3.3	$-CH_3$	10.8	CH_4	11.3	10.8
O	1.2	$-C_2H_5$	0.05	C_2H_6	-----	0.05
N	1.7	-COOH	0.0094	CO_2	1.52	1.23
S	0.7	C =O	0.76	CO	3.18	7.36
		-O-	7.81	H_2O	------	7.16
		-OH-	8.25			

The main observations are:

1. All the methyl and ethyl groups form methane and ethane respectively. For this case, first order kinetics can adequately describe the methane evolution rate. This observation is another point in favor of the secondary methane source required for lower ranked coals being the cleavage of alicyclic rings.

2. The water-shift reaction shifts in the direction

$$H_2O + CO \rightarrow CO_2 + H_2$$

The calculated carbon dioxide yield shown in Figure 7 is a direct result of the water-shift reaction. A negligible amount of the carbon dioxide evolved is the result of decarvoxylation reactions.

5. MODEL LIMITATIONS

The limitations of the model are:

1. The model does not predict tar yields.
2. The model is limited to low pressure applications due to the neglect of secondary reactions.
3. The rate constants for the release of the free radicals from the coal are applicable to low heating rates. A heating rate of as high as 60° C/sec will shift the calculated initial temperature for methane formation away from the experimental temperature by approximately 10°C.
4. Correlations predicting the initial functional group distribution are limited to coals containing between approximately 70% C and 92% C.

BIBLIOGRAPHY

1. Attar, A., Prep. Div. Fuel Chem., A.C.S., 23 (4), 169 (1978).

2. Messenger, L. and Attar, A., Fuel, 58 (9), 655 (1979).

3. Anthony, D. B. and Howard, J. B., A.I.Ch.E.J., 22 (4), 625 (1976).

4. Suuberg, E. M., W. A. Peters and J. B. Howard, I.E.C., Proc. Des. Div., 17 (1), 37 (1978).

5. Wen, C. Y. and T. Z. Chaung, I.E.C., Proc. Des. Div., 18 (4), 684 (1979).

6. Benson, S. W., "Thermochemical Kinetics", Wiley, N. Y., 1976, p. 229.

7. Campbell, J. H. and D. R. Stephens, A. C. S. Prep. For 1976 meeting in San Francisco.

8. Makino, M. and Y. Toda, Fuel, 58, 231 (1979).

9. Makino, M. and Y. Toda, Fuel, 58, 573 (1979).

10. Fitzgerald D. and D. W. Van Krevelen, Fuel, 38, 17 (1959).

11. Bredael, P. and T. H. Vinh, Fuel, 58, 211 (1979).

12. Madorsky, S. L. and S. Straus, J. Res. Nat'l. Bur. Standards, 53 (6), 361.

13. Eisenbert, A. and T. Yokoyama, A. C. S. Div. Polym. Chem., 9 (2), 1408 (1968).

14. Factor, A., J. Polym. Sci., Part A-1, 7, 363 (1969).

15. Kretschmer, C. B. and H. L. Peterson, J. Chem. Phys., 39, (7), 1772 (1963),

16. Mulcahy, M., "Gas Kinetics", Wiley, N. Y., 1973.

17. Kochi, J. K. (ed.), "Free Radicals" Vol. I., John Wiley and Sons, N. Y., 1973, p. 6.

18. Benson, S. W., "Thermochemical Kinetics", Wiley, N. Y., 1976, p. 164.

19. Loucks, L. F. and K. J. Laidler, Canadian J. Chem., 45, 2795, (1967).

20. Denisov, E. T., "Liquid Phase Reaction Rate Constants", I. F. I./Plenum, N. Y., 1974, pp. 286-287.

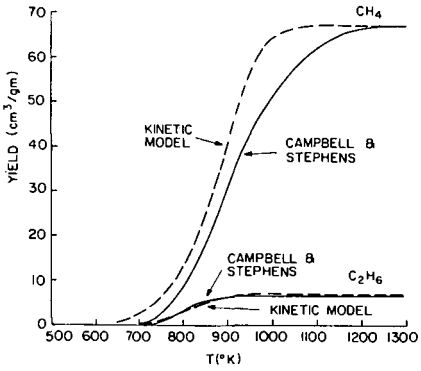

Figure 1. CH_4 and C_2H_6 Ref. (7)

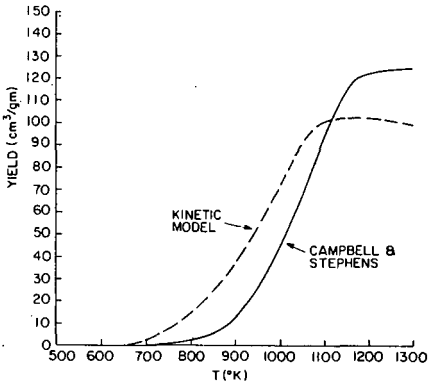

Figure 2. Hydrogen Ref. (7)

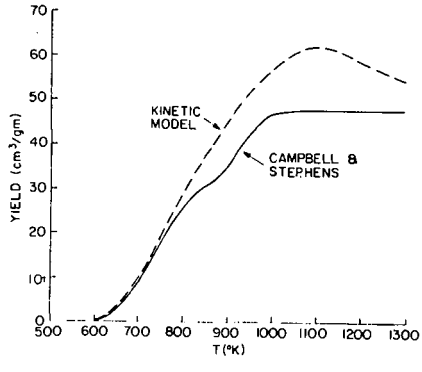

Figure 3. Carbon Dioxide Ref. (7)

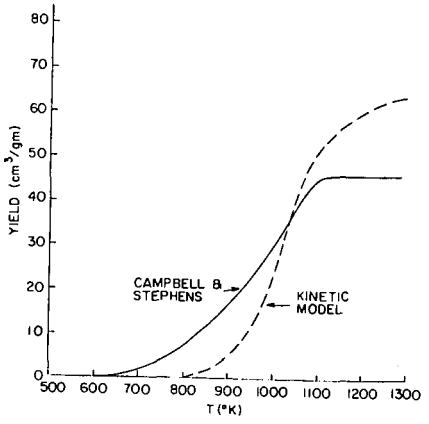

Figure 4. Carbon Monoxide Ref. (7)

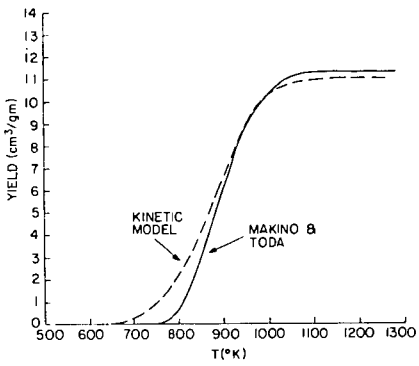

Figure 5. Methane Ref. (8,9)

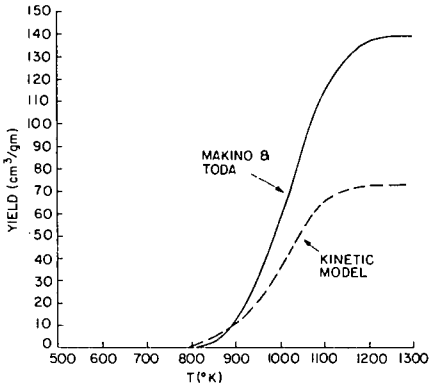

Figure 6. Hydrogen Ref. (8,9)

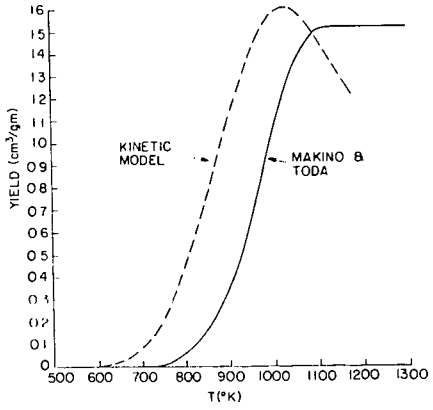

Figure 7. Carbon Dioxide Ref. (8,9)

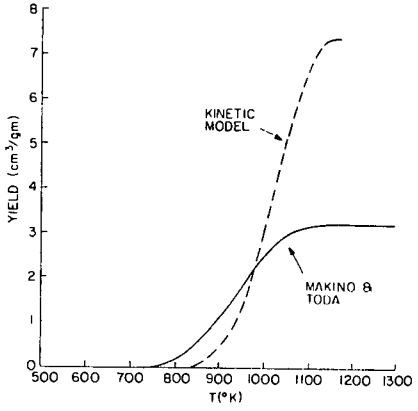

Figure 8. Carbon Monoxide Ref. (8,9

AN IN SITU STUDY OF RAPID COAL PYROLYSIS USING FTIR*

J. D. Freihaut, P. R. Solomon,** D. J. Seery

United Technologies Research Center, East Hartford, CT 06108

INTRODUCTION

Recent investigations of rapid coal pyrolysis have generally been limited to two approaches -- entrained flow techniques and heated grid devices. The entrained flow technique provides a method wherein injected coal samples experience heating rates comparable to those expected in combustion processes. However, the data collected is generally limited to weight loss as a function of apparent residence time in the reactor hot zone (1,2,3). The heated grid techniques provide a more clearly defined time-resolved thermal environment for small particles (60 - 100 μm) and allow determination of the volatile species evolved into a cold environment surrounding the grid (4-8). Due to the mode of heating of the particles in the grid technique one is limited to the particle size ranges that can be employed. Both approaches have provided useful information concerning the nature of rapid devolatilization. It is also clear that other techniques and reactor designs are needed to provide information concerning rapid pyrolysis phenomena for a range of temperatures, particle sizes and reactive atmospheres.

EXPERIMENTAL DESIGN

A reactor has been constructed in which small samples of coal (20 - 60 mg) are rapidly injected (~ 25 msec) into a preheated environment. The injection device allows one to deliver particles as small as 100 μm or as large as several millimeters in diameter. Injection of the small samples into a preheated zone insures that the particles experience initial heating rates comparable to those expected in coal combustors. The gases produced by the thermal decomposition process are monitored in situ by use of a Nicolet FTIR Spectrometer operated in the rapid scan mode. A schematic of the pyrolysis system is shown in Fig. 1.

PYROLYSIS GAS SPECTRA

Figure 2 displays a portion of the time-resolved spectra obtained from the devolatilization of a Pittsburgh bituminous coal (PSOC 170). Figure 3 displays the same spectral window obtained from the rapid scan FTIR data collected from the devolatilization of a Montana lignite. The difference in characteristics of the gaseous yields are apparent. The bituminous coal yielded the greater ratio of hydrocarbon species to carbon oxide species. The same trend is noted in the high resolution scans taken at the completion of the rapid scans (See Figs. 4 and 5). These trends

*Work supported by the Department of Energy under Contract ET-78-C-01-3167
**Present Address: Advanced Fuel Research, P.O. Box 18343, East Hartford, CT 06118

were to be expected on the basis of work previously preformed by use of a heated grid to devolatilize the coal. That is, the relative yields of the light gases reflect the functional group characteristics of the parent coal (8).

APPARENT FIRST ORDER ARRHENIUS RATE CONSTANTS

The rise times of the various gaseous species were used to extract apparent first order rate constants from the time-resolved FTIR data. For the sake of comparison, the method of extracting the rate constants was the same as that previously employed using the heated-grid apparatus. Figure 6 shows the results obtained for the Pittsburgh bituminous coal and the Montana lignite. Obviously, there is a significant difference in the apparent rate constants obtained by devolatilization in each of the two reactors. It is believed that the variation in rate constants reflect the variations in the thermal flux experienced by the coal particles within each reactor. The initial heating rate of 100 μm coal particles in the heated grid apparatus employed was determined by thermocouple measurements to be of the order of 10^2 to 10^3°C/sec. In the isothermal furnace the initial heating rates are estimated to be of the order of 10^4°C/sec and greater (9). The rate constants obtained in the furnace experiments are about a factor of ten higher than those obtained from the heated grid. It is believed that the non-isothermal nature of the pyrolysis process in the furnace is responsible for the apparent lack of temperature sensitivity in the rate constant values.

APPARENT FIRST ORDER RATE CONSTANTS AND COAL TYPE

Inspection of Fig. 6 indicates that, within the resolution of the experiment, the coal type does not have a significant effect upon the apparent first order rate constant for a particular gaseous species evolved. The reactor type has a much greater effect on apparent rates than does the coal type.

The independence of apparent rate constant with coal type is in agreement with results obtained by use of the heated grid that indicated that the amount of a particular gaseous species evolved to be highly dependent on coal type but the rate of evolution to be independent of coal type.

APPARENT RATE AND PARTICLE SIZE

As shown in Fig. 6 there is a decrease in rate with particle size if the particle size range of the sample is changed from -100 mesh to -40 mesh. There does not appear to be any significant difference in the yield structure of the light gases evolved. For the small sample sizes employed, the yield structure of the light gases appeared to vary more with the particular sample employed than with the particle size chosen.

FINAL REMARKS

As indicated by the comments above, the current pyrolysis configuration has been useful in determining the validity of hypotheses formulated by studies performed with the heated grid apparatus. However, in its current configuration it is not without

its disadvantages: calibration of the reactor is extremely difficult; the alumina walls tend to provide active sites for the transformation of sulfur-containing gases; the tar-soot mist formed at higher operating temperatures and by use of smaller particle sizes tends to interfere with the IR signal.

ACKNOWLEDGMENTS

The authors wish to express gratitude for the technical assistance of Dave Santos and Gerald Wagner.

REFERENCES

1. Badzioch, S. and Hawksley, P. G. W., Ind. Eng. Chem. Proc. Des. Develop. 9, No. 4, 521 (1970).
2. Nsakala, N. Essenhigh, R. H. and Walker, P. L., Jr., Studies on Coal Reactivity: Kinetics of Lignite Pyrolysis in Nitrogen at 808°C, Pennsylvania State Univ. (1977).
3. Scaroni, A. W., Walker, P. L., Jr. and Essenhigh, R. H., Amer. Chem. Soc. Div. of Fuel Chem. Preprints 24, No. 3, 123 (1979).
4. Juntgen, H. and van Heek, K. H., Fuel, 47, 103 (1968).
5. Anthony, D. B. and Howard, J. B., AIChE 22, No. 4, 625 (1976).
6. Suuberg, E. M. Peters, W. A. and Howard, J. B., Amer. Chem. Soc. Div. of Fuel Chem. Preprints 22, No. 1, 112 (1977).
7. Solomon, P. R. and Colket, M. B., Seventeenth Symp. (International) on Combustion, 131 (1978).
8. Solomon, P. R., Amer. Chem. Soc. Div. of Fuel Chem. Preprints 24, No. 2, 184 (1979).
9. Freihaut, J. D. and Vastola, F. J., Preprints -- Eastern States Section: The Combustion Institute, November (1978).

FIG. 1: PYROLYSIS SYSTEM

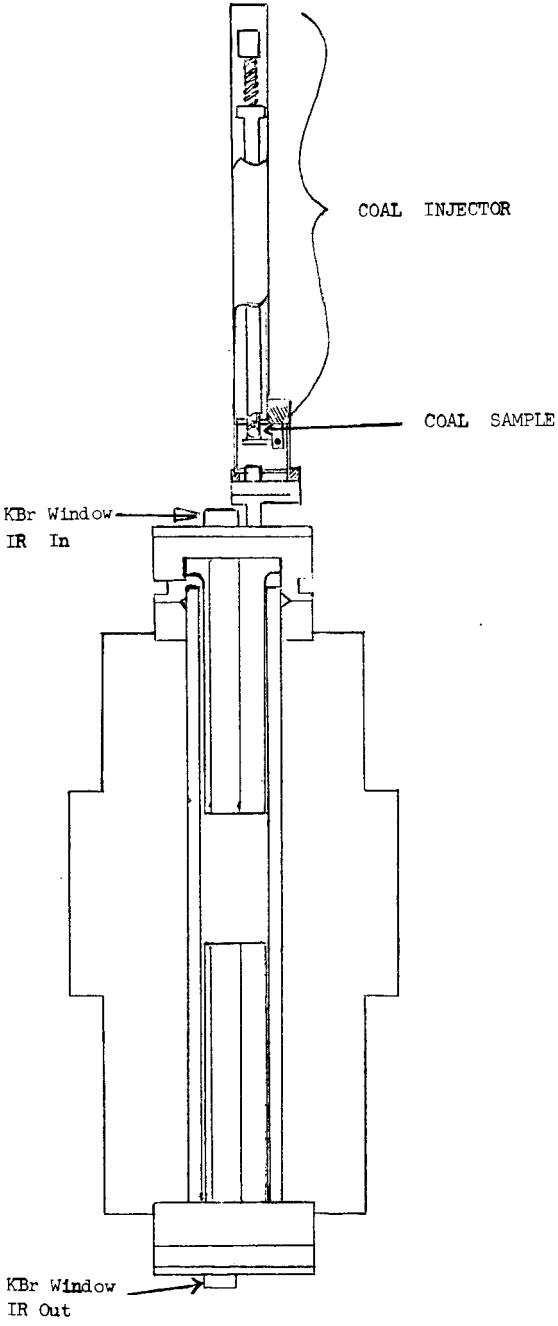

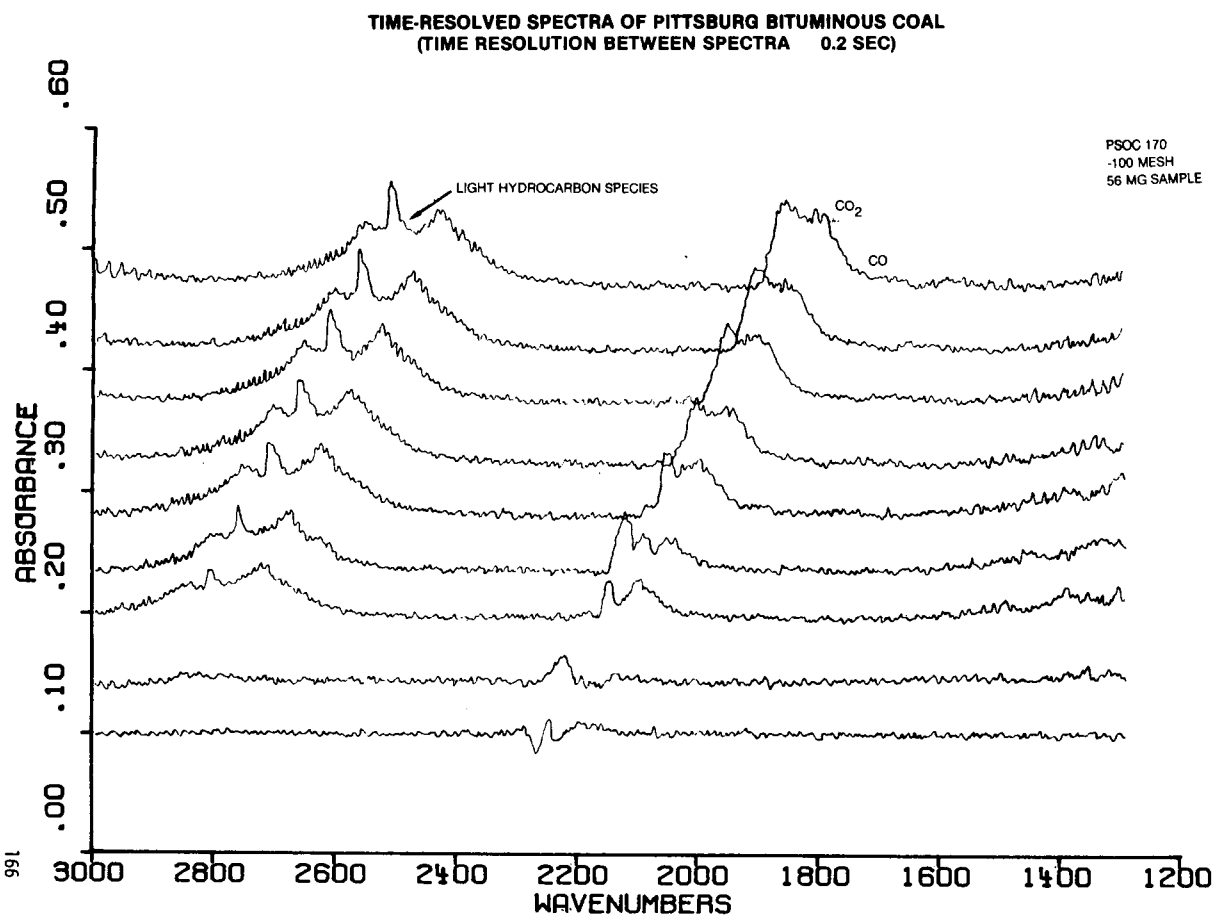
TIME-RESOLVED SPECTRA OF PITTSBURG BITUMINOUS COAL
(TIME RESOLUTION BETWEEN SPECTRA 0.2 SEC)
PSOC 170
-100 MESH
56 MG SAMPLE
LIGHT HYDROCARBON SPECIES
CO_2
CO
ABSORBANCE
.00
.10
.20
.30
.40
.50
.60
3000
2800
2600
2400
2200
2000
1800
1600
1400
1200
WAVENUMBERS

FIG. 2

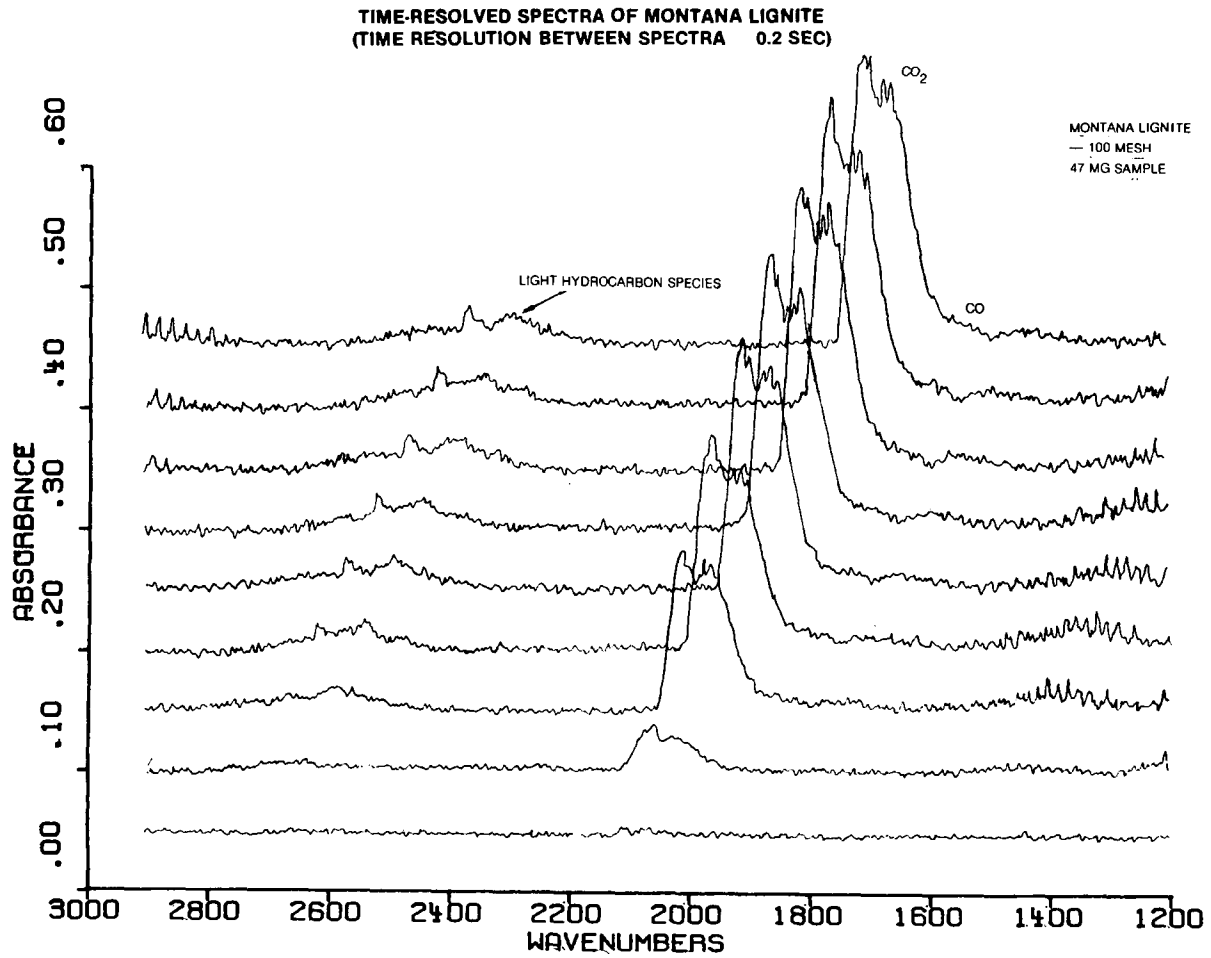
TIME-RESOLVED SPECTRA OF MONTANA LIGNITE
(TIME RESOLUTION BETWEEN SPECTRA 0.2 SEC)
MONTANA LIGNITE
— 100 MESH
47 MG SAMPLE
CO_2
CO
LIGHT HYDROCARBON SPECIES
ABSORBANCE
.00
.10
.20
.30
.40
.50
.60
3000
2800
2600
2400
2200
2000
1800
1600
1400
1200
WAVENUMBERS

FIG. 3

PYROLYSIS GAS — HIGH RESOLUTION SCAN

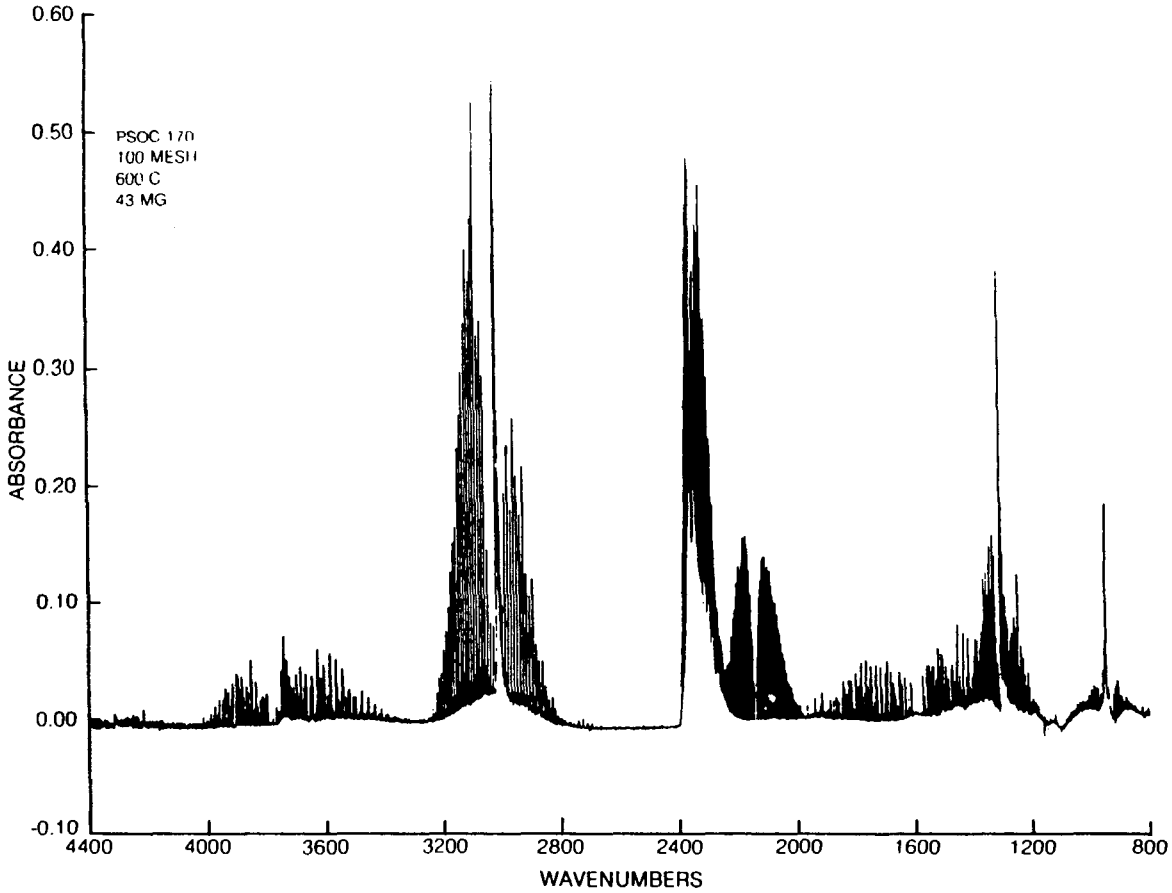

PYROLYSIS GAS — HIGH RESOLUTION SCAN

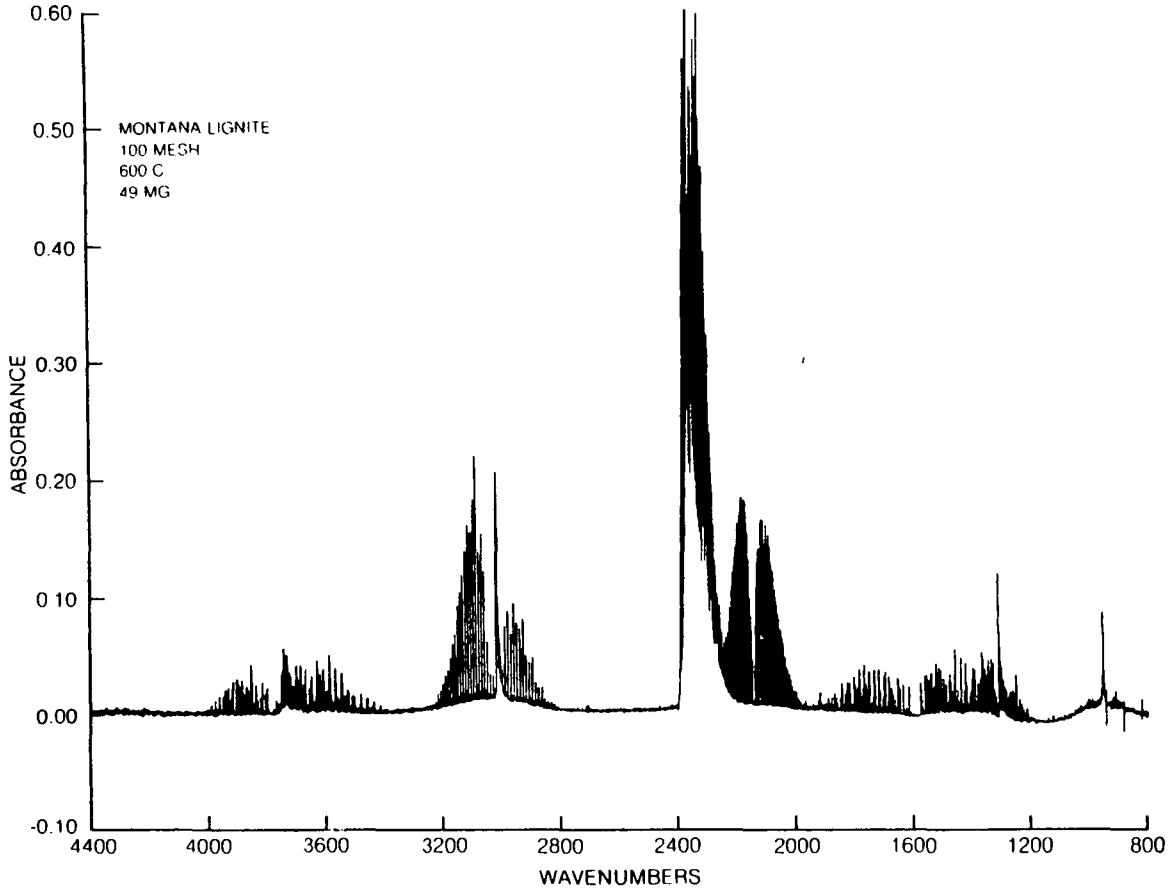

FIG. 6

RATE CONSTANT FOR METHANE EVOLUTION

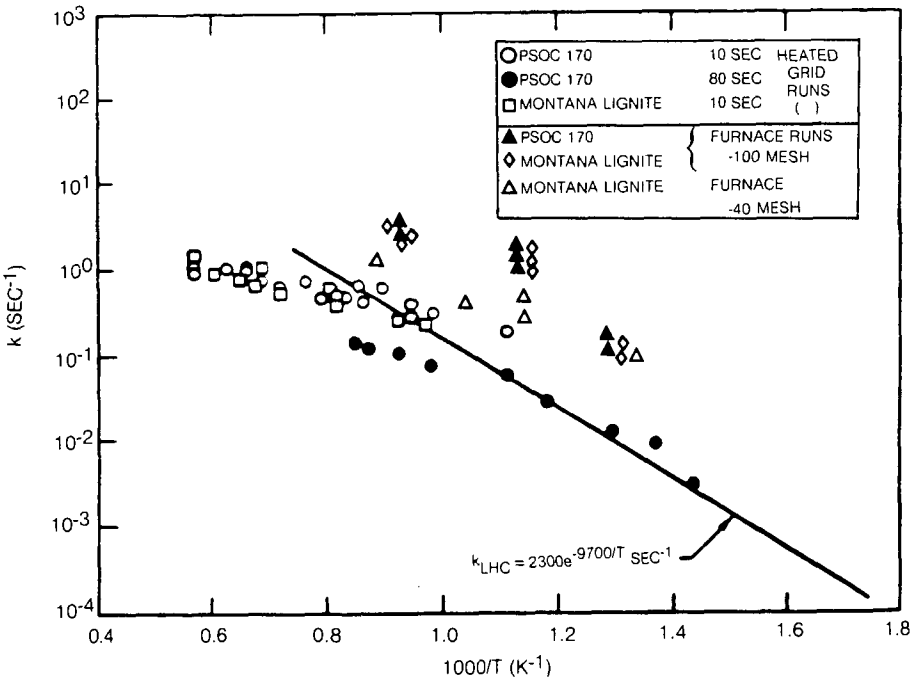

THE THERMOCHEMICAL EFFECTS OF GAS-COALS IN PYROLYSIS PROCESS

Zhaoxiong Wang and James K. Shou

Institute for Mining and Minerals Research, University of Kentucky
P.O. Box 13015, Lexington, Kentucky 40583

INTRODUCTION

The gas-coal is a young bituminous coal. In its organic matter there is a large quantity of thermally unstable constituents. The intense thermal decomposition may be initiated at a temperature as low as slightly above 300°C. Much tar, water of decomposition and gaseous products are liberated sharply (1). These features of thermochemical conversion influence the pyrolysis process.

During pyrolysis, chemical changes and phase transformation are accompanied by certain thermal effects. Chemical reactions occur in opposite directions - degradation and polycondensation. For instance, the high-molecular-weight substances of coal decompose and produce volatile products with low molecular weights, which evolve successively. On the other hand, organic matter remaining in the solid phase will continue to strengthen its linkage between structural units. The thermal effects alternate between exothermic and endothermic during the pyrolysis process. The alternation of thermal effects reflects the nature of chemical interreactions. At each turning point the chemical composition of coal organic matter will undergo a remarkable change.

EXPERIMENTAL PROCEDURE

The thermal effects generated by pyrolytic reactions and phase exchanges under the action of heat may be studied by means of differential thermal analysis (DTA) (2-6). Brief description of DTA experiments are as follows.

About 1g of finely ground coal with a particle size of less than 0.2mm was packed in a porcelain crucible. Another crucible contained the calcined magnesia, which was used as the inert reference. Both crucibles were separately covered with a lid, on which a thermowell was connected. Samples were heated to 850-950°C at a constant rate of 5°C/min. The thermographic curves were plotted by a mirror galvanometer in coordinates of coal temperature versus heating time and temperature difference versus heating time.

To detect chemical changes, the composition of heated coal organic matter at its peak temperature was determined. A series of 10g coal samples were taken and were heated in the same pyrothermograph furnace. The heating was strictly controlled to match that in the DTA tests. When each relative peak temperature was reached, the crucible was immediately taken off the furnace and cooled in the desiccator. The proximate and ultimate analyses of these samples were carried out.

RESULTS AND DISCUSSION

THE GENERALIZATION OF THERMOGRAPHIC PEAKS

DTA curves of several coals studied have shown general characteristics and also have revealed some differences, with respect to peak temperature, peak width, peak altitude and peak shape (Figure 1). Analytic data of these coals are given in Table 1. Coals No. 1 and No. 2 are good caking coals, the others are weakly caking coals.

TABLE 1. ASSAY DATA OF TESTED GAS-COALS

COAL SAMPLE	PROXIMATE ANALYSIS, WT.%				ULTIMATE ANALYSIS, WT.%,DAF				PLASTOMETRIC INDEX*, mm	
	MOISTURE AS DETERMINED	ASH CONTENT (dry)	VOLATILE MATTER (daf)	TOTAL SULFUR (dry)	C	H	N	(O+S)	X	Y
No. 1	1.90	7.86	39.9	3.04	80.51	5.83	1.97	11.69	43	17
No. 2	2.14	12.40	36.5	2.94	81.20	5.59	1.96	11.25	48	14
No. 3	3.29	5.39	46.3	0.52	78.10	5.72	1.94	14.24	40	7
No. 4	4.28	7.08	42.7	0.38	80.48	5.60	2.81	13.11	27	7
No. 5	3.55	9.64	43.9	0.50	80.88	5.90	——	———	40	7-8

*Index X (final shrinkage) and Y (maximum thickness of plastic layer) were determined by special plastometric testing equipment. The value of Y was served as the parameter for measuring the caking capacity of coal.

To interpret the thermograms, the following points should be considered.

1. The primary effect (the first endothermic peak) appears at about 100°C. This effect occurs only in connection with evaporation of physically absorbed water.

2. Above 150°C, the differential curve spreads upward. Its peak temperature indicates the initiation of intense thermal decomposition of organic matter. With respect to gas-coals, the temperature of this peak is located at about 270°C. The temperature of this exothermic peak will be affected by the heating rate. Structural studies had not shown the breakdown of coal structure when it was heated to below 250°C and there was a little possibility of chemical change. Some reactions, such as dehydrogenation, surface oxidation and dehydration, exhibit an exothermic effect (7). At this point water of decomposition is already yielded from gas-coals (1).

3. Beyond 300°C the differential curve starts to decline. The thermal effects of coal pyrolysis show endothermic character as a result of the decomposition reaction, polycondensation of pyrolysis products and phase transformation. The quantity of volatile yield between the second and third peaks makes up almost one half of the total volatile matter.

The existence of a W-shape peak expresses the situation of coal in plastic stage. As illustrated in Figure 2, there is little difference in the appearance of differential curves between the original coal and the fast preheated (50°C/min) to 280°C coal. It shows that deep destruction has not taken place during the fast heating of coal. However, on the thermogram of char, a similar W-shape peak disappears. The curve is smooth before the temperature reaches 536°C. This is because the primary decomposition and evolution of volatile matter and the phase conversion essentially have been completed. Therefore the existence of that W-shape peak is characteristic of the plastic state. The phenomenon of exothermic effect within a W-shape peak might also be affected by the increase in thermal conductivity when the particles became agglomerated. In essence, the first dip of the curve occurs when coal softens and changes to a plastic state. The second dip occurs during resolidification of the plastic mass.

4. The general thermal effect becomes clearly exothermic at temperatures of 510-550°C. The rise of the curve indicates the formation of a semi-hard structure. This secondary carbonization, accompanied by liberation of residual hydrogen from the periphery of aromatic clusters, in every case gives rise to an exothermic peak.

5. At temperatures above 760°C, slight endothermic effects could be observed. These effects are due to further regulation in the arrangement of hexagonal carbon network.

6. The effect of mineral matters under high temperatures may be reflected on the thermogram. The thermogram of coal sample No. 2 with a 20% lime additive is shown in Figure 3. To a certain degree, mineral matters affect thermal decomposition of organic matter. Particularly at temperature ranges of 750-850°C, there appears an obvious endothermic effect, which is characteristic of this additive.

CONSTITUENT CHANGES OF NONVOLATILIZED MATERIAL

The chemical reaction of thermal decomposition of gas-coal organic matter is extremely complex. While it is difficult to postulate the thermochemical reactions, the study of constituent alternation of gas-coal organic matter is helpful in explaining the mechanism of thermal decomposition.

Elemental composition data of nonvolatilized material from gas-coals No. 1 and No. 2 heated to each characteristic peak temperature are given in Tables 2 and 3. R_{HC} is the ratio of total hydrogen and carbon to total content of other elements. The hydrogen-containing grade (f_H) is the atomic ratio of hydrogen to carbon. The carbonization grade (f_C) is an index of the atomic ratio of carbon to noncarbon elements. This ratio for the original coal is assigned an index value of 1.0. The aromaticity (fa) is calculated according to Van Krevelen and Schuyer's formula (8).

These two gas-coals begin to decompose at about 270°C. It appears that thermochemical decomposition is initiated from hydrogen- and oxygen-rich groups. As data indicate, the hydrogen content of nonvolatilized material decreases sharply as the pyrolysis process proceeds. On the contrary, the main part of the carbon ring structure is strengthened because of the polycondensation reaction. The carbonization grade of nonvolatilized material increases steadily with the increase of temperature. For coal sample No. 1, carbon-to-hydrogen ratio changes from $C_6H_{5.2}$, approximated to the aromatic composition of benzene, to $C_6H_{0.9}$. As shown in Figure 4, fc rises from 0.722 to 0.999 and eventually stabilizes.

The carbonization process is carried out simultaneously with dehydrogenation. This is shown by the decreasing hydrogen-containing grade. Meanwhile, the carbonization of condensed carbon rings exhibits an aromatizing characteristic, as indicated by the increase of aromaticity. So it may be presumed that chemical structure changes only in the direction of high polycondensation of aromatic rings.

CONSTITUENT CHANGES IN VOLATILIZED MATERIAL

As a result of thermochemical decomposition, certain fractions of coal organic matter turn into volatile matter. The changes in volatile matter content of gas-coals No. 1 and No. 2 are listed in Tables 2 and 3.

As previously stated that in the temperature range between the second and third peaks, i.e. 258-435°C for gas-coal No. 1 and 274-438°C for gas-coal No. 2, the evolving rate of volatile products is higher than in other ranges. The higher evolution rate for gas-coal No. 2 appears in a higher temperature interval ranging from 372°C to 438°C. It shows that gas-coal No. 2 probably has a higher thermal stability than gas-coal No. 1.

The devolatilization process may be divided into three stages. Referring to the DTA curve for gas-coal No. 1, temperature ranges for the three stages are 20-435°C, 435-530°C and beyond 530°C. The chemical composition of evolved volatilized material changes significantly, depending on the various temperature ranges. These data are listed in Tables 4 and 5. Where, Cv, Hv, (O+S)v and Nv are contents of carbon, hydrogen, oxygen and sulfur, and nitrogen in volatilized material in wt.% respectively, δC, δH, $\delta(O+S)$ and δN (wt.%, daf) are the quantities of each element converted into volatile products in certain temperature ranges.

TABLE 2. CONSTITUENT CHANGES OF NONVOLATILIZED MATERIAL DURING HEATING OF COAL SAMPLE NO. 1

TYPE OF ANALYSIS DATA	PEAK TEMPERATURE, °C						
	ORIGINAL COAL	258	435	482	530	760	COKE
Volatile Matter*, VMo, %	39.9	34.1	15.6	12.3	7.63	3.71	1.32
Evolving Rate of Volatile Matter (ΔVMo/°C) X 100		3.6	10.4	7.0	9.7	1.7	1.3
Composition of non-volatilized material, %, daf							
Carbon	80.51	82.20	84.04	84.70	86.70	91.60	94.20
Hydrogen	5.83	5.51	4.11	3.51	3.11	1.93	1.19
Oxygen & Sulfur	11.69	10.29	9.57	9.40	7.85	4.18	2.74
Nitrogen	1.97	2.00	2.28	2.39	2.34	2.29	1.87
R_{HC}	6.3	7.1	7.4	7.5	8.8	14.4	20.7
f_H	0.87	0.81	0.59	0.50	0.43	0.25	0.15
f_C	1.00	1.09	1.44	1.65	1.92	3.23	5.27
fa	0.722	0.771	0.937	0.962	0.999	0.999	1.00

*VMo = $\frac{\text{Weight of VM of nonvolatilized sample}}{\text{Weight of original coal sample, daf}}$

TABLE 3. CONSTITUENT CHANGES OF NONVOLATILIZED MATERIAL DURING HEATING OF COAL SAMPLE NO. 2

TYPE OF ANALYSIS DATA	PEAK TEMPERATURE, °C							
	ORIGINAL COAL	274	372	438	514	563	735	COKE
Volatile Matter*, VMo, %	36.5	34.4	25.7	15.4	11.8	11.0	5.41	1.91
Evolving Rate of Volatile Matter (ΔVMo/°C) X 100		1.2	8.9	15.6	4.7	1.6	3.3	1.6
Composition of non-volatilized material, %, daf								
Carbon	81.20	82.11	82.50	84.77	85.18	87.44	90.76	94.27
Hydrogen	5.59	4.95	4.25	3.30	3.20	2.86	1.83	0.70
Oxygen & Sulfur	11.25	10.95	11.12	9.70	9.37	7.59	5.20	3.11
Nitrogen	1.96	1.99	2.13	2.23	2.19	2.11	2.21	1.92
R_{HC}	6.5	6.7	6.5	7.4	7.7	9.3	12.5	19.0
f_H	0.82	0.73	0.62	0.47	0.45	0.39	0.24	0.09
f_C	1.00	1.13	1.29	1.65	1.72	2.00	3.11	7.26
fa	0.757	0.770	0.854	0.936	0.973	0.957	0.988	0.998

TABLE 4. CHEMICAL COMPOSITION OF VOLATILIZED MATERIAL RELEASED FROM HEATING GAS-COAL NO. 1

CHEMICAL COMPOSITION	TEMPERATURE RANGE, °C 20-435	435-530	BEYOND 530
Element Converted, Wt.%, daf			
δC	11.30	5.01	2.85
δH	2.44	1.13	1.50
δ(O+S)	3.71	2.21	3.98
δN	0.08	0.17	0.50
Elemental Composition, %			
Cv	64.46	58.80	32.28
Hv	13.92	13.26	16.98
(O+S)v	21.16	25.94	45.08
Nv	0.46	2.00	5.66
Atomic Ratio			
C	5.4	4.9	2.7
H	13.9	13.3	17.0
O	1.3	1.6	2.8

TABLE 5. CHEMICAL COMPOSITION OF VOLATILIZED MATERIAL RELEASED FROM HEATING COAL SAMPLE NO. 2

CHEMICAL COMPOSITION	TEMPERATURE RANGE, °C 20-438	438-563	BEYOND 563
Element Converted, Wt.%, daf			
δC	9.93	4.03	3.59
δH	2.82	0.54	1.69
δ(O+S)	2.98	2.33	3.80
δN	0.06	0.07	0.13
Elemental Composition, %			
Cv	62.87	57.82	38.98
Hv	17.86	7.75	18.35
(O+S)v	18.87	33.43	41.26
Nv	0.40	1.00	1.41
Atomic Ratio			
C	5.2	4.8	3.2
H	17.9	7.8	18.3
O	1.2	2.1	2.6

Although carbon evolves during the pyrolysis of coal, most of the carbon remains nonvolatilized. Referring to Tables 6 and 7, only about 25% of the carbon in coal sample No. 1 converts into volatile products, and 21.6% of carbon in coal sample No. 2 converts into volatile products. Furthermore, the evolution of volatile carbon is relatively concentrated in the 270-550°C temperature range. Below 270°C, carbon hardly participates in devolatlilization.

TABLE 6. DECOMPOSITION AND DEVOLATILIZATION RATES OF EACH ELEMENT IN HEATED GAS-COAL NO. 1*

RATE OF ELEMENTAL DECOMPOSITION, %	PEAK TEMPERATURE, °C					
	258	435	482	530	760	COKE
ΔC	——	14.0	18.9	21.4	22.5	25.0
ΔH	6.0	41.7	53.3	61.2	77.4	86.8
Δ(O+S)	12.9	31.7	38.2	50.6	75.6	84.5

* $\Delta C = \frac{\text{Weight of carbon devolatilized}}{\text{Weight of carbon in original coal sample}} \times 100\%$

$\Delta H = \frac{\text{Weight of hydrogen devolatilized}}{\text{Weight of hydrogen in original coal sample}} \times 100\%$

$\Delta(O+S) = \frac{\text{Total weight of oxygen and sulfur devolatilized}}{\text{Total weight of oxygen and sulfur in original coal sample}} \times 100\%$

TABLE 7. DECOMPOSITION AND DEVOLATILIZATION RATES OF EACH ELEMENT IN HEATED GAS-COAL NO. 2

RATE OF ELEMENTAL DECOMPOSITION, %	PEAK TEMPERATURE, °C						
	274	372	438	514	563	735	COKE
ΔC	1.4	5.7	12.3	15.7	17.2	18.6	21.6
ΔH	13.4	29.1	50.5	53.1	60.1	76.0	90.4
Δ(O+S)	3.7	6.9	26.5	29.6	47.3	66.4	81.0

Hydrogen plays an important role in the coal pyrolysis process. The basis of pyrolytic change may be looked at as a redistribution of hydrogen among newly formed products (1). Large quantities of hydrogen are consumed for the formation of water, hydrogen sulphide and ammonia. The remaining hydrogen, called free hydrogen, is necessary for the yield of tarry products and for the formation of fusible matter in the plastic stage. The amount of liquid phase and the degree of softening increase with increasing amounts of free hydrogen in the coal. For coal sample No. 2, which produces a more stable plastic mass, the quantity of hydrogen evolved at the second stage (plastic stage) is lower than that in sample No. 1.

The free hydrogen may be better preserved in plastic mass under pressure. It has been proven by experiment that up to 600°C, plastic coal briquettes gave off less hydrogen than the same coal packed in a loose mass (9). Thus, pressurization is extremely important in the destructive hydrogenation of coal. In the conventional pyrolysis process, however, the nonvolatile part of carbon cannot be devolatilized because of a lack of thorough structural destruction. Furthermore, the amount of free hydrogen is limited, thus it is impossible to yield a great deal of liquid products.

After 550°C, the quantity of devolatilizable hydrogen is still sizable. It holds three-fourths of the total atomic amount of various elements (Tables 4 and 5). In a small degree, carbon converts into volatile products. At this stage volatile products should be light gaseous products, such as hydrogen and methane. Clearly, the production of liquid products by either pyrolysis or other conversion processes may be controlled only before reaching the exothermic peak within the W-shape (Figure 1).

CONCLUSIONS

1. This study of thermographical curves and corresponding assay data of gas-coals at peak temperatures has shown that thermal effects were closely connected with the decomposition of coal organic matter and its changes in chemical composition.

2. After the second peak (exothermic) temperature, gas-coals started to decompose intensely. Thermal decomposition was initiated from hydrogen- and oxygen-rich thermally unstable constituents.

3. The evolution of volatile carbon from solid substances was concentrated in the temperature range between the second and third peaks. The control of thermal decomposition before reaching the exothermic peak within the W-shape is of great importance. Improving interreaction between volatile carbon and free hydrogen, coal pyrolysis and other coal conversion processes could be improved to yield a greater amount of hydrocarbon products.

4. Beyond the second endothermic peak within the W-shape, the atomic ratio of carbon to the sum of other elements in nonvolatilized material increased markedly. The aromaticity of nonvolatilized material tends to increase with the rise of the carbonization degree.

REFERENCES

1. Wang, Zhaoxiong, Journal of Tienjin University, No. 13, 27 (1963), (in Chinese).

2. Wang, Zhaoxiong, Chemical World, No. 5, 224 (1962), (in Chinese).

3. Pope, M.I., et al., Differential Thermal Analysis, London (1977).

4. Shou, J.K., et al., Proceedings of 11th IECEC, 300 (1976).

5. Heilpern, S., Thermal Analysis, Vol. 3, 283, London (1974).

6. Arseneau, D.F., et al., Proceedings of the Coal and Coke Sessions, 28th Can. Chem. Eng. Conf., 56 (1978).

7. Takekawa, T., et al., Fuel, 57, 797 (1978).

8. Francis, W., Coal, London (1961).

9. Gryaznov, N.S., et al., Koks i Khimiya, No. 6, 1 (1975).

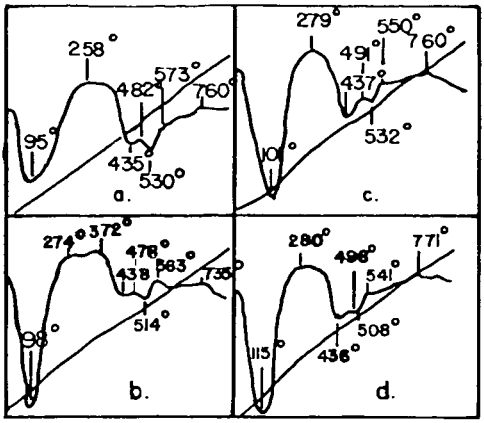

a. Coal Sample No. 1
b. Coal Sample No. 2
c. Coal Sample No. 3
d. Coal Sample No. 4

FIGURE 1. THERMOGRAMS OF GAS-COALS

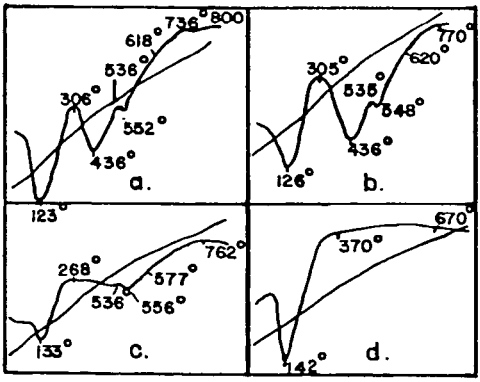

a. Original Coal
b. Fast Preheated Coal
c. Char From Preheated Coal
d. Coke From Preheated Coal

FIGURE 2. THERMOGRAMS OF GAS-COAL SAMPLE NO. 5

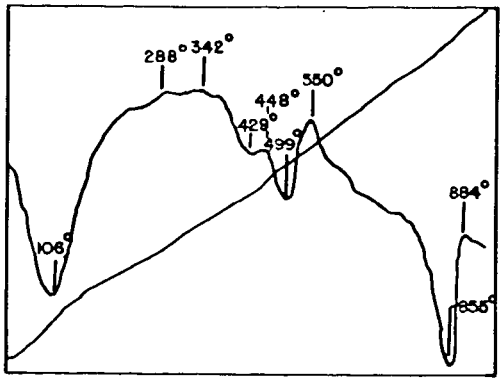

FIGURE 3. THERMOGRAM OF GAS-COAL SAMPLE NO. 2 WITH LIME ADDITIVE

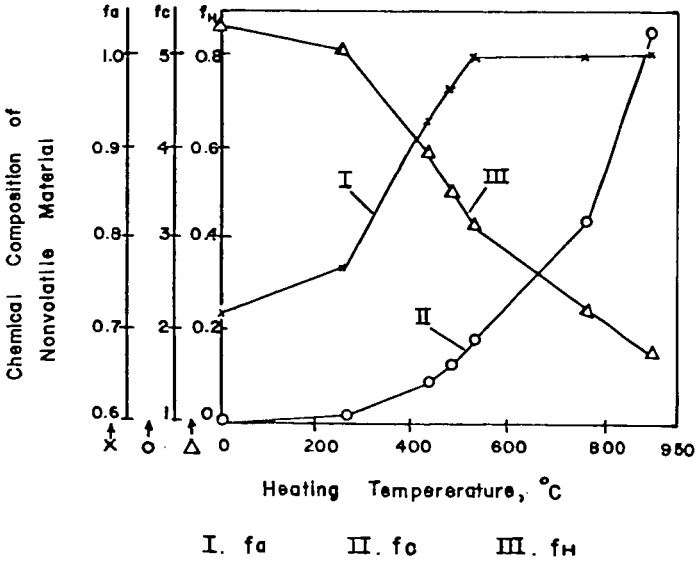

FIGURE 4. CHANGES OF AROMATICITY, CARBONIZATION GRADE AND HYDROGEN-CONTAINING GRADE OF COAL SAMPLE NO. 1 WITH HEATING TEMPERATURE

MODEL PATHWAYS FOR GAS RELEASE FROM LIGNITES

by
M.T. Klein and P.S. Virk
Department of Chemical Engineering
Massachusetts Institute of Technology
Cambridge, MA 02139

Introduction:

Recent developments limiting petroleum supplies have intensified the search for other sources of energy and chemical feedstocks. Two such alternatives are coal, of which lignites are especially abundant in the U.S. (1), and those renewable resources termed biomass, of which lignin is a major component (2). Commercial methods for processing both coal and biomass invariably involve high temperature treatments, aspects of which have been investigated in many laboratory pyrolyses of lignin and lignites (3-5). Unfortunately, the basic pathways and reaction mechanisms involved in these pyrolyses have remained obscure, on account both of the refractory nature of the substrates and the lack of unequivocal chemical structures to describe them. Pyrolyses of several very simple lignin-related substrates have also been reported, notably by Russian investigators (6-11). Among these, the pyrolyses of anisole and guaiacol (6-9) have been interpreted (11) in terms of analogous free radical demethylation and demethoxylation mechanisms which describe the formation of the observed gaseous products, methane and carbon monoxide, but are unable to rationalize the corresponding observed liquid products, benzene, phenol, and catechol. Overall, the literature still provides no framework, either theoretical or experimental, for modelling gas release during pyrolysis of lignites and lignin. This motivated the present work.

Our investigation derives from two hypotheses. First, the primary evolution of gas during lignite pyrolysis is presumed to occur from lignin-related residues in the coal. Second, it is hypothesized that the molecular topology of lignoid structures favors elimination of gases by concerted pericyclic reactions which are thermally (i.e., ground state)-allowed. In regard to the first hypothesis, the evolutionary link between biomass and coal is relatively well established (12,13) with lignin akin to peat, which is adjacent to lignite in the coalification series. It is therefore quite reasonable to expect lignin-related residues in lignite; indeed, such residues can be recognized in most structural models (1 ,14) of this coal. Our second hypothesis, which has not hitherto been mooted, is based on analysis of the Freudenberg model of lignin (2) in light of the Woodward-Hoffman (15) description of thermal pericyclic reactions. Such analyses revealed a variety of lignoid chemical moieties susceptible to pyrolysis by pericyclic pathways that involve elimination of gaseous products such as methane, carbon monoxide, carbon dioxide and water. According to the pericyclic formalism, methane might originate by concerted 6e($\sigma\pi\sigma$) group-transfer elimination from a guaiacyl moiety:

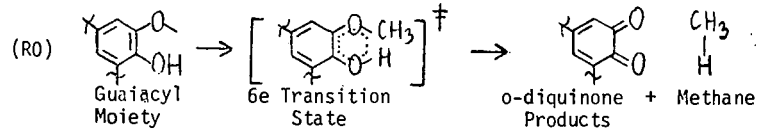

The guaiacyl moiety is relatively abundant in the lignin structure itself, within coniferyl alcohol monomer units which have suffered polymerization in the 5 and/or β positions; guaiacyl moieties can also arise from reversion of the prevalent β-ether linkage between monomer units. In similar vein, carbon monoxide could arise by cheletropic extrusion of a carbonyl unit, such as that in coniferaldehyde,

and carbon dioxide by cyclo-reversion of lactones and aryl-carboxylic ("humic") acids. Finally, pericyclic elimination of water could result from retro-ene reactions among the guaiacyl-glycerol units in lignin, possibly following β-ether reversion.

The preceding hypotheses for gas release from lignites are amenable to experimental probing by pyrolysis of appropriate model compounds. In the present paper we report preliminary results for two series of substrates respectively associated with methane and with carbon monoxide production. Methane formation was examined by pyrolyses of guaiacol, the prototypical guaiacyl moiety, along with anisole (control), and a number of substituted guaiacols, including 2,6 dimethoxyphenol, isoeugenol, and vanillin. Carbon monoxide release was investigated by pyrolysing benzaldehyde, the prototypical moiety, along with related carbonyl compounds including acetophenone (control), cinnamaldehyde and vanillin, the latter two respectively intended to illustrate the effects of extended conjugation and guaiacyl substitution.

Experimental:

The substrates pyrolysed were all commercially available in purities exceeding 98% and were used as received. The batch reactors employed were stainless steel "tubing bombs", fashioned from Swagelok components and ranging in volume from 0.6 to 10.5 cm^3. The larger reactors were equipped with valves for gas sampling, while the smaller reactors were used to minimize heat-up and quench times in experiments of short duration. Kinetic data were demonstrably unaffected by variations in reactor volume. All reactors were loaded and sealed in a glove box maintained with an inert atmosphere of either nitrogen or argon, the inert serving as an internal standard in later gas analyses. The reactors were then immersed in a fluidized sand bath for the duration of reaction and finally quenched in an ice water bath. The pyrolysis experiments were conducted at temperatures from 250 to 600 C, with holding times of 2 to 40 minutes. Substrate conversions were generally held to less than 30%, in an effort to emphasize primary reactions; however, kinetic data were also obtained at very low conversions, of < 10% for some substrates which were prone to form coke, and at high conversions, up to 90%, in other selected instances. The amount of substrate charged varied from 10 to 200 mg, to provide initial substrate concentrations ranging from 0.15to 3.0 mol/ℓ in the gas phase. Product analyses were effected by gas chromatography on a Hewlett-Packard 5730 instrument. Gaseous products, sampled by syringe, were analysed on molecular sieve, silica gel, and Porapak Q columns using helium carrier gas and thermal conductivity detectors. Liquid and solid reactor contents were dissolved in solvent and analysed on Porapak P and Q, and silicone oil columns, using either thermal conductivity or flame-ionization detection. Care was taken to effect material balance closures and to match gas and liquid product yields. In all cases, the liquid (and solid) phase material balance, which invariably included unreacted substrate, could be closed to within ±10%. In favorable cases, where reaction stoichiometry was known, the absolute gas and liquid products agreed to within ±10% of each other and separately equalled the amount of substrate converted. However in certain other cases, noted in the text, reaction stoichiometry was uncertain and precise matching of gaseous and liquid products impossible; in such instances, substrate decomposition kinetics were based on liquid phase analyses.

Results:

Table 1 summarizes the present experimental grid. For each substrate pyrolysed, the table lists chemical structure, purity, and reaction conditions of temperature, holding time and concentration. The experimental results will be described in three parts, namely (i) prototype pyrolyses, of guaiacol and benzal-

dehyde, which revealed major pathways for methane and carbon monoxide formation, (ii) substituenteffects, inferred from pyrolyses of substituted guaiacols and benzaldehydes, and (iii) control pyrolyses, of the relatively refractory substrates anisole and acetophenone, for comparisons with the prototype pyrolyses.

(i) Prototype Pyrolyses

Guaiacol pyrolysis yielded methane, carbon monoxide,catechol and phenol as the only products at low conversions; at high conversions a solid 'coke' also formed, being accompanied by reduced yields of catechol relative to the other products. Relationships among products are illustrated in Figure 1. The mol ratios of (methane/catechol), Figure 1a, and (carbon monoxide/phenol), Figure 1b, were each separately close to unity in essentially all cases, covering fractional substrate conversions $0.5 \times 10^{-3} < X < 0.10$ at all temperatures from 250 to 450 C. Also, the mol ratios of (CO/CH_4) and (phenol/catechol) were each substantially independent of substrate conversion at any given temperature, as shown in Figure 1c. These observations suggest two parallel pathways for guaiacol decomposition, respectively termed (R1) and (R2):

(R1) 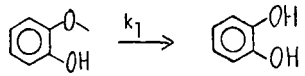 + CH_4 (-2H)

(R2) 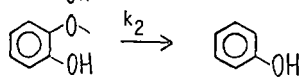 + CO (+2H)

The parentheses to the right of each expression indicate the difference in hydrogen atoms between the substrate and the observed pair of stable products. The order of reactions (R1) and (R2) with respect to guaiacol was examined by varying the initial substrate concentration from 0.45 to 3.0 mol/l in a series of experiments at T = 350C. These data are displayed in Figure 2, parts a, b, and c of which respectively plot the variation with time of guaiacol, catechol, and phenol concentrations, each normalized by the initial guaiacol concentration. On the co-ordinates of Figure 2, a reaction with rate expression $r = kC^{\alpha}$, i.e. rate constant k and order α ,would yield an initial slope $|\, d\ln (C/C_0)/\, dt|_{\, t \to 0} = kCo^{\alpha-1}$. In each of Figures 2a, 2b, and 2c, a single average slopesufficed to describe all of the data. No systematic variation of initial slope with initial substrate concentration could be discerned and the absolute uncertainties in the slope, respectively $\pm$20% in Figures 2a and 2b and $\pm$50% in Figure 2c, were small relative to the seven-fold range of initial concentrations used. The foregoing show that α=1 for each of reactions (R1) and (R2); that is, the kinetics of guaiacol disappearance, catechol appearance, and phenol appearance were all essentially first order in guaiacol. Further study of guaiacol pyrolyses at temperatures from 300 to 525 C with fixed initial concentration 0.45 mol/l revealed the temperature-dependence of the first order rate constants k_1 and k_2 respectively associated with reactions (R1) and (R2). These results are shown in Figure 3, an Arrhenius diagram with co-ordinates of $\log_{10}k$ (s^{-1}) vs. reciprocal temperature θ^{-1} where $\theta = 4.573 \times 10^{-3}$ T in Kelvins; on these co-ordinates, the usual Arrhenius relationship describes a straight line, $\log_{10}k = \log_{10}A - E^*/\theta$, where the pre-exponential factor A has units of the rate constant k and the activation energy E^* is expressed in kcal/mol. In Figure 3 it is evident that $\log_{10}k_1$ (shown by circles) increases linearly with decreasing reciprocal temperature θ^{-1}, obeying an Arrhenius relationship over a range of five orders of magnitude in k_1. The best fit of these data yields Arrhenius parameters of ($\log_{10}A$ (s^{-1}), E^* (kcal/mol)) = (10.9 $\pm$ 0.5 , 43.7 $\pm$ 1.4) for the reaction (R1). Also in Figure 3, $\log_{10}k_2$ (squares) is seen to increase linearly with θ^{-1} over a range

of four orders of magnitude in k_2 and this provides the Arrhenius parameters ($\log_{10}$A (s^{-1}), E* (kcal/mol)) = (11.5 ± 0.5, 47.4 ± 1.6) for reaction (R2). These results also reveal that the selectivity of (CO/CH_4) formation from guaiacol, given directly by the ratio (k_2/k_1), was typically on the order of 10^{-1} but increased with increasing temperature, from 0.05 at 300C to 0.25 at 450C.

Benzaldehyde pyrolysis yielded carbon monoxide and benzene as the major products; traces of biphenyl and phenolic products were also detected, their concentration being from one to two orders of magnitude less than that of benzene. The mole ratio of (CO/benzene) products was unity, 1.0 ± 0.1, while the mols of CO and of benzene formed each closely equalled the moles of benzaldehyde that disappeared in all cases, covering fractional substrate conversions from 0.01 to 0.30 at temperatures from 300 to 550C. Thus the benzaldehyde pyrolysis pathway was evidently:

(R3) 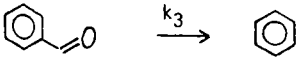 + CO

Variation of the initial substrate concentration from 0.45 to 3.0 mol/ℓ at T = 400C showed reaction (R3) to be strictly first order in benzaldehyde, with the rate constant $k_3 = (8.0 \pm 2.0) \times 10^{-3}\ s^{-1}$ essentially independent of concentration. Finally, measurements of reaction (R3) kinetics at temperatures from 300 to 500C provided the data shown in Figure 4, an Arrhenius plot. It is evident that $\log_{10} k_3$ (circles) increased linearly with decreasing θ^{-1}, the best fit Arrhenius parameters being ($\log_{10}$ A (s^{-1}), E* (kcal/mol)) = (9.5 ± 0.8, 41.5 ± 2.7).

(ii) Substituent Effects

Pyrolyses of 2,6 dimethoxyphenol, iso-eugenol, vanillin, and t-cinnamaldehyde probed the effect of substituents on the prototype pathways described above.

Both of the 2,6 dimethoxyphenol and iso-eugenol substrates decomposed clearly by pathways (R1) and (R2) analogous to guaiacol to yield methane, carbon monoxide, and the corresponding liquid products, namely:

(R1) 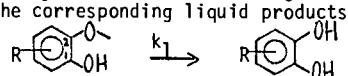 + CH_4 (-2H)

(R2) 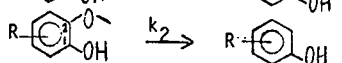 + CO (-2H)

where the substituent R is either 6-methoxy or 4-propenyl. The associated kinetic results are summarized in Table 2 which gives a matrix of first order rate constants, $\log_{10}k$ (s^{-1}), obtained at 400C for each substrate decomposing by each prototype pathway. In Table 2, values of k_1 and k_2 obtained for each of 2,6 dimethoxyphenol and iso-eugenol are close to the corresponding values for guaiacol. That is, the kinetics of both methane and carbon monoxide formation from these two substituted guaiacols were very similar to those from guaiacol itself.

Vanillin pyrolysis yielded CO and methane as the principal gaseous products, the former predominant. Among liquids, at low conversions, guaiacol and dihydroxybenzaldehyde were major products, the former predominant, while at higher conversions catechol also arose, along with lesser amounts of phenol; at the highest conversions solid coke formed. At conversions of $0.02 < X < 0.20$, the mol ratios of (CO/guaiacol) and (CH_4/dihydroxybenzaldehyde) were each approximately unity; the latter pair of products were always less than the former at low conversions, with the ratio $(CH_4/CO)_{X\to 0} \sim 0.1$ at T = 400C. These data suggest that vanillin decomposed by pathways of the type (R3) and (R1) earlier established for benzaldehyde and guaiacol:

(R3) 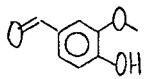 $\xrightarrow{k_3}$  + CO

(R1) 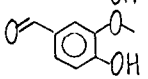 $\xrightarrow{k_1}$ 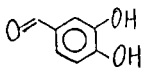 + CH_4 (-2H)

At high substrate conversions, the guaiacol and dihydroxybenzaldehyde products could further decompose by the same kinds of pathways to yield the catechol and phenol products observed. Kinetic data for vanillin pyrolysis at 400°C are summarized in Table 2. It is noteworthy that the rate constant k_3 for vanillin far exceeded that for benzaldehyde while the rate constant k_1 was essentially equal to that from guaiacol. Thus the rate of arylaldehyde decarbonylation was markedly enhanced by the guaiacyl substituents while the rate of guaiacyl demethanation was virtually unaffected by the carbonyl substituent.

Pyrolysis of t-cinnamaldehyde yielded CO as the major gaseous product, with much smaller amounts of hydrogen, methane, and acetylene also detected. A number of liquid products arose among which a dimeric condensation product, phenols, plus cresols, and styrene, were each appreciable, along with lesser amounts of toluene, benzene, other alkyl benzenes and biphenyl. Product pathways for this pyrolysis have not yet been fully established. However it was significant that the mol ratio of (CO/styrene) products always approached unity at low substrate conversions and the kinetics of styrene appearance were essentially first order in substrate over a three-fold range of initial concentrations at 350°C. This allows tentative isolation of a pathway of type (R3) for CO formation from cinnamaldehyde:

(R3) 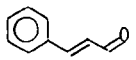 $\xrightarrow{k_3}$  + CO

The first order rate constant k_3 for cinnamaldehyde, shown in Table 2, was about three-fold greater than that for benzaldehyde, suggesting that decarbonylation rates are enhanced by conjugation.

(iii) Control Pyrolyses

Anisole pyrolysis produced methane and carbon monoxide as the major gaseous products with hydrogen also present in appreciable amounts. The major liquid products were ortho-cresol, phenol, and benzene, with smaller amounts of toluene, xylenes, and xylenols also detected. At low substrate conversions, the product proportions were strongly influenced by reaction temperature. Thus at 400°C it was found that CH_4:CO::1.0:0.4 and o-cresol:phenol:benzene::3:1:0.1, whereas at 550°C these ratios were CH_4:CO::1:1 and o-cresol:phenol:benzene::0.6:1:1. Among products, the ratios $_4$ (methane/phenol) = 0.2 ± 0.1 and (CO/benzene) = 0.6 ± 0.2 were roughly constant at substrate conversions $0.01 < x < 0.30$ and T = 450°C. Anisole pyrolysis thus appears to involve at least three major pathways, namely, re-arrangement to o-cresol, formation of methane and phenol, and the formation of CO and benzene. Further experiments at T = 450°C and spanning initial substrate concentrations from 0.45 to 3.1 mol/ℓ showed that the overall substrate disappearance, as well as the normalized phenol and benzene product appearances, were all essentially first order in anisole. This allowed association of a first order rate constant with the overall anisole disappearance, termed reaction (R4):

(R4)  $\xrightarrow{k_4}$ all products

where (R4) is, of course, a sum of the individual anisole decomposition pathways identified above but not as yet decisively delineated. Study of (R4) at various temperatures provided the values of k_4 depicted in figure 3 (diamonds); the corresponding Arrhenius parameters for overall anisole decomposition are

$(\log_{10}A(s^{-1}),\ E^*(kcal/mol)) = (12.1\pm 0.8,\ 51.4 \pm 2.4)$. The value of k_4 for anisole at T = 400°C is also quoted in Table 2, for comparison with guaiacol. From Figure 3 and Table 2 it is clear that the overall anisole decomposition by (R4) was typically at least an order of magnitude slower than guaiacol decomposition by (R1) in the present experiments. Exact comparisons between the kinetics of CH_4 and CO formation from guaiacol and from anisole cannot yet be made but the data suggest that both gases form roughly a hundred times faster from the former substrate.

Acetophenone pyrolysis led to carbon monoxide and methane as the major gaseous products with $(CO/CH_4) \sim 2$; hydrogen was also present. Liquid product spectra were complex, benzene, toluene, xylenes and styrene being the major components, along with apparent dimers; additionally present were benzaldehyde, biphenyl, cresols, and aromatic ethers. No clear link has yet been established between gas and liquid products, precluding enunciation of possible pyrolysis pathways. The overall decomposition of acetophenone was found to be roughly first order in substrate at T = 550°C for initial concentrations from 0.14 to 1.4 mol/ℓ. This allows use of a first order overall decomposition pathway of type (R4):

(R4) 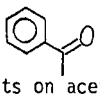 $\xrightarrow{k_4}$ all products

Experiments on acetophenone pyrolyses at various temperatures yielded the values of the rate constant k_4 shown in Figure 4 (diamonds); the corresponding Arrhenius parameters for overall acetophenone decomposition are

$(\log_{10}A(s^{-1}),\ E^*(kcal/mol)) = (10.3 \pm 1.6,\ 50.7 \pm 5.8)$. A value of k_4 for acetophenone at 400°C is given in Table 2, for comparison with benzaldehyde. From Figure 4 and Table 2 it can be seen that overall acetophenone decomposition by (R4) is more than two orders of magnitude slower than benzaldehyde decomposition by (R3) in the present experiments.

Discussion:

Comparisons of the present results with previous literature is possible only in a few instances. Prior studies of guaiacol pyrolysis (8-10) provide no activation parameters but do give overall decomposition rate constants $\log_{10}k(s^{-1}) = -1.0$ at 500C and ~0 at 540C which are of the order of magnitude of our $\log_{10}k_1$ for guaiacol in that temperature range. An earlier study of benzaldehyde pyrolysis (16) yielded an overall decomposition rate constant $\log_{10}k(s^{-1}) = -2.2$ at 550C which agrees with our value of $\log_{10}k_3 = -2.3$ at 550C. Two prior anisole pyrolysis (6,7) at 500C yield overall decomposition rate constants $\log_{10}k(s^{-1}) = -1.8$ and -1.9 which compare favorably with our value of $\log_{10}k_4 = -2.5$ at 490C. Also, an anisole pyrolysis (17) at 800C showed a product spectrum akin to ours but with the ratio of (CO/CH_4) and (benzene/phenol) each ~3, which accords with our observations showing these ratios to increase from ~0.3 at 350C to ~1.0 at 550C. In summary, pyrolysis data from the present study are in reasonable agreement with the available literature for guaiacol, benzaldehyde and anisole, lending credence to our experimental methods and hence to those results reported here for the first time.

The kinetic data obtained invite mechanistic interpretations. First, in regard to methane formation, guaiacol and anisole offer striking contrasts. The former substrate produced methane at rates a hundred times faster than the latter; also, methane formation from guaiacol was stochiometrically linked with production of catechol whereas that from anisole was associated with appreciably less than stochiometric amounts of phenol; finally, the products from anisole pyrolysis included numerous methyl-benzenes and methyl-phenols, suggestive of radical methylation, whereas such products were absent from guaiacol pyrolyses. Thus the guaiacol evidently had access to a methane-forming pathway that was far more facile than the radical pathway likely responsible (11) for methane formation from anisole. A possible pericyclic reaction path accessible to guaiacol, but not to anisole, involves the concerted group transfer shown in (R0). Here the experimental activation parameters obtained for (R1), which was first order with ($\log_{10}$A, E*) = (10.9, 43.7), are relevant. The value of $\log_{10}$A implies a tight transition state with activation entropy $\Delta S^{\ddagger}$ = -12 cal/mol K; this is close to the magnitude expected for the loss of two bond rotations that must accompany guaiacyl moiety alignment for concerted methane elimination. Further, the observed activation energy for (R1) is close to the values of 45±3 kcal/mol that have been reported for isoelectronic group transfer eliminations of hydrogen and methane from various 1,4 cyclohexadienes (18). Finally, if (R1) is indeed pericyclic like (R0), then its kinetics should be dominated by frontier orbital interactions between the methane and o-diquinone products. However, methane has a relatively large HOMO-LUMO energy gap, while the diquinone, which is further conjugated, must have a small HOMO-LUMO separation. Thus the dominant frontier orbital energy differences, of the form HOMO(methane)-LUMO(diquinone) and v.v., should be relatively large and only little influenced by substituents on the diquinone. Experimentally, it was seen in Table 2 that the kinetics of methane formation from guaiacol were insensitive to substituents. Turning next to carbon monoxide formation, it was clear that benzaldehyde produced CO via (R3) far faster than acetophenone, which latter yielded a product spectrum suggestive of a radical decomposition. In regard to benzaldehyde, we suspect that the pathway (R3) might involve a non-linear cheletropic mechanism (15), with the concerted shift of hydrogen, as in the aldehyde, being more facile than that of methyl, as in the ketone. Although molecular mechanisms for CO release from benzaldehyde have previously been mentioned (16,17), cheletropic extrusions specifically have not hitherto been proposed. In the present case, Arrhenius parameters for the first order forward reaction (R3), namely ($\log_{10}$A, E*) = (9.5, 41.5), can be combined with thermochemical data of (ΔH_r(kcal/mol), ΔS_r(cal/mol K)) = (2.3, 25.5) to provide activation parameters for the bimolecular reverse reaction, namely ($\log_{10}$A (ℓ/mol s), E*) = (5.7, 39.2). The reverse of cheletropic extrusion is, of course, cheletropic addition, which is well known (15,19) to possess tight transition states akin to cycloaddition. It is therefore interesting that the parameters inferred for the reverse of reaction (R3) yield an activation entropy $\Delta S^{\ddagger}$ = -36 cal/mol K, of magnitude typically encountered in cycloadditions. Also, cheletropic decarbonylation reactions are reported in the literature (20) to exhibit great sensitivity to stereoelectronic factors and indeed the present kinetic data showed CO formation to be appreciably affected by modifications of the benzaldehyde structure to vanillin and cinnamaldehyde. The foregoing arguments suggest that pericyclic group transfer elimination and cheletropic extrusion constitute plausible reaction mechanisms for methane and carbon monoxide formation respectively from guaiacol and benzaldehyde pyrolyses.

Acknowledgement:

This work was financially supported by the US DOE through seed funds distributed by the MIT Energy Laboratory.

References:

1. Wender, I., ACS Div. Fuel Chem. preprints, 20(4) 16(1975)

2. Freudenberg, K. and Neish, A.C., Constitution and Biosynthesis of Lignin, Springer-Verlag, New York (1968)

3. Allan, G.G. and Mattila, T., in Sarkanen, K.V. and Ludwig, C.H., ed., Lignins Occurrence, Formation, Structure and Reactions, Wiley Interscience, New York (1971)

4. Suuberg, E.M., Sc.D. Thesis, M.I.T., August 1977

5. Solomon, P.R., ACS Div. Fuel Chem. preprints, 24(3), 154-9(1979)

6. Obolentsev, R.D., J. Gen. Chem. (U.S.S.R.) 16, 1959-70(1946)

7. Friedlin, L.Kh; Balandin, A.A; Nazarova, N.M; Izvest. Akad. Nauk S.S.S.R., Otdel Khim. Nauk ,no. 1, 102-9(1949)

8. Shaposhnikov, Yu. K. and Kosyukova, L.V., Khim. Pererabotka Drev., Ref. Inform., no. 3, 6-9 (1965)

9. Kravchenko, M.I.; Kiprianov, A.I.; Korotov, S. Ya; Nauch. Tr. Leningrad Lesotekh. Akad., 135(2), 60-4(1970)

10. Kiprianov, A.I. and Kravchenko, M.I., Izv. Vyssh. Ucheb. Zaved., Les Zh. 15(5), p121-5(1972)

11. Kislitsyn, A.N.; Rodionova, Z.M.; Savinykh, V.I.; Ill'ina, E.I.; Abakhumov, G.A., Sb. Tr., T sent. Nauch - Issled. Prockt. Inst. Lesokhim. Prom., no. 22, p4-16 (1971)

12. Flaig, W., Chemistry of Humic Substances in Relation to Coalification, in Coal Science, Advances in Chemistry Series, ACS, Wash., D.C. (1966)

13. van Krevelen, D.W., Coal, Elsevier, Amsterdam (1961)

14. Hill, G. and Lyon, L., Ind. Eng. Chem., 54(6), 30-9(1962)

15. Woodward, K.B. and Hoffmann, R., The Conservation of Orbital Symmetry, Verlag Chimie, Academic Press, Germany (1971)

16. Smith, R.E. and Hinshlewood, C.N., Proc. Roy. Soc., (London)A, 175, 131-142 (1940)

17. Ingold, K.V. and Lossing, F.P., Can. J. of Chem., 31, 30-41(1953)

18. Frey, H.M., and Walsh, R., Chem. Rev., 69 103(1969)

19. Mock, W.L. in Pericyclic Reactions Volume II, A.P. Marchand and R.E. Lehr, Editors, Academic Press, New York (1977)

20. Clarke,S.C. and Johnson,B.L., Tetrahedron, 27,3555-61(1971)

Table 1. Experimental Grid

Set	Substrate	Structure	Purity wt%	Reaction Conditions: Temperature Range C	Holding Times s	Initial Concentration mol/l
1	Guaiacol		99	250-525	110-6000	0.46-3.07
2	Benzaldehyde		99	300-500	120-3600	0.16-3.3
3	2,6 dimethoxyphenol		99	300-500	120-1800	0.32
4	Iso-eugenol		99	300-500	60-1560	0.33
5	Vanillin		99	300-500	120-1500	0.85
6	t-Cinnamaldehyde		99	250-400	120-1500	0.38-1.3
7	Anisole		98	344-550	180-1500	0.46-3.07
8	Acetophenone		98	350-550	120-4980	0.14-1.4

Table 2. Summary of Kinetic Data at 400C

Set	Substrate	Pathway: / Rate Constant:	R1 $\log_{10}k_1$	R2 $\log_{10}k_2$	R3 $\log_{10}k_3$	R4 $\log_{10}k_4$
1	Guaiacol		-3.2	-3.8	-	-
2	Benzaldehyde		-	-	-3.7	-
3	2,6 dimethoxyphenol		-3.1	-3.6	-	-
4	Isoeugenol		-3.2	-3.7	-	-
5	Vanillin		-3.4	-	-2.5	-
6	t-Cinnamaldehyde		-	-	-3.4	-
7	Anisole		-	-	-	-4.5
8	Acetophenone		-	-	-	-6.3

Notes: See text for pathway definitions. All k in s^{-1}.

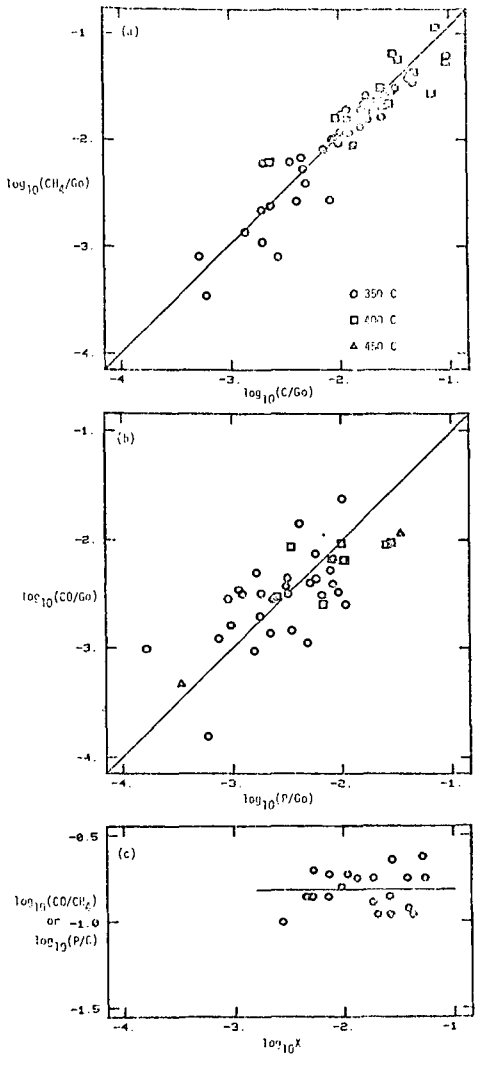

Figure 1. Product relationships in guaiacol pyrolysis:
(a) Methane vs. Catechol
(b) Carbon Monoxide vs. Phenol
(c) (Phenol/Catechol) ratio vs. Substrate conversion

Note: P-Phenol, C-Catechol, Go-Guaiacol,initial, X- Guaiacol conversion

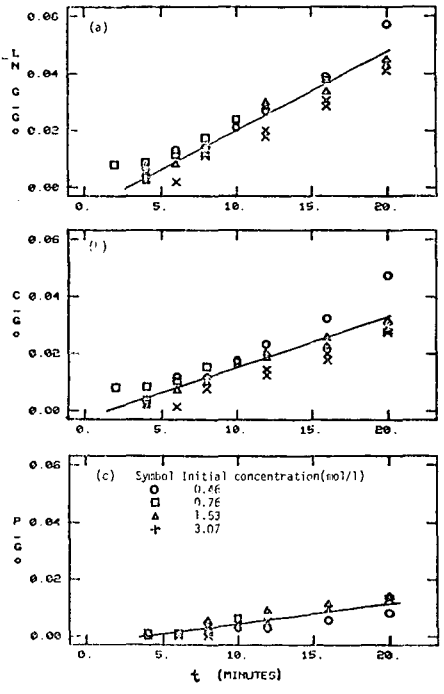

Figure 2. Guaiacol pyrolysis kinetics, T= 350 C:
(a) Substrate disappearance
(b) Catechol appearance
(c) Phenol appearance

Substrate	Path	$\log_{10}A(s^{-1})$	E^*(kcal/mol)
○ Guaiacol	R1	10.9±0.5	43.7±1.4
□ Guaiacol	R2	11.5±0.5	47.4±1.6
◇ Anisole	R4	12.1±0.8	51.4±2.4

Substrate	Path	$\log_{10}A(s^{-1})$	E^*(kcal/mol)
○ Benzaldehyde	R3	9.5±0.8	41.5±2.7
□ Acetophenone	R4	10.3±1.6	50.7±5.8

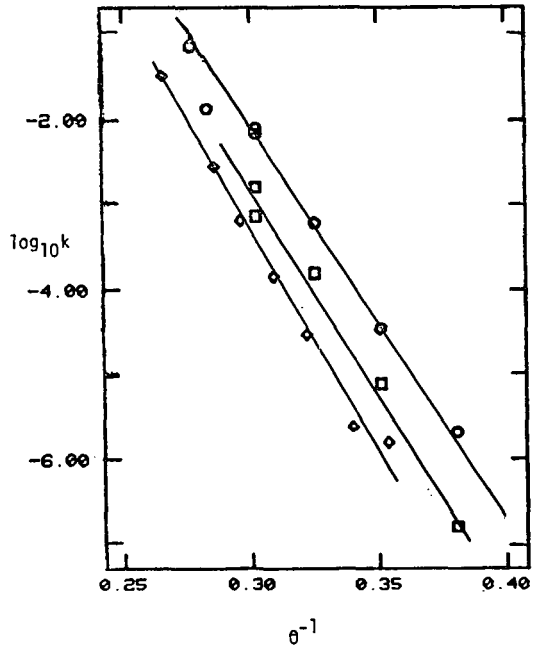

Figure 3. Arrhenius diagram for Guaiacol and Anisole pyrolyses.

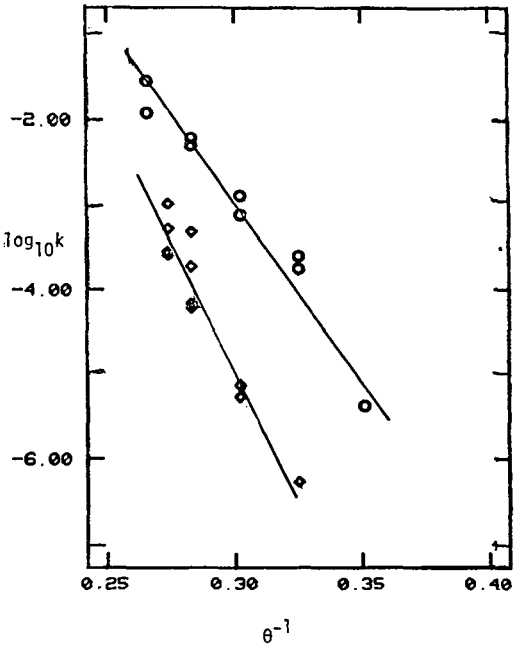

Figure 4. Arrhenius diagram for Benzaldehyde and Acetophenone pyrolyses.